DISPERSION OF A CONTINUOUS POLLUTANT SOURCE IN OPEN CHANNEL FLOW

A thesis

submitted in partial fulfilment

of the requirements for the Degree

of

Doctor of Philosophy in Civil Engineering

in the

University of Canterbury

by

ANTHONY JOHN MCNULTY

University of Canterbury

May 1983

ABSTRACT

In this study a new algorithm is developed to obtain a solution for the complete dispersion equation for a continuous release of pollutant into open channel flow. The technique used is based on Aris moment transforms and gives longitudinal moments of the concentration distribution. To ensure that these moments are finite, a deficit concentration is defined such that at steady state the concentration of pollutant tends to zero at large distances downstream from the source. Once computed, the "deficit" moments of concentration may be used to produce approximate deficit concentration profiles at any point in the channel cross-section. A simple transformation to these profiles yields the actual concentration distribution. The solution is very accurate far from the source but accuracy is less satisfactory close to the source.

The solution technique permits any combination of velocity and diffusivity distributions to be used to define the flow field. This allows the model to be compared with known solutions for a constant velocity and diffusivity, and verified with a set of laboratory experiments where a more realistic flow field is observed.

The verified model is also used to examine the assumptions and conclusions of previous investigations of a continuous pollutant source. As previously assumed, it is found that the effect of the longitudinal diffusion on the concentration distribution is negligible. The constant velocity/constant diffusivity field, as used by most investigators of a continuous source, is shown to give conservative predictions for the pollutant dispersion. Finally, the dead zone mechanism, recognised by several studies as an important factor in the dispersion of a pollutant introduced as a slug, is found to be of little importance for a continuous pollutant release. Such bed effects are adequately described by the friction factor.

The two dimensional model is applied to the transverse dispersion of a continuous pollutant released into two natural channels. A comparison is made between measurements of concentration in each field test reach and from the two-dimensional model, using vertical averages. The model is shown to give good overall predictions if the reach averaged velocity and diffusivity distributions are available.

Finally, the applicability of the two-dimensional model, as applied to natural channels, is tested with a three-dimensional model. This model is developed in an identical manner to the two-dimensional model. With the three-dimensional model the degree of vertical mixing is examined at the measurement sections in the field experiments. This indicates that vertical mixing is complete long before the transverse mixing in both natural channels and a two-dimensional model is appropriate.

ACKNOWLEDGEMENTS

This study was performed in the Department of Civil Engineering, University of Canterbury, and thanks are extended to its head, Professor R. Park for the opportunity to use the facilities and equipment of the Department.

Sincere gratitude is expressed to Professor I.R. Wood, who supervised this project, for his unlimited enthusiasm, provoking criticism and guidance.

I gratefully acknowledge the assistance of the academic and technical staff of the Civil Engineering Department, in particular:

Dr. R.H. Spigel for his guidance during Professor Wood's absence;

Drs. B.W. Hunt, A.J. Sutherland and Mr. E.P. Giddens for their helpful advice;

Messrs H. Pearce, A. Stokes, I. Sheppard and F. Archer for their technical advice and assistance in the construction and performance of experiments;

Mr. J. Ritchie for the construction and help with the data capture equipment;

Mr. L. Gardiner for the photography;

Mrs. J.E. Stewart for her excellent effort typing the manuscript.

I am grateful to Dr. R. Smith of the Department of Applied Mathematics and Theoretical Physics, University of Cambridge for his interest in analytical solutions and the academic staff of the Department of Mathematics, University of Canterbury, for their assistance.

Thanks are extended to Mr. D. Johnstone of the Ministry of Works for his and his staff's assistance with the field experiments.

I would like to thank my fellow students for many helpful discussions and my family and friends for their patience and support during this study.

This research was funded by the National Water and Soil Conservation Organisation. During this study the writer was supported by the University Grants Committee of New Zealand.

TABLE OF CONTENTS

LIST OF FIGURES

FIGURE PAGE

FIGURE PAGE

FIGURE PAGE

LIST OF PLATES

LIST OF TABLES

LIST OF SYMBOLS

A - Area of flow section or % of bed occupied by dead zones;

A_n - Coefficient in the exponential series, $c = \sum_n A_n e^{-\alpha_n x}$;

B - Flux of buoyancy in the tracer;

b - Channel flow width;

c - Concentration of pollutant;

c' - Fluctuating component of concentration (about the mean concentration);

c_{dp} - Pth moment of non-dimensional deficit concentration about $\xi = 0$ $\left(= \int_0^\infty c_{d*}\ \xi^p\ d\xi\right)$;

c_{d*} - Non-dimensional deficit concentration ($c_{d*} = c_* - 1$);

c_e - Fully mixed concentration of dispersant;

c_p - Pth moment of concentration about $\xi = 0$ $\left(= \int_0^\infty c\ \xi^p\ d\xi\right)$;

c_s - Source concentration;

c_{s*} - Non-dimensional source concentration;

c_* - Non-dimensional concentration;

D_x - Longitudinal dispersion coefficient;

D_y - Depth-averaged vertical dispersion coefficient;

D_z - Width-averaged transverse dispersion coefficient;

d - Depth of dead zones (in mm);

E - Non-dimensional shift of the origin into the eddy caused by dead zones;

e - Shift of the origin into the eddy ($= E.\frac{dA}{y_R}$);

F - Arbitrary function;

f - Friction factor;

G - Arbitrary function;

g - Gravitational acceleration,

H - Element size in the numerical scheme;

I - Counter in the numerical scheme (= element number);

J_ν - Bessels function of the 1st kind of order ν;

$j'_{n,\nu}$ - Nth zero of the first derivative of J_ν;

K - Entrainment coefficient for the dead zone eddy;

K_p - Constant of integration for c_{dp};

K_x, K_y, K_z - Longitudinal, vertical and transverse mixing coefficient;

L - Order of moments for large p ($c_{dp} \equiv c_{dL}$);

M - Source strength in series solution for the dispersion equation;

m_p - Second moment transform as defined by Aris $\left(= \int_0^1 c_p\ d\eta\right)$;

$\tilde{n}$ - Unit outward pointing normal to a control surface;

PTZ - Percentage of rectangular dead zone occupied by the eddy;

p - Order of moments;

Q_p - Flux pth moment through a horizontal plane $\left(= \psi(\eta) \frac{\partial c_{dp}}{\partial \eta}\right)$;

q - Flux or discharge;

$R(\tau)$ - Velocity correlation function;

s - Control surface;

s_0 - Channel bed slope;

T_L - Lagrangian time scale;

t - Time variable;

u, v, w - Velocity components in x, y and z directions respectively;

u', v' - Velocity fluctuation about u and v respectively;

$\tilde{u}$ - Velocity vector (= (u, v, w));

$\bar{u}$ - Section averaged velocity (in longitudinal direction);

u_* - Shear velocity $(= \sqrt{\tau_0/\rho})$;

V - Control volume;

v_i^e, v_i^b - Equilibrium and background readings on the conductivity for probe i, respectively;

w - Channel width or concentration in the dead zone eddy;

x, y, z - Longitudinal, vertical and transverse distance co-ordinates, respectively;

y_n - Mean flow depth;

y_s - Location of a point source;

y_{su}, $y_{s\ell}$ - Upper and lower bounds of a source, respectively;

z_n - Mean flow width;

α - Power for the power-law velocity distribution (generally, $\alpha = \frac{1}{7}$);

α_n - Decay coefficient in the exponential series, $c = \sum_n A_n e^{-\alpha_n x}$;

β - Constant in the diffusion equation;

γ_n - Coefficient in the Bessels function;

Δ - Source half-width;

δ - Dirac delta function;

ε_M - Molecular diffusivity coefficient;

ε_m - Momentum diffusivity coefficient;

ε_{Tij} - Turbulent diffusivity tensor;

ε_x, ε_y, ε_z - Longitudinal, vertical and transverse diffusivities, respectively;

ε_ξ, ε_η - Longitudinal and vertical diffusivities, respectively;

ζ, η, ξ, - Dimensionless transverse, vertical and longitudinal distance co-ordinates, respectively;

η_s - Dimensionless source location;

η_{su}, $\eta_{s\ell}$ - Dimensionless upper and lower bounds of a source, respectively;

κ - von Karman turbulence coefficient;

λ_n - Coefficient in the Bessels function solution;

μ - Non-dimensional mean velocity $(=(\overline{u}/u_*)^2)$;

ν - Viscosity or the order of Bessels function;

ρ - Fluid density;

τ - Non-dimensional time, time increment or shear stress;

τ_{xy} - Shear stress at any point in a two-dimensional flow field;

τ_0 - Bed shear stress;

$\phi(y,z)$, $\phi(\eta,\zeta)$ - Transverse diffusivity function;

$\chi(y,z)$, $\chi(\eta,\zeta)$ - Local velocity function;

$\psi(y,z)$, $\psi(\eta,\zeta)$ - Vertical diffusivity function ($\equiv \psi(\eta)$ in 2-D model).

BLANK PAGE IN ORIGINAL - PART OF PAGINATION

CHAPTER I

INTRODUCTION

1.1 Pollution in the Environment

One of the many roles a river plays is to return waste water from land masses to the oceans. Even before man began discharging his wastes into the environment, via the rivers, there were naturally occurring forms of contamination. For instance, in a storm the wash from the land may contain significant volumes of soil resulting in heavy siltation of the river systems. In any body of water, there will be a balance between the physical environment and the life processes of the plant and animal community. Any contaminant introduced into the waterway will upset this system. The extent to which this balance is upset depends on the type of pollution and the river characteristics.

Ideally, any waste waters returned to the environment by man should not result in a lasting detrimental effect on the water system. Unless a large amount of cheap power is available it is not economical to remove all the contaminants from the waste water, and it must then be accepted that polluted water will be released into the rivers. It is the task of the water quality engineer to dispose of the waste water such that certain pollution limitations are satisfied. These limits will depend on various factors, like the downstream use of the water and the standards that are set by governing bodies. To fulfill his role, the engineer must be able to present a reliable prediction of the dispersive ability of any particular waterway. This will enable the potential impact of the release of a pollutant into a natural channel to be assessed.

1.2 Dispersion in Open Channel Flow

1.2.1 Longitudinal Dispersion

When a pollutant is introduced into a natural channel it is dispersed in and is diluted by the water mass. There are two major processes which dominate the mixing occurring in a river. The pollutant is dispersed by the turbulent eddies which exist in the flow and by the velocity shear resulting in the downstream transportation of pollutant at different rates. This later process is termed longitudinal dispersion. A large proportion

BLANK PAGE IN ORIGINAL - PART OF PAGINATION

of the previous work on the dispersive properties of natural channels has been devoted to predicting longitudinal dispersion properties, theoretically and experimentally. Indeed this process is very important when a slug (instantaneous) type injection is being considered.

Theoretical predictions of mixing coefficients have been made for steady flow in open channels (Elder 1959). However, in most natural channels the variations in channel geometry and velocity fields, both along and across a reach, render these predictions unrealistic. To obtain a first estimate of the mixing characteristics, a comparison can be made with data collected from the large number of experimental studies that have been reported (see Rutherford 1981). If this estimate predicts pollutant concentrations close to the limits imposed on the specific problem then a more detailed study of the reach is necessary. The inability of present models to predict dispersion patterns for any given reach reflects the difficulty in modelling the channel geometry and flow conditions that exist in natural channels.

While longitudinal dispersion processes have been well investigated, there are still gaps in the knowledge of the vertical and transverse mixing properties of a natural flow. It is these mechanisms which are important for a continuous pollutant release.

1.2.2 A Continuous Pollutant Release

Whereas an instanteous pollutant release will continue spreading longitudinally as the pollutant cloud moves downstream, a continuous source (after an inital unsteady period) will attain a fully mixed condition after some distance. Further mixing will only occur if there is some additional input into the river (e.g. a side channel). In a continuous release situation, longitudinal concentration gradients are expected to be very small. Consequently, the longitudinal dispersion parameters produced by most of the experimental studies are of little use.

Analytical solutions are available for the continuous injection of pollutant into a constant velocity and constant diffusivity field but the application of this model to natural channels is limited. Although dispersion coefficients are available for vertical mixing (Elder 1959 and subsequent investigators) no analytical solutions have been presented to incorporate typical non-uniform velocity/diffusivity distributions for continuous pollutant sources.

BLANK PAGE IN ORIGINAL - PART OF PAGINATION

There are two water quality criteria which may regulate the continuous discharge of contaminant into an open channel. These criteria will depend on factors like the type of pollutant being introduced into the waterway and the uses of the water downstream of the release point. One requirement is the maximum concentration permissible for the final fully mixed pollutant at a large distance downstream. This concentration may be determined by a simple ratio between the initial pollutant concentration, and the pollutant discharge and river discharge. Thus the allowable pollutant discharge is directly related to the river discharge. A second and more demanding requirement is usually imposed on the mixing in a channel. This condition acknowledges that close to the source pollutant concentrations will be high but limits these excessive concentrations to within a certain distance from the source. For example, water quality authorities may require that from 2 km downstream of the pollutant source, the concentration of pollutant at any point in the channel does not exceed twice the final allowable concentration. In this type of situation the limiting factors are the amount of contaminant being released and the ability of the river to disperse the contaminant in the given distance. It is the task of the engineer to predict the dispersion pattern, which will enable estimates of concentrations at all points in the river.

1.3 The Aims and Scope of this Investigation

The previous work on dispersion with a continuous source has focused on the predictions obtained if certain restrictive assumptions are made. While these assumptions permit a solution to the dispersion problem, it is only a first estimate for most real situations. In this study a model is proposed which will solve the complete dispersion equations. This will enable the previous assumptions that,

(a) the longitudinal concentration gradients are negligible,
(b) the velocity does not vary with depth,
(c) the diffusivity does not vary with depth,

to be examined.

The pollutants modelled in this study are conservative substances which have identical properties to those of the ambient river water. Although the extension to buoyant or decaying substances is not considered in this study, properties relating to individual pollutants may be included in the analysis to obtain appropriate solutions. That is, the approach in

BLANK PAGE IN ORIGINAL - PART OF PAGINATION

this study considers only the mixing characteristics already existing in a channel.

A summary of the relevant literature is presented in Chapter 2. This is followed by the development and discussion of the three major aspects of this investigation.

Chapters 3 and 4 describe the theoretical development of the model, and the corresponding numerical model, for the dispersion of a continuous pollutant source in steady two-dimensional open channel flow. Each of the above assumptions is investigated and the effects of dead zones in the channel bed are discussed. An extension of this model, to enable an estimate of the three-dimensional dispersion processes, is included in Chapter 9.

The series of laboratory experiments performed to verify the model predictions are reported in Chapters 5 and 6. Chapter 5 outlines the laboratory equipment and experimental techniques and the following Chapter presents the results of the laboratory experiments.

The field experiments performed are described in Chapter 7. A modified version of the two-dimnensional program is applied to the field experimental reaches and results compared with collected data in Chapter 8.

Finally, Chapter 10 summarises the conclusions arising from this study and outlines the areas which require further investigation.

Table 2.1: A summary of terms used to describe mixing processes.

Convection	- the transportation of particles by the bulk movement of the fluid.
Diffusion (molecular)	- the scattering of particles by random molecular motion (this may be described by the classical diffusion equation).
Diffusion (turbulent)	- The scattering of particles by random turbulent motion, considered roughly analogous with molecular diffusion on a much larger scale.
Diffusivity	- this is identical to the turbulent diffusion.
Dispersion	- the scattering of particles or a pollutant cloud by the combined effects of shear and diffusion.
Shear	- the convection of fluid at different velocities at different locations in the flow (e.g. a normal velocity profile in open-channel flow has slower velocities near the boundaries than at the surface).

CHAPTER II

LITERATURE REVIEW

2.1 Introduction

Whilst some aspects of the dispersion problem have been well investigated, the release of a continuous pollutant has had limited attention. However, previous contributions to the mixing theory as a whole form the background for this study. There are several factors contributing to the mixing of a contaminant in a turbulent open-channel flow. A summary of the terms used to describe these factors is included (table 2.1) and should be referred to throughout this chapter.

The major developments in mixing theory are outlined, along with a review of previous approaches to modelling the continuous pollutant release.

2.2 Historical Background

In 1822 Fourier presented his law of heat flow to describe the physical process of heat flow that he had observed. Following this heat flow law, in 1855 a German physiologist Adolph Fick hypothesised that an identical law existed for the molecular diffusion of salt in its solvent. Fick suggested that the flux of salt, the mass of salt crossing a unit area per unit time in a given direction, is proportional to the salt concentration gradient in that direction. Mathematically this law is written as

$$q = - D \frac{\partial c}{\partial x} \qquad (2.1)$$

where q is the flux of salt, C the salt concentration and D a constant of proportionality. If this law and the conservation of mass principle are applied to a control volume then a molecular diffusion equation may be derived.

Subsequent investigators, beginning with Sir G.I. Taylor (1921), recognised that turbulent motion is capable of diffusing heat and other diffusible properties in much the same way that molecular agitation gives rise to molecular diffusion. Taylor hypothesized that the dispersive

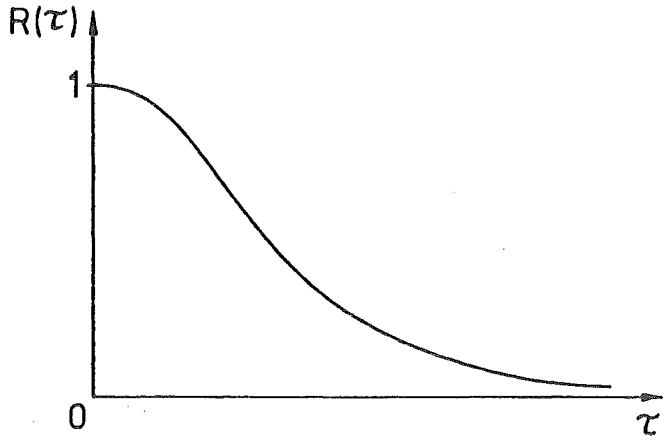

Figure 2.1 : The correlation $R(\tau)$ between the velocity at a point at time t and time $t + \tau$.

ability of a flow is related directly to simple statistical measures of turbulent velocity fluctuations. Although Taylor's original analysis was for a homogeneous turbulence field requiring the mean flow properties to be stationary random functions of time, the method is applicable for a turbulent shear flow. In this case, as Batchelor and Townsend (1956) pointed out, a fluid particle may migrate randomly through the entire flow field such that the velocity of the fluid particle may be described as a fluctuation about the mean velocity (i.e. as a stationary random function of time). Taylor's analysis is Lagrangian (that is, it is describing discrete fluid particles).

The variance of particles (the mean square position) in a turbulent shear flow as described by Taylor is,

$$\sigma^2(t) = 2\,\overline{u'^2}\; t \int_0^\infty R(\tau)\, d\tau \qquad (2.2)$$

where $u' = u - \bar{u}$, is the instantaneous velocity of a particle about an origin moving at the mean velocity, $\bar{u}$. $R(\tau)$ is the correlation between the velocity of a fluid particle at time t and time $(t + \tau)$, i.e.

$$R(\tau) = \frac{\overline{u'(t)\, u'(t+\tau)}}{\overline{u'(t)^2}}$$

The overbar designates a mean over a large number of particles. A typical distribution of $R(\tau)$ is shown in Figure 2.1.

Equation 2.2 describes the diffusion of particles originally concentrated at the origin about a plane moving with the mean velocity. Taylor proceeded to use this relationship for large values of τ, since $\lim_{\tau\to\infty} R(\tau) = 0$ (see figure 2.1), to obtain $\sigma^2(t) = 2\,\overline{u'^2}\, T_L t$. T_L is the Lagrangian integral time scale of turbulence and is defined by

$$T_L = \int_0^\infty R(\tau)\, d\tau$$

Therefore, at large times the variance of a pollutant cloud will be directly proportional to time. That is, the diffusion coefficient is constant.

In his later papers Taylor (1953, 1954) computed values for this constant diffusivity and verified this analysis in laboratory experiments.

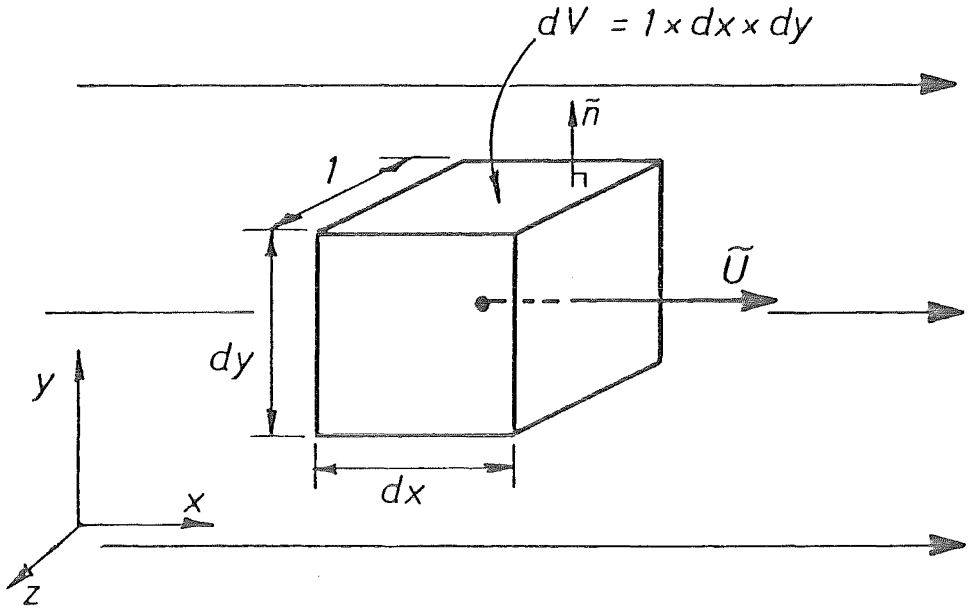

Figure 2.2 : Stationary incremental control volume of fluid.

Although the Lagrangian approach provides a useful insight into the mechanics of the dispersion processes, it appears less suitable than the Eulerian theory for describing dispersion in a turbulent shear flow.

2.3 The Eulerian Dispersion Equation

Whilst the theory developed by Taylor is Lagrangian, one of the most direct theoretical approaches to the dispersion process is Eulerian. This involves the application of the principle of conservation of mass to an arbitrary control volume in the flow (Sayre 1968). The Lagrangian approach investigates the behaviour of discrete particles.

If an incremental volume of flow is considered (see figure 2.2), then the flux of solute through the surface of the control volume must be balanced by the flux due to convection and the flux due to molecular diffusion across the surface of the control volume. This is expressed as

$$\int_V \frac{\partial c}{\partial t}\, dv = -\int_S c\tilde{u}.\tilde{n}\, ds + \int_S \varepsilon_M \nabla c.\tilde{n}\, ds \qquad (2.3)$$

where c is the concentration of solute, $\tilde{u}$ is the velocity field, ε_M is the molecular diffusion coefficient and $\tilde{n}$ is the outward pointing unit normal to the surface of the control volume. The first term on the right hand side represents the convection of tracer (solute) through the control volume surface and second term the molecular diffusion (c.f. Fick's law). If the divergence theorem is applied to each of the surface integrals then

$$\frac{dc}{dt} = \int_V \frac{\partial c}{\partial t}\, dv = -\int_V \nabla.(c\tilde{u})\, dv + \int_V \varepsilon_M \nabla^2 c\, dv \qquad (2.4)$$

For incompressible flow, $\nabla.\tilde{u} = 0$ and equation 2.4 reduces to

$$\frac{\partial c}{\partial t} = -\tilde{u}.\nabla c + \varepsilon_M \nabla^2 c \qquad (2.5)$$

This equation along with the boundary and initial conditions gives an exact description of dispersion in a laminar flow.

In turbulent flow, the instantaneous concentration and velocity vectors are represented by a time-averaged value plus a fluctuation component,

$$\begin{aligned} c &= \bar{c} + c' \\ u_i &= \bar{u}_i + u_i' \end{aligned} \qquad (2.6)$$

BLANK PAGE IN ORIGINAL - PART OF PAGINATION

where the subscript i denotes the ith co-ordinate direction, and the overbar represents a time average, obtained using the Reynolds averaging procedure. The averaging period is sufficiently long for the averages to converge.

The contribution of molecular diffusion to the mixing process in turbulent flow is generally negligible in comparison to the turbulent diffusion and this term, the last in equation 2.4 is usually neglected (it may be considered to be incorporated in the turbulent diffusion term). Equation 2.5 averaged over time becomes, in tensor form,

$$\frac{\partial \bar{c}}{\partial t} + \bar{u}_i \frac{\partial \bar{c}}{\partial x_i} = \frac{-\partial}{\partial x_i} \overline{c' u_i'} \tag{2.7}$$

The concentration co-variance is normally written as,

$$- \overline{c' u_j'} = \varepsilon_{Tji} \frac{\partial \bar{c}}{\partial x_i} \tag{2.8}$$

where ε_{Tji} is turbulent diffusion tensor. In the general case, turbulent mixing in all directions plays an important role in the dispersion pattern. However, as pointed out by Dagan (1969), the diffusivity tensor is symmetric. This means that for some choice of axes (the principle axes of the diffusivity field) the off-diagonal terms in the tensor will become zero. In most cases (Dagan 1969 and Fischer 1970) the principle axes of the diffusivity field will correspond to the Cartesian co-ordinate system used in open channels (i.e. horizontal, vertical and longitudinal co-ordinates). Consequently, the tensor ε_{Tji} reduces to a diagonal tensor whose non-zero elements correspond to the principle diffusivities, ε_x, ε_y and ε_z.

Omitting the time average overbars and expanding to the conventional rectangular Cartesian notation, equation 2.8 substituted into equation 2.7 results in the general form of the convection-diffusion equation for a conservative substance in turbulent open-channel flow,

$$\frac{\partial c}{\partial t} + u \frac{\partial c}{\partial x} + v \frac{\partial c}{\partial y} + w \frac{\partial c}{\partial z} = \frac{\partial}{\partial x}\left(\varepsilon_x \frac{\partial c}{\partial x}\right) + \frac{\partial}{\partial y}\left(\varepsilon_y \frac{\partial c}{\partial y}\right) + \frac{\partial}{\partial z}\left(\varepsilon_z \frac{\partial c}{\partial z}\right) \tag{2.9}$$

where u, v, w are velocity components in the x, y and z directions (see figure 2.1).

It is this equation upon which this study is based. The solution of this equation in a natural river is extremely difficult, even if all the values of u, v, w and ε_x, ε_y, ε_z were known at every point in the

BLANK PAGE IN ORIGINAL - PART OF PAGINATION

river, which they never are. Previous theoretical investigations of dispersion in open channel flow have been devoted mainly to

(1) establishing a theoretical basis for predicting ε_x, ε_y and ε_z,
(2) the analysis of certain limiting cases of equation 2.9 for which solutions can be obtained,
(3) the transformation of equation 2.9 into forms which are more amenable to solution,
(4) the solution of equation 2.9 by numerical methods.

As each of these points are relevant to this investigation the foregoing studies on each aspect are outlined in the following sections.

2.4 The Diffusion Coefficients

The vertical diffusion coefficient ε_y is usually evaluated by assuming that the turbulent transfer of mass and momentum are equivalent (Reynolds Analogy). Consider the flux of mass and momentum in the y direction in a channel with steady, uniform two-dimensional flow; the total transfer rate for mass,

$$\text{Mass flux} = (\varepsilon_y + \varepsilon_M) \frac{\partial c}{\partial y}$$

and for momentum

$$\text{Momentum flux} = \rho(\varepsilon_m + \nu) \frac{\partial u}{\partial y}$$

Then the analogy is complete if (Rohsenow and Choi 1961),

(a) the mechanisms which control mass transfer and momentum transfer are identical,
(b) $\varepsilon_M \ll \varepsilon_y$ and $\nu \ll \varepsilon_m$,
(c) the momentum transfer is unaffected by the mass transfer.

Here ε_M is the molecular diffusion, ν the viscosity and ε_m the momentum diffusion coefficient. Condition c is automatically satisfied for a dispersant of identical properties to the receiving fluid. The second condition is satisfied in open-channel flow. Although eddy diffusion theory suggests that the first condition is satisfied, present knowledge of the processes of mass and momentum transfer is insufficient for an analytical proof. In the following development it is assumed that the Reynolds analogy is valid.

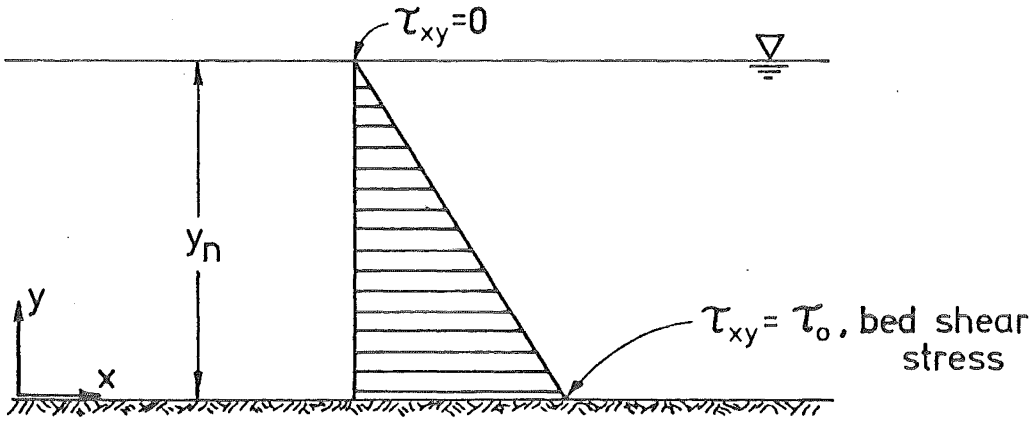

Figure 2.3 : Shear stress distribution over the flow depth.

The momentum diffusivity is defined as,

$$\varepsilon_m = \frac{-\overline{u'v'}}{\frac{du}{dy}} \tag{2.10}$$

From the momentum equation in turbulent flow, the velocity co-variance and shear stress are found to be related by

$$\tau_{xy} = -\rho\,\overline{u'v'} + \rho\nu\frac{du}{dy} \tag{2.11}$$

The shear stress, τ_{xy}, is linearly distributed over the depth, varying from τ_0, the bed shear stress, at $y = 0$ to zero at $y = y_n$ (see figure 2.3) and for $\nu << \varepsilon_m$,

$$\tau_{xy} = -\rho\,\overline{u'v'} = \tau_0\left(1 - \frac{y}{y_n}\right) \tag{2.12}$$

Then, noting that $\tau_0 = \rho u_*^2$ (u_* = shear velocity),

$$\varepsilon_m = \varepsilon_y = \frac{u_*^2\left(1 - \frac{y}{y_n}\right)}{\frac{du}{dy}} \tag{2.13}$$

For any given velocity distribution, u(y), the vertical diffusion coefficient may be now calculated using equation 2.13.

Using the von Karman-Prandtl logarithmic velocity distribution function,

$$u = \bar{u} + \frac{u_*}{\kappa}\left(\ln\frac{y}{y_n} + 1\right) \tag{2.14}$$

where κ is von Karman's constant, the diffusivity coefficient becomes,

$$\varepsilon_y = \kappa u_* y_n \frac{y}{y_n}\left(1 - \frac{y}{y_n}\right) \tag{2.15}$$

If equation 2.15 is averaged over the depth, then the vertical mixing coefficient $K_y = \frac{\kappa}{6} u_* y_n$ is obtained. This average diffusion result and equation 2.13 have both been verified by laboratory studies (Jobson and Sayre 1970).

Since turbulence is not isotropic and transverse velocity distributions are not analytically available as is the case for the vertical velocity, no acceptable theory for predicting the transverse diffusion coefficient ε_z has yet been developed. However, numerous experiments

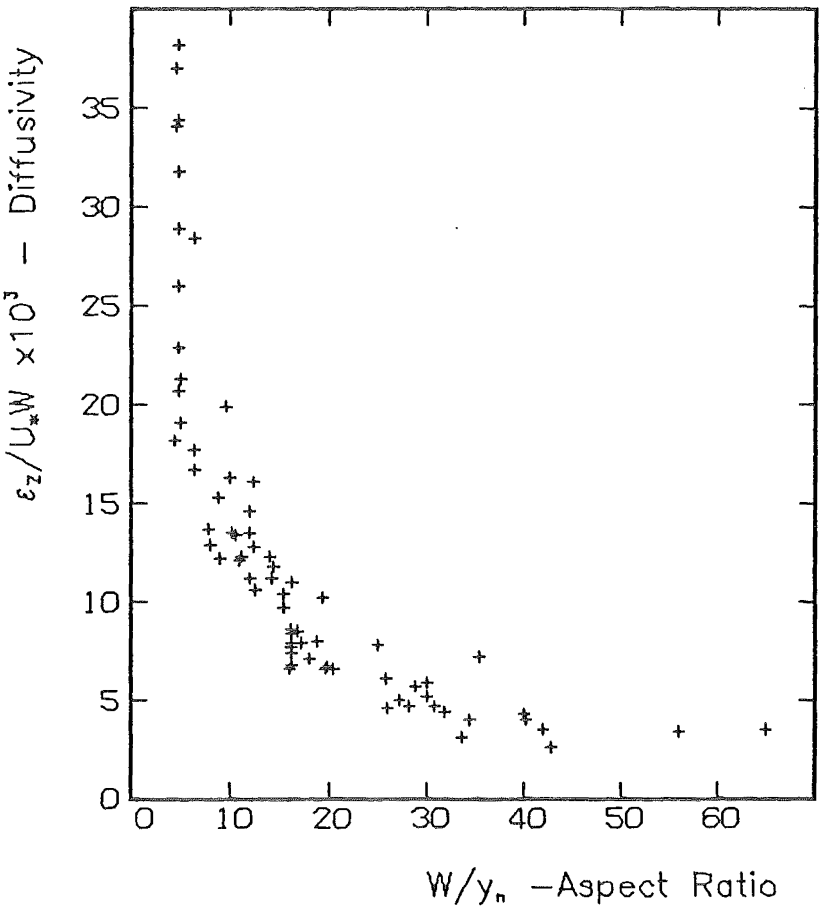

Figure 2.4 : Variation of ε_z/u_*w with w/h for published data for rectangular channels.

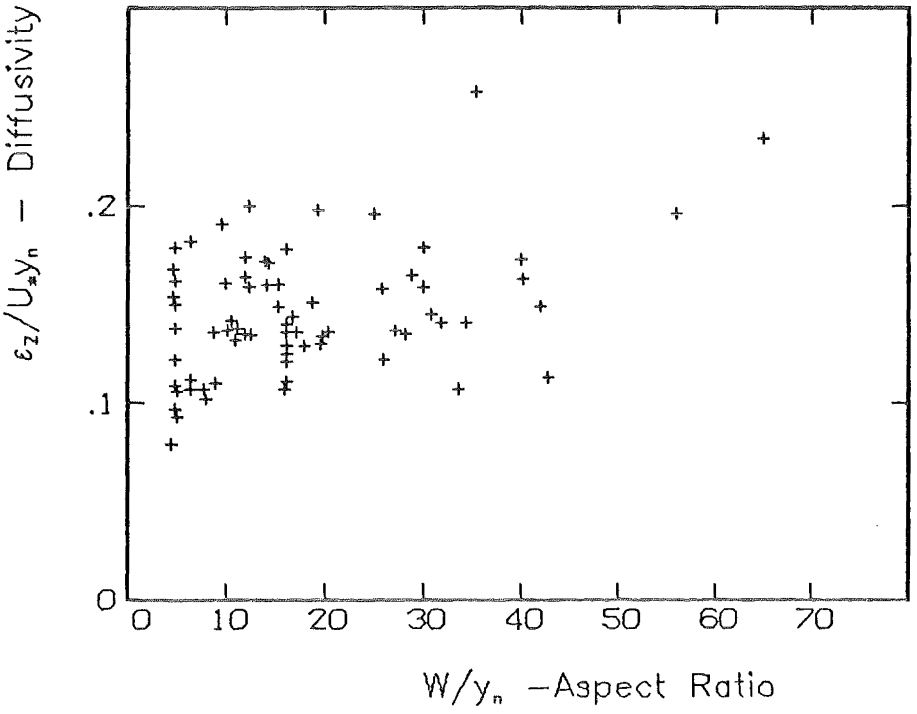

Figure 2.5 : Published data of ε_z/u_*h versus w/h for rectangular channels.

have been performed in laboratory and natural channels. Okoye (1970) found for experiments on dissolved tracers that the depth-averaged transverse mixing coefficient was dependent on the aspect ratio, b/y_n where b is the channel width and y_n the flow depth. Furthermore, he found that the diffusion coefficient, ε_z varied over the depth, tending to be largest near the water surface.

Figure 2.4 shows the variation of K_z/u_*w with w/y_n, where K_z is the average transverse diffusion coefficient and w is the width, taken from 10 separate publications (Lau and Krishnappen, 1977). Although this presentation appears to collapse the data onto one curve it does not allow the friction factor to be taken into account. Figure 2.5 compares the usual dimensionless diffusion coefficient K_z/u_*y_n with w/y_n. Clearly K_z/u_*w is a better dimensionless diffusion coefficient than K_z/u_*y_n. However, figure 2.5 does infer the average value of K_z/u_*y_n of 0.15 that has been reported for laboratory studies. Fischer (1973) found that in natural channels where the thalweg tends to meander and hence induce secondary currents, the average transverse coefficient was $K_z = 0.22\ u_*y_n$. Bends and changes in channel cross-section which result in stronger transverse circulations will further increase transverse mixing rates.

Although most investigators have focused on predicting average transverse coefficients it is also recognised that there is some variation in the local transverse coefficient. The most promising results in this area have been presented by Lau and Krishnappen (1981). In this study, a three-dimensional river problem was treated as a depth averaged two-dimensional mixing problem. They compared measured concentration profiles with profiles predicted using various forms for the transverse variation of flow properties. The best model for accurate simulation of the measured profiles used local values of velocity and depth with the section average transverse diffusion coefficient which can vary in the downstream direction. However, even the analytical solution (for constant diffusivity) of the model equation gave a good approximation to the measured profiles.

Smith (1981) proposed that the variation in local diffusivity be described by

$$\varepsilon_z = 0.15\ y(z)\ u_*(z) \qquad (2.16)$$

where $y(z)$ and $u_*(z)$ are the functions describing the depth profile and shear velocity across the channel. A similar variation in diffusivity was

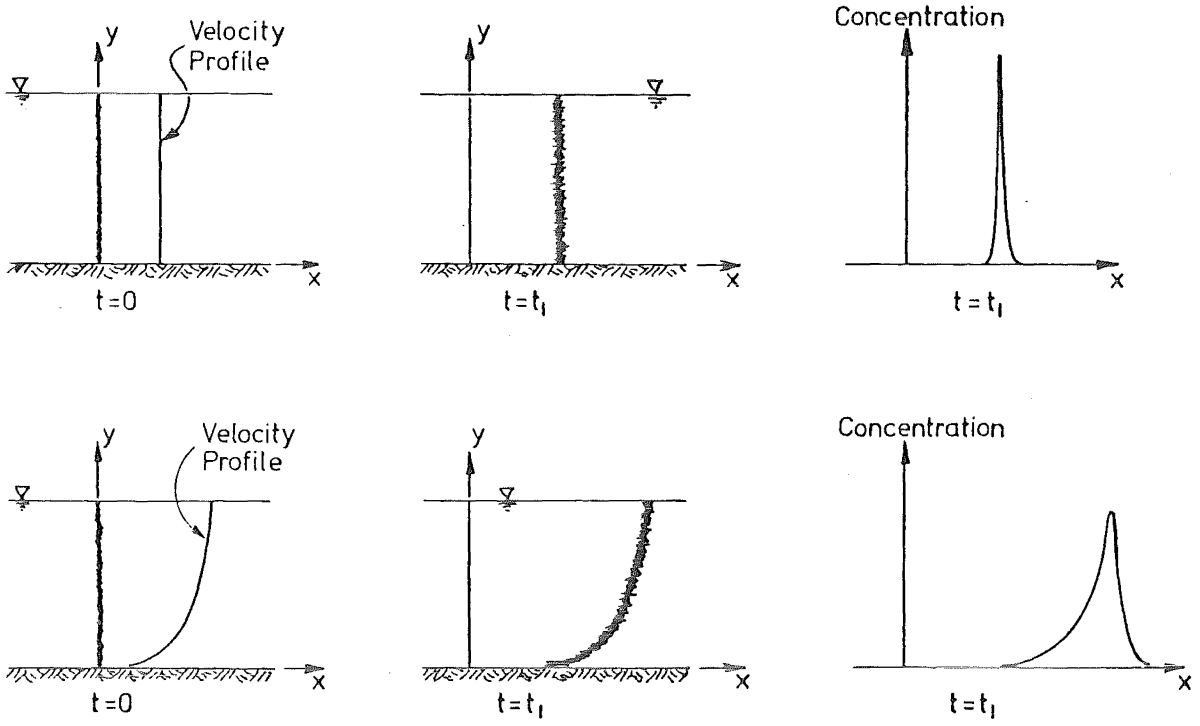

Figure 2.6 : Comparison of turbulent diffusion in a uniform flow and a shear flow.

the second best model of those investigated by Lau and Krishnappen (1981).

The remaining diffusion coefficient is for the longitudinal (streamwise) turbulent diffusion. This coefficient, ε_x, is generally assumed to be the same as the vertical coefficient, ε_y. That is, the vertical and longitudinal diffusivities are isotropic. However, it appears that the longitudinal diffusion is generally insignificant when compared to the mixing caused by the shear effect of velocity profiles. This is shown in figure 2.6 where dispersion is compared for a vertical line source in a uniform flow and a shear velocity flow. Elder (1959) calculated the longitudinal dispersion coefficient for a logarithmic velocity profile to be $D_x = 5.86\, y_n u_*$, which is approximately 90 times the magnitude of the turbulent diffusion coefficient given by equation 2.15 $\left(K_y = \frac{\kappa}{6} u_* y_n\right)$. Most subsequent investigators have neglected the longitudinal diffusion term in favour of the dispersion coefficient. Furthermore, for a continuous pollutant source, the longitudinal concentration gradient will be very small everywhere except close to the source. In this study the longitudinal term is included in the development of model equations in order to assess its effect.

2.5 Solutions to the Dispersion Equation

2.5.1 Fickian Diffusion Theory

In this approach, which was the earliest and still a common approach, a complete analogy with molecular diffusion or heat conduction is assumed. That is, the local diffusion coefficients ε_x, ε_y, ε_z are assumed to be constants (K_x, K_y and K_z) and the local longitudinal velocity is replaced by the cross-sectional average, $\bar{u}$. Furthermore, any effects due to the variation of u within the cross-section are absorbed into K_x and any effects due to the secondary flow velocities v, w can be absorbed into K_y and K_z. With these assumptions, equation 2.9 becomes,

$$\frac{\partial c}{\partial t} + \bar{u}\frac{\partial c}{\partial x} = K_x \frac{\partial^2 c}{\partial x^2} + K_y \frac{\partial^2 c}{\partial y^2} + K_z \frac{\partial^2 c}{\partial z^2} \qquad (2.17)$$

Solutions to this type of equation are available for a large variety of boundary and initial boundary conditions (Carslaw and Jaeger 1959). The application of Taylor's theory to open channel flow produces a one-dimensional form of equation 2.17 (Elder 1959).

Comparisons between solutions of the Fickian equation and

BLANK PAGE IN ORIGINAL - PART OF PAGINATION

experimental observations in channels that are fairly straight and uniform tend to show reasonably good agreement for the transverse and vertical mixing processes except very close to the source, and for the longitudinal mixing processes after x and t become very large (Sayre 1973).

In a two-dimensional flow with a continuous release the steady state form of equation 2.14 is

$$\bar{u} \frac{\partial c}{\partial x} = K_x \frac{\partial^2 c}{\partial x^2} + K_y \frac{\partial^2 c}{\partial y^2} \qquad (2.15)$$

This equation is identical to the steady state two-dimensional version of equation 2.9 with $u = \bar{u}$ and an assumption of constant diffusivities. It is frequently used as a first approximation to the two-dimensional mixing problem.

2.5.2 Aris Moment Transforms

The most promising analytical approach to longitudinal dispersion in turbulent open channel flow is the Aris moment equation transforms (Aris 1956). With no loss of rigor the moment transforms introduced provide a substantial simplification by reducing the number of variables in the dispersion equation. Aris defined an arbitrary local velocity as,

$$u(y, z) = \bar{u}\{1 + \chi(y, z)\} \qquad (2.16)$$

where $\bar{u}$ is the mean velocity and χ defines the velocity variation relative to the mean velocity. The turbulence distribution was assumed to be isotropic thus,

$$\varepsilon_z = \varepsilon_y = \varepsilon_z = D\,\psi(y, z) \qquad (2.17)$$

where D is the section averaged mixing coefficient and ψ is a function describing the distribution of eddy diffusivity across the section. Dimensionless variables are defined by the mean channel depth, y_n,

$$\xi = \frac{(x-\bar{u}t)}{y_n}, \quad \eta = \frac{y}{y_n}, \quad \zeta = \frac{z}{y_n}$$
$$\tau = \frac{Dt}{y_n^2} \text{ and } \mu = \frac{\bar{u}y_n}{D} \qquad (2.18)$$

Now equation 2.9 may be rewritten,

BLANK PAGE IN ORIGINAL - PART OF PAGINATION

$$\frac{\partial c}{\partial \tau} + \mu\chi \frac{\partial c}{\partial \xi} = \psi \frac{\partial^2 c}{\partial \xi^2} + \frac{\partial}{\partial \eta}\left(\psi \frac{\partial c}{\partial \eta}\right) + \frac{\partial}{\partial \zeta}\left(\psi \frac{\partial c}{\partial \zeta}\right) \qquad (2.19)$$

The initial and boundary conditions to be applied to the equation are,

$$\begin{aligned} &c(\xi, \eta, \zeta, \tau = 0) = c_0(\xi, \eta, \zeta), \text{ a known function} \\ &\text{and } \psi \frac{\partial c}{\partial \xi} = \psi \frac{\partial c}{\partial \eta} = \psi \frac{\partial c}{\partial \zeta} = 0 \text{ on the boundary} \end{aligned} \qquad (2.20)$$

The boundary condition implies that there is no flux of solute across the flow boundaries.

Aris then defined the pth moment of the concentration distribution,

$$c_p(\eta, \zeta, \tau) = \int_{-\infty}^{+\infty} \xi^p \, c(\xi, \eta, \zeta, \tau) \, d\xi \qquad (2.21)$$

If equation 2.19 is multiplied by ξ^p and integrated with respect to ξ from $-\infty$ to $+\infty$, then the moment equation is obtained,

$$\frac{\partial c_p}{\partial \tau} = \frac{\partial}{\partial \eta}\left(\psi \frac{\partial c_p}{\partial \eta}\right) + \frac{\partial}{\partial \zeta}\left(\psi \frac{\partial c_p}{\partial \zeta}\right) + p\mu\chi \, c_{p-1} + p(p-1)\psi \, c_{p-2} \qquad (2.22)$$

for which the appropriate initial and boundary conditions are,

$$\begin{aligned} &c_p(\eta, \zeta, 0) = \text{known value}, \\ &\psi \frac{\partial c_p}{\partial \eta} = \psi \frac{\partial c_p}{\partial \zeta} = 0 \text{ at the boundaries}, \\ &\frac{1}{A} \iint_A c_0(\eta, \zeta, \tau) \, d\eta d\zeta = \text{constant} \end{aligned} \qquad (2.23)$$

To render these equations complete, Aris defined his second moment transformation

$$m_p = \int_0^1 c_p \, d\eta \qquad (2.24)$$

This permits the further simplification by applying this transformation to equation 2.22,

$$\frac{dm_p}{d\tau} = p\mu \, \overline{\chi \, c_{p-1}} + p(p-1) \, \overline{\psi \, c_{p-2}} \qquad (2.25)$$

where the overbars signify vertical averaging. The conditions are now,

$$\begin{aligned} &m_p(\tau) \text{ is fixed for } \tau = 0 \\ &\frac{dm_0}{d\tau} = 0 \text{ (mass is conserved)} \end{aligned} \qquad (2.26)$$

BLANK PAGE IN ORIGINAL - PART OF PAGINATION

The equations are now complete and solutions may be obtained for all moments.

Whilst Aris did not solve the moment equations for turbulent open channel flow, he did show that the moments m_p behave as the moments of the normal distribution as $\tau \to \infty$. Therefore the mean concentration is ultimately distributed about a point, moving downstream at the mean velocity, according to the normal law of distribution. Consequently, at large dispersion times the one-dimensional diffusion theory appears to be applicable.

Although the Aris moment transform method provides a very useful tool for investigating dispersion processes for instantaneous releases of contaminant, the method has not been used to investigate a continuous release. In this situation the moments of concentration will clearly become infinite. It is this problem and the technique used to facilitate the use of moment transforms to which this study is addressed.

2.5.3 Numerical Solutions

Yotsukura and Fiering (1964) employed an explicit numerical scheme to solve the two-dimensional dispersion equation in turbulent open-channel flow with a parabolic and a logarithmic velocity distribution. Although this method was limited by the excessive amount of computer time required to reach an informative stage in the dispersion process, longitudinal distribution curves appeared to exhibit Gaussian characteristics after a certain dispersion time.

More recently numerical models have been developed for three-dimensional finite-difference solutions for steady-state near-field mixing in straight rectangular channels (Rastogi and Rodi 1978). The technique used by Rastogi and Rodi is a down-stream marching, non-iterative procedure with a typical calculation taking 30 minutes on a UNIVAC 1108 to cover a longitudinal distance of 18 channel widths.

Unsteady problems are generally solved in two-dimensions only. Even then the techniques used by many investigators (explicit finite-difference techniques) require relatively large amounts of computer time for all but the simplest of problems. Harden and Shen (1979) obtained reasonable solutions to the transient two-dimensional mixing problem using a combined implicit/explicit finite difference scheme proposed by

BLANK PAGE IN ORIGINAL - PART OF PAGINATION

Stone and Brian (1963) and Peaceman and Rachford (1955). In their study a 50 x 50 grid was used to model a 150 - 210 m wide by 1245 m long section of the Missouri River in a steady state condition. This reach was some 2.66 km downstream from the release point and used measured data as an upstream condition.

A more promising approach appears to be that used by Sayre (1968), who applied the Aris moment transform (Aris 1956) to the two-dimensional dispersion equation. He proceeded to solve the transient two-dimensional problem for a neutrally buoyant pollutant and also for particles with a fall velocity. The transformation of the dispersion equation by the moment method effectively reduces the problem by one dimension. This enables significant reductions in computer time required to solve the two-dimensional problem. This method was extended by Valentine (1978) to incorporate trapping elements in the flow region and was applied to the three-dimensional problem in the same study.

The numerical techniques used in this investigation are largely based on the methods used by Sayre and Valentine.

2.6 Dispersion in Natural Channels

Most of the earlier work in natural channels was concerned with the verification of the Fickian dispersion equation. Many of these investigations showed a large increase in the value of the longitudinal dispersion coefficient that had been predicted by laboratory experiments. A table of data compiled by Rutherford (1981) for over 30 rivers and canals shows a variation in the longitudinal dispersion coefficient, K_x, of $10\ y_n u_* < K_x < 7500\ y_n u_*$. For turbulent two-dimensional open channel flow, Elder (1959) derived a theoretical value of $K_x = 5.9\ y_n u_*$. Part of the variation may be attributable to measurements being taken in a region where the Fickian model is not valid (prior to a point discharge becoming well-mixed across the channel when K_x is not constant). However, much of the variation reflects the real differences between the idealised two-dimensional case and natural channels with intrinsic meanders, sandbars, side pockets, obstructions and so on.

While the longitudinal dispersion characteristics of a natural channel may not be significant for a continuous pollutant release, the transverse and vertical dispersion coefficients will certainly be important. Confident predictions of these coefficients for every point

BLANK PAGE IN ORIGINAL - PART OF PAGINATION

in the channel is difficult. Some streams may be so irregular that no model can be applied. However in most cases approximate methods may be used. The variety of channel characteristics between rivers and the variation along a reach generally means each channel must be treated individually. Until more capable models are available the emphasis will still be placed on field measurements.

Some individual aspects of natural channels have been investigated with some success. Aris (1959) appears to have been the first to report on the trapping effect which he studied in pipes. The stretched tail of a slug released in an open channel has been attributed to various forms of entrainment (Chatwin 1971). Fischer (1973) likened the tail on a pollutant cloud due to the trapping regions in a river to the tail observed in a smooth laboratory channel due to the viscous sublayer. Subsequent investigators have developed models which incorporate trapping elements for instantaneous pollutant releases. A review of these methods is given by Valentine (1978). The so-called dead zone mechanism, with a slug release, involves the entrainment of contaminant in the dead zone when the contaminant cloud passes, followed by the slow release of material back into the main flow after the cloud has moved downstream. In this study the dead zone mechanism is investigated for a continuous release.

A second major area of investigation is the effect of channel curvature. It is recognised that bends enhance the transverse mixing (Fischer 1969) due to the induced secondary circulation. In a gradual bend centrifugal forces distort the transverse velocity distribution resulting in a deeper flow region on the outside of the bend (in an erodible channel). If there is a sequence of bends in alternating directions the problem is further complicated. The most promising approach to meandering flows is that introduced by Yotsukura and Sayre (1976) who define a cumulative discharge variable to be used in place of transverse distance. This stream tube concept appears to be capable of accounting for changes in river geometry and curvature quite easily. Subsequent experiments have confirmed the applicability of this method (Lau and Krishnappen 1981). While this study is concerned with straight channels, this technique may be a useful tool for an extension to meandering channels.

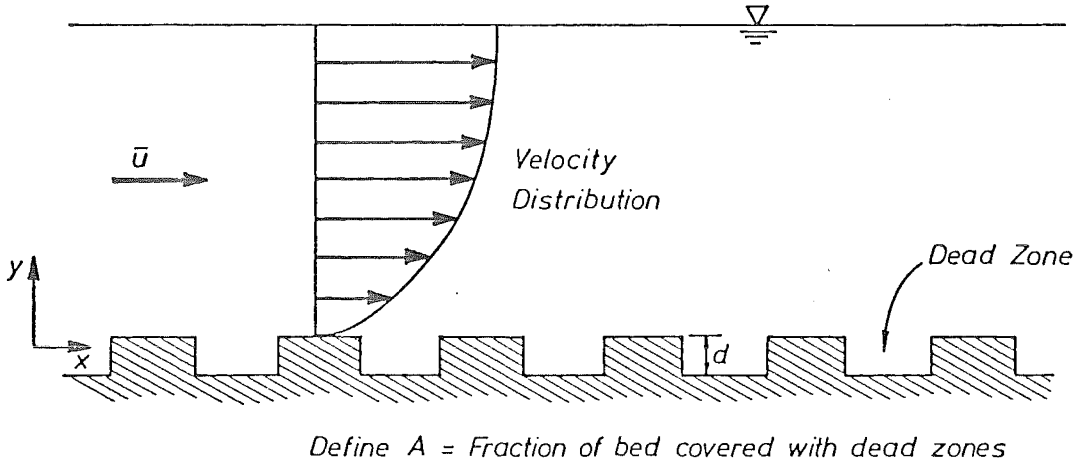

Figure 3.1 : Idealised model including trapping elements (dead zones) with a typical velocity distribution.

CHAPTER III

ANALYTICAL DEVELOPMENT OF A TWO-DIMENSIONAL MODEL FOR DISPERSION

3.1 Summary

This chapter introduces an idealised model for a two-dimensional channel and the equations which the model must satisfy. An algorithm is developed for two-dimensional turbulent shear flow, to obtain the complete downstream concentration distribution. Comparisons are made between this solution and available solutions where the velocity and diffusivity are constant.

3.2 Idealised Model

The model is designed to incorporate as much of the physical characteristics of a natural stream as possible yet still enable a convenient numerical simulation. Figure 3.1 shows the model with a typical velocity distribution. Velocity and diffusivity distributions are arbitrary but must be steady with time.

As depicted, the flow can be seen to pass over a series of cells in the bed, labelled "dead zones". These regions contain water isolated from the main flow which is circulating and continuously exchanging fluid with the region directly above in the main flow. They represent boundary roughnesses and trapped pockets of fluid present in most natural streams. As will be shown later in the chapter the form of the dead zones in the model is not as important as in previous studies (Valentine 1978). It is envisaged that d, the dead zone element depth and A the fraction of the bed covered with dead zones, can be chosen in such a way as to match, as closely as possible, both the channel roughness (via A) and the amount of fluid trapped behind objects (via d). As developed in this chapter there is no option in the model for any variation of either of the above parameters along a reach.

3.3 Flow Equations

The derivation of the conservation of mass equation is well documented and has been outlined in chapter 2. This results in the usual form of the general convective-diffusive equation in two-dimensions for a

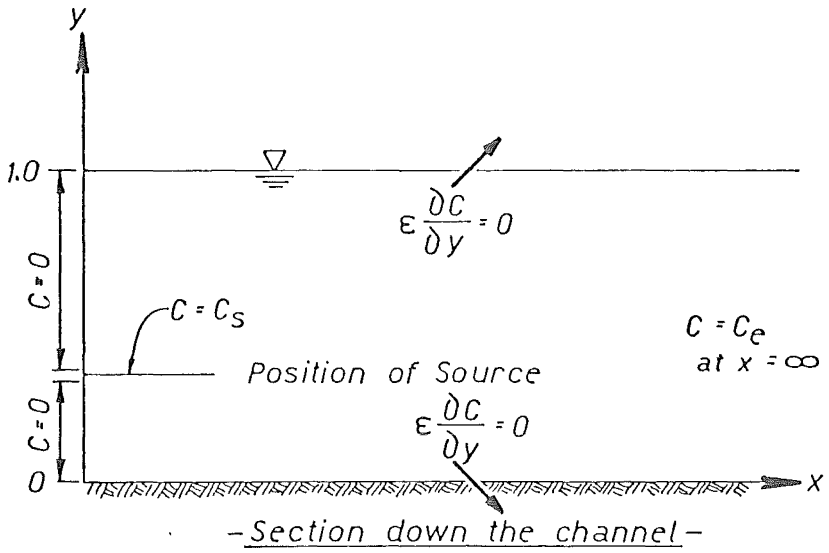

Figure 3.2 : Boundary conditions for a typical flow section.

conservative substance in turbulent open channel flow,

$$\frac{\partial c}{\partial t} + u \frac{\partial c}{\partial x} = \frac{\partial}{\partial x}\left(\varepsilon_x \frac{\partial c}{\partial x}\right) + \frac{\partial}{\partial y}\left(\varepsilon_y \frac{\partial c}{\partial y}\right) \tag{3.1}$$

For a conservative substance there can be no flux of mass across any of the flow boundaries (either the water surface or the wetted perimeter). Mathematically, this is expressed as

$$\varepsilon_y \frac{\partial c}{\partial y} = 0 \tag{3.2}$$

since the y-axis is perpendicular to the boundaries.

If x is defined as zero at the same location as the continuous source, then the upstream and downstream boundary conditions are described by, (figure 3.2),

$$c = 0 \text{ at } x = 0, \begin{cases} 0 \leq y < y_{s\ell} \\ y_{su} < y \leq y_n \end{cases} \tag{3.3}$$

$$c = c_s \text{ at } x = 0, \quad y_{s\ell} \leq y \leq y_{su}$$

$$\text{and } c = c_e \text{ at } x = \infty \tag{3.4}$$

where $y_{s\ell}$ and y_{su} are the lower and upper bounds of the source respectively and y_n is the flow depth.

The concentration when the pollutant has been fully mixed, c_e, is determined by

$$\int_0^{y_n} u\, c_s \, dy = \bar{u}\, c_e \tag{3.5}$$

Thus

$$c_e = \frac{c_s}{\bar{u}} \int_{y_{s\ell}}^{y_{su}} u \, dy \tag{3.6}$$

A point source may also be considered by letting $y_{s\ell}$ tend to y_{su} and replacing the integral in equation 3.5 by a delta function at the source height such that

$$c_e = \frac{u(y_s)}{\bar{u}} c_s \tag{3.5a}$$

BLANK PAGE IN ORIGINAL - PART OF PAGINATION

with $$c = c_s \, \delta(y - y_s) \text{ at } x = 0 \qquad (3.3a)$$

3.4 Dead Zones

When dead zones are present there will be a continual interchange of fluid between the dead zones and the main flow. If it is assumed that the mass transfer of tracer across the interface between the dead zone and the main flow is proportional to the concentration difference across it and the mean velocity $\bar{u}$, the flux per unit length of bed can be written as

$$q = K\bar{u}A \, (c - w) \qquad (3.7)$$

where K is a non-dimensional entrainment coefficient, w is the mean concentration in the eddy and c the mean concentration in the main flow directly above the interface.

Thus for conservation of mass of dispersant between the dead zone and flow zone

$$\frac{\partial}{\partial t} (wAd) = K\bar{u}A \, (c - w) \qquad (3.8)$$

Therefore the equation describing the concentration in the dead zone is

$$\frac{\partial w}{\partial t} = \frac{K\bar{u}}{d} (c - w) \qquad (3.9)$$

Once steady state conditions are reached $\frac{\partial w}{\partial t} = 0$, so there is no net vertical transfer of mass between the main flow and the eddy (i.e. $c = w$).

In physical terms, consider the main flow to be divided into a "bundle" of stream tubes. In any stream tube there will be a downstream transportation of tracer. As one particle moves downstream there will be another from some upstream location moving down to replace it. There will also be an exchange of tracer between stream tubes where a concentration gradient exists. In steady state there will be no change in concentration at any point. Similarly any tracer particle trapped in an eddy in the dead zone will after some time be released into the main flow and will be replaced by another particle from upstream. So even though there is no change in concentration in any eddy there is still a net downstream movement of tracer. It is proposed then, that the dead zones be considered as a further stream tube, which will have the same concentration of pollutant

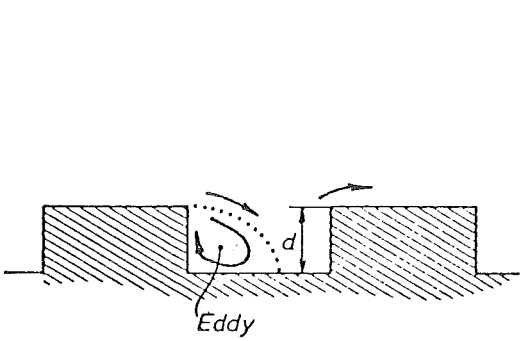

Figure 3.3a : Flow pattern around a dead zone.

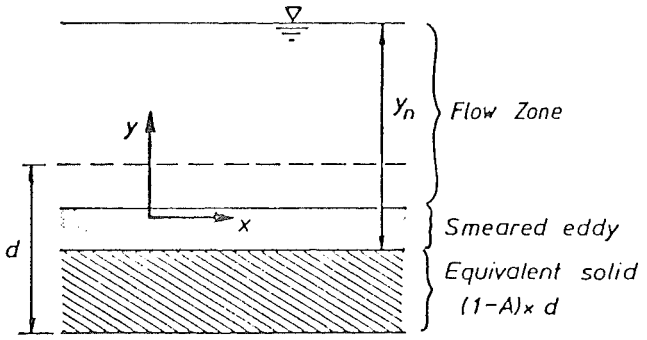

Figure 3.3b : Equivalent "smeared" dead zones. Note the origin is below the lower flow boundary.

as the fluid immediately above the dead zone but will have no net downstream movement of tracer since none of the dead zones are actually connected. The only modification to the mainflow dispersion equation will be an adjustment to the velocity and diffusivity at the bottom following a similar approach to that of Antonia and Wood (1975), who redefined the origin for the velocity profile below the eddy surface. This accounts for the non-zero velocity at the eddy/main flow interface.

The procedure for modifying the bed conditions is illustrated in figures 3.3. The basic flow pattern around the dead zone is illustrated by figure 3.3(a). (As the pitch of the elements is reduced flow will no longer reattach between the elements). With this flow configuration an equivalent model is suggested. This consists of "smearing" each region giving the average conditions (figure 3.3(b)). For any given bed form there are two parameters required to define the equivalent bed conditions. The equivalent solid area is determined from the element size and spacing, such that

$$\text{Equivalent Solid Area} = (1 - A)d \tag{3.10}$$

with A the fraction of bed covered with dead zones and d the depth of the trapping regions.

Two further parameters are required to define the equivalent eddy geometry. One parameter is needed to describe the fraction of the dead zone occupied by the eddy and another to define the location of the origin (which will correspond to the location of $u = 0$). The mainflow equations are now applied to the entire region above the smeared eddy, as depicted in Figure 3.3(b).

It is now assumed that $\varepsilon \frac{\partial c}{\partial y} = 0$ at the top of the smeared eddy ($y \neq 0$) and the region below this behaves as a storage element only, retaining an amount of tracer of identical concentrations to that in the bottom flow element. This is discussed further in the Numerical Scheme.

3.5 Definition of Dimensionless Variables

Dimensionless variables introduced following Valentine (1978) are,

$$\xi = \frac{x}{y_n}, \quad \eta = \frac{y}{y_n}, \quad \tau = \frac{\bar{u}t}{y_n}$$
$$\frac{u}{\bar{u}} = \chi(\eta), \quad \varepsilon = D[\psi(\eta)] \tag{3.11}$$

BLANK PAGE IN ORIGINAL - PART OF PAGINATION

where $$D = u_*^2 \, y_\eta / \bar{u} \text{ and } \psi(\eta) = (1 - \eta)/\frac{\partial \chi}{\partial \eta} \tag{3.12}$$

Substituting these into equation 3.2 gives

$$\frac{8}{f} \frac{\partial c}{\partial \tau} + \frac{8}{f} \chi(\eta) \frac{\partial c}{\partial \xi} = \psi(\eta) \frac{\partial^2 c}{\partial \xi^2} + \frac{\partial}{\partial \eta} \psi(\eta) \frac{\partial c}{\partial \eta} \tag{3.13}$$

since $$\frac{8}{f} = \left[\frac{\bar{u}}{u_*}\right]^2 \tag{3.14}$$

The boundary conditions become,

$$\psi(\eta) \frac{\partial c}{\partial \eta} = 0 \text{ for } \eta = E, 1 \tag{3.15}$$

(Note that for no dead zones E = 0).

It is also convenient to express all concentrations in terms of c_e by defining,

$$c_* = c/c_e \tag{3.16}$$

This does not alter equation 3.13 or the boundary conditions.

3.6 Analytical Solutions

3.6.1 Series Solution to the Diffusion Equation Without Dead-Zones

The simplest solution to equation 3.13 is obtained by assuming

$$\chi(\eta) = 1, \; \psi(\eta) = \text{constant} = \frac{\kappa}{6} \sqrt{\frac{8}{f}} \tag{3.17}$$

and that the longitudinal concentration gradients are negligible. The constant diffusivity corresponds to the mean diffusivity reported for vertical dispersion (see section 4.2.2). The equation now reduces, for steady source conditions, to

$$\beta \frac{\partial c}{\partial \xi} = \frac{\partial^2 c}{\partial \eta^2} \tag{3.18}$$

where $\beta = \frac{6}{\kappa} \sqrt{\frac{8}{f}}$. ($\kappa$ is von Karman's constant). Standard solution techniques are available for this equation, the general form is,

$$c(\xi, \eta) = a_0 + \sum_{m=1}^{\infty} a_m \, e^{-\frac{1}{\beta} (m\pi)^2 \xi} \cos(m\pi\xi) \tag{3.19}$$

The coefficients, a_m, in 3.19 are solved for using the upstream boundary

BLANK PAGE IN ORIGINAL - PART OF PAGINATION

conditions, (non-dimensional form of equations 3.3), resulting in (see Appendix B),

$$c(\xi, \eta) = c_s (\eta_{su} - \eta_{s\ell}) + \frac{4c_s}{\pi} \sum_{n=1}^{\infty} \frac{\sin[n\pi(\eta_{su} - \eta_{s\ell})/2] \cos[n\pi(\eta_{su} + \eta_{s\ell})/2] \cos(n\pi\eta)}{n} \times \exp\left[-\frac{(\eta\pi)^2 \xi}{\beta}\right] \quad (3.20)$$

This equation was used as a base to test all numerical schemes before they were applied to non-uniform flow conditions.

It should be noted that equation 3.19 may be written as

$$c(\xi) = \sum_{n=0}^{n=\infty} A_n \exp(\alpha_n \xi) \quad (3.21)$$

and that the coefficient α_n may be written as

$$\alpha_n = \alpha_0 (n+1)^2, \text{ for } n = 1, 2, \ldots \quad (3.22)$$

3.6.2 Bessel's Solution to the Diffusion Equation

As outlined in Appendix B an approximate solution may be obtained using a power-law velocity distribution and an assumed form for the diffusivity. That is, it is assumed that $\varepsilon(\eta)$ varies as

$$\varepsilon(\eta) = \frac{u_*^2 y_n}{\frac{\partial u}{\partial \eta}} \quad (3.23)$$

rather than the form derived from the Reynold s analogy (the equivalence of mass and momentum transfer),

$$\varepsilon(\eta) = \frac{u_*^2 y_n (1 - \eta)}{\frac{\partial u}{\partial \eta}} \quad (3.24)$$

The solution to equation 3.13 for these flow conditions with a point source at η_s is,

$$c(\xi, \eta) \simeq 1 + \sum_{n=2}^{\infty} \exp\left[-\left(j'_{n,0}\right)^2 \frac{u_*^2 \xi}{4\alpha \bar{u}^{-2}}\right] J_0\left(j'_{n,0}\, \eta^{\frac{1}{2}+\alpha}\right) J_0\left(j'_{n,0}\, \eta_s^{\frac{1}{2}+\alpha}\right) / J_0\left(j'_{n,0}\right)^2 \quad (3.25)$$

BLANK PAGE IN ORIGINAL - PART OF PAGINATION

where $J_0(z)$ is a Bessel function of the first kind of order 0 and $j'_{n,0}$ is the nth zero of $J_0'(z)$. Once again for a constant depth in the flow the equation reduces to equation 3.21,

$$c(\xi) = \sum_{n=1}^{n=\infty} A_n \exp(\alpha_n \xi) \tag{3.26}$$

Now the variation of α_n is given by (note $j'_{1,0} = 0$)

$$\alpha_n = \left(\frac{j'_{n+2,0}}{j'_{2,0}}\right)^2 \alpha_0, \quad n = 1, 2, \ldots. \tag{3.27}$$

The significance of this relationship is discussed in the following chapter.

3.7 Method of Solution Without Uniform Flow Assumptions

3.7.1 Aris Moment Transform

Of the available analytical approaches to handle the convective-diffusive transport equation the method of Aris (1956) moment transforms appears the most promising. The application of the moment transforms reduces the problem from two-dimensions to essentially one-dimension. However, instead of a complete solution, statistical moment parameters which describe the solution are obtained, by integrating in the x-direction the moment of the concentration. Moments are taken about a fixed origin at the same location as the source.

For a sudden release of a slug of pollutant Aris multiplied equation 3.13 by ξ^p and integrated from $\xi = -\infty$ to ∞, obtaining a set of equations from which moments of the solution could be obtained for all values of p. That is, the pth moment of concentration is described by,

$$c_p = \int_0^{\infty} c\ \xi^p\ d\xi \tag{3.28}$$

It is apparent that with the problem set up in the present form this method will lead to infinite moments, as $c \to c_e$ at $\xi = \infty$.

The method proposed here focuses on the introduction of a new variable, c_{d*} the concentration deficit which is defined by

$$c_{d*} = c_* - 1 \tag{3.29}$$

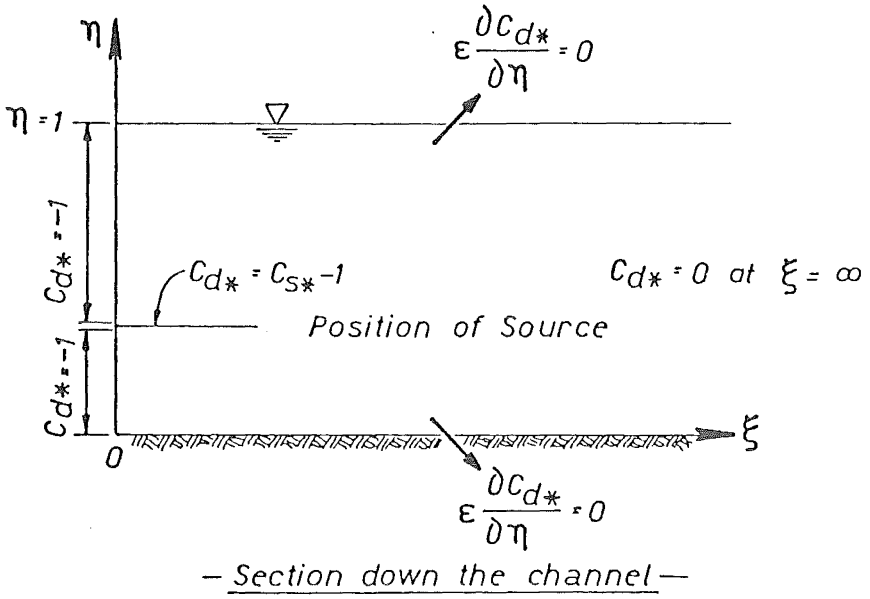

Figure 3.4 : Boundary conditions for deficit concentration.

Now equation 3.13 remains unchanged,

$$\frac{8}{f}\frac{\partial c_{d*}}{\partial \tau} + \frac{8}{f}\chi(\eta)\frac{\partial c_{d*}}{\partial \xi} = \psi(\eta)\frac{\partial^2 c_{d*}}{\partial \xi^2} + \frac{\partial}{\partial \eta}\psi(\eta)\frac{\partial c_{d*}}{\partial \eta} \qquad (3.30)$$

The boundary conditions at $\xi = 0$ and $\xi = \infty$ nevertheless, change as shown in figure 3.4. They become,

$$\begin{aligned} c_{d*} &= -1 \text{ at } \xi = 0 \begin{cases} 0 \leq \eta < \eta_{s\ell} \\ \eta_{su} < \eta \leq 1 \end{cases} \\ c_{d*} &= c_{s*} - 1 \text{ at } \xi = 0,\ \eta_{s\ell} \leq \eta \leq \eta_{su} \\ &\text{and } c_{d*} = 0 \text{ at } \xi = \infty \end{aligned} \qquad (3.31)$$

This enables finite moments to be computed. Indeed defining

$$c_{dp} = \int_0^\infty c_{d*}\,\xi^p\,d\xi \qquad (3.32)$$

and multiplying equation 3.30 by ξ^p and integrating (see Appendix A) we obtain for the steady state situation $\left(\frac{\partial c_{d*}}{\partial \tau} = 0\right)$ with,

$$p = 0, \qquad \frac{\partial}{\partial \eta}\left[\psi(\eta)\frac{\partial c_{d0}}{\partial \eta}\right] = -\frac{8}{f}\chi(\eta)\,c_{d*}\Big|_{\xi=0} + \psi(\eta)\frac{\partial c_{d*}}{\partial \xi}\Big|_{\xi=0} \qquad (3.33)$$

$$p = 1, \qquad \frac{\partial}{\partial \eta}\left[\psi(\eta)\frac{\partial c_{d1}}{\partial \eta}\right] = -\frac{8}{f}\chi(\eta)\,c_{d0} - \psi(\eta)\,c_{d*}\Big|_{\xi=0} \qquad (3.34)$$

$$p = 2,\ldots,\infty \qquad \frac{\partial}{\partial \eta}\left[\psi(\eta)\frac{\partial c_{dp}}{\partial \eta}\right] = -\frac{8}{f}\chi(\eta)\,p\,c_{d(p-1)} - \psi(\eta)\,p(p-1)\,c_{d(p-2)} \qquad (3.35)$$

Furthermore, one can define $Q_p(\eta)$ by,

$$Q_p(\eta) = \psi(\eta)\frac{\partial c_{dp}}{\partial \eta} \qquad (3.36)$$

which is the flux of mass through the line η = constant from $\xi = 0$ to $\xi = \infty$ (figure 3.5). Thus,

$$Q_0(\eta) = \int_0^\eta \left[-\frac{8}{f}\chi(\eta)\,c_{d*}\Big|_{\xi=0} + \psi(\eta)\frac{\partial c_{d*}}{\partial \xi}\Big|_{\xi=0}\right] d\eta + \text{constant} \qquad (3.37)$$

Since there is no flux of mass through the flow boundaries, at

Note: The term $\frac{\partial c_{d^*}}{\partial \xi}$ is derived from the longitudinal term in equation 3.30, which is shown in the following chapter to have negligible effect on dispersion from a continuous source, consequently this term may be neglected completely in the derivation. The statement $\left.\frac{\partial c_{d^*}}{\partial \xi}\right|_{\xi=0} = 0$ is not mathematically correct due to the behaviour at the source boundaries, however it appears physically justifiable over the remainder of the flow field.

$\eta = 0$, and $\eta = 1$,

$$\psi(\eta) \frac{\partial c_{dp}}{\partial \eta} = Q_p(0) = Q_p(1) = 0 \qquad (3.38)$$

Furthermore, if we are considering a simple source (point source or distributed source) then the term $\frac{\partial c_{d*}}{\partial \xi}\Big|_{\xi=0}$ in equation 3.37 will be zero at all points on $\xi = 0$ except the boundaries of the source, and therefore it may be neglected.

Once the above condition is imposed on 3.37, then,

$$Q_0(\eta) = \int_0^{\eta} - \frac{8}{f} \chi(\eta)\, c_{d*}\Big|_{\xi=0} d\eta + \text{constant} \qquad (3.39)$$

is defined for all η. The right hand side is the inflow over the section at $\xi = 0$, from $\eta = 0$ to $\eta = \eta$.

The constant of integration is determined from the lower boundary condition, $Q_0(0) = 0$, and must be zero. The boundary condition at $Q_0(1) = 0$ is used to define the source strength (equation 3.6) such that,

$$\int_0^1 \chi(\eta)\, c_{d*}\Big|_{\xi=0} d\eta = 0 \qquad (3.40)$$

Equation 3.40 is the non-dimensional concentration deficit form of equation 3.6.

Now, the zeroeth moment, as defined by equation 3.36 becomes

$$c_{d0} = \int_0^{\eta} \frac{Q_0(\eta)}{\psi(\eta)} d\eta + \text{constant} \qquad (3.41)$$

which will have a constraint placed on it by equations 3.34 and 3.38,

$$Q_1(1) = 0 = - \int_0^1 \left(\frac{8}{f} \chi(\eta)\, c_{d0} + \psi(\eta)\, c_{d*}\Big|_{\xi=0} \right) d\eta \qquad (3.42)$$

Equation 3.34 is required to determine the constant of integration for equation 3.41, and is solved using the substitution $c_{d0} = c'_{d0} +$ constant. This solution procedure is demonstrated in Appendix B where analytical moment solutions are obtained.

BLANK PAGE IN ORIGINAL - PART OF PAGINATION

Using values obtained for c_{d0}, a similar procedure can be followed for c_{d1}, with

$$Q_1(\eta) = \int_0^{\eta} \left[-\frac{8}{f} \chi(\eta)\, c_{d0} - \psi(\eta)\, c_{d*}\Big|_{\xi=0} \right] d\eta \qquad (3.43)$$

Clearly now each moment c_{dp} is defined entirely in terms of boundary conditions or lower moments, so equation 3.35 may be used to solve for any c_{dp}. The only limitation is the accuracy of the numerical scheme, which for numerical integration (a "smoothing" process) is of the order of $h^2/12$, where h = spacing of nodes in the integration scheme. It remains to obtain from these moments and the boundary conditions the complete distribution of c_{d*}. Profiles of c_{d*} versus ξ found for various values of η = constant are used to construct a picture of the complete concentration distribution. Individual profiles are fitted in terms of far field solutions and near field solutions.

3.7.2 Far Field Solution

Well downstream from the source longitudinal concentration gradients become very small. Hence, for a steady release equation 3.30 becomes

$$\frac{8}{f} \chi(\eta) \frac{\partial c_{d*}}{\partial \xi} = \frac{\partial}{\partial \eta} \psi(\eta) \frac{\partial c_{d*}}{\partial \eta} \qquad (3.44)$$

As both sides of this equation can be written in terms of a single variable, a separated solution for c_{d*} is appropriate, i.e.

$$c_{d*} = F(\xi)\, G(\eta) \qquad (3.45)$$

Thus equation 3.44 can be written as

$$\frac{F'(\xi)}{F(\xi)} = \frac{1}{\frac{8}{f} \chi(\eta)\, G(\eta)} \frac{\partial}{\partial \eta} [\psi(\eta)\, G'(\eta)] \qquad (3.46)$$

Since each side of equation 3.46 involves functions of separate independent variables both sides may be equated to a constant (say $-\alpha_n$, where α_n are positive). For a constant η, the dependency of c_{d*} on ξ will be described by,

$$F'(\xi) + \alpha_n F(\xi) = 0 \qquad (3.47)$$

The general solution of 3.47 is,

BLANK PAGE IN ORIGINAL - PART OF PAGINATION

$$F(\xi) = \sum_{n=0}^{\infty} A_n \, e^{-\alpha_n \xi} \tag{3.48}$$

where A_n are constant coefficients (A_n are not independent of η). This satisfies the conditions that c_{d*} is zero at $\xi = \infty$. For a constant η, $F(\xi)$ will be equivalent to $c_{d*}(\xi)$, so moments calculated from the equation 3.48 may be compared to numerically computed moments. The moments of concentration yielded by 3.48 are,

$$c_{dp} = \sum_{n=0}^{\infty} \frac{A_n \, p!}{(\alpha_n)^{p+1}} \tag{3.49}$$

Now
$$\frac{c_{dp+1}}{c_{dp}} = (p+1) \left[\frac{\dfrac{A_0}{\alpha_0^{p+2}} + \dfrac{A_1}{\alpha_1^{p+2}} + \cdots}{\dfrac{A_0}{\alpha_0^{p+1}} + \dfrac{A_1}{\alpha_0^{p+1}} + \cdots} \right] \tag{3.50}$$

If $\alpha_0 < \alpha_1 < \alpha_2 \ldots$ and p is large, say p = L, such that $\alpha_0^{L+1} \ll \alpha_1^{L+1}$ and $\alpha_0^{L+2} \ll \alpha_1^{L+2}$, then equation 3.50 will reduce to,

$$\alpha_0 = \frac{c_{dL}}{c_{dL+1}} (L+1) \tag{3.51}$$

Substituting this value of α_0 back into the expression 3.49 for c_{dp} with the same assumption yields,

$$A_0 = \frac{\alpha_0^{L+1} \, c_{dL}}{L!} = \frac{c_{dL}^{L+2} \, (L+1)^{L+1}}{L! \, c_{dL+1}^{L+1}} \tag{3.52}$$

Thus the term that dominates at large ξ is

$$c_{d*} = \frac{[c_{dL}]^{L+2} \, (L+1)^{L+1}}{L! \, [c_{dL+1}]^{L+1}} \cdot \exp\left[\frac{-c_{dL}(L+1)\,\xi}{c_{dL+1}} \right] \tag{3.53}$$

3.7.3 Near Field Solution

A solution near to the source is obtained numerically by assuming the solution form is that of equation 3.48. For the uniform flow conditions, the variation of α_n with n is known to be, (Appendix B)

$$\alpha_n = (n+1)^2 \, \alpha_0 \quad \text{for } n = 1, \ldots \infty \tag{3.54}$$

Note: Equation 3.38 is used as a smoothing device only. It is used to force the concentration profile to behave correctly for small ξ, where the profile will be perpendicular to the η-axis. (This is observed in profiles produced by analytical solutions.)

This may also be used as a first approximation for non-uniform flow conditions, however, a better solution is obtained if the Bessels type variation is used. As shown in section 3.6.2, a power-law velocity and linear diffusivity (correct close to the bed) yields a variation in α_n described by

$$\alpha_n = \left(\frac{j'_{n,0}}{j'_{2,0}}\right)^2 \alpha_n \quad , n = 2,3,\ldots \tag{3.55}$$

Although the assumption made to obtain this solution is only valid near the bed, where $\eta << 1$ and the term $(1 - \eta)$ is close to 1, it is shown (and discussed) in chapter 4 that there is a significant improvement in the fitted profile over the entire depth.

Once the variation in α_n is chosen equation 3.48 may be multiplied by ξ^p and integrated from $\xi = 0$ and $\xi = \infty$ to obtain moments for any height in the flow (η = constant);

$$c_{dp} = \sum_{n=0}^{\infty} \frac{A_n\, p!}{(\alpha_n)^{p+1}} \tag{3.56}$$

In addition to these equations, the boundary condition at $\xi = 0$ is known, thus

$$c_{d*}\Big|_{\xi=0} = \sum_{n=0}^{\infty} A_n \tag{3.57}$$

and away from the source $\left.\frac{\partial c_{d*}}{\partial \xi}\right|_{\xi=0} = 0$, as do all higher derivatives, which yield further equations:

$$\left.\frac{\partial^m c_{d*}}{\partial \xi^m}\right|_{\xi=0} = \sum_{n=0}^{\infty} (\alpha_n)^m A_n = 0 \tag{3.58}$$

It remains then to determine a criterion which will detail the number of moment equations 3.56 and the number of derivative equations 3.58 to combine with the boundary condition 3.57. Once this is decided, a matrix can be generated and solved for the coefficients A_n. The number of coefficients will define the number of terms used in equation 3.48.

The basis for the equations used in the matrix generation is the distance, at $\xi = 0$, from the source. If it is known how c_{d*} is likely to

BLANK PAGE IN ORIGINAL - PART OF PAGINATION

vary with ξ at any particular vertical distance from the source then this will be the foundation for the matrix generation. For instance, as the source is approached (i.e. $\eta \to \eta_s$) the effect of the source will be noticed sooner moving along η = constant (with increasing ξ) and the peak concentration will increase. Conversely, well away from the source (η away from η_s) the profile will be slow changing with ξ and will peak at the equilibrium concentration a long way downstream from the source. In the regions where there are rapid changes in c_{d*} (with ξ), it is apparent that more moments will be required to describe c_{d*} and away from the source more derivatives are needed. Although this scheme is limited by the numerical stability when large moments are used, very accurate solutions are obtained when α_n is known and higher terms in the exponential expansion are negligible (i.e. as $\xi \to \infty$). For small ξ, higher terms become important and the solution may depart from predicted solutions. This will be seen in the following chapter when the numerical scheme is described and results outlined.

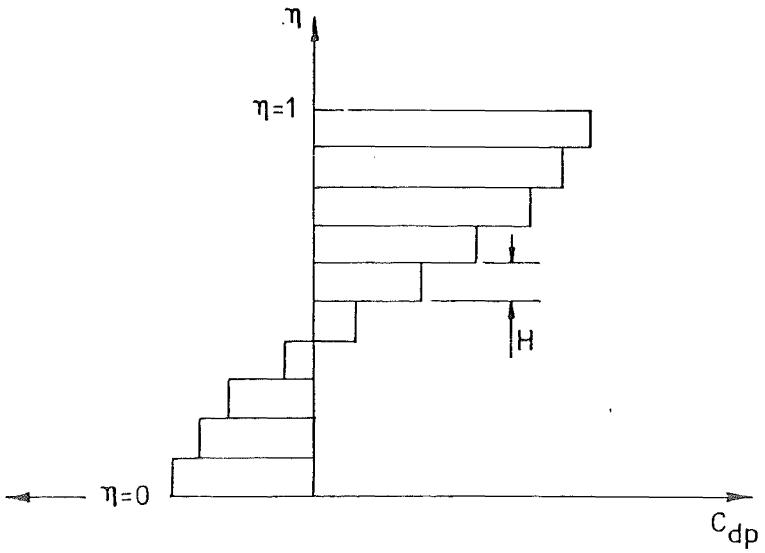

Figure 4.1 : Typical distribution of c_{dp} for a flow section divided into 10 elements (normally the computer solution would use 1000 elements).

CHAPTER IV

DEVELOPMENT OF THE NUMERICAL SOLUTION FOR TWO DIMENSIONS AND RESULTS

4.1 Summary

A numerical scheme is developed to solve the equations obtained in the previous chapter. The scheme provides exact moments of the concentration distribution and, via fitting techniques, produces concentration plots. These are compared with known solutions.

4.2 Numerical Solutions

The application of Aris moment transforms reduces the diffusion equation from two-dimensions to a one-dimensional partial differential equation for c_{dp}. Of the numerical solution techniques available for such equations (equations 3.33 - 3.35) numerical integration was chosen (via equations 3.37 and 3.41). The methods of numerical integration used require discrete valued functions at equally spaced intervals. To achieve this the flow region was divided up into elements, which may be considered as extending from $\xi = 0$ to $\xi = \infty$, of thickness H. The trapezoidal rule was employed when information was required in each element (for subsequent integrations) and Simpson's rule applied for integrations over the entire flow region (to obtain constants of previous integrations). Both of these methods are stable and as shown later in this chapter they are sufficiently accurate for this application. A typical resultant distribution of c_{dp} is shown in figure 4.1 for ten elements.

4.2.1 Velocity Distributions

The velocity used for each computer run was determined by the data input into the program. Typically this took the form of a logarithmic, power or a uniform velocity distribution function, although a parabolic pofile was also available. These are defined by the functions:

(i) von Karman-Prandtl velocity profile,

$$u(\eta) = \bar{u} + \frac{u_*}{\kappa} (\ln \eta + 1)$$

(ii) Power law velocity profile,

BLANK PAGE IN ORIGINAL - PART OF PAGINATION

$$u(\eta) = \bar{u}(1 + \alpha)\eta^{\alpha} \quad \left[\text{generally } \alpha = \frac{1}{7}\right]$$

(iii) Parabolic velocity profile,

$$u(\eta) = \bar{u} + \frac{u_*}{\kappa}(-3\eta^2 + 6\eta - 2) \tag{4.1}$$

(iv) Uniform velocity profile

$$u(\eta) = \bar{u}$$

The velocity in any element in the numerical scheme is defined as the average value over the depth increment,

$$u(I) = \frac{1}{H}\int_{IH}^{(I+1)H} u(\eta)\, d\eta \tag{4.2}$$

where u(I) is the velocity in the Ith element and $u(\eta)$ is any of the above velocity functions.

4.2.2 Diffusivity Distributions

The eddy diffusivity is involved in two terms in the moment diffusion equations 3.33 - 3.35. The longitudinal diffusion term is evaluated as the mean diffusivity over an element; the vertical diffusion term used in the integration scheme is computed as the integral of the diffusivity or the numerical integral of the product of a moment and the diffusivity (for all cases when p is greater than one).

It is a good approximation (Elder 1959) that in a boundary layer flow the transfer of momentum and mass are equivalent (Reynold s analogy),

$$\varepsilon_y \equiv -\frac{\overline{v'c'}}{\frac{\partial c}{\partial y}} \simeq -\frac{\overline{v'u'}}{\frac{\partial u}{\partial y}} \tag{4.3}$$

The flux of momentum through a surface is the shear stress at the surface divided by the fluid density, τ/ρ. It is shown in elementary texts (Henderson 1966) that ~~that~~ the shear stress, τ, varies linearly with depth,

$$\tau = \tau_0(1 - \eta) \tag{4.4}$$

where $\tau_0 = u_*^2\rho$ (see figure 2.3). Thus equation 4.3 becomes

$$\varepsilon_y \equiv \frac{u_*^2 y_n (1 - \eta)}{\frac{\partial u}{\partial \eta}} \tag{4.5}$$

BLANK PAGE IN ORIGINAL - PART OF PAGINATION

This equation has been verified in laboratory flumes (Sayre 1973). Using this relationship, $\varepsilon(\eta)$ is obtained for each velocity profile,

(i) From the von Karman-Prandtl velocity,

$$\varepsilon(\eta) = \kappa u_* y_n \eta(1 - \eta)$$

(ii) From the power law velocity,

$$\varepsilon(\eta) = \frac{u_*^2 y_n (1 - \eta)}{\bar{u}(1 + \alpha)\alpha \eta^{\alpha-1}} \tag{4.6}$$

(iii) From the parabolic velocity,

$$\varepsilon(\eta) = \frac{\kappa u_* y_n}{6}$$

It should be noted that equation 4.5 does not enable a diffusivity distribution to be obtained for a uniform velocity. It is possible however to obtain a depth averaged value of ε_y from equations 4.6 by integrating each distribution from $\eta = 0$ to $\eta = 1$. Experiments have shown that for many practical problems the mean diffusivity is given by (Fischer 1973),

$$D_y = \frac{\kappa}{6} u_* y_n \tag{4.7}$$

This mean diffusivity is used with the uniform velocity.

For non-uniform velocities, the integration of equations 4.6 yields equation 4.7 for both the von Karman-Prandtl and parabolic velocities. For consistency, the remaining diffusivity distribution derived from the power law velocity profile is multiplied by a constant such that the mean diffusivity is given by equation 4.7.

The average diffusivity over an element is then defined by,

$$\varepsilon(I) = \frac{1}{H} \int_{IH}^{(I+1)H} \varepsilon(\eta)\, d\eta \tag{4.8}$$

For vertical diffusivity, the integral from $y = 0$ is used when $p = 1$,

$$\varepsilon_{integral}(I) = \int_{0}^{IH} \varepsilon(\eta)\, d\eta \tag{4.9}$$

BLANK PAGE IN ORIGINAL - PART OF PAGINATION

and a numerical integration to calculate $\int_0^\eta c_{dp}\, \varepsilon(\eta)\, d\eta$ when $p > 1$.

4.2.3 The Numerical Scheme

The model for the numerical solution may be split into three distinct sections, corresponding to the three stages of the solution procedure. Step one is the evaluation of the moments by numerical integration. Step two is to find a curve of best fit for the calculated moments, followed by the final plotting step. The first two steps are discussed here.

4.2.3.1 Evaluation of Moments

To obtain each set of moments (that is, for each value of p) three numerical integrations are performed. As there were no apparant advantages with higher order integration techniques, numerical integrations were trapezoidal or Simpson's Rule type schemes. Sufficient accuracy was obtained by dividing the flow into 1000 elements. On the University of Canterbury's Burroughs B6900 computer for each moment calculated (using 1000 elements) there was approximately 1 second of computing time. Typically, the procedure for calculating any moment initially involves the calculation, via numerical integration, of two arrays of terms for $Q_p(I)$, where $Q_p(I)$ is the flux of pth moment into the Ith element. These two arrays account for the two terms on the right hand side of the equation for $Q_p(I)$ (from equation 3.35),

$$Q_p(\eta) = \int_0^\eta \left[-\frac{8}{f}\chi(\eta)\, pC_{dp-1} - \psi(\eta)\, p(p-1)\, c_{dp-2} \right] d\eta \qquad (4.10)$$

It should be recalled that equation 4.10 is applicable for $p \geq 2$. For lower moments the terms in the equation for the flux may be analytically integrated, e.g.

$$Q_0(\eta) = \int_0^\eta -\frac{8}{f}\chi(\eta)\, c_{d*}\Big|_{\xi=0} d\eta \qquad (4.11)$$

which is a known piecewise function of η.

A second numerical integration is applied to the flux to obtain moments as described by a similar equation to equation 3.41,

$$c_{dp} = \int_0^\eta \frac{Q_p(\eta)}{\psi(\eta)}\, d\eta + \text{constant} \qquad (4.12)$$

BLANK PAGE IN ORIGINAL - PART OF PAGINATION

This integration has the form,

$$c_{dp}(I) = c_{dp}(I - 1) + \frac{H}{2} (Q(I.H)/\psi(I) + Q((I + 1).H)/\psi(I + 1) \quad (4.13)$$

The final integration required determines the constant of equation 4.12. The boundary condition at $\eta = 1$ must be satisfied by c_{dp}, i.e. equation 4.10.

$$Q_p(1) = 0 = \int_0^1 \left\{ \frac{8}{f} \chi(\eta) p \, c_{p-1} - \psi(\eta) \, p(p - 1) \, c_{dp-2} \right\} d\eta \quad (4.10a)$$

Thus the constant of integration for c_{dp} is determined from the zero flux condition of Q_{p+1} at $\eta = 1$.

If dead zones are present, then from the appropriate input parameters (described in section 3.4), the average ("smeared") properties of the dead zones are determined. This will produce a parameter YST which is the shift of the velocity "zero" from the bottom of the flow zone into the smeared eddy. Everything below the flow zone is ignored in the calculation of moments. It is assumed that the concentration in the eddy region is identical to that directly above in the flow zone. This enables the interface between the flow zone and the smeared eddy to be treated as a solid boundary.

4.2.3.2 Fitting A Concentration Profile

When sufficient moments have been obtained, the fitting procedure described in chapter 3 may be applied. Coefficients for equation 3.48,

$$c_{d*} = A_n \, e^{-\alpha_n \xi} \quad (4.14)$$

are found by solving a matrix containing equations 3.56 - 3.58, for the moments, derivatives and the boundary condition at $\xi = 0$. The matrix solution technique used is Gauss-Siedel.

4.2.4 Program Requirements and Capabilities

The computer program discussed in this chapter is given in Appendix D. This program is designed to be self-supporting and only the major input requirements will be mentioned here.

Velocity and diffusivity distributions are built into the program for the analytical profiles given in sections 4.2.1 and 4.2.2. The choice of profiles to be used is determined by the value given to various

BLANK PAGE IN ORIGINAL - PART OF PAGINATION

input parameters. For this two-dimensional solution the properties of the channel to be examined are completely described by the parameter MU, where $MU = \frac{f}{8}$, and by the channel bottom conditions if dead zones are present. For the dead zone case the input required is the dead zone geometry variables, A(AREA), d(DZO), PTZ and E. PTZ is the fraction of the dead zone occupied by the eddy and E is the depth into the dead zone at which u = 0. In the corresponding laboratory experiments A and d are directly measurable from the channel properties. PTZ is estimated from observations of dye movements in the dead zones. E is based on the work of Antonia and Wood (1975) in which the shift of origin into an eddy is given as E = 0.25 for the type of roughness used in these experiments (refer to section 3.4).

The value of the von Karman turbulence coefficient, κ, is considered a variable (AK) by the program and was chosen to correspond to measured velocity profiles. This gave a range of κ from 0.33 to 0.37, with the average of κ = 0.35 being used in most cases.

For convenience the equilibrium concentration was chosen to be 1. Consequently solutions obtained will be in the form of a non-dimensional concentration.

The computer program is designed to run with only non-dimensional variables (by setting YNN = 1.0). However, it was more convenient for modelling the experiments described in subsequent chapters to use real dimensions for probe heights, flow depths (YNN) and bed form size. This enabled physical measurements to be used as input which were non-dimensionalised within the program.

Output from the computer program may include the moments calculated, the matrix generated to solve for coefficients in the exponential series and the coefficients produced from the matrix, if the variables MOMUSE, DUMPM and COEFF are set not equal to zero. The important output, however, is the concentration profiles produced by the program. The way in which this output is presented depends on the method used to portray the individual concentration profiles (each for a given η). This may be as a longitudinal section at a given height (η = constant), a complete concentration contour diagram, or one of various three-dimensional plots available. As a contour plot portrays more information this is the most common output form for the solution.

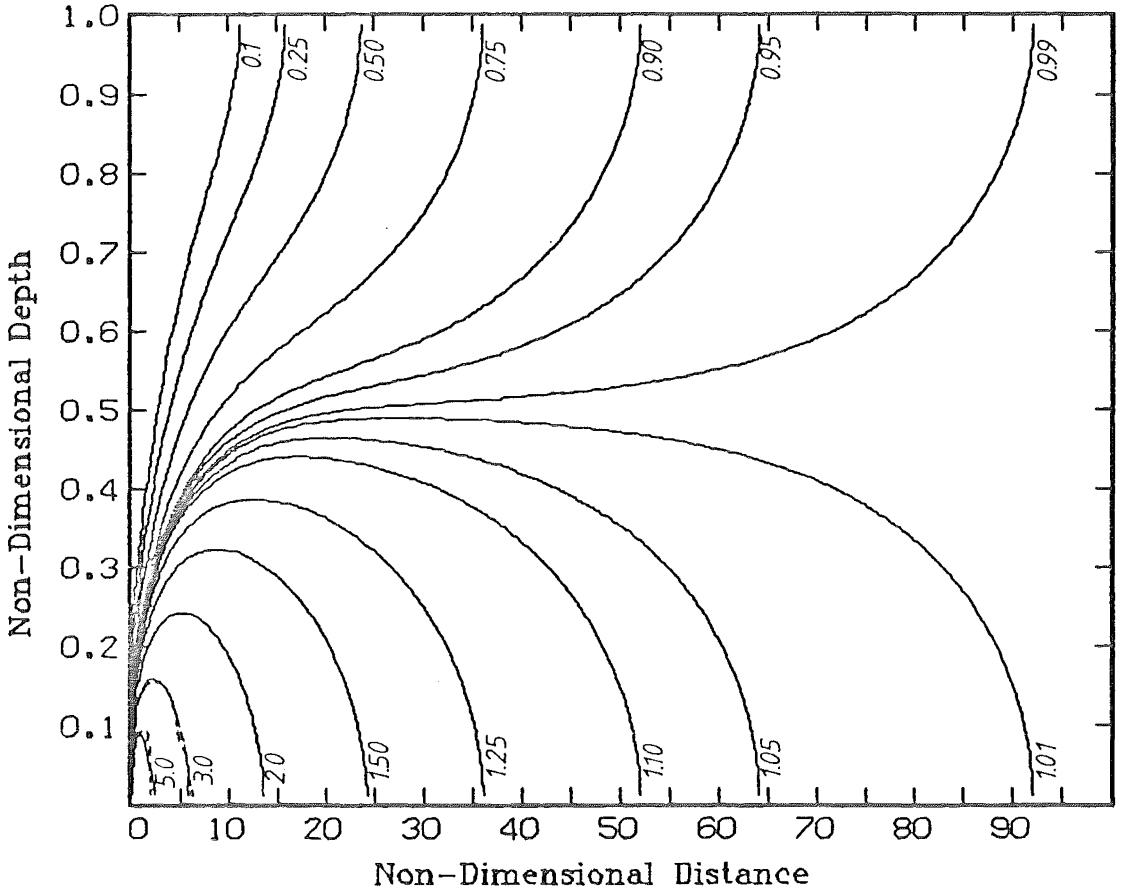

—— Correct (Series) Solution, --- Moment Solution

Figure 4.2 : Uniform Velocity With Source At 0.003 (f=.08)

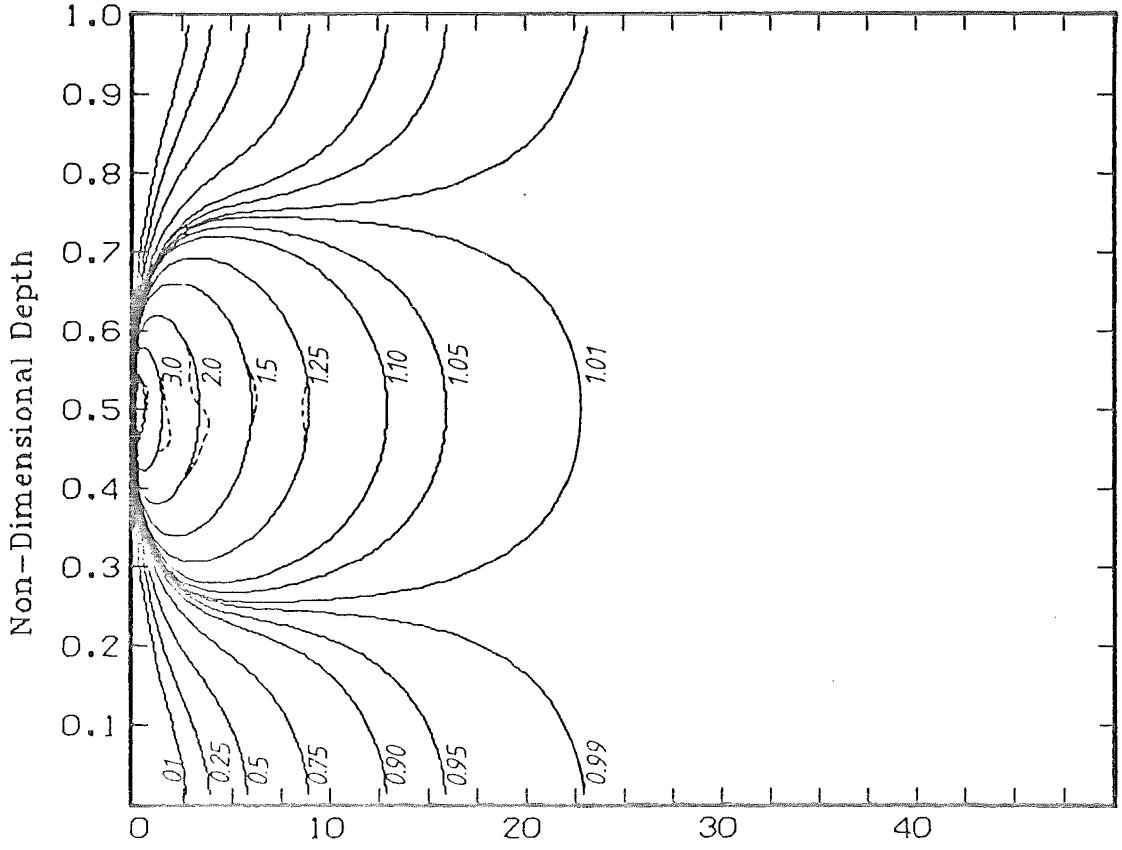

—— Correct (Series) Solution, --- Moment Solution

Figure 4.3 : Uniform Velocity With Source At 0.5 (f=.08)

A typical plot of concentration contours would be produced by a package contouring routine using profiles fitted at 40 evenly spaced heights with 180 points given on each profile. That is, the contouring routine input was a 40 by 180 array of "spot" concentrations. The entire procedure of computing moments, fitting profiles and producing such a contour plot required approximately 90 seconds of process time on the Burroughts B6900.

4.3 Presentation of Computer Model Results

4.3.1 Program Evaluation

Before applying the computer model to real situations it is essential to test it against known solutions, particularly the readily available uniform flow/uniform diffusivity solution. A routine is included in the program to calculate the series solution and plot this in an identical form to the moment solution. The series solution is only applicable to smooth bed cases and requires $\frac{f}{8}$ and the source location to generate a solution. Two comparisons are given in figures 4.2 and 4.3, for the source at the bed and at the mid-depth respectively. The solid lines represent the correct (series) solution with the deviation of the moment solution shown by the dashed lines. Complete agreement is obtained between the two solutions from about five flow depths downstream from the source. Closer to the source agreement is reasonable and certainly sufficient for engineering applications.

It is also possible to compare moments obtained from the computer program with those derived from the analytical solution by applying the moment transform equation to equation 3.20, resulting in

$$c_{dp} = \frac{2}{\pi\Delta}\left(\frac{f}{8\pi^2}\right)^{p+1} p! \sum_{m=1}^{\infty} \frac{\sin(m\pi\Delta)\cos(m\pi\eta_s)\cos(m\pi\eta)}{m^{2p+3}} \qquad (4.15)$$

Agreement between moments produced by the program (which were also checked analytically for uniform flow conditions) and those obtained from equation 4.15 was exact to 5 significant figures for all moments, (that is, the percentage error was always less than 0.01%). It should be recalled that equation 4.15 is the moment solution to the simplest possible form of the diffusion equation, $\beta \frac{\partial c}{\partial \xi} = \frac{\partial^2 c}{\partial \eta^2}$ (equation 3.18), and that in this equation the longitudinal term has been neglected. The uniform solution used above to compare with the moments obtained from the series solution (equation 4.15) also had the longitudinal term removed. To test the solution with

Source Location	Moment	Computer Soln.	Analytical	% diff.
0.2	c_{d0}	21.90476786	21.90476190	0.000027
	c_{d1}	343.4633387	343.4639907	0.000190
	c_{d2}	9873.145059	9873.181881	0.000373
0.5	c_{d0}	-5.952374994	-5.952380957	0.000100
	c_{d1}	-24.84307659	-24.84325409	0.000714
	c_{d2}	-187.4870148	-187.4896884	0.001426
0.8	c_{d0}	-20.95237499	-20.95238096	0.000028
	c_{d1}	-330.3047726	-330.3053970	0.000189
	c_{d2}	-9760.800174	-9760.835607	0.000363

Table 4.1 : Moments at $\eta = 0$ for three source locations.

Source Location	Velocity	Computer Soln.	Analytical	% diff.
0.2	Power-law	26.54885615	26.54885992	0.00001
	Logarithmic	30.51667443	30.51669295	0.00006
0.5	Power-law	-3.330870849	-3.330869178	0.00005
	Logarithmic	-0.976713135	-0.976698077	0.00154
0.8	Power-law	-19.95496385	-19.95496363	1.1×10^{-5}
	Logarithmic	-18.77414043	-18.77412755	0.00007

Table 4.2 : Zeroeth moments at $\eta = 0$ for computer and analytical solutions with non-uniform velocity fields.

this term included, an analytical solution for moments was obtained (see Appendix B). Since there are three separate cases for the flux function (the right hand side of equations 3.33-3.35, for $p = 0$, $p = 1$ and $p \geq 2$ respectively), it is necessary to evaluate the first three moments to verify the computer solution. Table 4.1 gives the first three moments for three different source locations. The differences between analytical and computed moments are small and within the limits of numerical accuracy.

Moments may also be obtained analytically for a power-law velocity distribution and a logarithmic velocity distribution if a uniform diffusivity field is assumed. If adequate agreement is obtained for the zeroeth moment then it is reasonable to assume that agreement between higher moments will be satisfactory since the algorithm is identical to that used for the uniform conditions solution. Analytical derivations for the moments are included in Appendix B and the resulting comparisons in table 4.2. Again deviations in the computer generated moments may be attributed to numerical accuracy.

The preceding results clearly indicate that errors observed in figures 4.2 and 4.3 arise entirely from the fitting techniques used to obtain $c_{d*}(\xi)$ from moments generated. It was noted in chapter 3 that regardless of the velocity and diffusivity fields the same basic form was assumed for the variation of concentration with distance downstream,

$$c_{d*}(\xi) = \sum_{n=0}^{\infty} A_n \, e^{-\alpha_n \xi} \qquad (4.16)$$

Using this relationship it was demonstrated in chapter 3 that A_0 and α_0 may be determined from high order moments. Also discussed was the variation of α_n for the uniform flow conditions, where $\alpha_n = (n + 1)^2 \, \alpha_0$ and the variation of α_n for a power-law velocity field with an approximate form of the associated diffusivity field, where $\alpha_n = (j'_{n+2,0}/j'_{2,0})^2 \, \alpha_0$. It is apparent therefore that there should be some type of "goodness of fit" test which would enable a comparison between the two preceding equations for α_n and also give some estimation of the errors involved in the fitting technique. An approximate test is obtained by comparing moments given by the computer solution with those calculated from the fitted profile. The general procedure is,

(i) Determine A_0, α_0 from large moments.
(ii) Determine the number of terms in $c_{d*}(\xi) = A_n \, e^{-\alpha_n \xi}$.
(iii) Determine the number of moments to be used to calculate coefficients A_n.

Height (η)	No. of moments used in fitting	% error in uniform solution	% error for $(\frac{n}{\eta}+1)^2$ coeffs.	% error for Bessels coeffs.
0.025	4	0.0017	0.0486	0.0155
0.075	4	0.0003	0.0418	0.0048
0.125	3	0.0005	0.1228	0.0311
0.175	3	0.0039	0.0950	0.0282
0.225	3	0.0022	0.0572	0.0172
0.275	3	0.0014	0.0198	0.0086
0.325	3	0.0012	0.0224	0.0029
0.375	3	0.0006	0.0775	0.0066
0.425	3	0.0002	0.1534	0.0164
0.475	3	0.0023	0.3036	0.0348
0.525	3	0.0021	0.7847	0.0905
0.575	3	0.0007	3.1705	0.4331
0.625	3	0.0003	0.5009	0.0647
0.675	3	0.0001	0.2516	0.0326
0.725	3	0.00004	0.1380	0.0193
0.775	3	0.00002	0.0684	0.0125
0.825	3	0.0001	0.0145	0.0100
0.875	3	0.0001	0.0299	0.0106
0.925	3	0.0001	0.0681	0.0178
0.975	3	0.0002	0.0956	0.0381

Table 4.3 : Maximum percentage differences in moments calculated from the fitted profile and moments calculated from the computer model for a source at η = 0.0035.

Height (η)	No. of moments used in fitting	% error in uniform solution	% error in $(\frac{n}{\pi}+1)^2$ coeffs.	% error in Bessels coeffs.
0.025	3	0.0005	0.3090	0.0363
0.075	3	0.0004	0.2819	0.0324
0.125	3	0.0005	0.2351	0.0255
0.175	3	0.0005	0.1855	0.0188
0.225	3	0.0007	0.1130	0.0095
0.275	3	0.0011	0.0271	0.0049
0.325	3	0.0019	0.0895	0.0231
0.375	3	0.0038	0.2552	0.0308
0.425	3	0.0092	0.5348	0.0806
0.475	3	0.0104	1.0300	0.0574
0.525	3	0.0255	3.2289	0.3697
0.575	3	0.0331	8.1780	0.7169
0.625	4	0.0028	0.5293	0.1228
0.675	4	0.0052	0.2688	0.1018
0.725	4	0.0008	0.1386	0.0289
0.775	3	0.0034	0.1991	0.0184
0.825	3	0.0035	0.0279	0.0248
0.875	3	0.0010	0.1212	0.0144
0.925	3	0.0005	0.2483	0.0676
0.975	3	0.0010	0.4036	0.1714

Table 4.4 : Maximum percentage differences in moments calculated from the fitted profile and moments calculated from the computer model for a source at $\eta = 0.6665$.

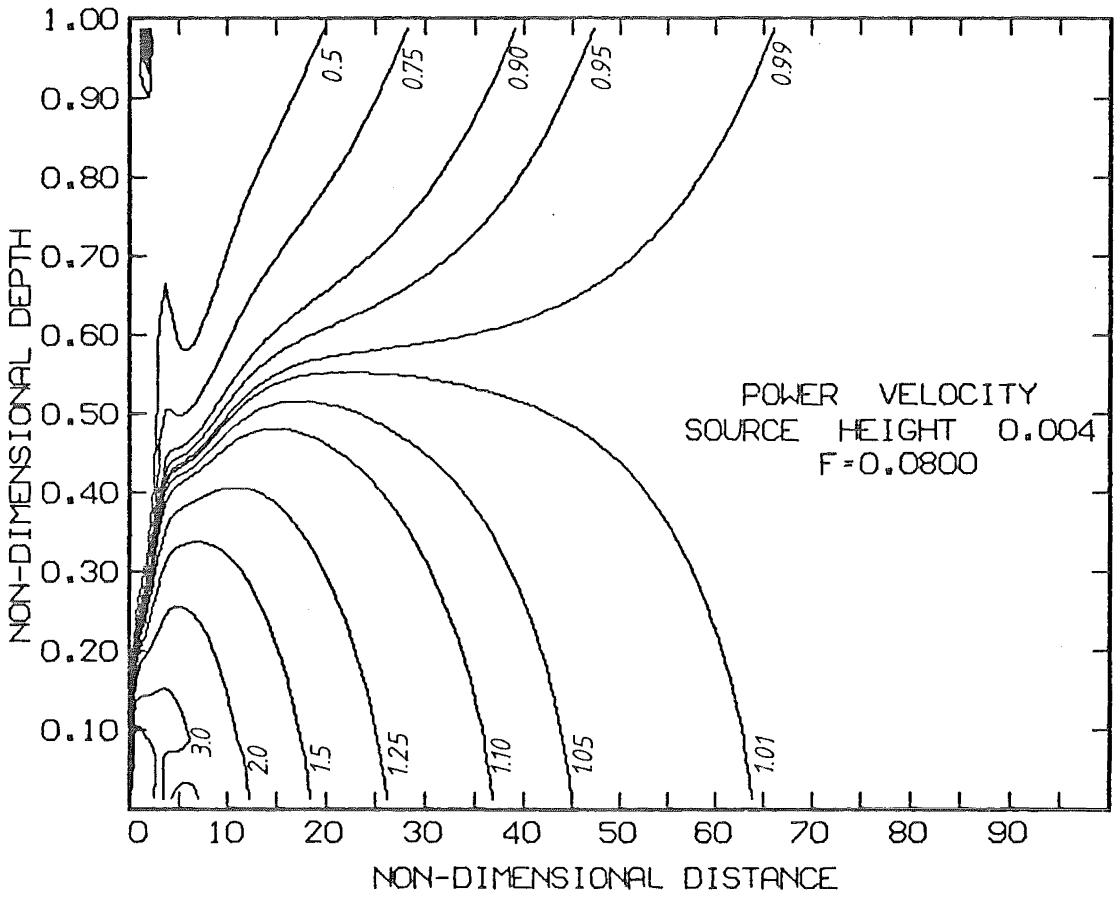

Figure 4.4a : Moment solution with a power velocity distribution using $\alpha_n = (n+1)^2 \alpha_0$ for a source at the bed.

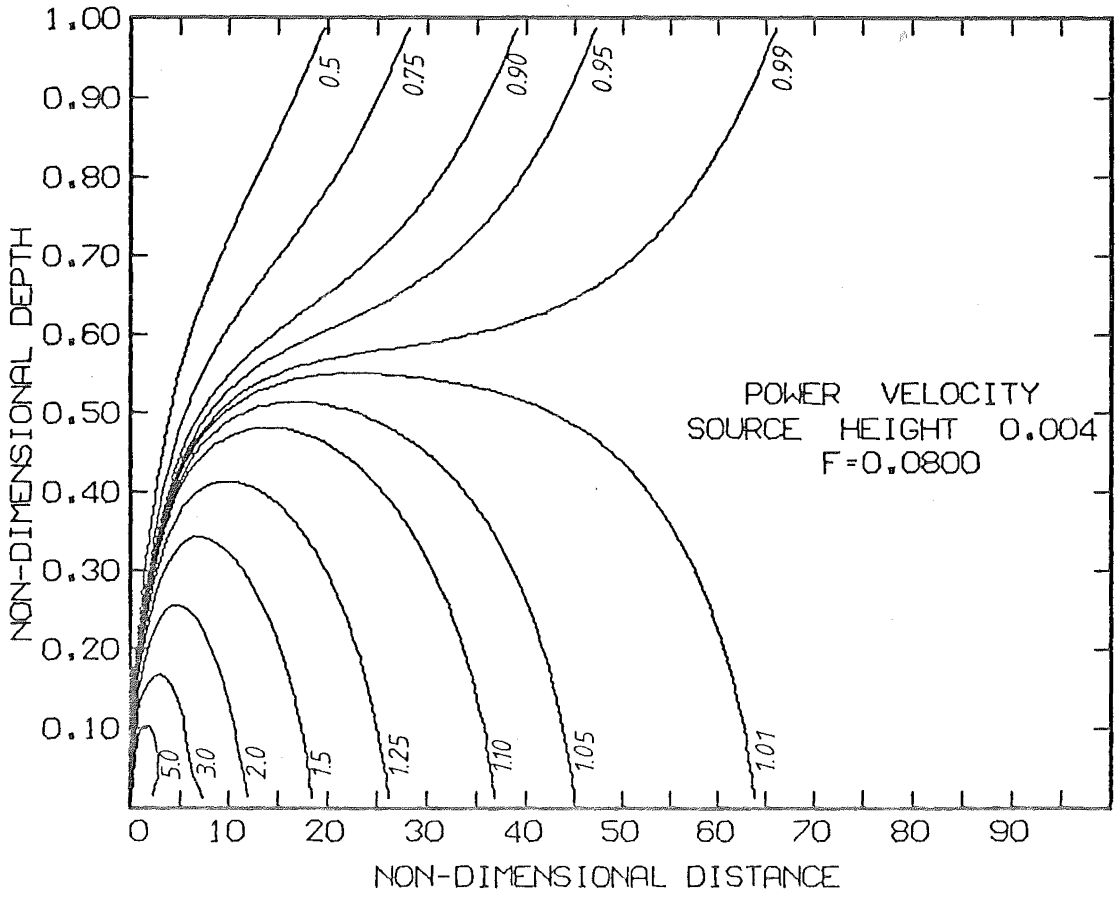

Figure 4.4b : Moment solution with a power velocity distribution using $\alpha_n = (j'_{n+2,0}/j'_{2,0})^2 \alpha_0$ for a source at the bed.

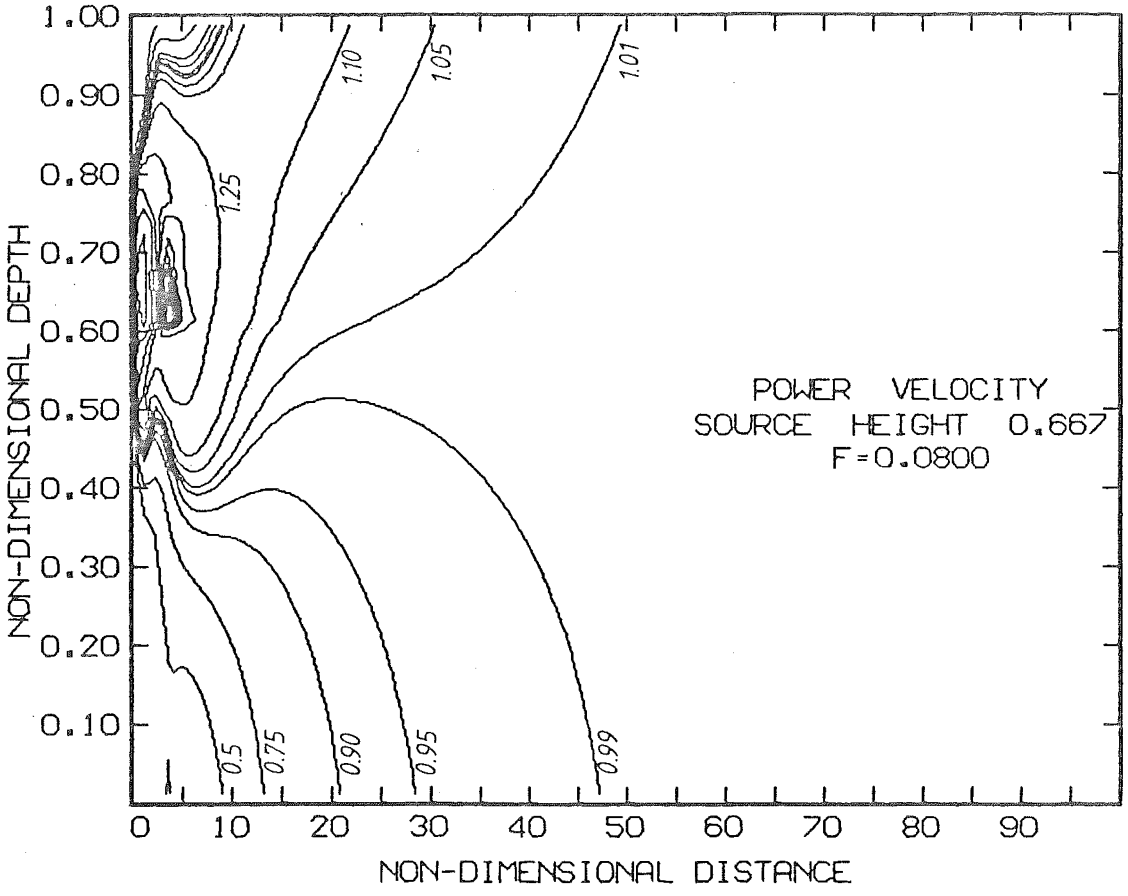

Figure 4.5a : Moment solution with a power velocity distribution using $\alpha_n = (n+1)^2 \alpha_0$ for a source at $\eta = 0.667$.

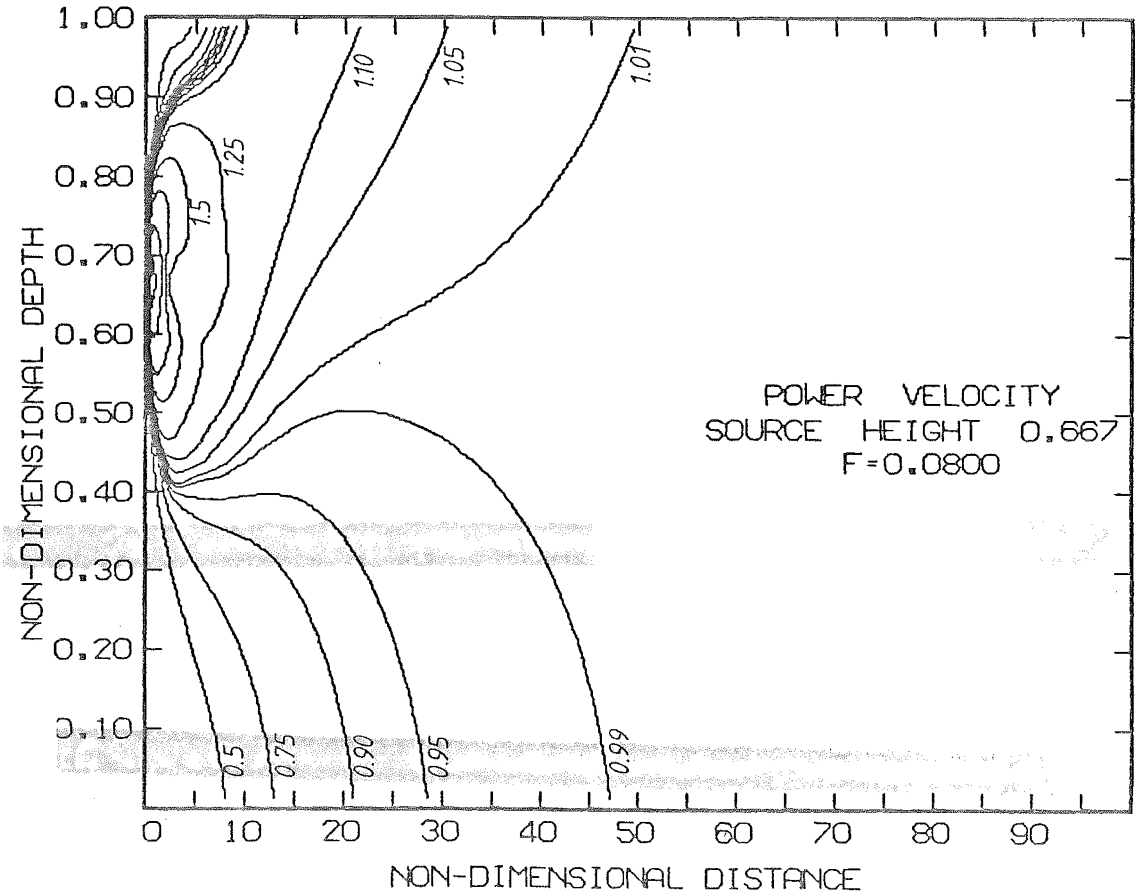

Figure 4.5b : Moment solution with a power velocity distribution using $\alpha_n = (j'_{n+2,0}/j'_{2,0})^2 \alpha_0$ for a source at $\eta = 0.667$.

Note: The contouring routines used to produce all contour plots presented here were package programs. Consequently, some contour diagrams may appear physically incorrect. This is partly due to difficulties in fitting concentration profiles to moments but also to the incorrect interpretation of these profiles by the contouring routines.

(iv) Calculate moments of fitted curve, $\int_0^\infty \xi^p \left(\sum_{m=0}^{n} A_m e^{-\alpha_n \xi} \right) d\xi$.

Since some moments have been used to find the coefficients, A_n, the first few moments will be exact and generally the largest deviation is in the first moment beyond those used in the fitting procedure. Tables 4.3 and 4.4 present the maximum percentage differences in moments calculated from the fitted concentration profile and moments calculated by numerical integration (in the computer program), for a source of 0.0035 and 0.6665 respectively. Column 3, for the uniform flow conditions, indicates that sufficient agreement is obtained in fitting computed moments. Any deviations noticed in the uniform solution (figures 4.2 and 4.3) must therefore occur because of the inability of the chosen distribution (an exponential series) to duplicate the very steep concentration gradients experienced close to the source.

Also given in tables 4.3 and 4.4 are maximum percentage differences for a power-law velocity using in one case $\alpha_n = (n + 1)^2 \alpha_0$ and in the other $\alpha_n = (j'_{n+2,0}/j'_{2,0})^2 \alpha_0$. If the same variation in α_n, as is appropriate for uniform flow conditions, is used with the non-uniform velocity there is a dramatic increase in the percentage error. The choice of $\alpha_n = (j'_{n+2,0}/j'_{2,0})^2 \alpha_0$ significantly reduces the errors in observed moments. Since the Bessel's type variation is only appropriate for an approximate velocity/diffusivity field it is not expected to provide the same degree of fit that is observed in the uniform flow case. However, it is interesting to note that while the approximation made in the diffusivity field to obtain the Bessel's variation in α_n is certainly appropriate near the bed there is no apparent decrease in the goodness of fit away from the bed. Errors are larger just above the mid-depth but this is mainly due to a decrease in the magnitude of the moments. At this height in the flow, moments change sign and some may be close to zero.

The results presented in tables 4.3 and 4.4 are reinforced when plots of concentration contours are examined for the two choices for α_n. This comparison is shown in figures 4.4 and 4.5. It is apparent in these diagrams that the use of $\alpha_n = (n + 1)^2 \alpha_0$ causes instabilities for small values of ξ at all heights in the flow. A significant improvement is seen when $\alpha_n = (j'_{n+2,0}/j'_{2,0}) \alpha_0$. Distant from the source agreement is exact since the 1st term of the exponential series dominates and this is independent of the choice of α_n.

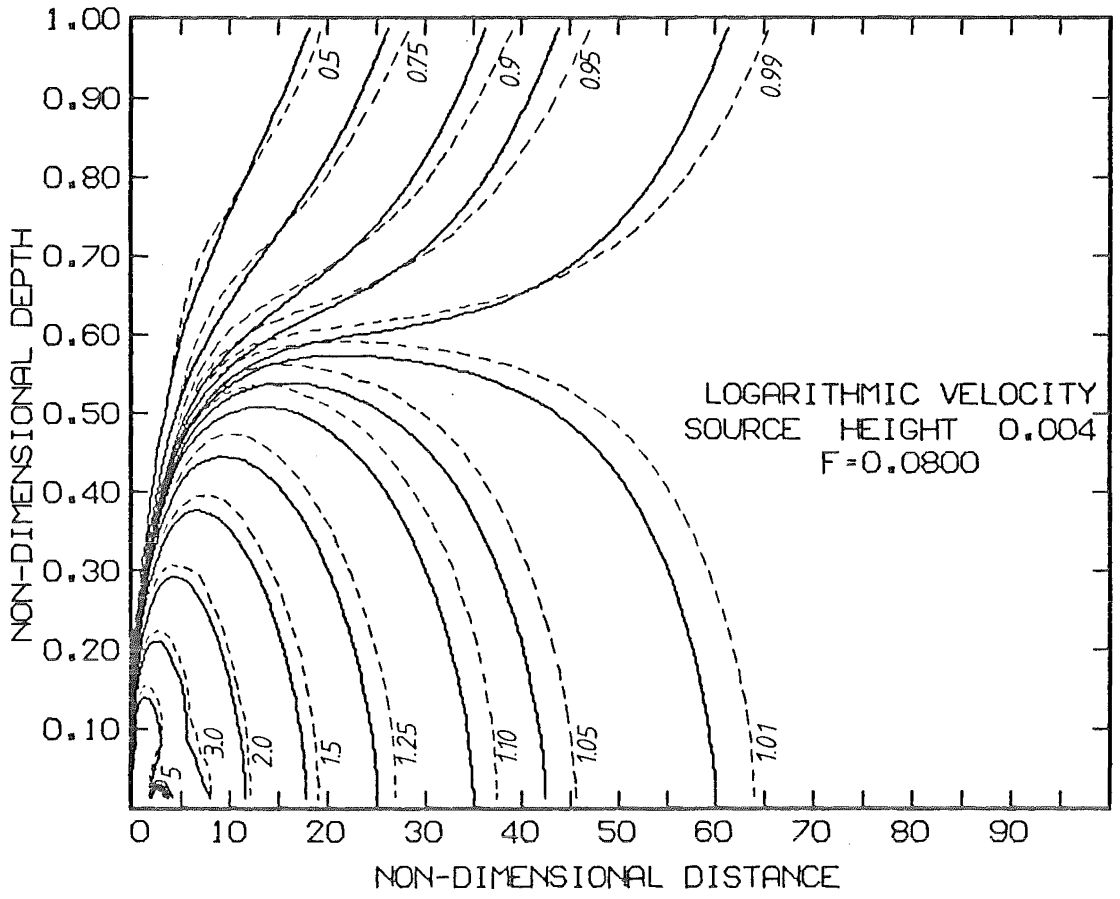

Figure 4.6 : Comparison of solutions with (---) and without (——) dead zones. Note that the % increase in mixing length (~ 7%) is the same as the % increase in flow area due to the inclusion of dead zones.

As the logarithmic velocity field is approximated fairly closely by the power-law profile and both distributions produce similar diffusivity profiles, it would seem reasonable to assume that the same decay term will be appropriate. In fact, the Bessel's decay (α_n) is the best approximation presently available after that used for uniform conditions, since no analytical solution (or approximate solution) is possible for the logarithmic velocity/parabolic diffusivity case. If the same test as described for the power-law velocity by tables 4.3 and 4.4 is applied to the concentration profile fitted with the logarithmic velocity, identical results are produced (approximately the same errors for $\alpha_n = (n + 1)^2 \alpha_0$ and the same improvement with $\alpha_n = (j'_{n+2,0}/j'_{2,0})^2 \alpha_0$). In the absence of any better relationship for α_n, the Bessel's variation is used for fitting profiles for both non-uniform flow fields examined.

4.3.2 Dead Zone Effects

The consequence of introducing trapping mechanisms into the flow is twofold. Firstly the location of $\eta = 0$, the point at which the velocity equals zero (for the non-uniform cases) will shift into the bed. This effectively increases the area of flow available for dispersion, and the mixing length increases. The second result of the dead zones is to completely change the channel boundary conditions in terms of roughness. This will produce an entirely different flow than that of the smooth bed case. Hence it is unrealistic to compare effects of trapping by simply altering the dead zone geometry without considering the corresponding alterations to the flow field. In a typical flow situation the friction factor is, in general, readily obtainable. With the channel roughness defined (using the friction factor) it is then possible to estimate the dead zone geometry and calculate a solution for the concentration distribution. A comparison may now be made between the various choices of dead zone parameters, which will not affect the main flow since that has been fixed by determining the friction factor. Such a comparison is shown in figure 4.6 where the friction factor has been chosen as $f = 0.08$. Solid lines represent contours with no trapping mechanisms present and the dashed lines portray contours for a rectangular trapping element case. The size of the dead zones is such that the flow region is increased by about 7%, which is the same as the increase in mixing length. Increasing the flow region and the corresponding shift of $\eta = 0$ into the bed occurs because of the way dead zones have been defined. Numerically they are considered to be additions to the bed of the channel below the existing bed level therefore increasing the mean flow depth and necessitating a translation

BLANK PAGE IN ORIGINAL - PART OF PAGINATION

of the origin. Moving the origin into the bed will also "stretch" the velocity distribution. The lower flow boundary will no longer be characterised by zero velocity. The example given in figure 4.6 is an extreme case where the physical size of the trapping element is large $\left(\simeq \frac{1}{5} y_n\right)$ compared to the flow depth, y_n. In most cases the dead zone effect is expected to be less significant.

4.3.3 Longitudinal Diffusion

One of the aims of this study was to examine previous assumptions that have been applied to effect a solution to the dispersion equation for a continuous pollutant source. The assumption that the longitudinal dispersion is small enables the term $\varepsilon_\xi \frac{\partial^2 c}{\partial \xi^2}$ to be removed from the relevant equation leaving,

$$u(\eta) \frac{\partial c}{\partial \xi} = \frac{\partial}{\partial \eta} \varepsilon_\eta \frac{\partial c}{\partial \eta} \qquad (4.17)$$

It was found that in the computer solution the magnitude of this term was about 5 orders smaller than the remaining term in equation 4.17. Although the effect of longitudinal dispersion on calculated moments is more noticeable in non-uniform flow conditions, there is negligible difference in plotted contours. This is not unusual since it is expected that with a continuous source the longitudinal concentration gradients will be small.

It is concluded therefore that this assumption is reasonable.

4.3.4 The Effect of Variations in the Velocity and Diffusivity Profiles

A common assumption made when solving the dispersion equation, is to let the velocity and diffusivity fields be represented by constant functions of depth. The model has been developed to included non-uniform flow fields which has enabled this assumption to be examined.

The simplest way to compare solutions obtained for the dispersion equation is to calculate how large a distance is required to attain a certain degree of mixing throughout the channel cross-section. Conequently, a "mixing length" is defined as the non-dimensional distance required for the pollutant to be mixed to within some predetermined percentage of the fully mixed concentration across the entire section. Contour plots of the non-dimensional concentration distribution, as produced by the

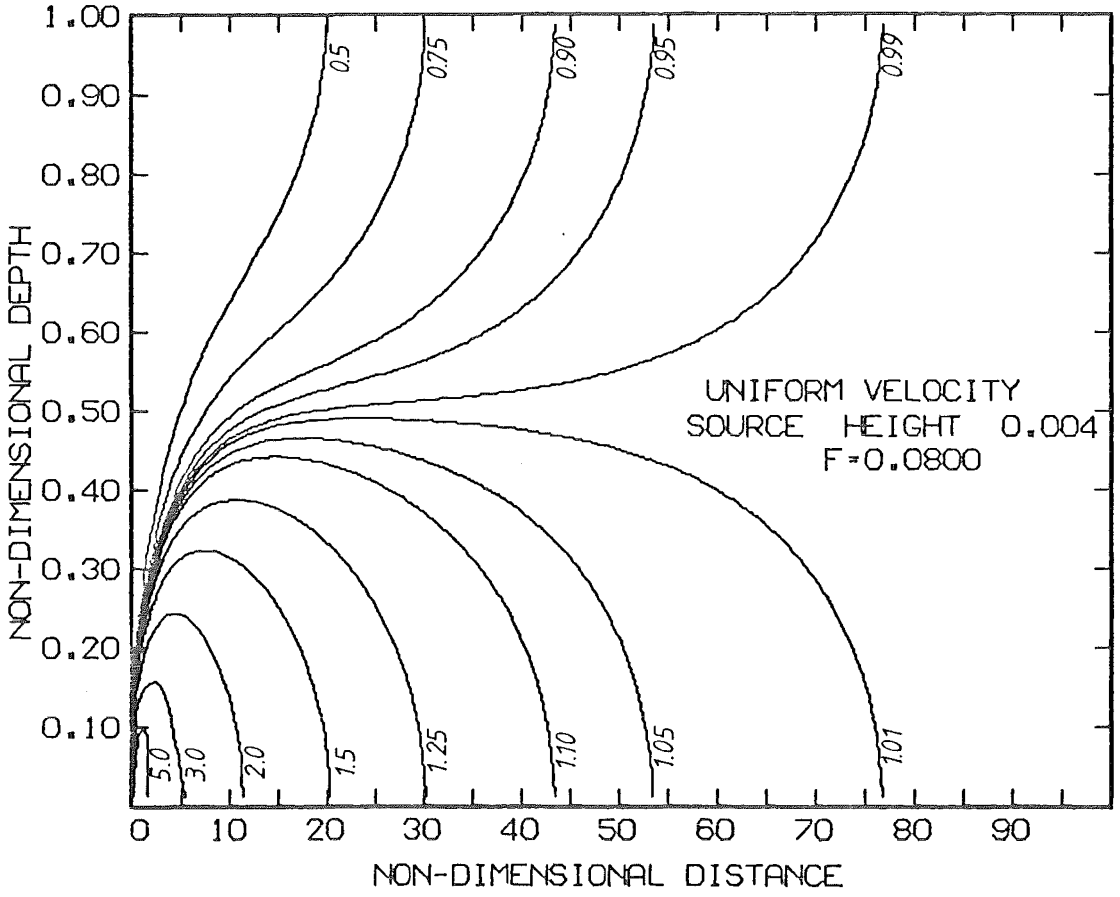

Figure 4.7a.

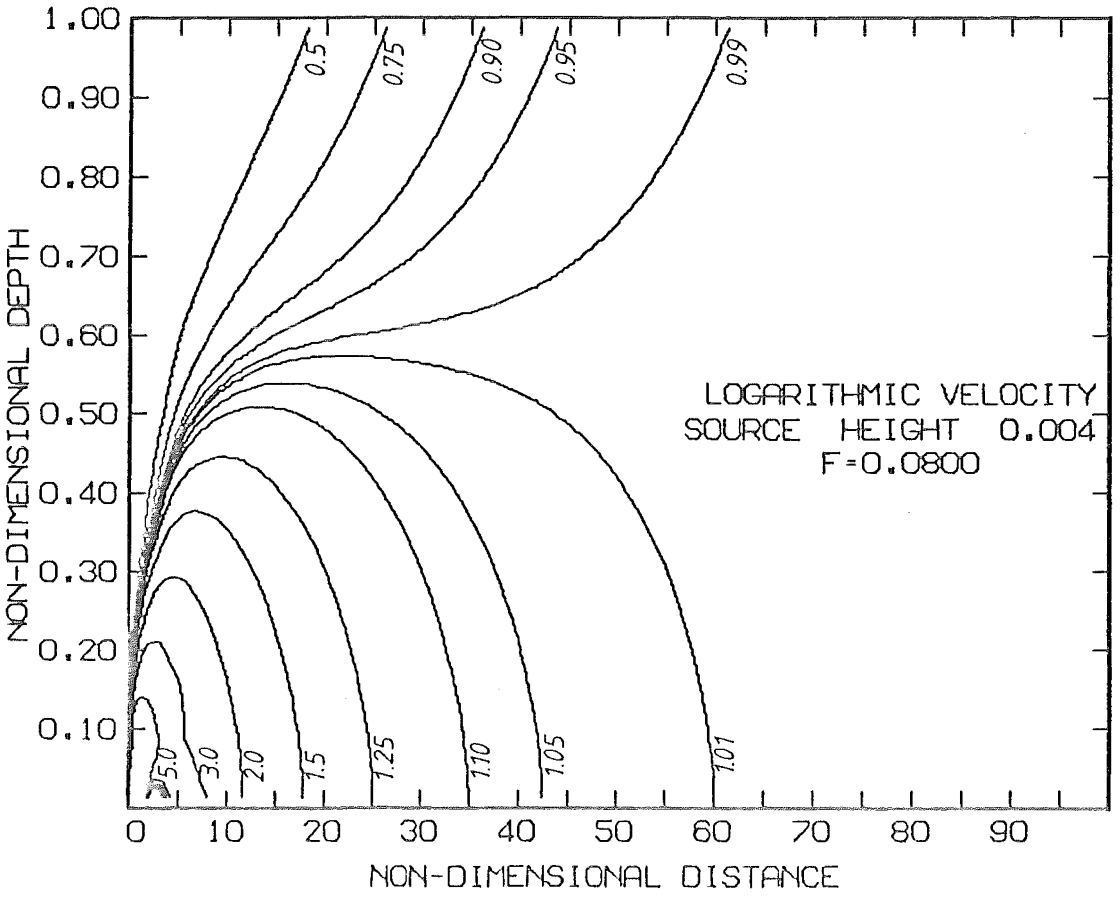

Figure 4.7b : Comparison in mixing length for a uniform velocity and a logarithmic velocity with the source at the bed.

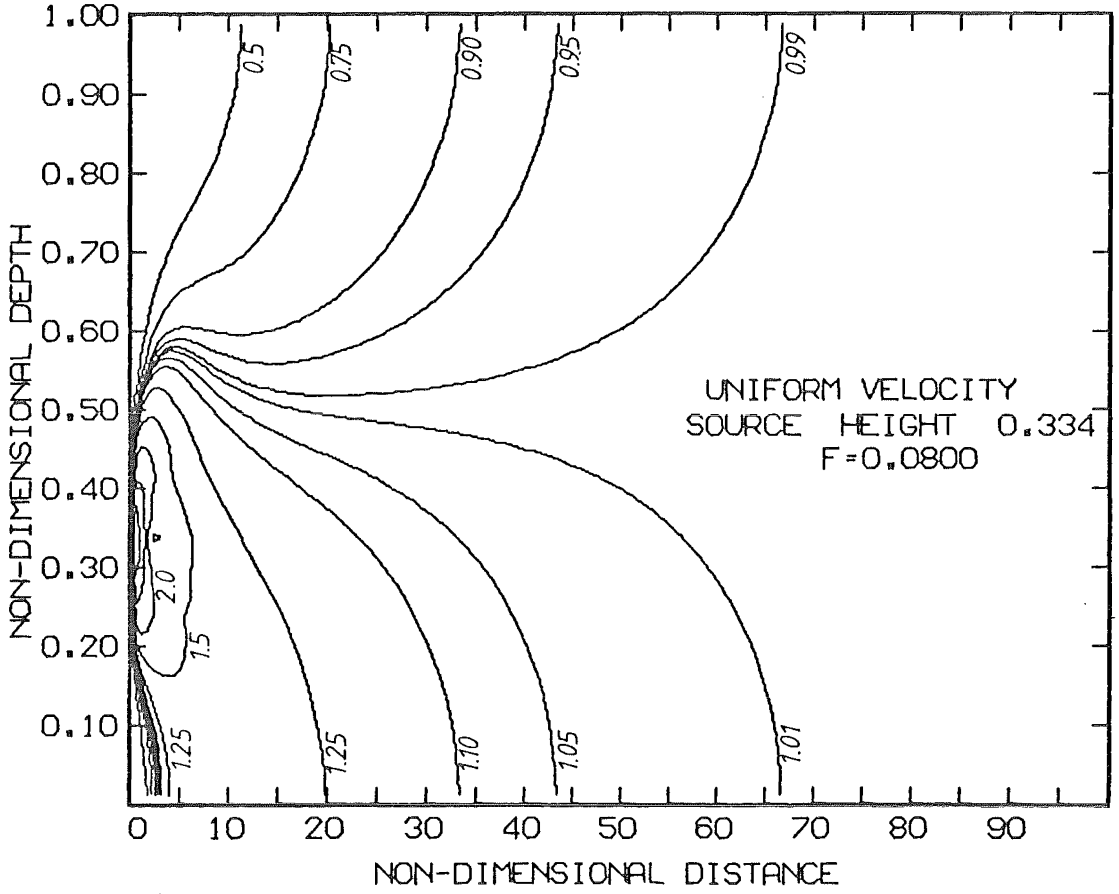

Figure 4.8a.

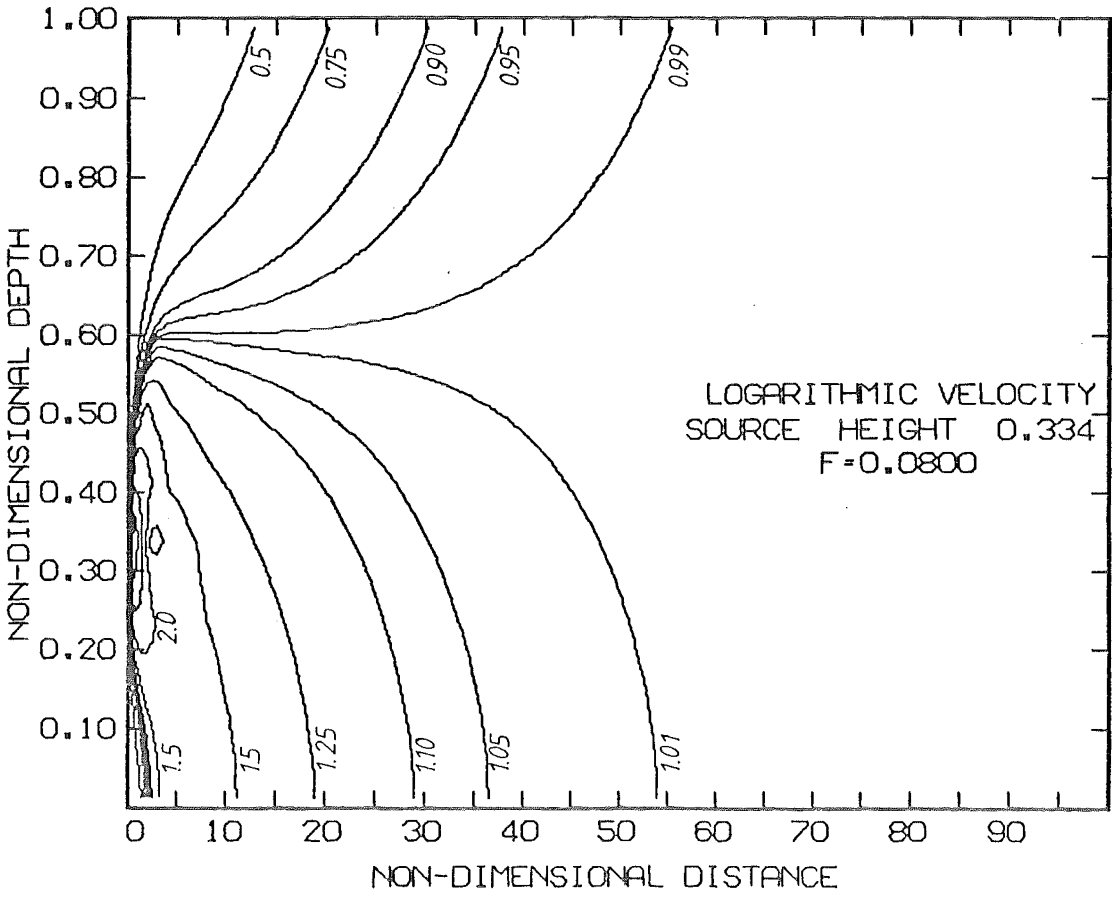

Figure 4.8b : Comparison in mixing length for a uniform velocity and a logarithmic velocity with the source at $\eta = 0.333$.

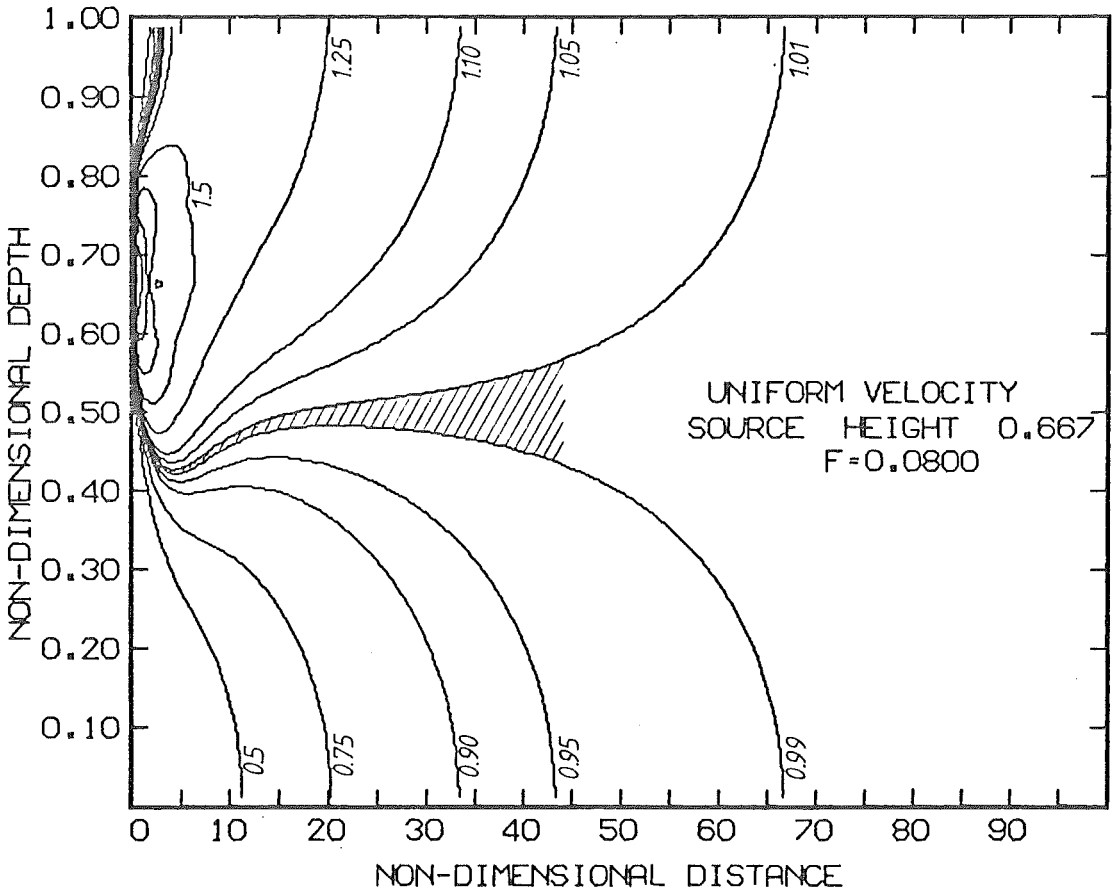

Figure 4.9a.

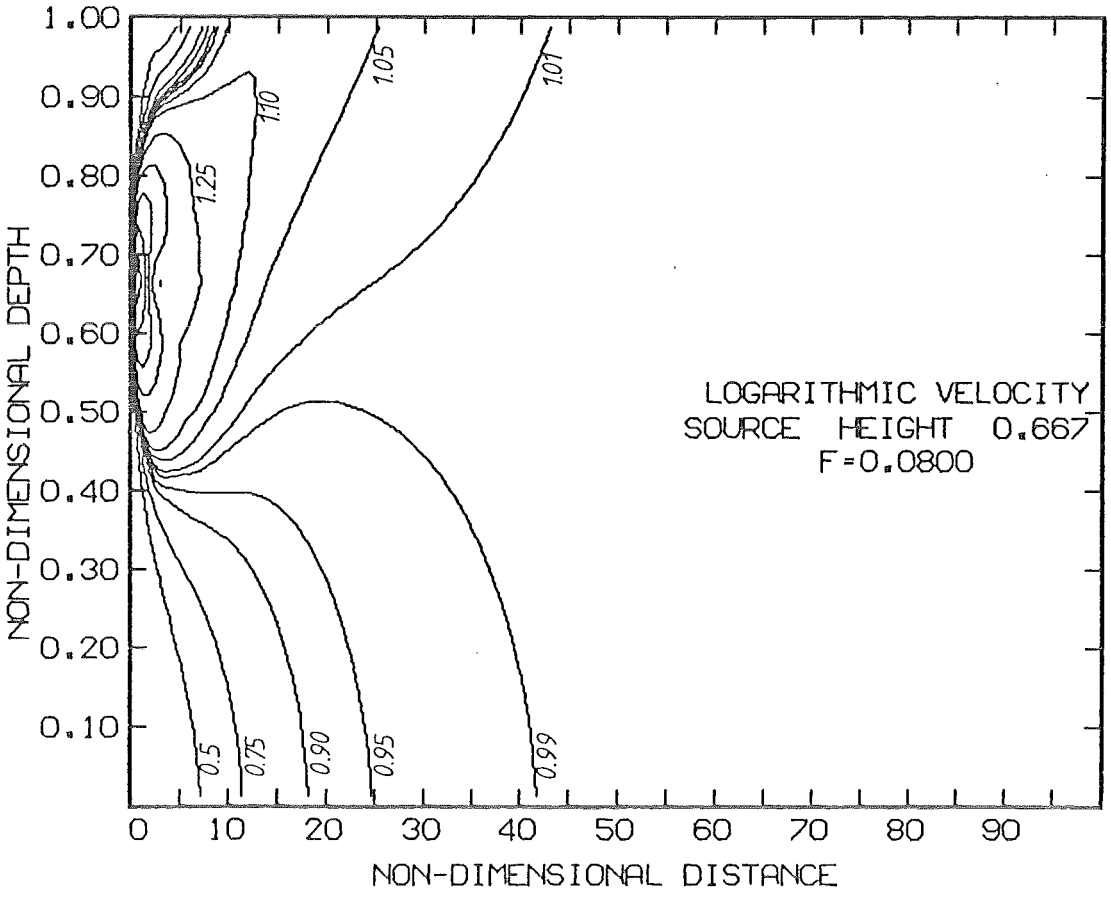

Figure 4.9b : Comparison in mixing length for a uniform velocity and a logarithmic velocity with the source at $\eta = 0.667$.

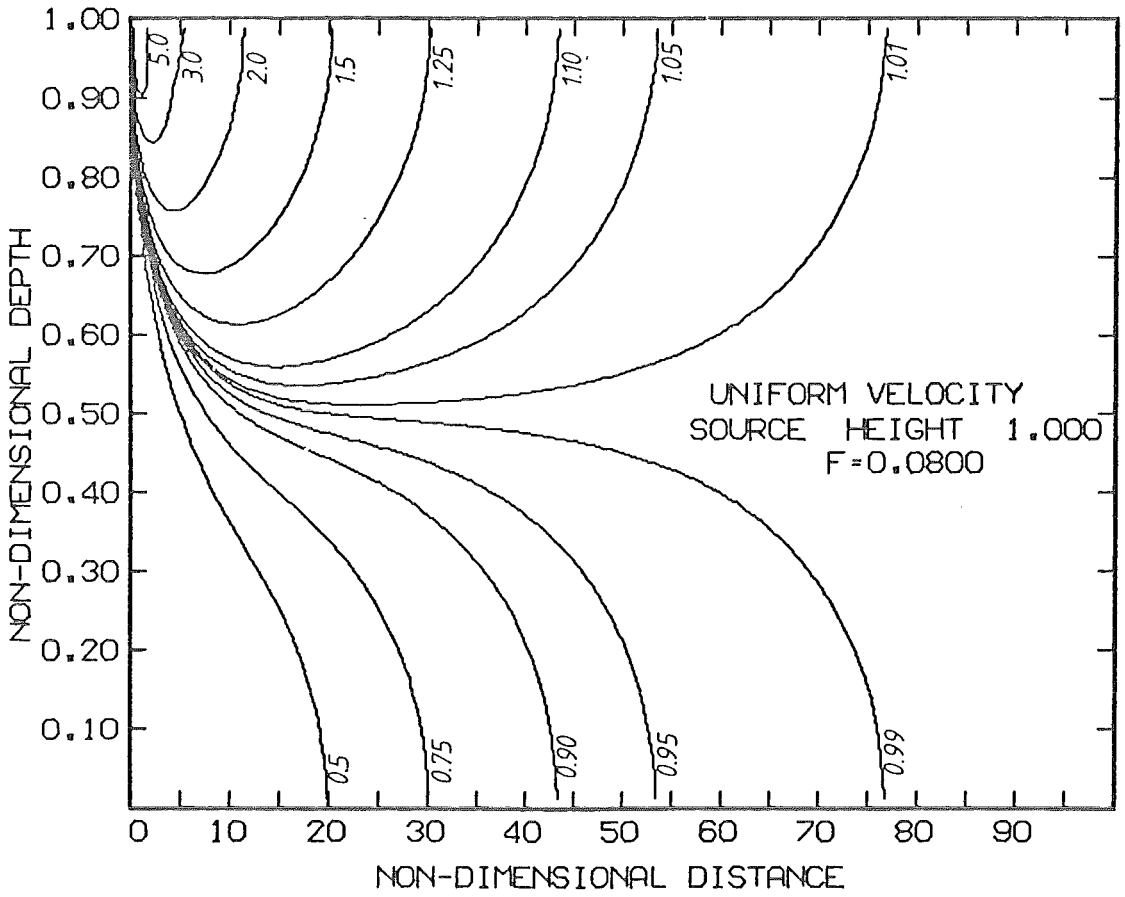

Figure 4.10a.

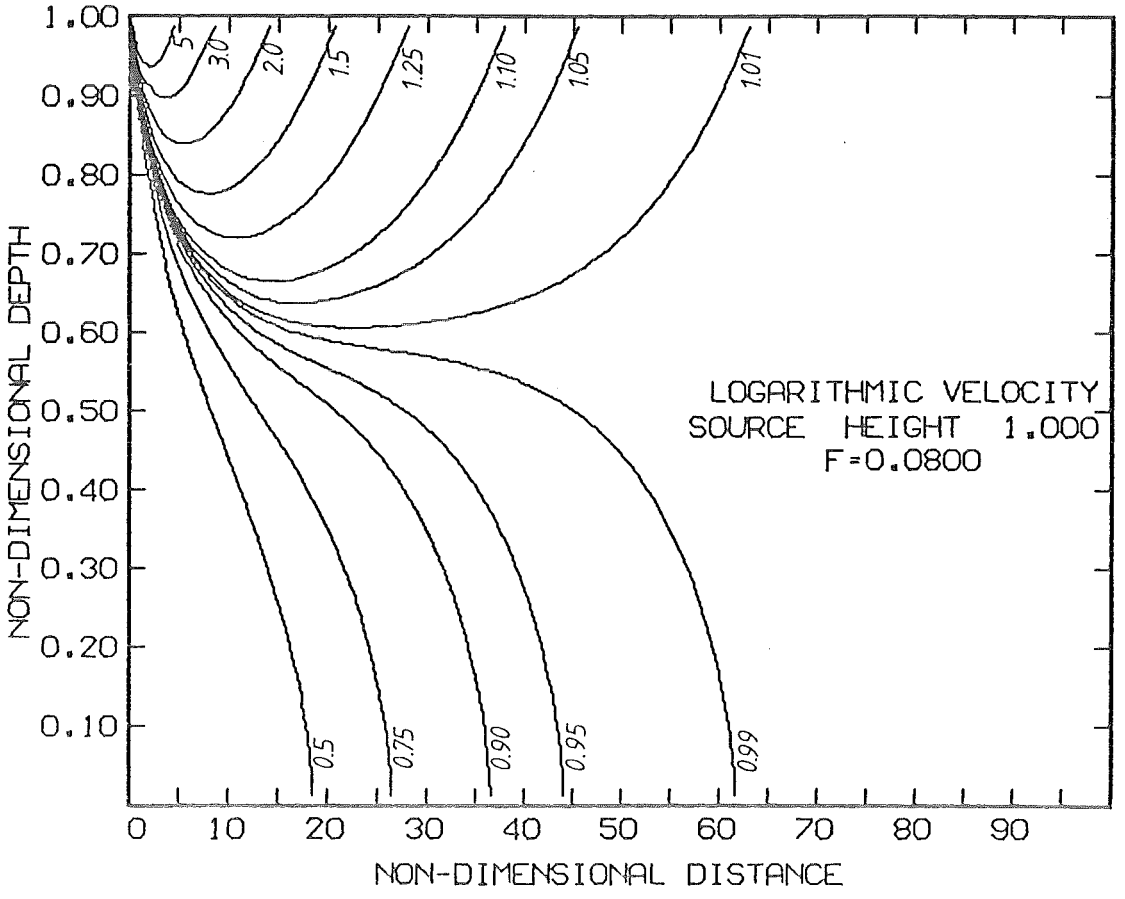

Figure 4.10b : Comparison in mixing length for a uniform velocity and a logarithmic velocity with the source at the surface.

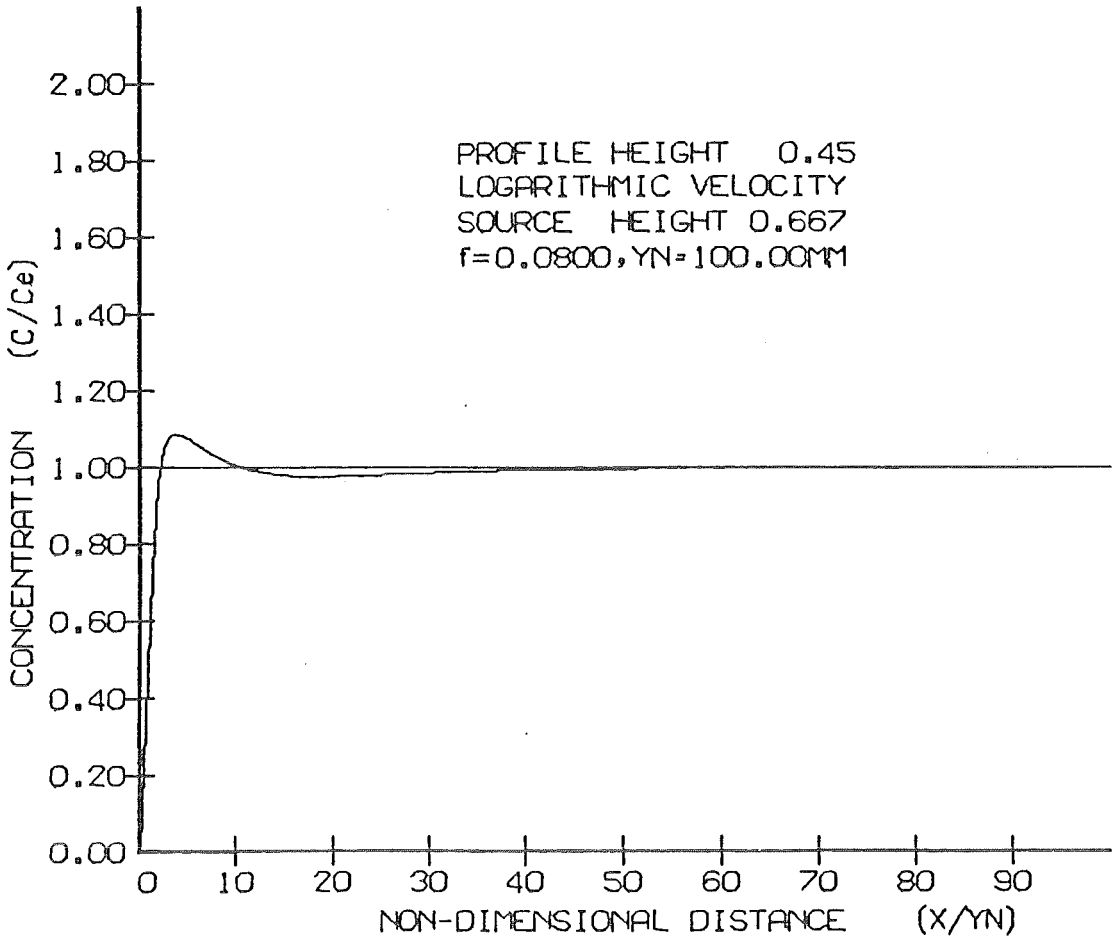

Figure 4.11 : Longitudinal concentration profile from figure 4.9b at η = 0.45.

computer, indicate the different degrees of mixing along the channel. The plots presented in this chapter have contours showing concentrations 1%, 5%, 10%, 25%... from the fully mixed concentration (that is, non-dimensional concentration contours for $c_* = 1.01$ and 0.99, 1.05 and 0.95, 1.10 and 0.90, 1.25 and 0.75... respectively). For the discussion following, the distance to reach 1% of the fully mixed conditions, over the entire depth, shall be taken as the mixing length.

The plots shown in figures 4.7 to 4.10 are the respective contour plots for the uniform velocity field and logarithmic velocity field corresponding to four source locations. Each of these diagrams indicate the conservative nature of uniform velocity/diffusivity distribution. If the more correct logarithmic velocity and parabolic diffusivity is used there is a 20% to 35% reduction in mixing length depending on the position of the source. The power-law velocity with a parabolic diffusivity results in a slightly more conservative solution than that obtained for the logarithmic velocity distribution.

One interesting point arising from figures 4.8 and 4.9 is the behaviour of the dispersing pollutant at $\eta = 0.55$ in figures 4.8 and $\eta = 0.45$ in figures 4.9. At these heights in the flow, the longitudinal variation in concentrations predict that the equilibrium concentration will be experienced more than twice. This is illustrated in figure 4.11, where after an initial rise above $c_e (c_e = 1.0)$, the concentration decays to less than 1.0 before approaching the final mixing concentration c_e asymptotically. At small distances downstream from the source the dispersion is dominated by the local concentration gradients. As the plume spreads the influence of the channel boundaries becomes apparent and these will tend to control the dispersion pattern. In the uniform velocity case this results in the fully mixed region (that is, the area between the contours for $c_* = 0.99$ and 1.01) moving back towards the centre of the channel. This is shown by the shaded area in figure 4.9(a). The same effect is distinguishable in figure 4.9(b) however this fully mixed region does not centre at the mid-depth but at $\eta \simeq .58$.

In uniform flow conditions it is intuitively obvious that the minimum mixing length will occur when the source is at the mid-depth. For this location the pollutant has equal opportunity to spread to the surface, as it does to the bed. When a non-uniform velocity and the corresponding diffusivity distribution is considered it is not immediately

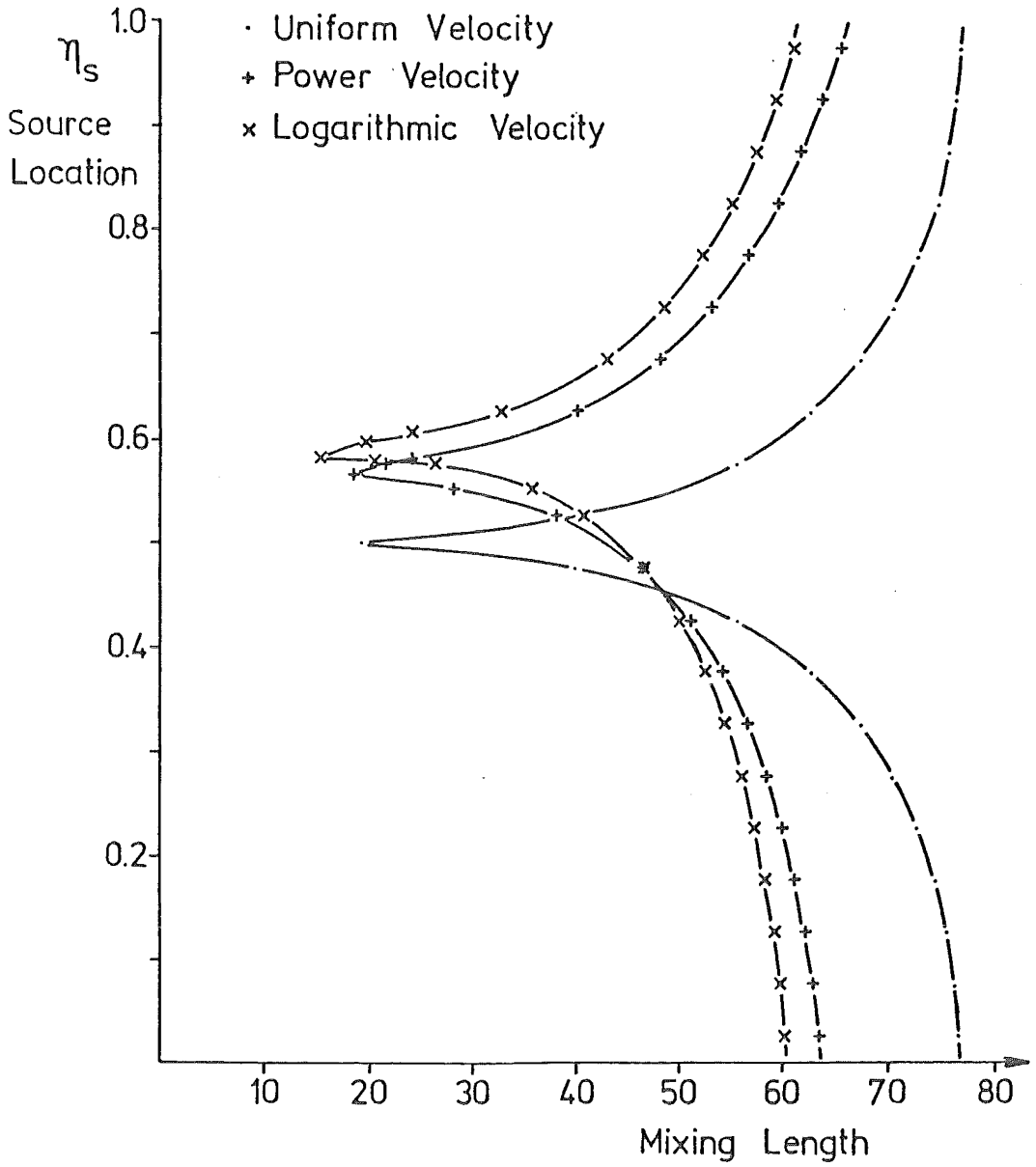

Figure 4.12 : Comparison of mixing length for different velocity distributions (and their corresponding diffusivities) against source location.

apparent which source location will give the minimum mixing length. If the source is below the mid-depth the pollutant will initially experience a larger velocity gradient but a lower convectivity and above the mid-depth the converse is true. To determine the source position for minimum mixing length in various velocity fields a plot of source locations versus mixing length was constructed (see figure 4.12). This plot shows the minimum mixing length occurs for a source at $\eta = 0.58$ for the logarithmic velocity distribution. If figure 4.9(b) is examined again, the height about which mixing ultimately centers is $\eta = 0.58$.

A second point to note from figure 4.12 is that there is a region over which the uniform assumption will result in more rapid mixing. However, this region is small ($\sim$ 7% of the flow depth) and on the whole the non-uniform velocity will result in better pollutant mixing.

Figure 4.12 is useful to predict the effect of the location of the pollutant source in a bounded region for a chosen velocity/diffusivity distribution and is the most significant result of this chapter.

BLANK PAGE IN ORIGINAL - PART OF PAGINATION

CHAPTER V

LABORATORY EXPERIMENTS: TECHNIQUES AND APPARATUS

5.1 Summary

This chapter outlines the experimental model, experimental programme and the methods of data analysis that have been employed. The laboratory equipment used is also described.

5.2 Introduction and Aims

A series of laboratory experiments, designed to test the results achieved in preceeding chapters, was conducted in the Fluid Mechanics Laboratory, Civil Engineering Department, University of Canterbury, during the period 1981 - 1982. The aims of the laboratory experiments are as follows:

(a) To provide a qualitative assessment of the computer model developed in two dimensions.
(b) To test the predictive powers of the model quantitatively.
(c) To provide data to enable a comparison between results obtained in an idealised laboratory situation and those obtained in the field experiments.

5.3 Experimental Model

Experiments were designed to simulate the results obtained from the computer studies. Since the numerical model is independent of time, experiments were all performed using a spatial co-ordinate system. Nearly all previous workers have employed methods to measure the concentration at a fixed point as a continuous function of time. However, for a continuous source, after an initial unsteady period, the time averaged concentration at any point in the flow will be constant providing the flow and the source are steady. Thus, a direct comparison is possible between numerical results and experimental results, both of which are expressed in the spatial domain.

Experimental data was obtained by running the flume and source until a steady state was reached and then taking time averaged

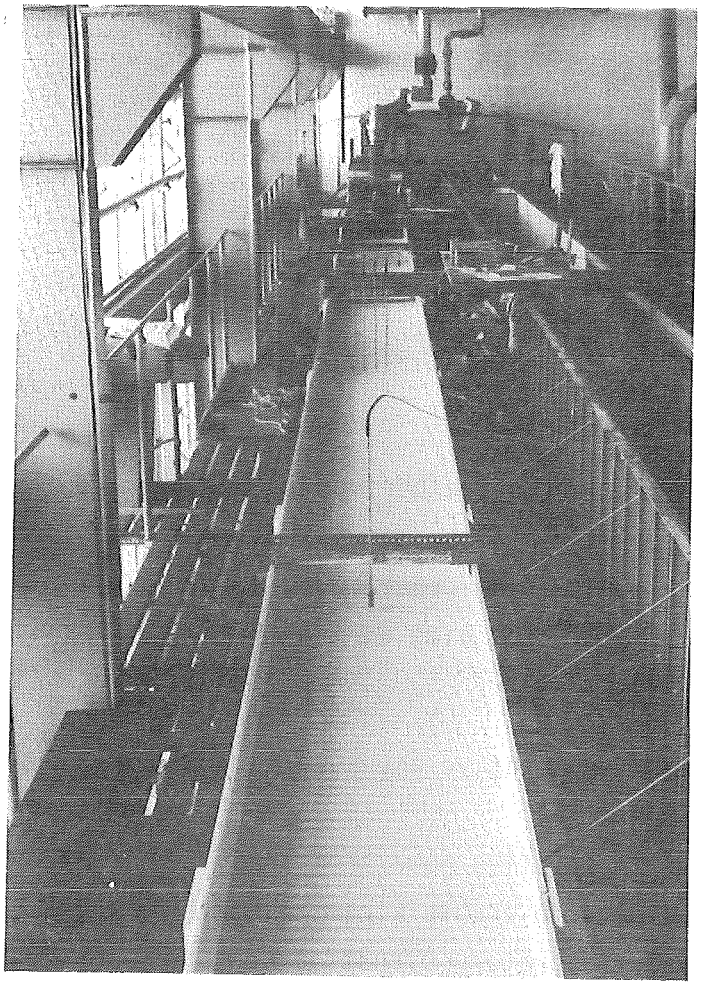

Plate 5.1 : The 22 m Plywood Laboratory Flume.

concentrations at several sections downstream from the source. The manner in which this was achieved is outlined in following sections.

5.4 Experimental Programme

The laboratory experiments involved the execution of 6 different runs in the tilting flume. The constant parameters and varying conditions are summarised as follows:

(1) Constant Parameters - 22 m long flume, flume width (z_n) = 562.5 mm flume slope (s_0) = 0.0045 and flume roughness constant.

(2) Two Dimensional Experimental Variables - Line source located at the channel bed and on the surface, with various flow depths.

5.5 Laboratory Apparatus and Measurements

5.5.1 Tilting Flume

Experiments were performed in a 22 m flume built for a previous study on dispersion and described by Valentine (1978) and shown in plate 5.1. The flume slope was adjustable by means of screw jacks at the mid-point and upstream end of the flume. The flume was constructed from ply-wood and has a 562.5 mm by 150 mm rectangular cross-section.

At the upstream end of the flume there was a series of grills which "straightened" the flow as it entered the channel. For this series of experiments, the two-dimensional series, complete mixing was obtained well within the length of flume available.

In order to obtain a truly two-dimensional velocity field it was necessary to destroy any secondary flow which may have been established. This was achieved by attaching roughness strips to the channel bed. The bed forms were 20 mm by 7 mm plastic strips extending across the entire width of the flume. Strips were placed at 40 mm centres, creating "dead zones" 20 mm by 7 mm over half of the channel bed. (That is, the dead zone fraction, A, is 0.5).

5.5.2 Water Supply and Control

Water was supplied from the recirculating laboratory system. Water from the laboratory sump was introduced via the constant head tower at the upstream end of the flume through a single valve controlled pipe, 152 mm

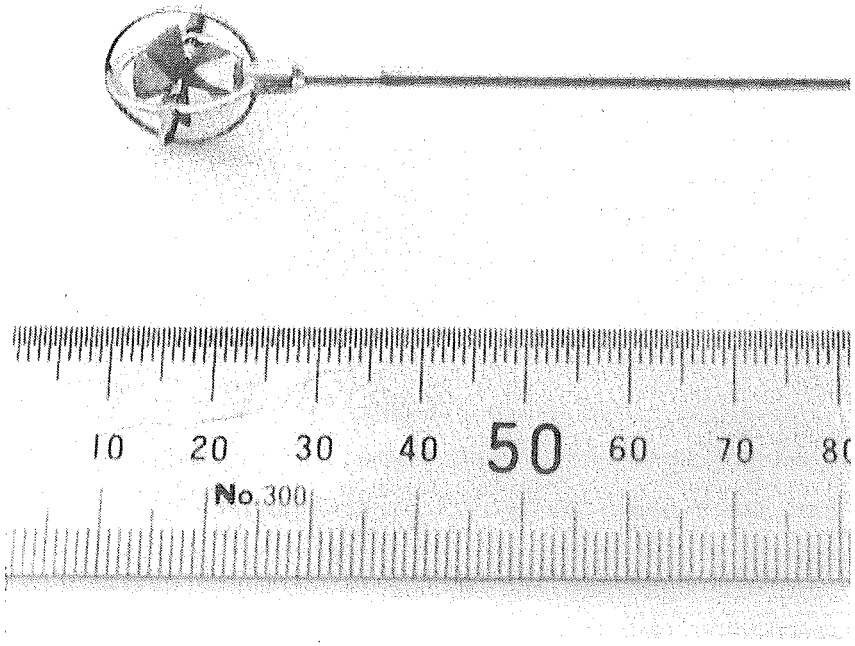

Plate 5.2 : Kent Mini-flow impellor.

in diameter. From the stilling basin at the downstream end of the flume water flows through a series of channels and pits back to the underground sump. Water from the constant head tower may also be discharged into a waste system. Fresh artesian water was pumped from a well serving the Engineering School. Sump water was replaced once a week or when tracer levels become excessive.

For large discharges and hence relatively large amounts of tracer being released into the system, water was continually discharged to waste and fresh water pumped into the sump. This maintained a constant background concentration enabling experiments to be performed continuously for as long as required.

5.5.3 Discharge and Depth Measurements

The inlet valve was graduated and once a flow depth was chosen the valve setting was noted and repeated for each experiment at this depth. The flow depth was measured with a vernier point gauge at at least four locations along the channel to obtain a mean depth for the experiment. Flow measurement was achieved by filling a laboratory calibrated pit over timed intervals. The calibrated pit is in series with the recirculatory system.

5.5.4 Velocity Profiles

Two methods were employed to obtain velocity profiles. A Kent Miniflow impellor-type meter (see plate 5.2) was attached to the movable trolley to produce velocity profiles as desired. The impellor is 15 mm in diameter and could therefore only be used for deeper flows and was unable to measure closer than 8 mm from any boundary. Readings were recorded on a chart recorder.

For shallow flows and as a method of checking the Miniflow meter, velocities were also measured with a pitot tube. The 6 mm outside diameter tube (1.3 mm inside diameter), allowed measurements much closer to the boundaries, and manometer tubes positioned at 15° to the horizontal enabled small changes in velocity to be recorded.

All velocity measurements were taken on separate days from the main experiments by obtaining hydraulic conditions as close as possible to those of a particular experiment. Velocity profiles were measured at two cross-sections and at 50 mm intervals across the flume.

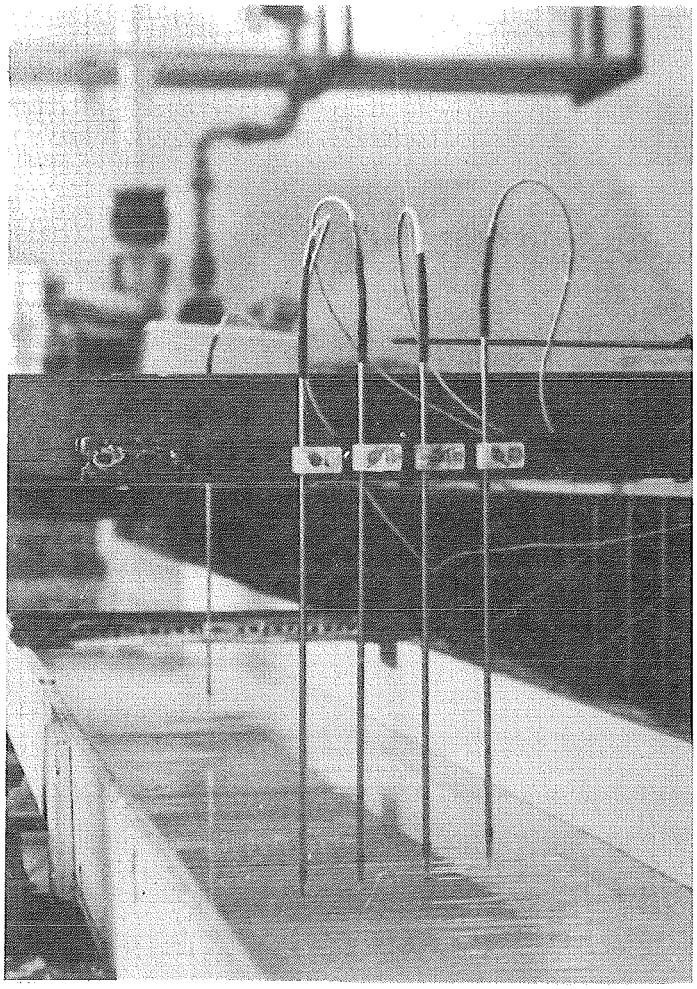

Plate 5.3 : Probes mounted on dexion attached to the moveable trolley.

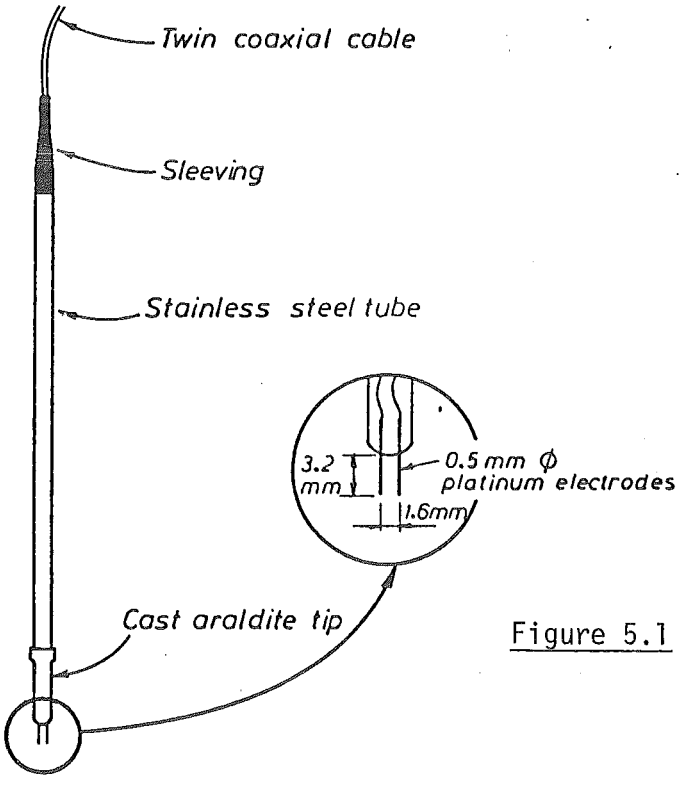

Figure 5.1 : The Conductivity Probe.

5.5.5 Concentration Measurement

The method chosen to record the dispersant movement was a conductivity method. This consisted of a six-channel conductivity meter and a series of probes placed at various points in the flow.

(a) The Meter. The meter used follows a design developed by Iowa Institute of Hydraulic Research (Glover, 1970) to measure the level of conductivity of a solution at a probe due to the presence of an electrolytic tracer material. A detailed description of the requirements of such a meter is given by Valentine (1978). Once the instrument was in use it was left on permanently to eliminate any warm-up period and maintain it under "constant" conditions.

(b) The Probes. All laboratory work was performed using the same probes. These were platinum electrodes (0.5 mm diameter) cast into an araldite tip, which in turn was cast onto the end of a hollow stainless steel tube. These were mounted in small clamps which could be bolted onto a dexion frame (see plate 5.3). The probe tips were identical to previous probes used in conjunction with the conductivity meter, that is, 0.5 mm diameter platinum extending 3.2 mm out of the araldite at a 1.6 mm spacing (see figure 5.1). Probes were tested to ensure that a linear response was obtained for expected operating concentrations.

5.5.6 Recording Equipment

The output from the salinity meter was recorded on the Civil Engineering Data Acquisition System (CEDACS). This system utilises a PDP11/10 computer to control the channel selection and scan rate at which data was collected from instruments. The six conductivity channels were connected to the PDP11/10 via a switch box connected to a digital voltmeter. The Data Acquisition micro processer chip reads a voltage up to 5V from any instrument. There was no data storage on the PDP11/10, so readings were sent by the PDP11/10 to the Departmental PDP11/34. Instructions to the PDP11/10 were issued using a ASR-33 Teletype and those to the PDP11/34 via a VDU Terminal.

There were two analogue to digital converters (A-D converters) attached to the PDP11/10. These were used to read the electrical output of the transducers connected. On command each channel would convert the analogue signal present on their inputs to a digit number, after which the

BLANK PAGE IN ORIGINAL - PART OF PAGINATION

PDP11/10 sent the reading(s) obtained to the PDP11/34. The A-D converter used for these experiments had 256 analogue channels with a 0 to 5 Volt range, which may be altered down to 0 to 5 millivolts, and 12 bit resolution. Technical details of the system are described in CEDACS Users Manual, an internal publication of the University of Canterbury.

Since the data capture system is capable of reading discrete values only (as opposed to the continuous nature of a chart recorder) the appropriate number of readings over a given time period must be determined. The two factors affecting the rate at which data was collected were the limitations of the data capture equipment and the amount of data required to adequately describe the concentration. The basic limitation of CEDACS was the ability of the PDP11/10 to receive and subsequently send information. It was also desirable to collect as little data as necessary so as to reduce handling and storage problems. The amount of data required to satisfactorily determine average concentrations depends on the magnitude and frequency of concentration fluctuations. These may be examined using a chart recorder across the output of the salinity meter. Hence it was possible to deduce the number of readings required per second and duration of record to produce average concentrations. This will vary with distance from the source (fluctuations will decrease in magnitude as the tracer becomes better mixed) and the scan rate was adjusted accordingly.

Once the PDP11/34 had received the data it was stored in a file. At the end of each experiment this data file was saved on floppy disk for permanent storage.

Velocity traces from the Kent Miniflow were recorded on a twin-channel Toa chart recorder.

5.6 Tracer

The electrolytic tracer was a 7.6% solution of common salt (NaCl). Dye was added to this in order to visualise the spread of dispersant. Tracer was made up in batches of about 500 ℓ and was thoroughly mixed before use. It has been shown (Fischer et. al. 1979) that vertical mixing will be independent of density effects if $\frac{B}{z_n u_*^3} < 1$, where $B = (\Delta\rho/\rho)gq$. Taking the worst combination of variables for these experiments $\frac{B}{z_n u_*^3} = 0.25$. Consequently, density effects were neglected.

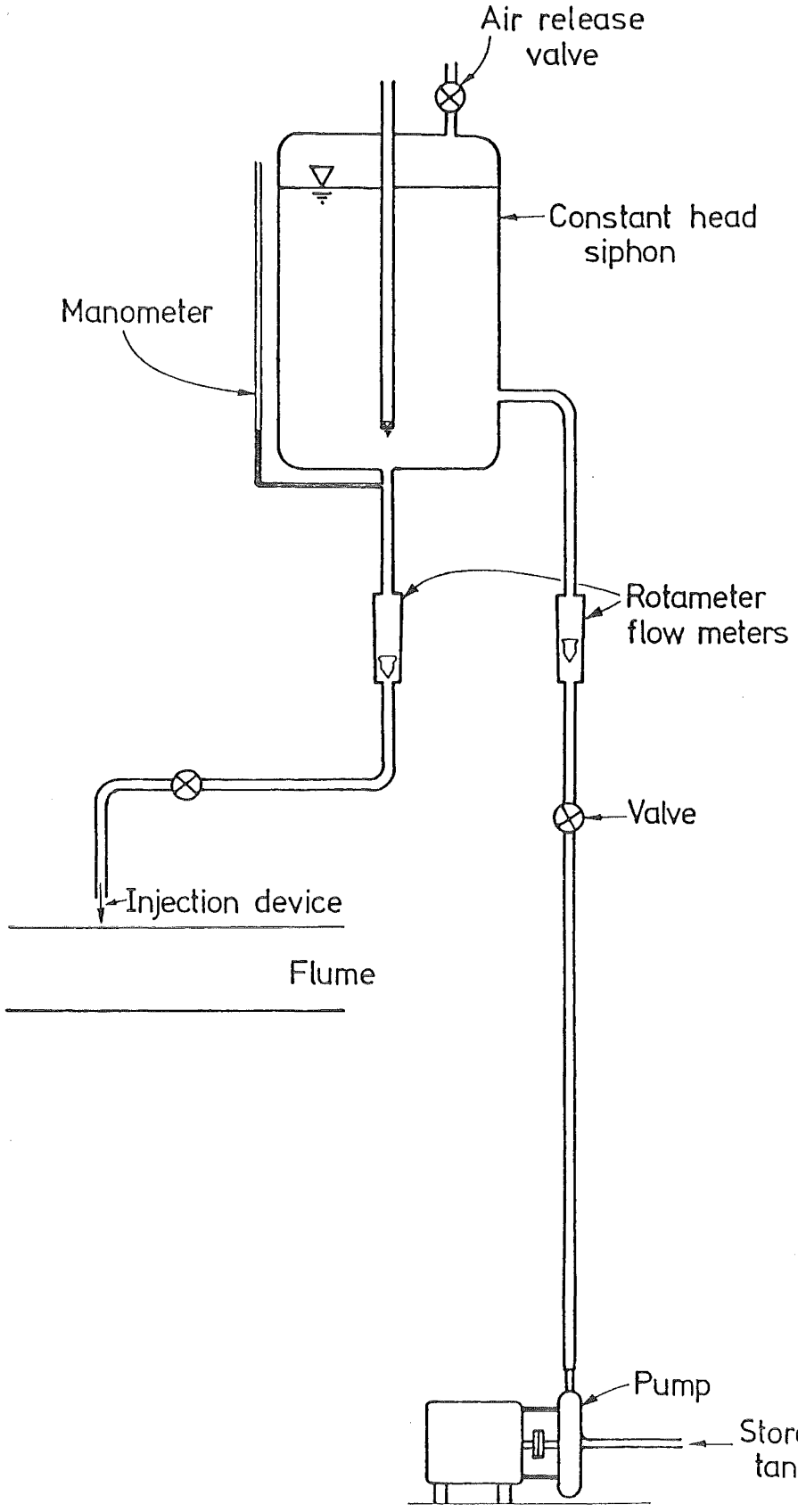

Figure 5.2 : Tracer reticulation equipment (Note: this is a schematic diagram only).

5.7 Tracer Injection

To maintain a constant injection rate a Marriot Syphon placed 2.0 m above the flume bed was employed. Tracer was pumped into the stainless steel tank which has an air release valve at the top, a delivery valve at the bottom and a manometer tube attached to the outlet. The constant head level was determined by a copper tube through the top of the tank, sealed where it entered the tank and open at both ends. Tracer flowed from the constant head tank to one of two devices for releasing the tracer into the mainflow. Figure 5.2 is a schematic diagram of the tracer injection equipment.

The injection of the tracer into the channel was as a line source across the channel at either the surface or in one of the dead zones on the bed. Pollutant releases at other points were not considered owing to the difficulty of obtaining a line source without disturbing the flow. For the surface release an airtight trough was constructed (figure 5.3) with 0.5 mm diameter holes spaced at 5 mm centres. This extended across the complete channel width and was clamped to the flume walls. The trough was positioned such that the downstream edge was continually in contact with the water surface. The second release mechanism was a hollow roughness strip which had 0.5 mm diameter holes at 5 mm centres at the mid-height of the downstream edge of the roughness element. This was attached to the bed at the normal spacing, resulting in tracer being introduced into the eddy behind the element (i.e. the dead zone) as shown in figure 5.4. Tracer was introduced from underneath the flume via a series of plastic tubes placed at 25 mm centres across the bottom of the channel.

Tracer flow for both injection devices was controlled with a valve in the line from the constant head tank. This was set at the beginning of the experiment such that flow was disturbed as little as possible by the tracer whilst maintaining sufficient levels of concentration for detection downstream.

The tracer injection points were at least 2.5 m downstream from the start of the bedforms. This ensured that uniform (steady) flow conditions were well established. This was verified by velocity profile measurements.

5.8 Experimental Procedure

Prior to experiments being performed each channel on the salinity

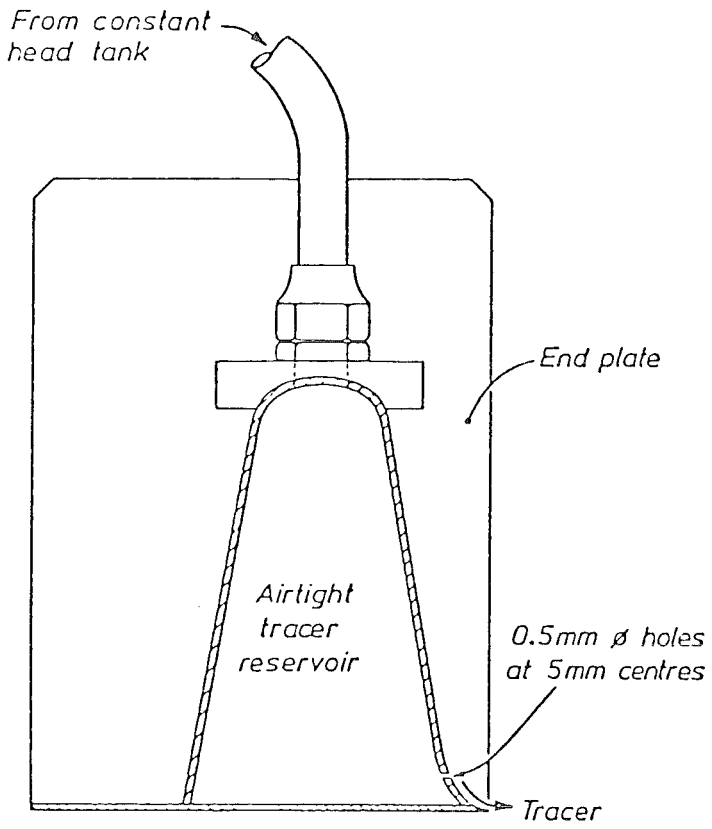

Figure 5.3 : Airtight tracer reservoir for a line source on the surface.

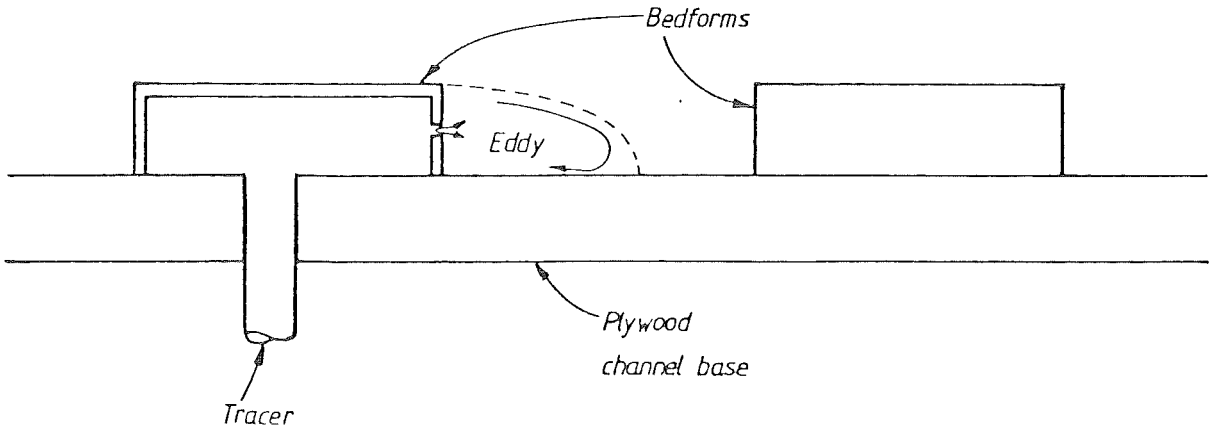

Figure 5.4 : The bed release mechanism; Tracer enters the bedform from tubes at 25 mm centres and exits through 5 mm holes at 5 mm centres in the front face of the bedform.

meter was calibrated against standard solutions. The salinity meter was then installed on an adjacent concrete structure, to avoid vibrations from the movement of the trolley along the flume. Once the instruments were set up, they were switched on and left on for the duration of the experimental programme. This was to eliminate warm-up periods required for some of the equipment.

Before the flow was established, the probes were set at varying heights above the bed. Since the flow conditions were constant across the central region of the channel, probes could be placed side by side at different heights to obtain four concentration profiles from each experiment. The exact height of each probe was measured at this stage and checked at the completion of the run.

Once the probes were arranged, the flow to be examined was established in the flume. Depth and discharge measurements were taken after uniform conditions were reached. For this series of experiments the calibrated pit was used to store contaminated water during an experiment and released into the sump at the end of a run. The recirculating system water was then allowed to mix thoroughly by recirculation prior to the next set of measurements being taken. Sump water was replaced weekly or when background levels of tracer exceeded desirable proportions.

Subsequent to the tracer discharge being established, conductivity measurements could begin. These measurements were generally completed within a period of twenty minutes, over which time flow conditions were essentially constant. Temperature fluctuations were small, normally much less than 1°C.

The initial two sets of conductivity readings taken were calibration readings, firstly with all the probes placed in the flume above the source to give background readings. The second set of conductivity readings were taken with all the probes in a fully mixed sample. This was either in the downstream end of the flume, for cases when mixing was complete at this point or in a trough, with a sample collected from below the stilling basin at the downstream end of the flume. These readings were followed by a set of measurements at twelve to sixteen locations down the flow channel. The number of data points collected depended on the scan rate (number of readings per second) and the duration of each sampling period. These parameters were identical for each channel at any particular sampling location but

BLANK PAGE IN ORIGINAL - PART OF PAGINATION

could be varied between locations. The total amount of data collected was limited by the amount of storage available on floppy disk. It was found that sufficient information could be obtained by scanning at 15 readings per second over 30 seconds for most locations. Lower scan rates were used for background and fully mixed sampling, and locations well downstream from the source (as the tracer approached the fully mixed condition, fluctuations decreased, thus less readings were required to produce the mean concentration value). At all times there were only four probes which were moved from section to section downstream from the source. Of the other two probes available, one was permanently located above the source. This probe gave a continual reading of the background conductivity. The remaining probe was kept in the fully mixed flume water, constantly recording any fluctuations in "fully mixed conductivity". At the completion of the traverse downstream, the initial two sets of readings were repeated. That is, probes were placed in the background and fully mixed flow regions. Immediately, this complete set of readings was transferred to floppy disk for permanent storage.

5.9 Method Of Analysis Of Laboratory Data

Since all experimental data had been stored on the departmental computer, a simple program could be written to read back the stored conductivity measurements. Readings were then averaged over the sampling period to give one mean conductivity reading for each probe for each sampling point. From these results, values of $c_* = c/c_e$ were calculated using the initial two sets of readings (background and equilibrium conductivities for each probe) and the background and equilibrium probe readings to adjust for any fluctuations.

The procedure for adjusting readings at each section requires the probes to be operating within their linear response range. Since this is the case adjustments may be made by simple proportions. For reference background and equilibrium conductivities the first two sets of readings are used.

If the background (upstream) probe fluctuates between readings then each of the remaining five probes is given a new background conductivity. As probes respond linearly then the adjustment to channel i will be

$$\Delta V_i^b = \Delta V_1^b \frac{V_i^e}{V_1^e} \qquad (5.1)$$

BLANK PAGE IN ORIGINAL - PART OF PAGINATION

where ΔV_1^b is the change in background conductivity of the upstream probe and V_1^e is the deflection recorded for the equilibrium concentration on the upstream channel (i.e. V_1^e = fully mixed conductivity - background conductivity on channel 1). Note that V_i^e will be unchanged by a change in background concentration only. Following any background adjustments, the equilibrium deflection on channel 6 is examined and corrections are made if this is not equal to the previously calculated V_6^e.

Again
$$\Delta V_i^e = \Delta V_6^e \frac{V_i^e}{V_6^e} \qquad (5.2)$$

Once equations 5.1 and 5.2 have been applied, non-dimensional concentrations may be calculated from

$$c_{*i} = (\text{Mean Reading}_i - V_i^b)/V_i^e \qquad (5.3)$$

Along with non-dimensional concentrations, the variance and skew were also calculated from individual readings on each channel. These gave an idea of how large concentration fluctuations were.

It was found in some instances that the method used to adjust background and equilibrium concentrations was unable to correctly predict the required adjustments. Typically this was due to the fluctuations of individual channels occurring for no apparent reason. When this did occur corrections could be made manually using the average concentration readings which the data reduction program also produced. These corrections were based on the background and equilibrium concentration measurements made on all probes at the beginning and at the end of an experiment plus the record during the experiment obtained from the background and equilibrium probes. The ability of the built in correction in the data reduction program is evaluated by considering this second set of background and equilibrium concentrations taken at the end of an experiment. If these were found to be 0.0 and 1.0 respectively on each probe then the program has applied all corrections required. Generally this second set of readings agreed within 2% of values expected.

As mentioned in section 5.5.6 the amount of data collected is limited by the computer system utilised. This may cause some deviation from true mean concentration measurements particularly closer to the source where fluctuations in conductivities are larger and more erratic.
The variance of concentration was calculated from the collected data. This was found to be of the order of the actual concentration readings, close to the source, but tends to zero before equilibrium is reached.

BLANK PAGE IN ORIGINAL - PART OF PAGINATION

Unfortunately the equipment used was operating close to its capacity and a more detailed analysis of these fluctuations was not practical.

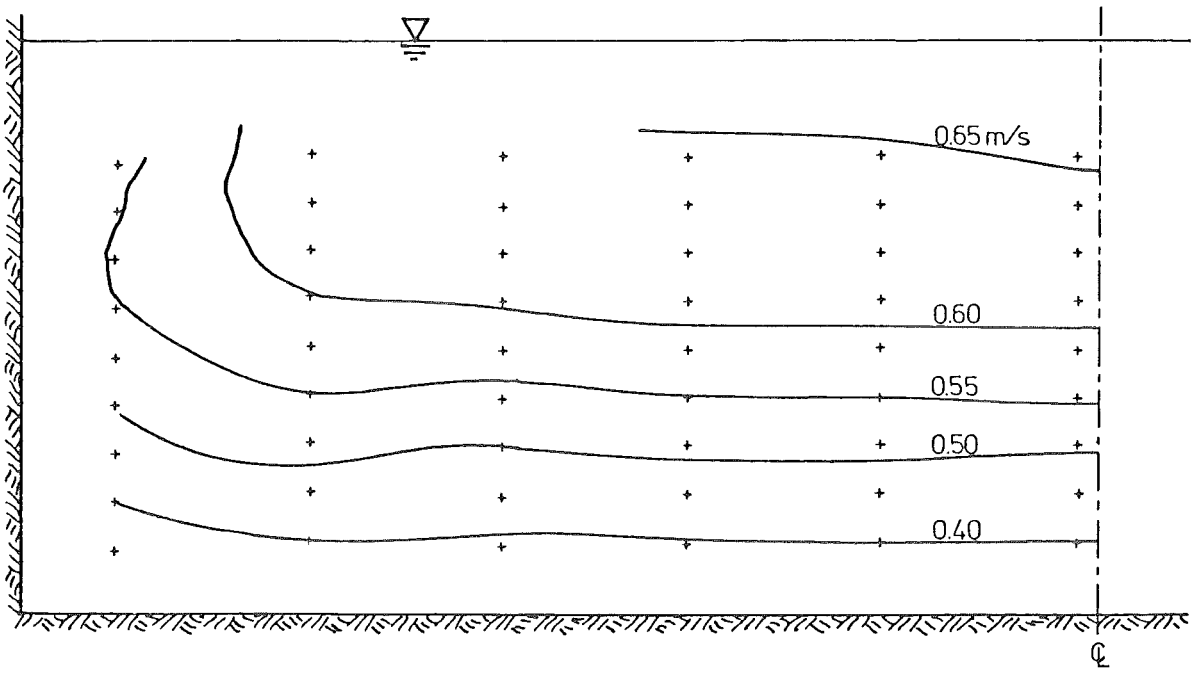

Figure 6.1 : Velocity contours in the laboratory flume for a flow depth of 59.5 mm (flume width = 562.5 mm, + velocity measurement points).

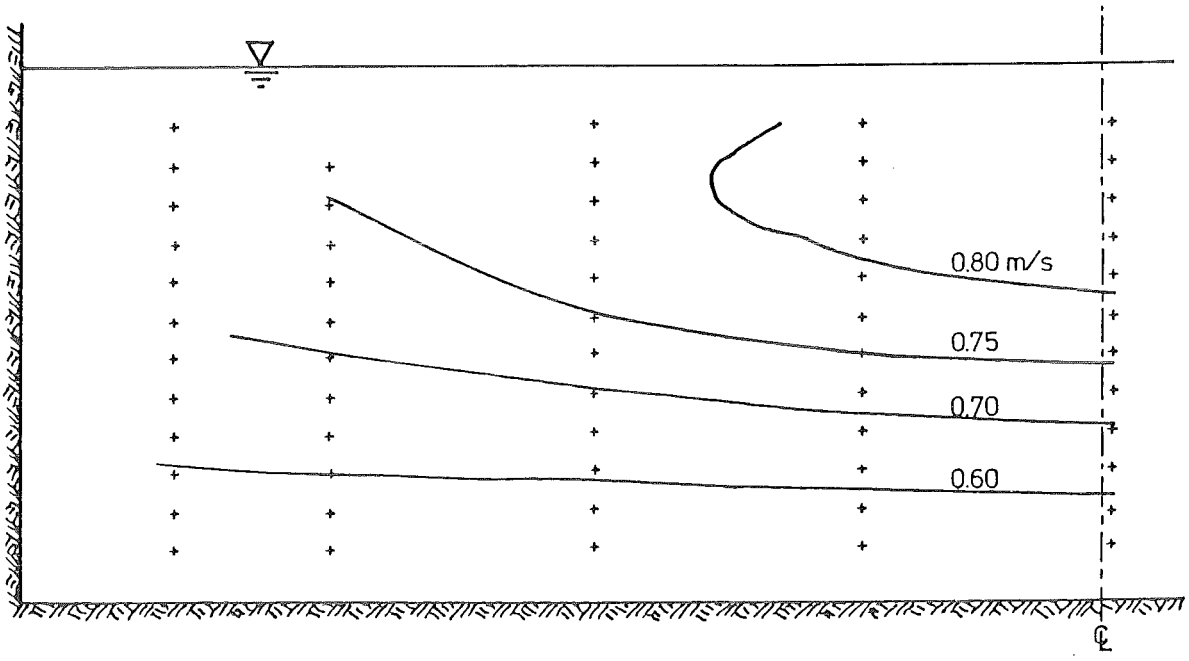

Figure 6.2 : Velocity contours for a flow depth of 72.1 mm (flume width = 562.5 mm, + velocity measurement points).

CHAPTER VI

RESULTS OF LABORATORY EXPERIMENTS AND COMPARISONS WITH PREDICTED NUMERICAL SOLUTIONS

6.1 Summary

The experiments described in the preceding chapter were performed and plots of concentration versus distance are presented. Comparisons are made between experimental data and computed numerical results. The effects of the velocity and diffusivity distribution are discussed and examined using the computer model.

6.2 Data Required for the Application of the Two-Dimensional Model

To obtain a corresponding model solution for each experiment, the appropriate flow parameters must be entered into the computer program. A complete description of an experiment is given by the velocity distribution, the diffusivity distribution and the channel boundary conditions (i.e. the dead zone geometry in these experiments).

6.2.1 Velocity Distributions

Velocity measurements were made with a Kent Miniflow current meter or a 1.3 mm inside diameter pitot tube as described in section 5.5.4. For the two-dimensional experiments sufficient velocity measurements were required to both define the vertical velocity profile and confirm the two-dimensionality of this profile (i.e. transverse velocity gradients are small enough to neglect). Typical plots of velocity distributions over the entire channel are shown in figures 6.1 and 6.2 for mean flow depths of 59.5 mm and 72.1 mm respectively. These contour diagrams were constructed from vertical velocity profiles (e.g. figure 6.3) spaced at 50 mm across the flume. Both diagrams show a limited central region which is approximately two-dimensional. Consequently, conductivity probes were placed as close to the centre of the channel as possible (Probes were staggered over a transverse distance of 30 mm to ensure there was no blocking effect on the flow). Although the effects of transverse velocity gradients are not fully understood, they appear small enough to neglect at the centre of the channel. This assumption would not be

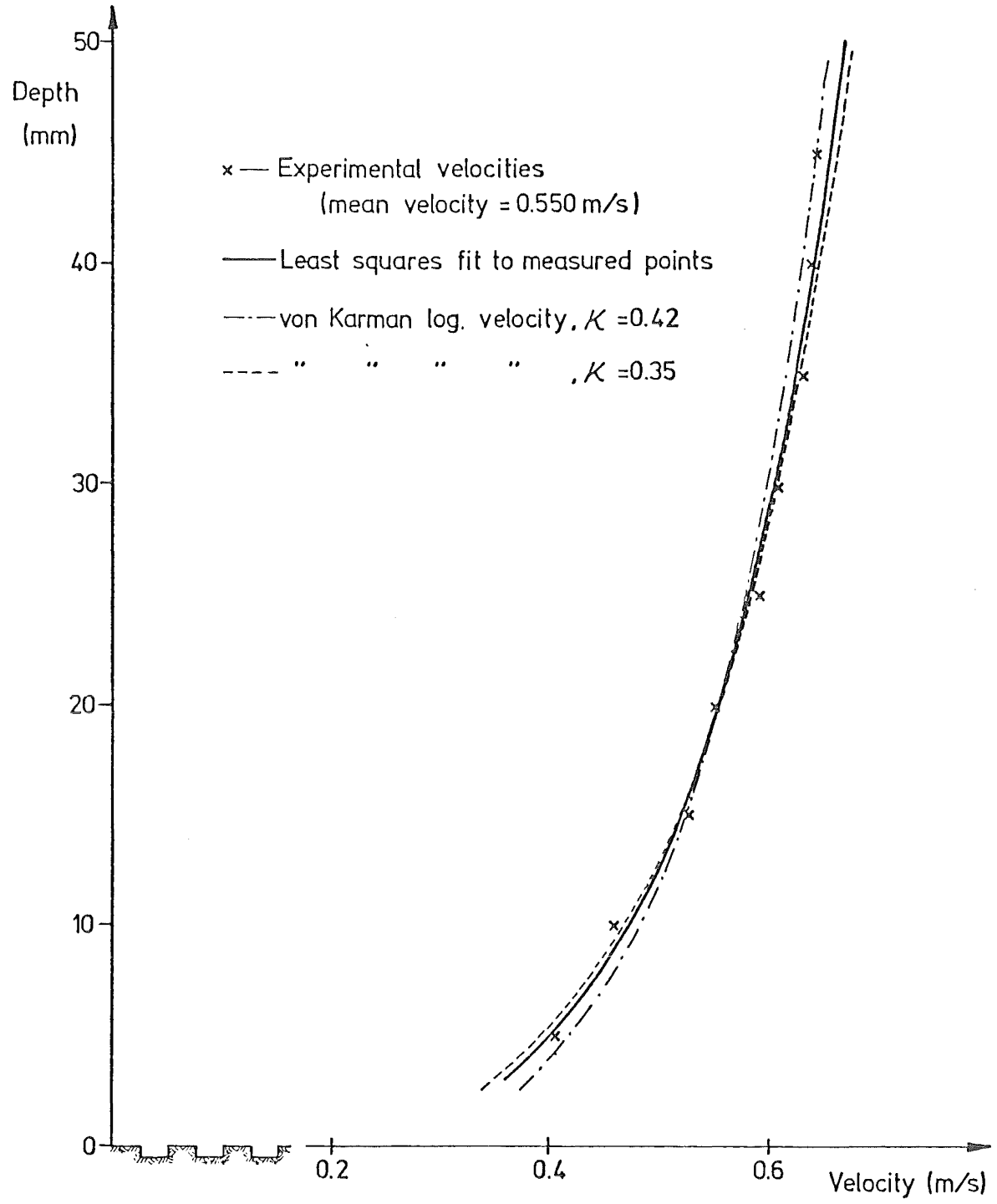

Figure 6.3 : Measured velocity points and fitted logarithmic velocity profiles (Note: bed forms are not to scale).

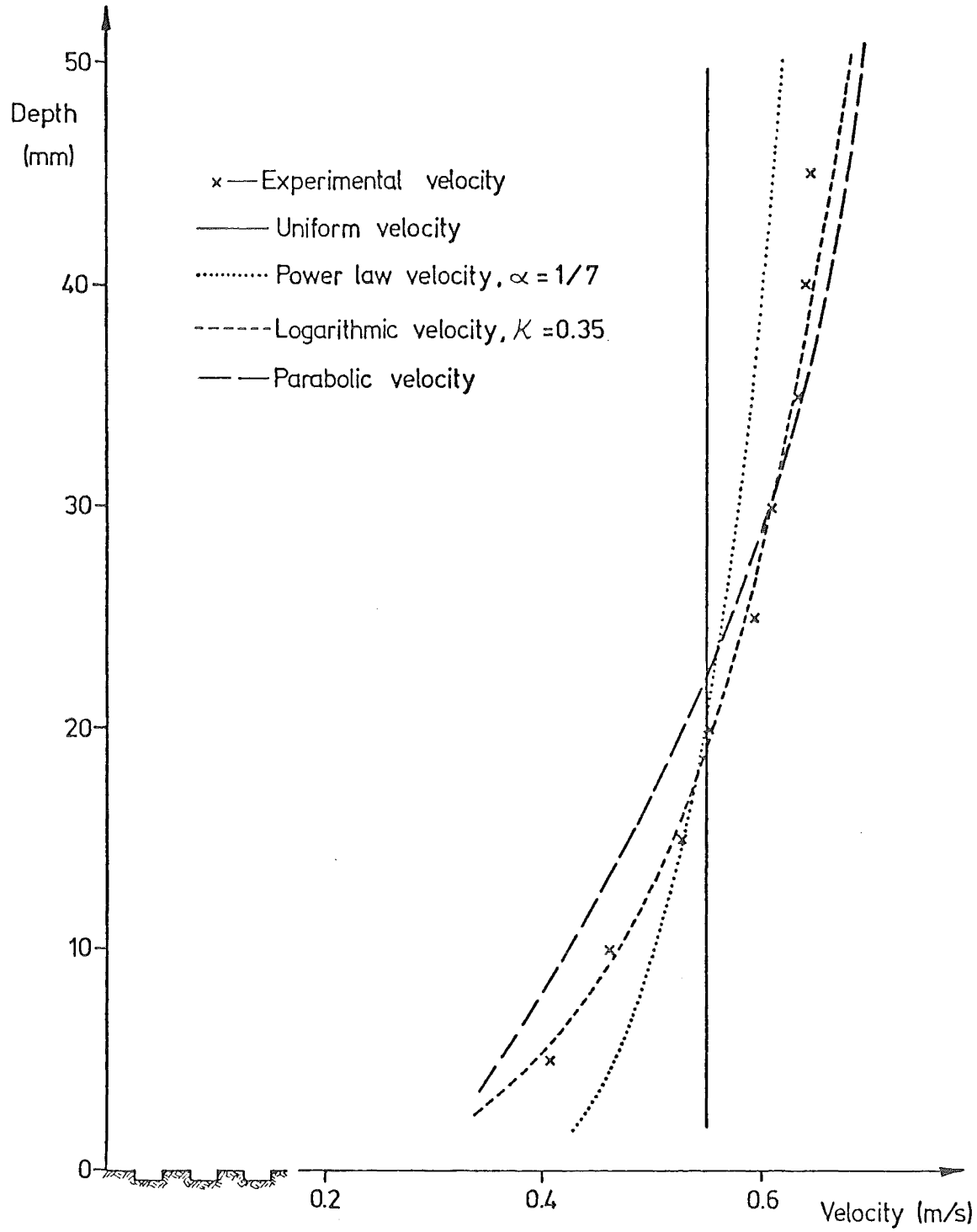

Figure 6.4 : Measured velocity points and available velocity distributions (Note: bed forms are not to scale).

BLANK PAGE IN ORIGINAL - PART OF PAGINATION

valid for flows significantly deeper than that shown in figure 6.2, in the same flume.

Whilst it is desirable to perform experiments in as shallow a flow as possible to obtain two-dimensionality, it is likely that the artificial roughness elements will have more effect on the flow at low depths. This is discussed in section 6.3.

Figure 6.3 depicts one of the central vertical velocity profiles used to plot figure 6.1. Measured points are shown with the solid line representing the least squares logarithmic curve fitted to these points. Also shown are curves for the von Karman logarithmic velocity profile using the appropriate mean velocity with $\kappa = 0.42$ and $\kappa = 0.35$. All of these curves would be appropriate representations of the velocity field in the flume considering the local variation of measured points and the slightly transverse variations. For the model, κ was taken as 0.35 (corresponding to the dotted curve), which is the mean value of κ from measured profiles.

Since the von Karman logarithmic velocity, $u = \bar{u} + \frac{u_*}{\kappa}(\ln\eta + 1)$, closely represents the measured velocity profile (with appropriate coefficients), this may be used to estimate actual values for κ. From measured points, a least squares logarithmic curve is computed in the form $u = a + b\ln\eta$ (where b and a are regression constants). A comparison of this curve with the von Karman distribution suggests $\kappa = \frac{u_*}{b}$ or $\kappa = \frac{u_*}{a - \bar{u}}$. Either of these expressions may be used to estimate von Karman's constant, κ. For the velocity distribution shown in figure 6.3 the best logarithmic fit yields $\kappa = 0.373$.

Section 4.2.1 describes the four available velocity profiles available in the computer model. These alternative velocity forms are compared with measured points in figure 6.4. It is quite apparent from this diagram that the best fit to the measured velocity profile is obtained with the logarithmic type velocity profile.

As discussed in section 5.5.4, the physical dimensions of both velocity measuring devices do not enable velocity measurements to be made within 3.5 mm of the top of the element. Some assumption must be made about the form of the velocity distribution below the measured points. As the flow depth decreases the validity of any assumptions made become more critical since the inaccessible region is constant (approximately

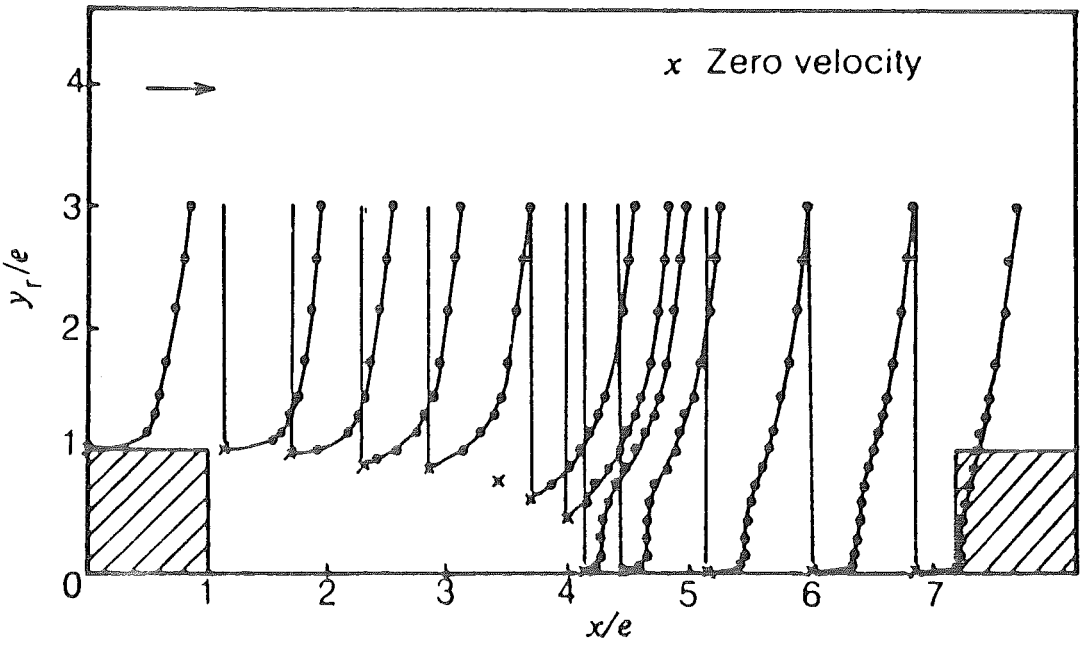

Figure 6.5 : Velocity measurements around rectangular bed forms (Aytekin and Berger (1979)).

7.5 mm above the average bed level). Actual measurments of velocities close to this type of roughness have been presented by previous investigators. An example is shown in figure 6.5 taken directly from Aytekin and Berger (1979). Their investigation showed that the mean flow field does not become independent of ξ until about 1.5 element heights above the crests of the elements (in this study about 10 mm). Obviously, the distribution of velocity shown in figure 6.5 will be the same for each trapping region and consequently the complete velocity field may be described as a periodic function of ξ. This longitudinal variation of velocity could be expressed as a variation about the mean velocity profile, with a vertical decay (as ξ increases away from the bed). However, the application of moment transforms to the initial problem eliminates the longitudinal dimension. Consequently, for the computer model only the average longitudinal conditions are considered (for both velocities and diffusivities). As a first estimate of average flow properties for the particular roughness elements used in this study, the logarithmic velocity profile was taken as extending over the entire channel. The exact location of $u = 0$ is determined by the bed roughness parameters described in the following section.

6.2.2 Turbulent Diffusivity Distributions

Section 4.2.2 outlines the forms of diffusivity that are derived from chosen velocity distributions. Each of the diffusivity profiles described in section 4.2.2 was available in the computer model. Since the logarithmic velocity profile best fits the measured velocities, the related parabolic distribution was used for the vertical turbulent diffusivity. The hydraulic conditions for each particular experiment were employed to calculate the average cross-section diffusivity, D, where D is given by equation 4.7,

$$D = \frac{\kappa}{6} u_* y_n \qquad (6.1)$$

with $u_* = \sqrt{g y_n s_0}$

y_n = mean flow depth

s_0 = channel bed slope

g = gravitational acceleration

The value of κ was taken as 0.35, which was the mean value calculated from experimental measurements of velocities.

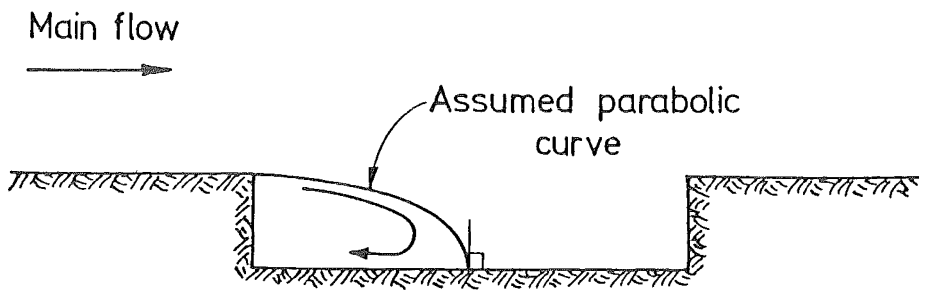

Figure 6.6 : Observed eddy in dead zones. (c.f. eddy in Figure 6.5).

6.2.3 Dead Zone Parameters

The trapping elements used in all experiments were inverted plastic channels with outside dimensions of 20 mm by 7 mm. These elements were centered at 40 mm, resulting in trapping regions 20 mm by 7 mm between elements. This results in 50% of the bed being covered with trapping regions (A = 0.5). As well as the depth of trapping region, DZO, and area covered, A, the parameters required by the model also includes variables which define the eddy properties (section 4.2.4). These are the fraction of dead zone occupied by the eddy, PTZ, and the depth into the dead zone at which u = 0, E. PTZ appears to be independent of the flow depth and has been estimated from dye patterns to be 0.35. This figure is calculated from the re-attachment point of the eddy (from dye movement) and the assumption that the eddy has a parabolic shape. Figure 6.6 illustrates the observed flow pattern.

The remaining parameter, E, was taken as 0.25 following Antonia and Wood (1975) (section 3.4), and previous investigators who found e/DZO to be about 0.125, where e is the shift of the origin into the eddy (in a dimensional form). Since dead zone parameters used in this model are for smeared non-dimensional bedforms, $E = \frac{e}{A \times DZO}$. Hence, for this study, with A = 0.5, the corresponding value of E is 0.25.

6.3 Results of the Two-Dimensional Experiments and Comparisons with Theory

The two-dimensional experiments were performed at three different depths with the source at the surface and the source in a dead zone (injection techniques are described in section 5.7). As expected, low flow depths with the source in a dead zone did not agree with corresponding curves derived using the logarithmic velocity in the model. However, when the nature of the velocity field is known (i.e. at the top of the flow) agreement is very good. This indicates that the assumptions of a logarithmic velocity distribution over the entire section and the smearing of channel bottom conditions do not represent the real situation very well. Since these assumptions do not affect results for source positions at the top of the flow and affect to a lesser extent bottom releases in deep flows, verification of the model is still possible.

Experimental points (●) having been adjusted for equilibrium and background changes, are plotted on computer produced figures of theoretical

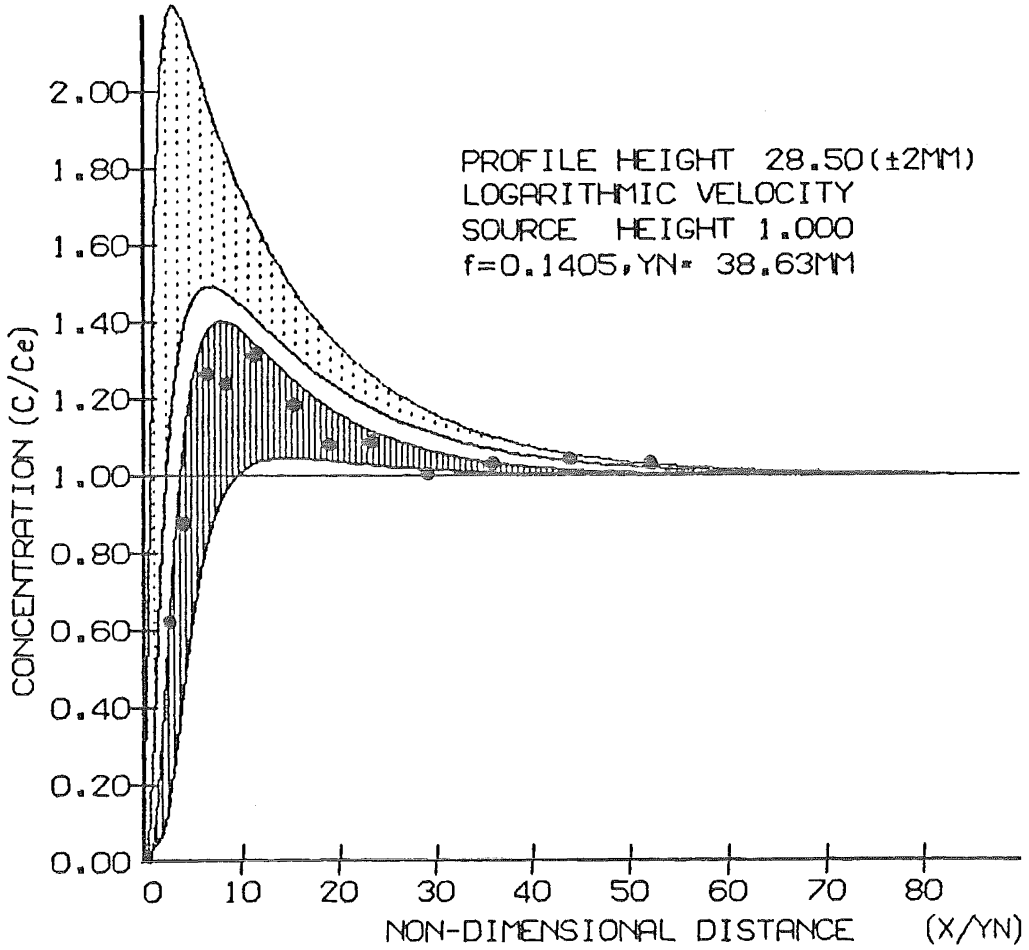

Figure 6.7a : A comparison between the experimental profile and computer predictions (▨ logarithmic velocity, ▧ uniform velocity) for a flow depth of y_n = 38.63 mm.

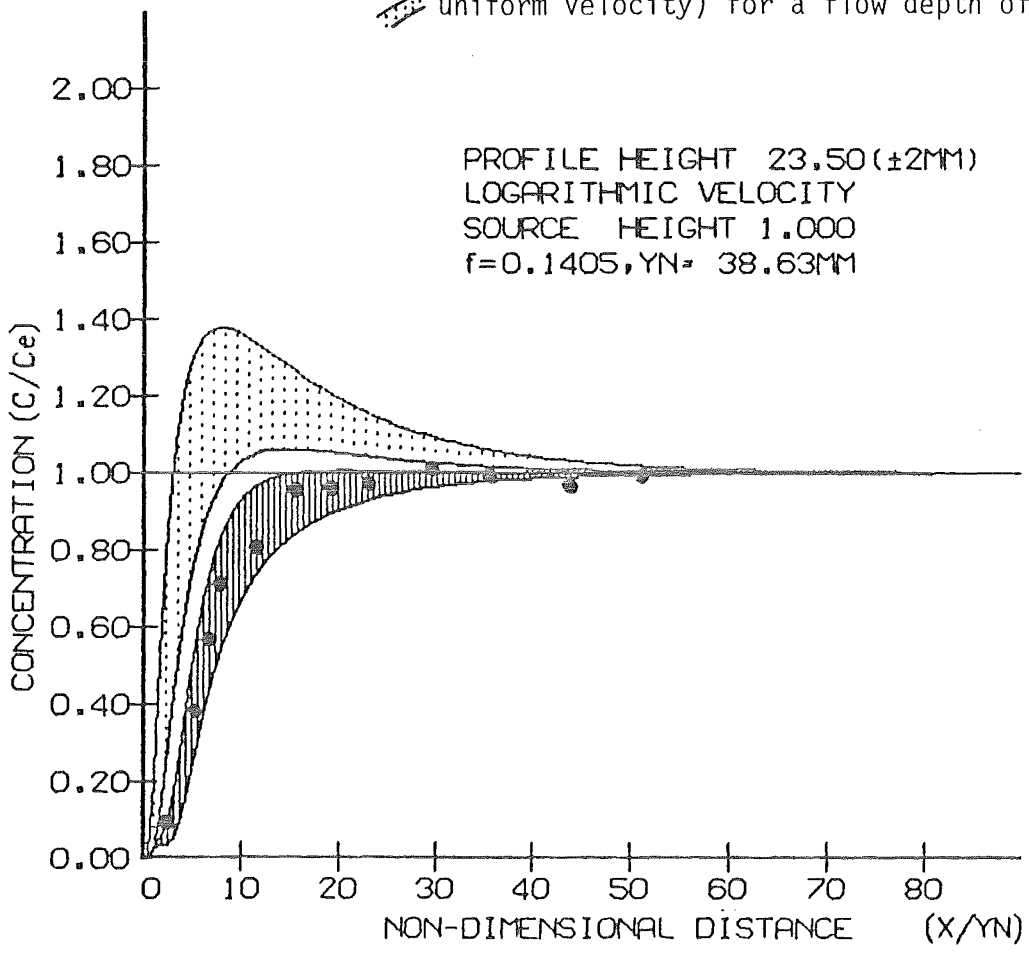

Figure 6.7b.

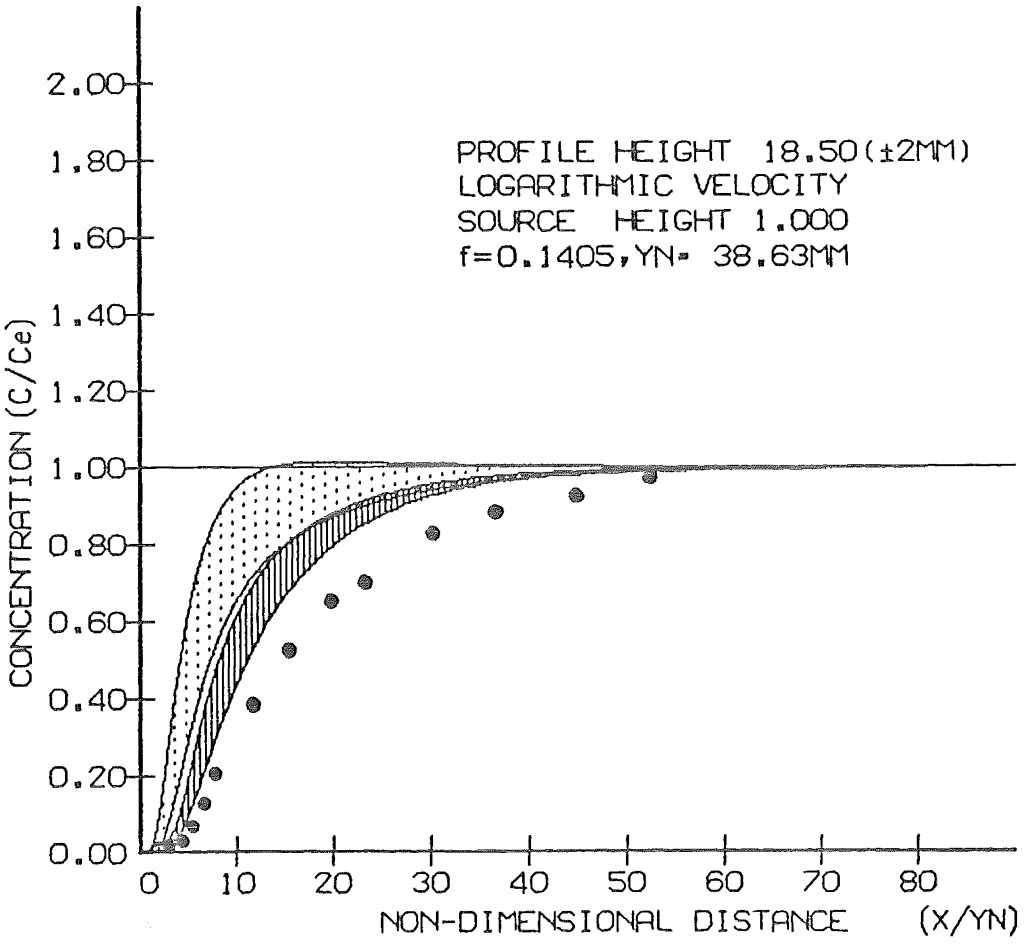

Figure 6.7c.

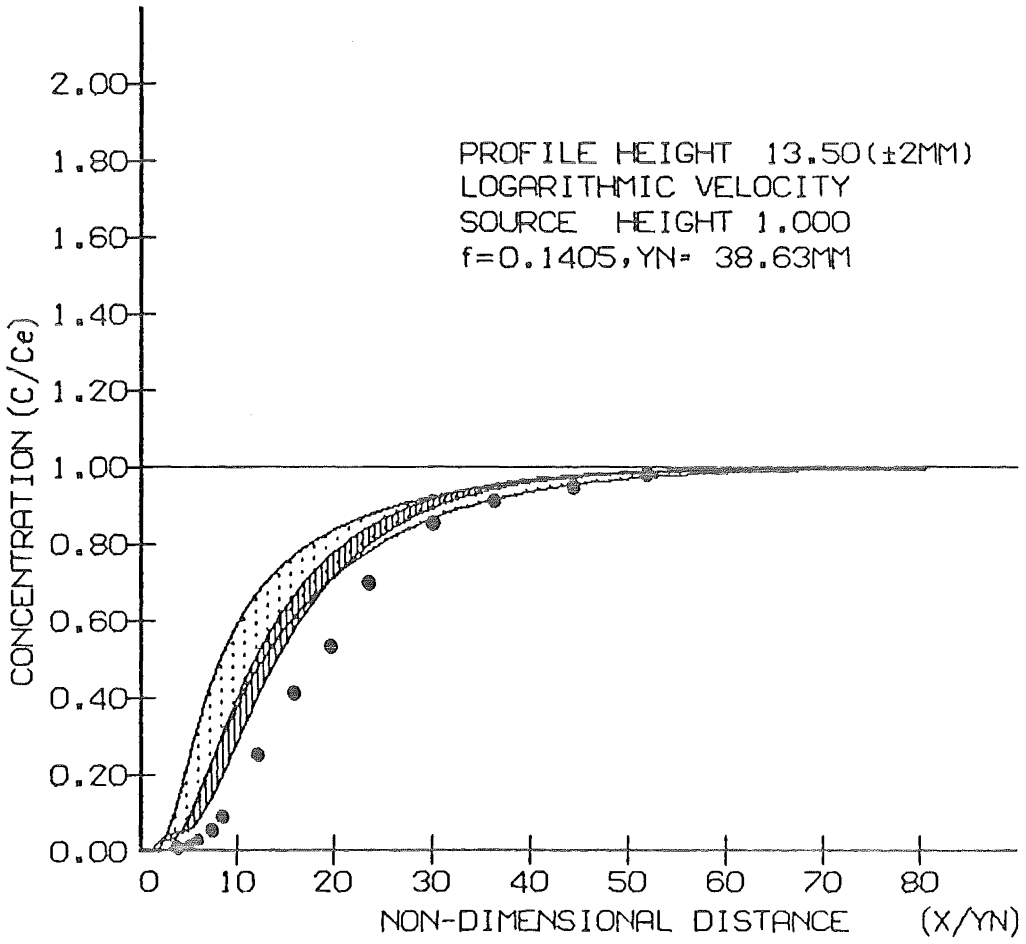

Figure 6.7d.

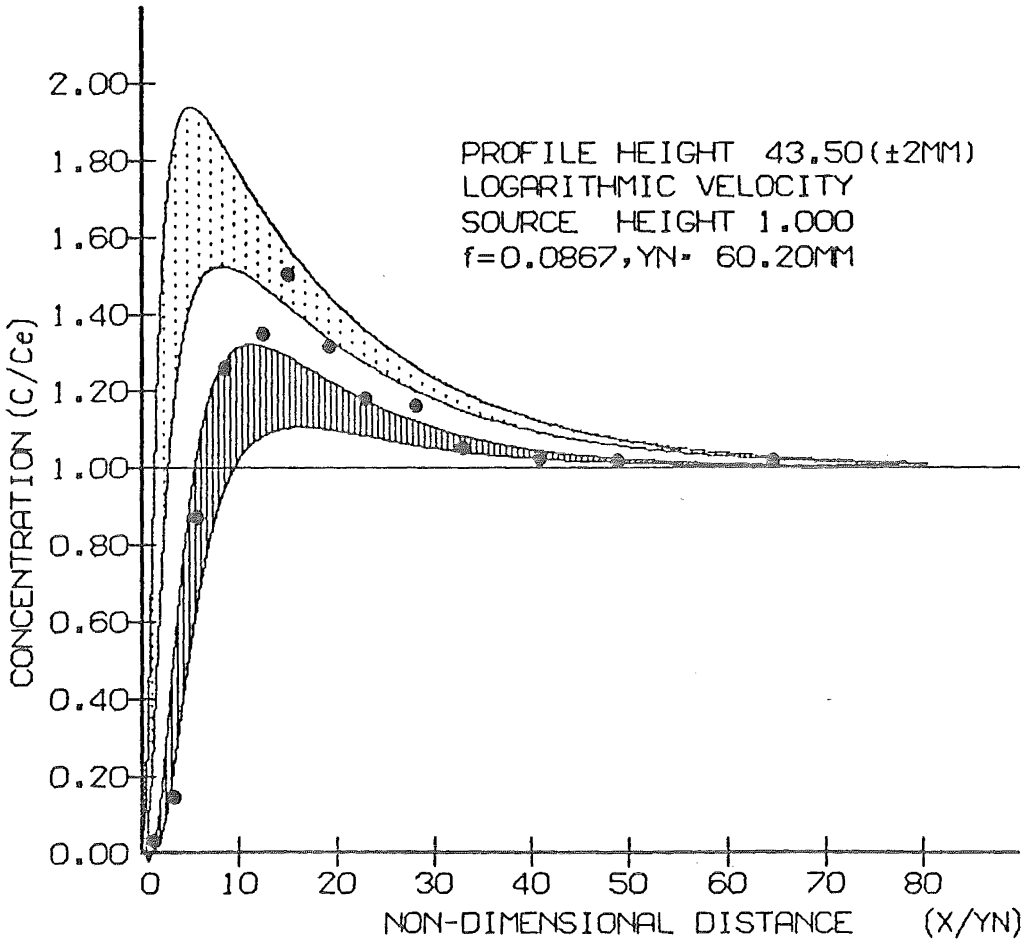

Figure 6.8a : A comparison between the experimental profile and computer predictions (▨ logarithmic velocity, ▩ uniform velocity) for a flow depth of y_n = 60.2 mm.

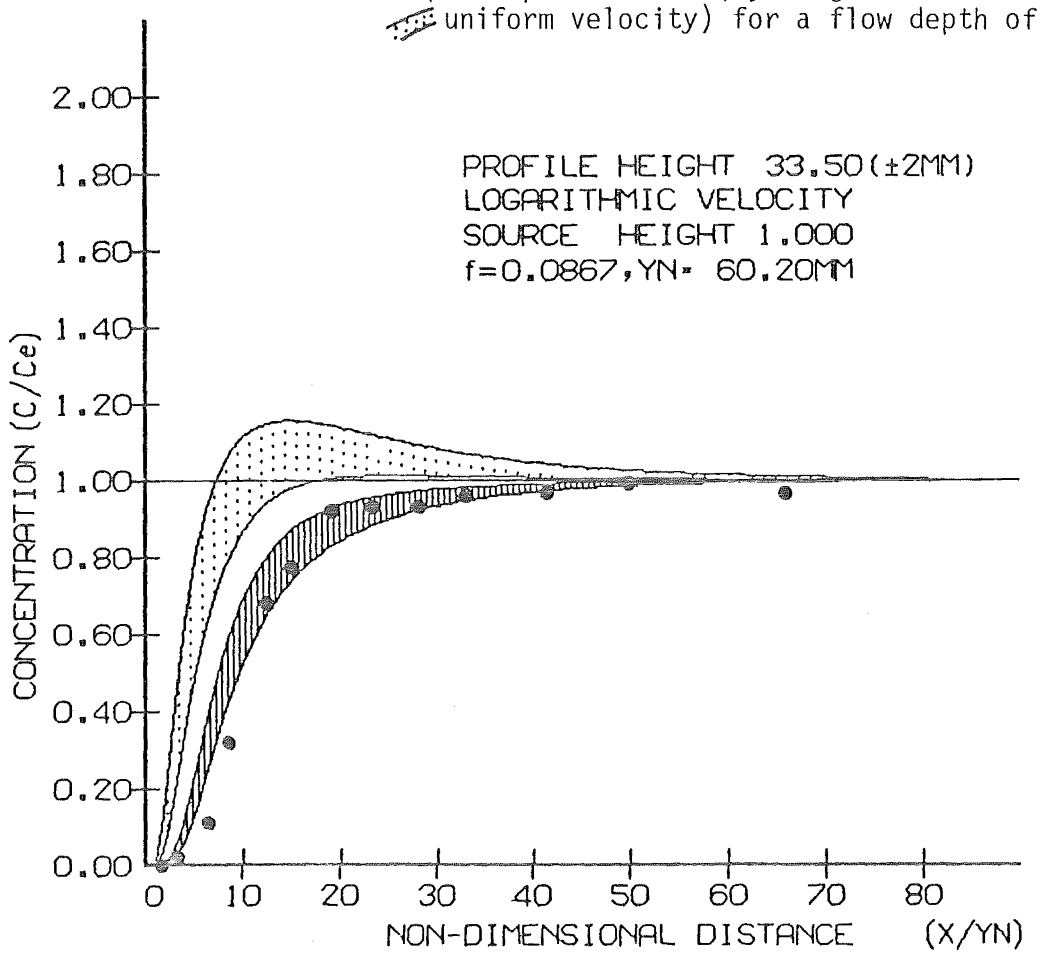

Figure 6.8b.

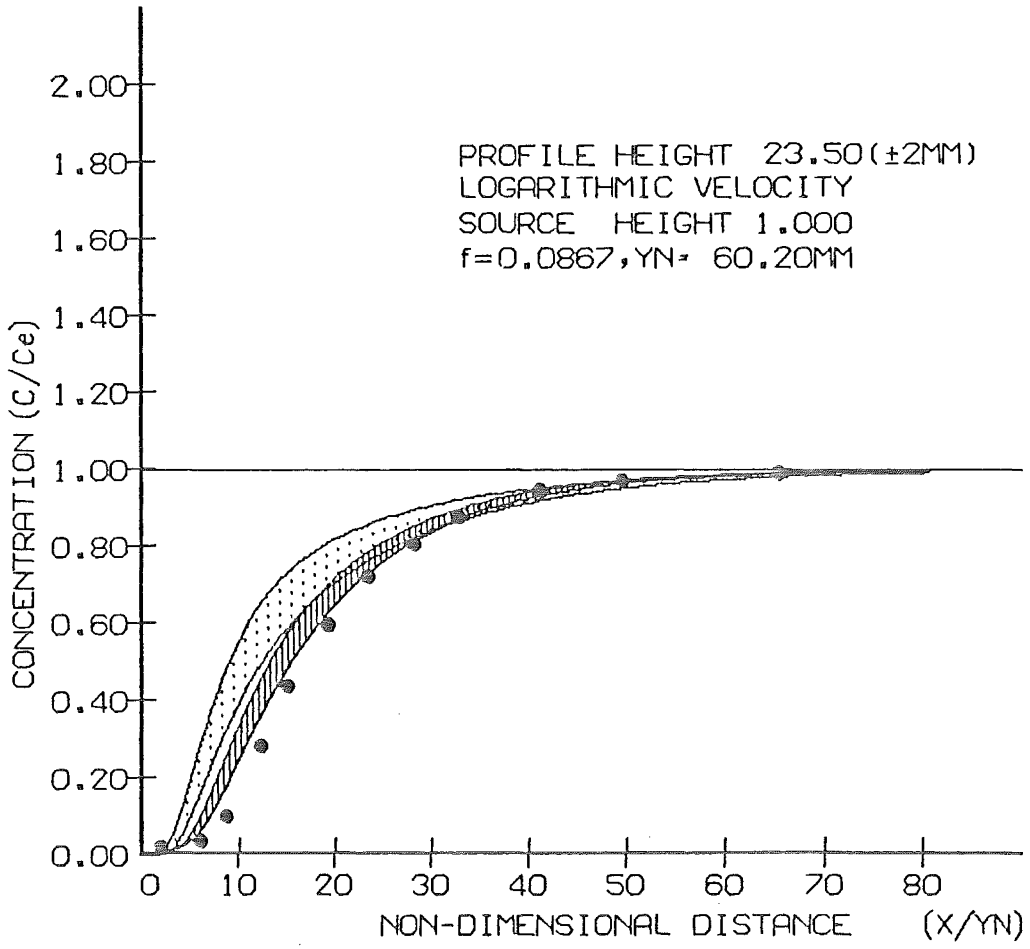

Figure 6.8c.

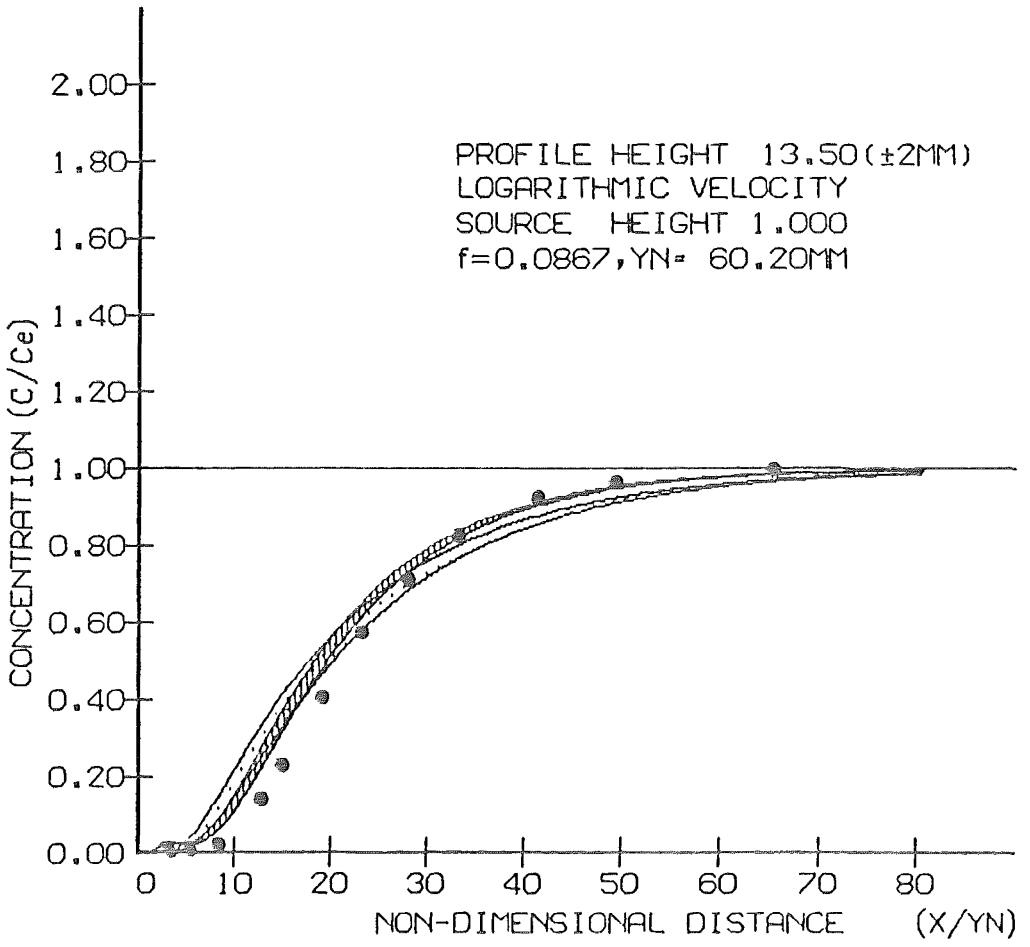

Figure 6.8d.

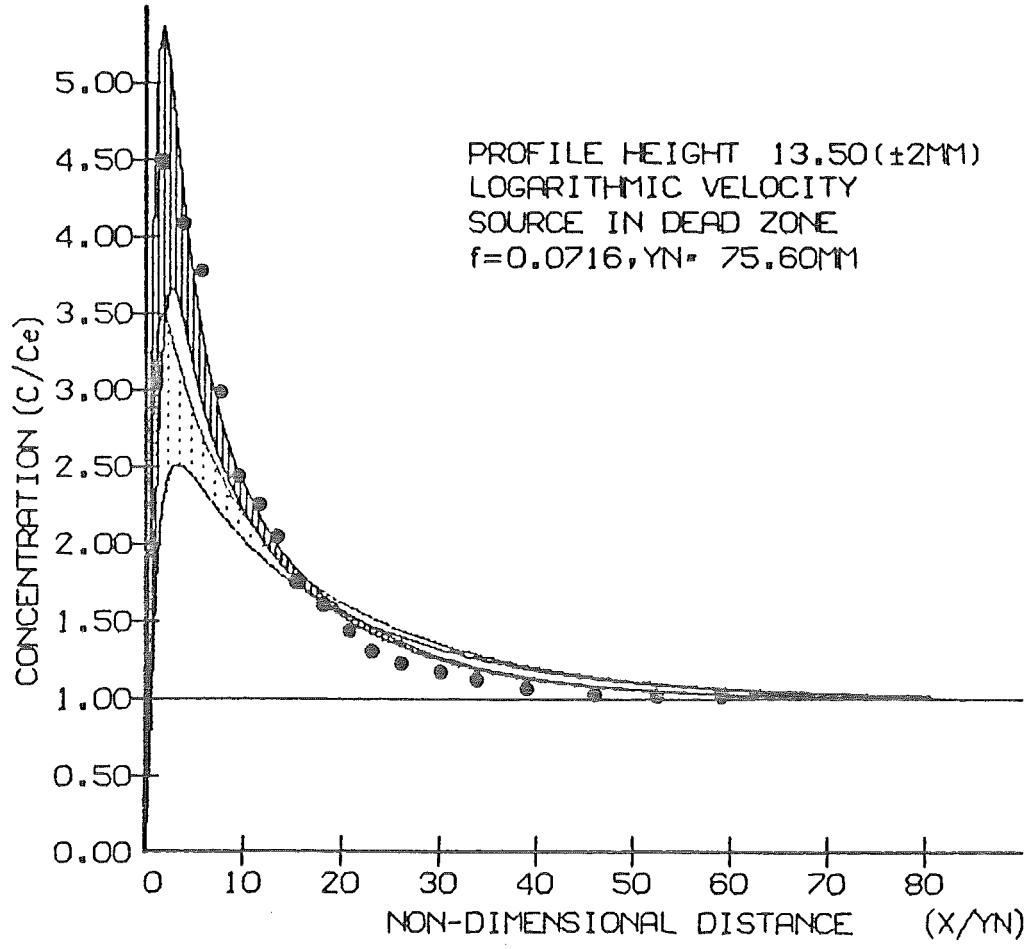

Figure 6.9a : A comparison between the experimental profile and computer predictions (▨ logarithmic velocity, ▩ uniform velocity) for a flow depth of y_n = 75.60 mm.

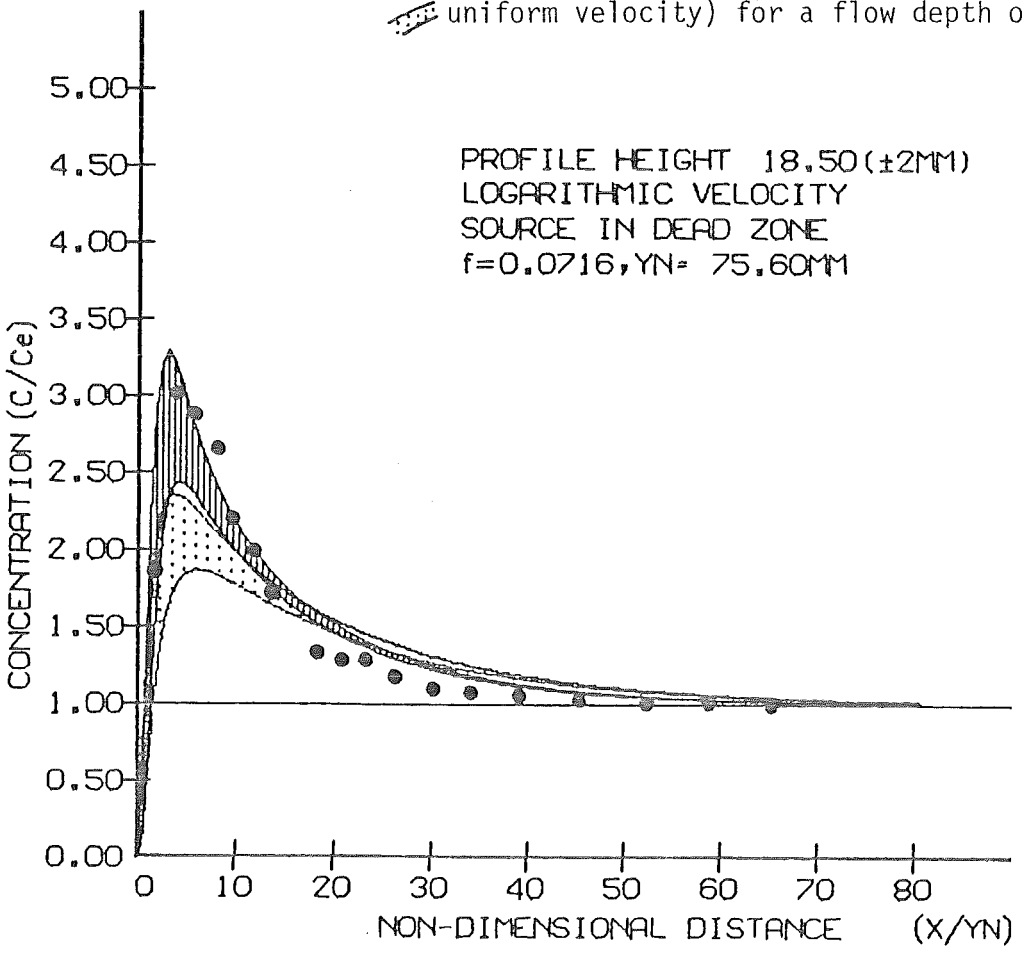

Figure 6.9b.

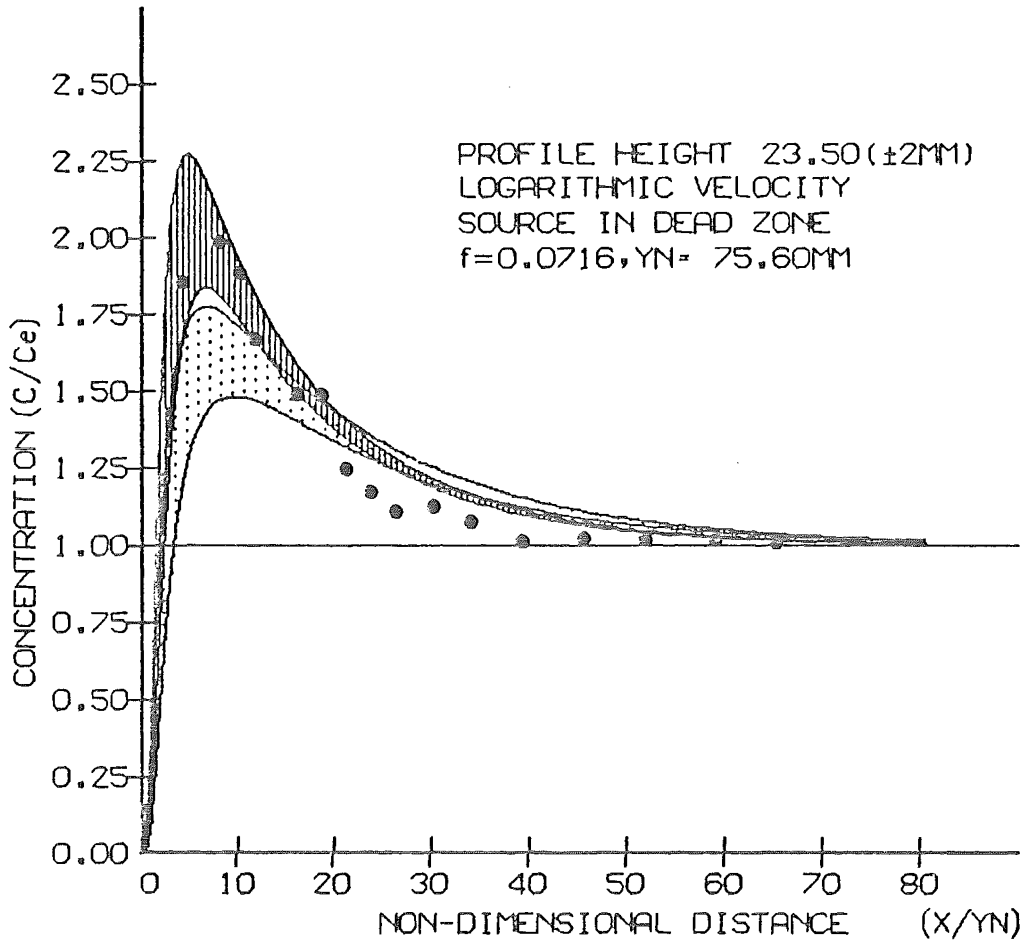

Figure 6.9c.

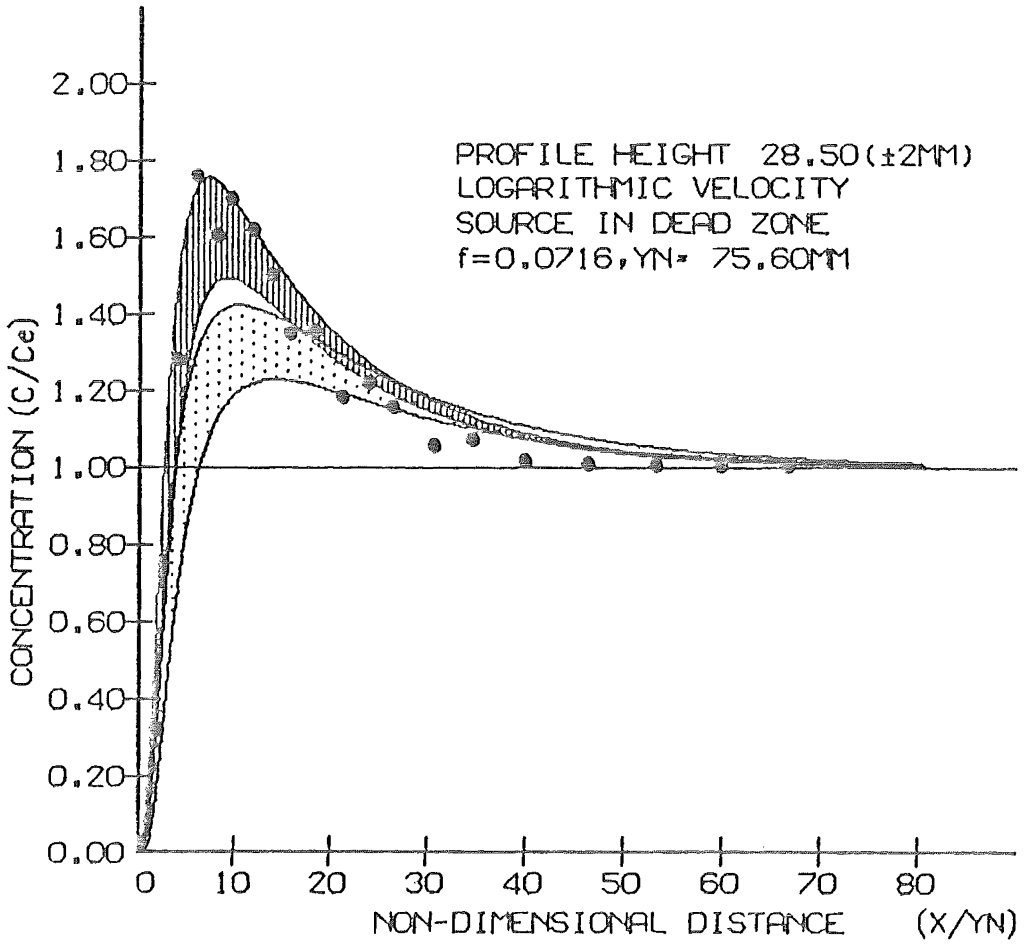

Figure 6.9d.

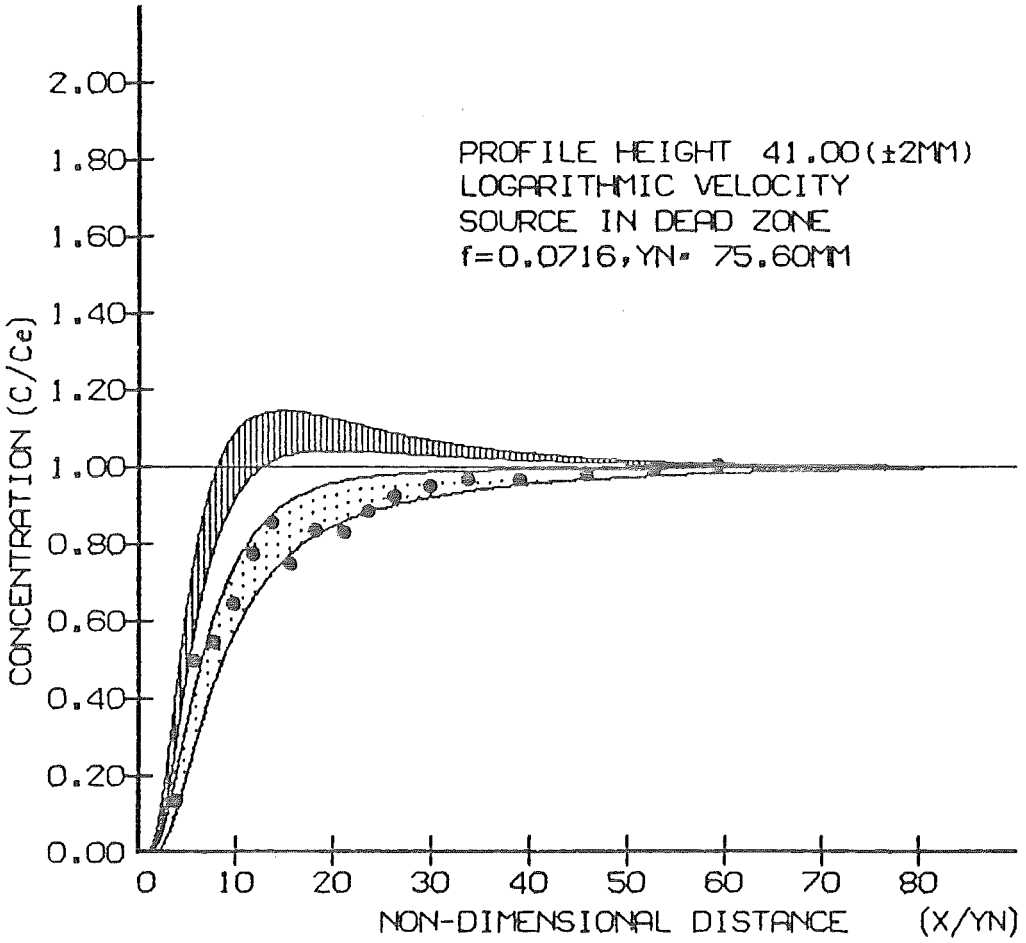

Figure 6.9e.

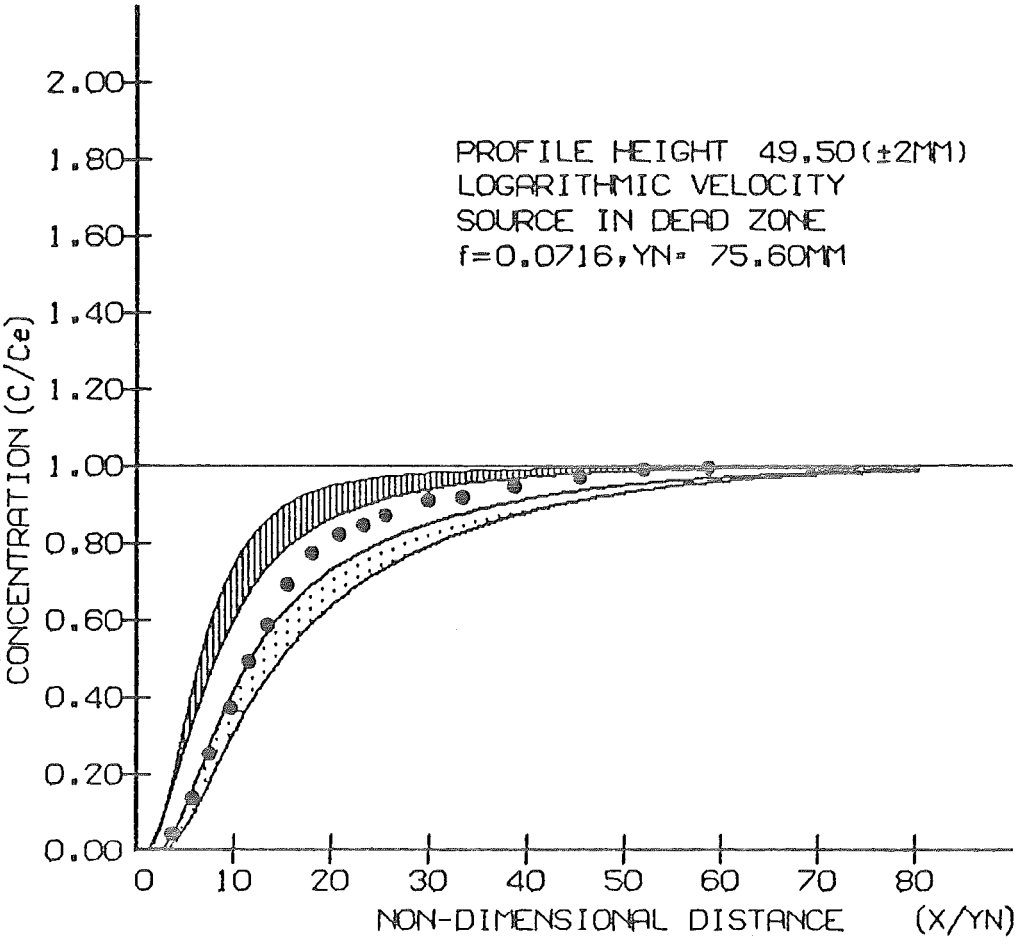

Figure 6.9f.

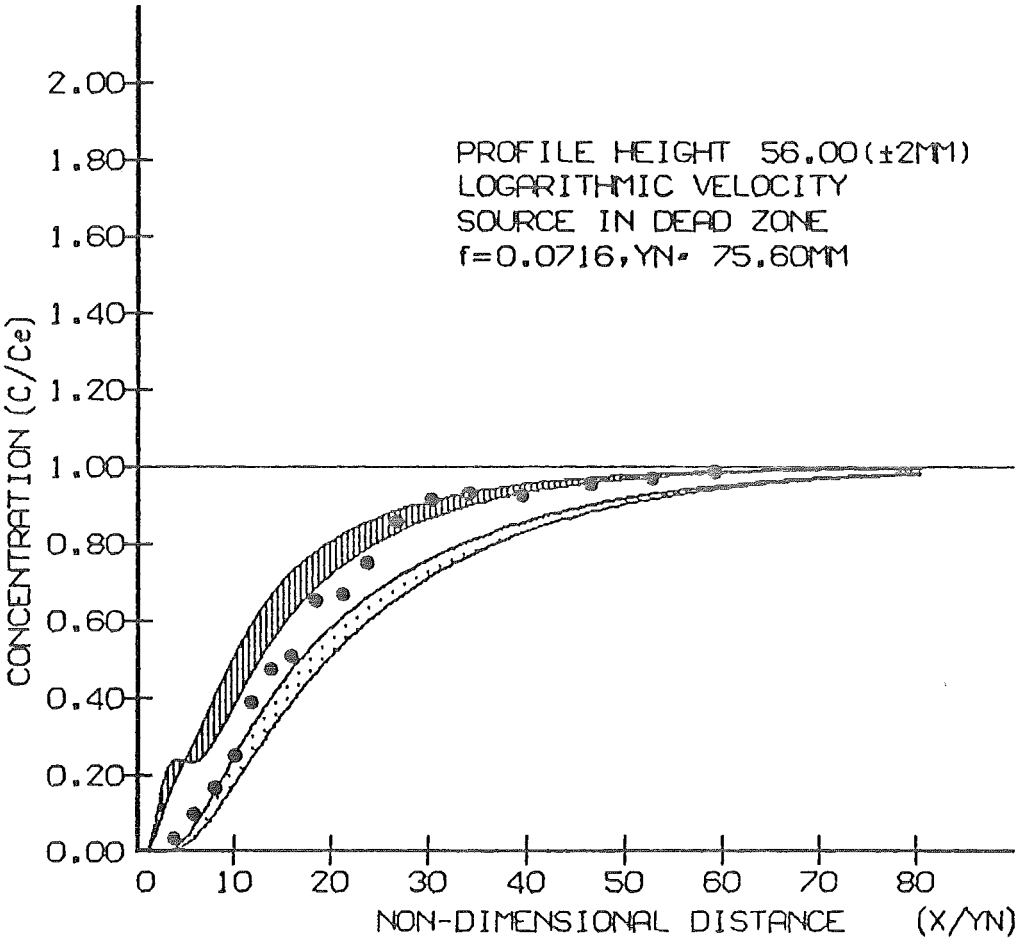
PROFILE HEIGHT 56.00(±2MM)
LOGARITHMIC VELOCITY
SOURCE IN DEAD ZONE
f=0.0716,YN= 75.60MM
CONCENTRATION (C/Ce)
2.00
1.80
1.60
1.40
1.20
1.00
0.80
0.60
0.40
0.20
0.00
0
10
20
30
40
50
60
70
80
NON-DIMENSIONAL DISTANCE (X/YN)

Figure 6.9g.

BLANK PAGE IN ORIGINAL - PART OF PAGINATION

curves. These plots are shown in figures 6.7 - 6.9. The two shaded regions shown in each plot correspond to theoretical concentration profiles for a logarithmic velocity distribution () and a uniform velocity distribution (). The bounds of each region are given by profiles at 2 mm either side of the measured probe height, representing the accuracy to which the probe height may be determined. Errors in locating the probes arise from fluctuations in the bed position ($\pm$ 1 mm), measurement of the probe height ($\pm$ 0.5 mm) and fluctuations of the water surface ($\pm$ 1 mm). It should also be recalled that the probes themselves have tips which will cover from 1 - 3 mm vertically, depending on the probe slope. The probe height was taken at the centre of the electrodes.

At the shallowest flow depth (y_n = 38.63 mm), shown in figures 6.7, measured points conform well with the predicted concentrations from the logarithmic velocity distribution for profiles at the top of the flow. The bottom two profiles do not match the logarithmic type profile as well, but the log-type concentration profile is a better prediction than that obtained with a uniform velocity field. When the flow depth is increased, the overall agreement between measured points and the log-type concentration predictions improves. This is illustrated by figures 6.8 where agreement is very good for each of the measured profiles.

Figures 6.9 shows the profile for the deepest two-dimensional flow, with the source in a dead zone. Measured peak concentrations are as predicted from the logarithmic velocity curves and for the four profiles closest to the source, measured points are always closer to the logarithmic curves than the uniform predictions. Moving further away from the source, agreement with the logarithmic curves is not as apparent. Figure 6.9e shows measured points matching the uniform predicted curves. This appears to be a transition region where measured profiles tend to the equilibrium concentration quickly, between the extremes observed close to the source and well away from the source. Still further from the source measured points tend more towards the logarithmic predictions. Since the actual velocity distribution is not defined exactly for the computer model, and most of the disagreement with the actual velocity will occur around the dead zones it would be unreasonable to expect as good agreement in this situation as for a surface release. Unfortunately a surface release experiment was not practical at this depth. This was due to the fluctuations in the water surface. If these fluctuations are to be removed, restraints must be placed on the water surface, resulting in a restricted

BLANK PAGE IN ORIGINAL - PART OF PAGINATION

surface velocity.

6.4 Conclusions

The aim of the two-dimensional experiments performed was to verify the model developed in chapter 3. The model is capable of using any velocity/diffusivity distributions desired. In order to ensure two-dimensionality in the laboratory experiments it was necessary to eliminate the possibility of secondary currents. This was achieved by placing roughness strips on the channel bed to promote vertical eddies. The inclusion of the roughnesses introduced trapping regions into the flow, resulting in changed boundary conditions on the channel bed. Velocity measurements show good agreement with the expected logarithmic velocity profile, however measurements are not possible closer than 3.5 mm from the crests of roughness elements. The use of the logarithmic velocity distribution in the model appears more appropriate for deeper flows where the influence of the dead zones is not as significant. Better agreement is also noted with the source at the surface rather than in the bed, again attributable to the unknown velocity field near the dead zones. These two trends infer the validity of the model if the correct velocity distribution is used for two-dimensional flow.

BLANK PAGE IN ORIGINAL - PART OF PAGINATION

CHAPTER VII

FIELD EXPERIMENTS: TECHNIQUES AND APPARATUS

7.1 Summary

This chapter outlines the rationale for the field experiments and the choice of reaches in which this work was performed. The apparatus employed is described and a typical field experimental procedure is given.

7.2 The Aims of the Field Experiments

A series of experiments were designed to extend the laboratory work to a field situation. The aims of these field experiments are as follows:

(a) To test the applicability of laboratory experiments to a similar channel shape but with natural bed conditions.

(b) To provide data which could be used to test and calibrate the computer model qualitatively.

(c) To examine a range of channel conditions from relatively smooth channels (which are similar to the laboratory channel) to rough channels with very turbulent flow. This will enable the effects of the channel bed conditions to be examined.

7.3 The Test Reaches

For the field experiments, it was necessary to consider a range of flow conditions and channels. Initial work was performed in an irrigation race since this was as similar to the laboratory channel as possible. This would enable a comparison between the artificial roughnesses used in the laboratory flume and the natural roughness of a geometrically similar channel without complications from sinuosity and streamwise flow. In particular, the factors influencing the choice of the first test reach were,

(a) A straight channel with as little as possible secondary flow effects (such as a meandering thalweg).

(b) Uniform flow conditions over the test reach. Ideally, a suitable channel would have a uniform slope, no variation in the cross-

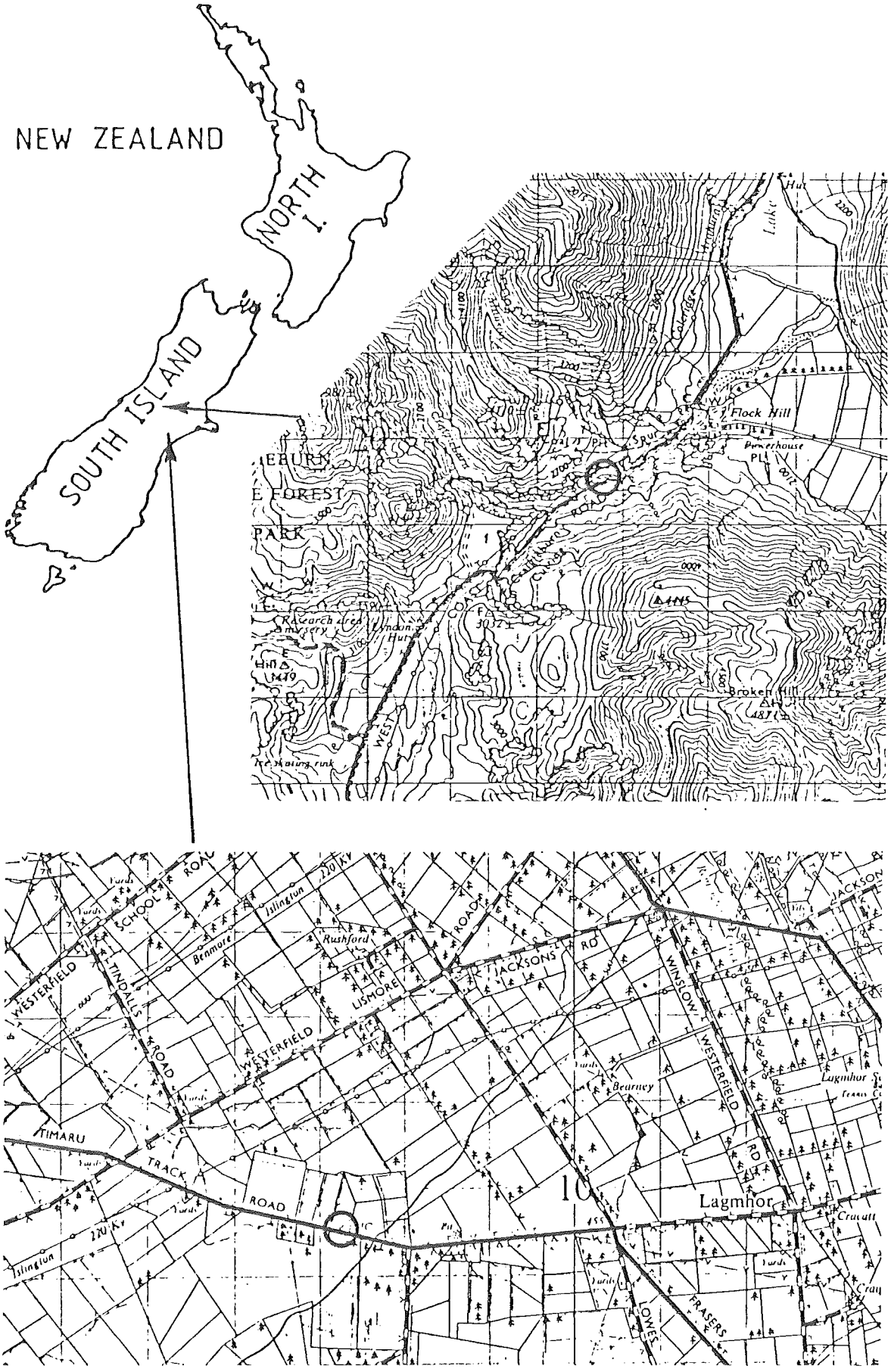

Figure 7.1 : Location maps for field experimental channels. The Craigieburn River section is marked on the top map and the lower map locates the irrigation channel.

(b) Cont. section along the reach and no fluctuation in flow rate during experiments.

(c) A channel that can easily be gauged and waded for sampling. This limits the size of the channel and the discharge. If the channel is not wadeable both the manpower and equipment required increases beyond that available for initial field work.

(d) The reach should be accessible by vehicle such that a trailer on which the injection tank rests may be placed as close to the injection point as possible.

This first test reach was located in Mid-Canterbury in one of the numerous man-made irrigation channels that are found on the Canterbury plains. These races are fed from the rivers of the Southern Alps via control structures. This particular water race, located in figure 7.1, is approximately 100 km from Christchurch and is fed by the Ashburton River. The flow rate varied from 0.8 - 1.0 m^3/s but was constant during any experiment. As seen in plate 7.1, the flow width is approximately constant (~ 3.2 m) and the race is essentially straight over the 130 m in which measurements were taken.

The Craigieburn River provided the second test reach in which a series of experiments was performed. This river is in the foothills of the Southern Alps (figure 7.1), about 110 km from Christchurch, and has bed conditions typical of the small mountain streams of the region. A typical section of channel is illustrated in plate 7.2. The average channel width is 4.1 m and the discharge varied from .25 m^3/s to .4 m^3/s. Measurements were taken over a reasonably straight 30 m section of the river.

For both reaches sampling sections were set out at positions located by taping from the injection point. The slope of the channel and channel cross-sections at each sampling section, were taken from a levelling exercise performed at both reaches. Sampling sections were marked with a string across the channel. Markers were placed on each string to indicate the transverse location of a sampling point. Typically there would be seven such sampling points at each sampling section.

Bed roughness conditions were examined using the Wolman Sampling technique (Wolman, 1954). This method of sampling the bed material aims to give a grain size distribution that is representative of the entire

Plate 7.1 : The Irrigation Canal.

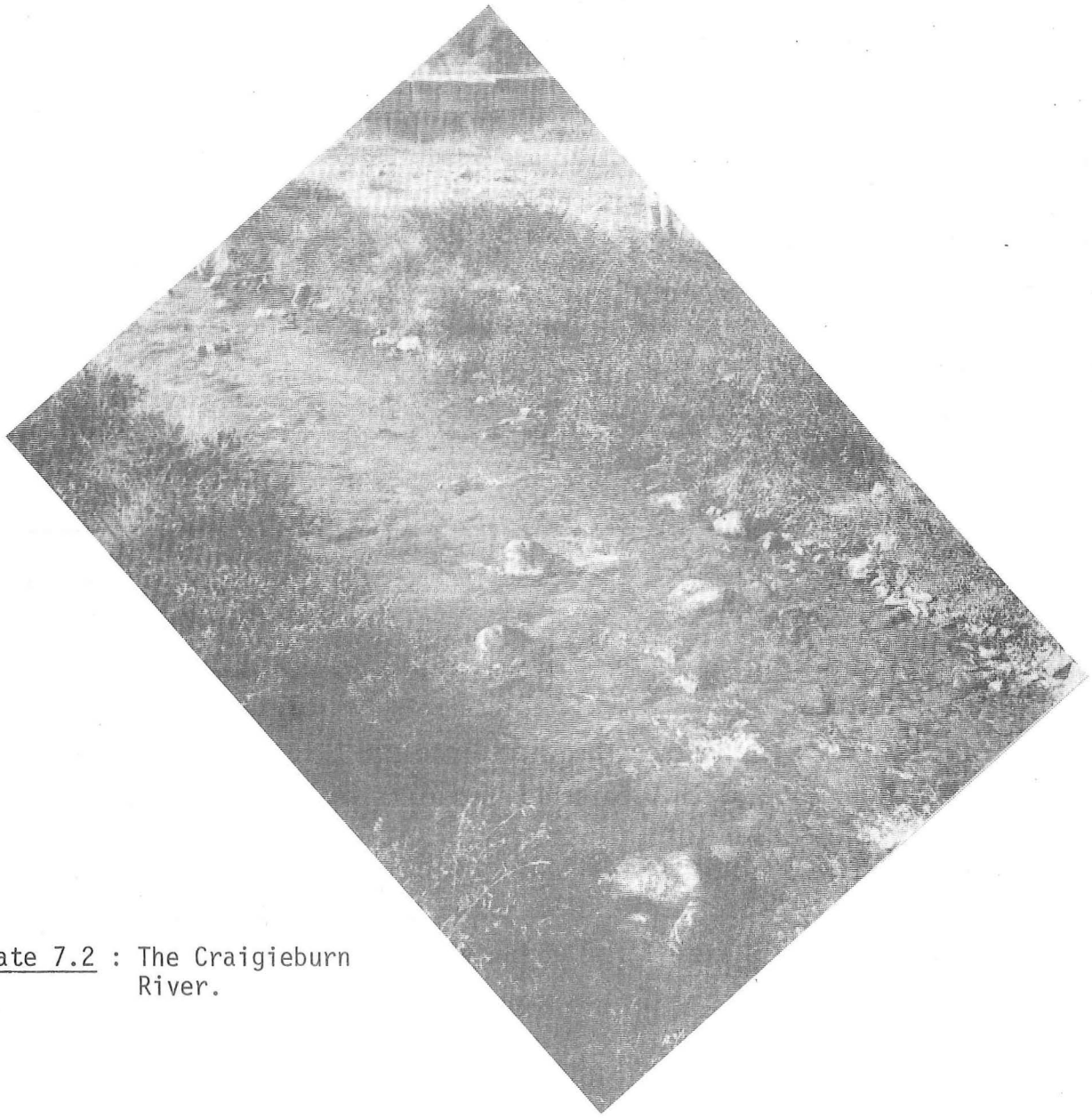

Plate 7.2 : The Craigieburn River.

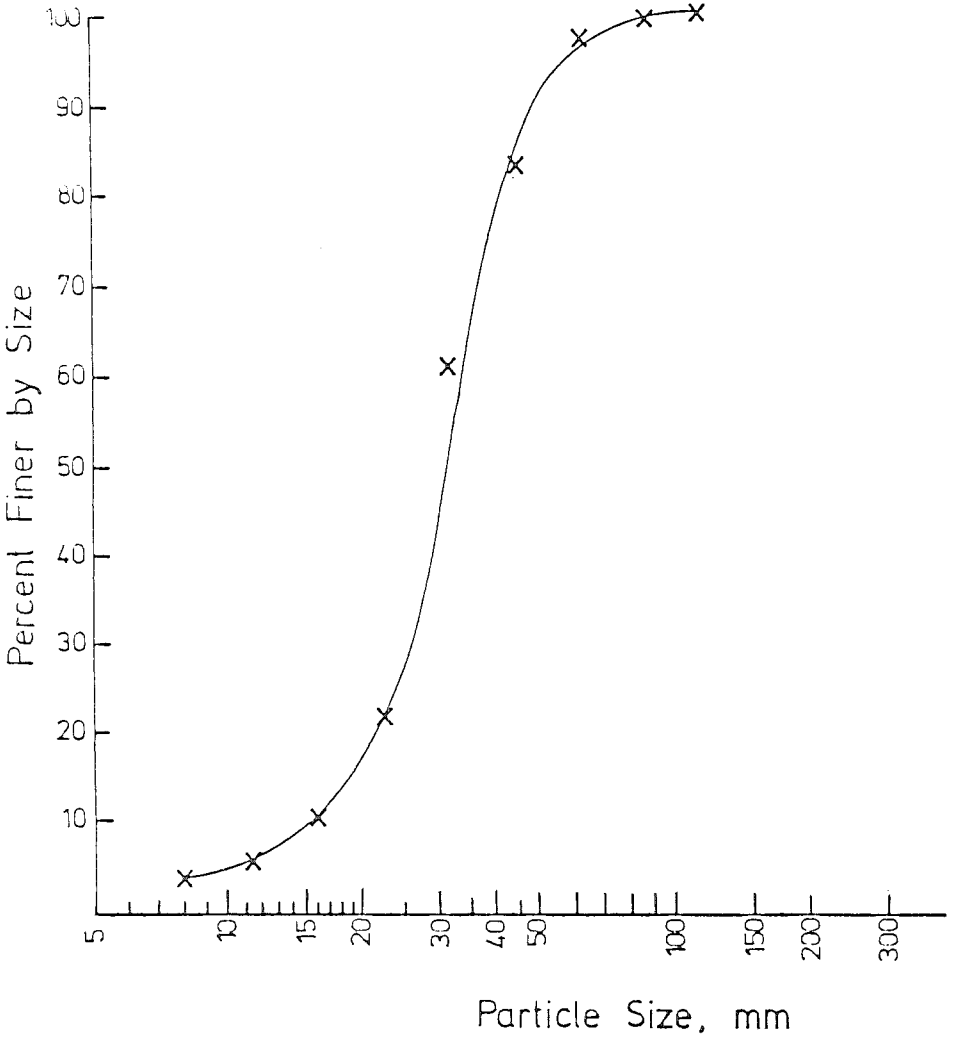

Figure 7.2a : Irrigation Canal.

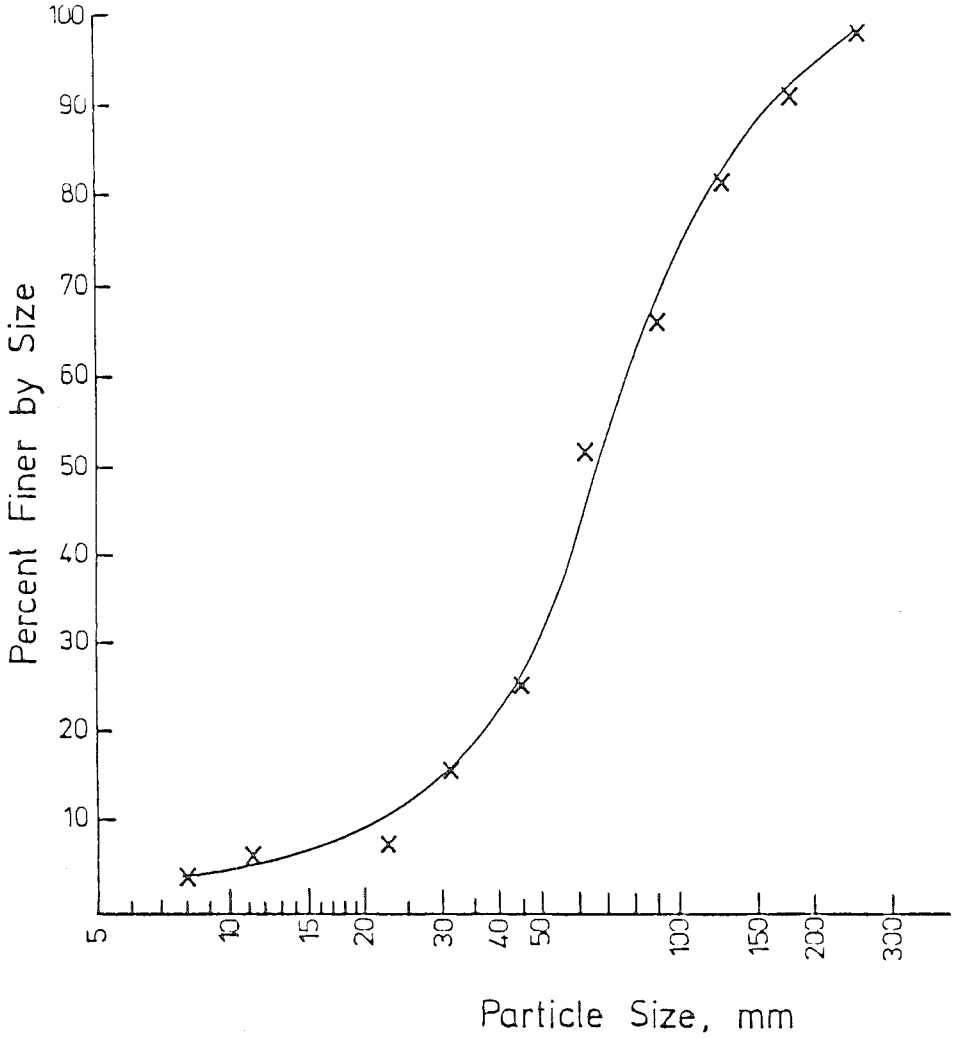

Figure 7.2b : Craigieburn River.

Plots of cumulative frequency of the grain size in the irrigation canal (7.2a) and in the natural bed of the Craigieburn River (7.2b).

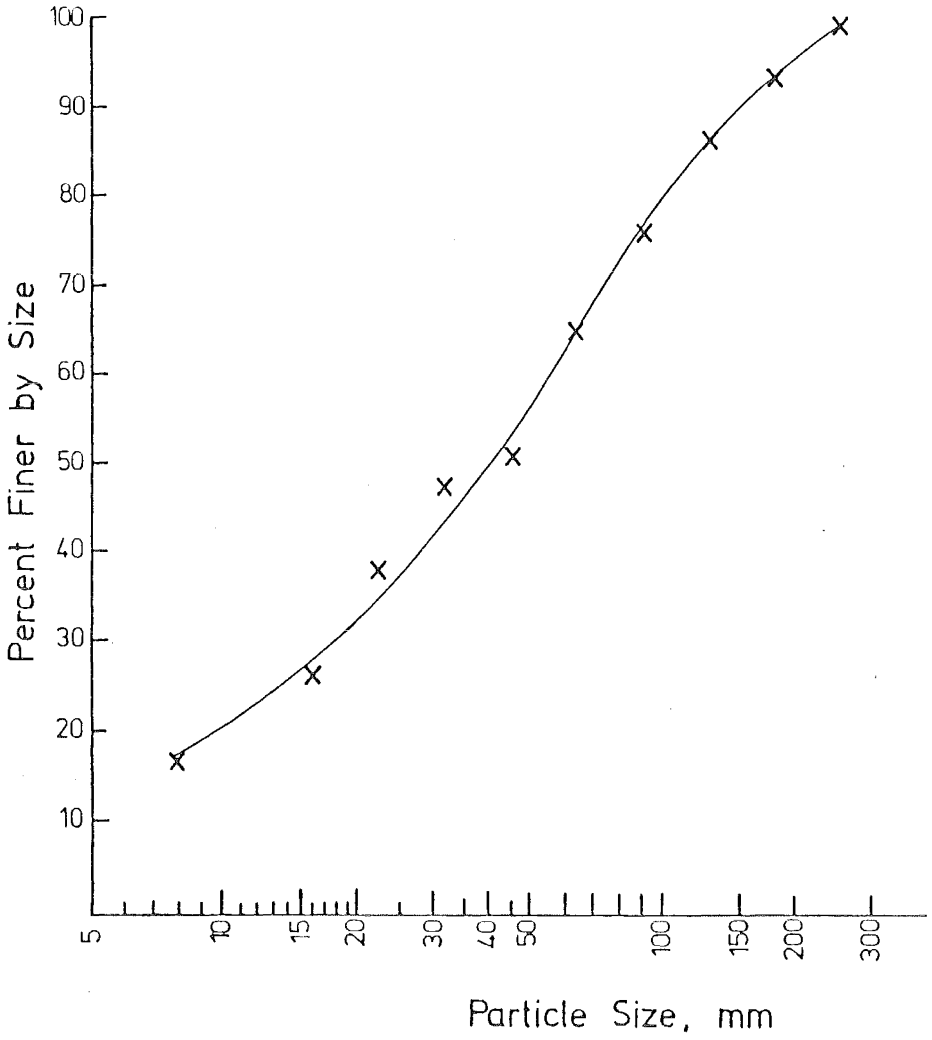

Figure 7.3 : Plot of cumulative frequency of grain size for the "smoothed" bed in the Craigieburn River.

reach. A sample of approximately 100 grains is picked from the bed of the channel on the basis of a grid system. (An equal number of grains were chosen from each section that had been taped and marked for concentration measurement). The intermediate axis of each grain is measured and tallied against the appropriate size limits. The cumulative frequency curves may be plotted directly from the data. The resulting curves for the two test reaches are shown in figures 7.2a and 7.2b. Photographs of the reach and the cumulative frequency distribution typify the channel conditions and enable comparisons with other reaches.

After a set of experiments was performed in the second test reach, the original bed was modifed by removing large rocks and filling holes. This produced a grain size distribution as shown in figure 7.3. Experiments were performed in the "smoothed" reach and in the smoothed reach with obstructions in the flow. These obstructions were introduced to enhance the mixing and were formed using sandbags and polythene in various patterns.

7.4 Apparatus and Measurements

7.4.1 Gauging

Stream gauging was carried out before and after a set of experiments. This was necessary to ensure no change in discharge during an experiment and provide flow parameters for numerical predictions.

The gauging was performed using a current meter and stop watch. A Gurley meter and a Pygmy meter were used, the first for normal gauging and the second in conjunction with a digital counter for a complete velocity distribution.

7.4.2 Measurement of Concentration

Once again in these experiments, the movement of pollutant was modelled by the movement of salt which was traced by conductivity measurements. This method was chosen for reasons of economy and ease of measurement. Salt also has minimal effects on the environment, particularly at levels which were of the same order of magnitude as the background dissolved salts.

At any point downstream from the tracer (salt) source it is expected that concentration and hence conductivity readings will fluctuate

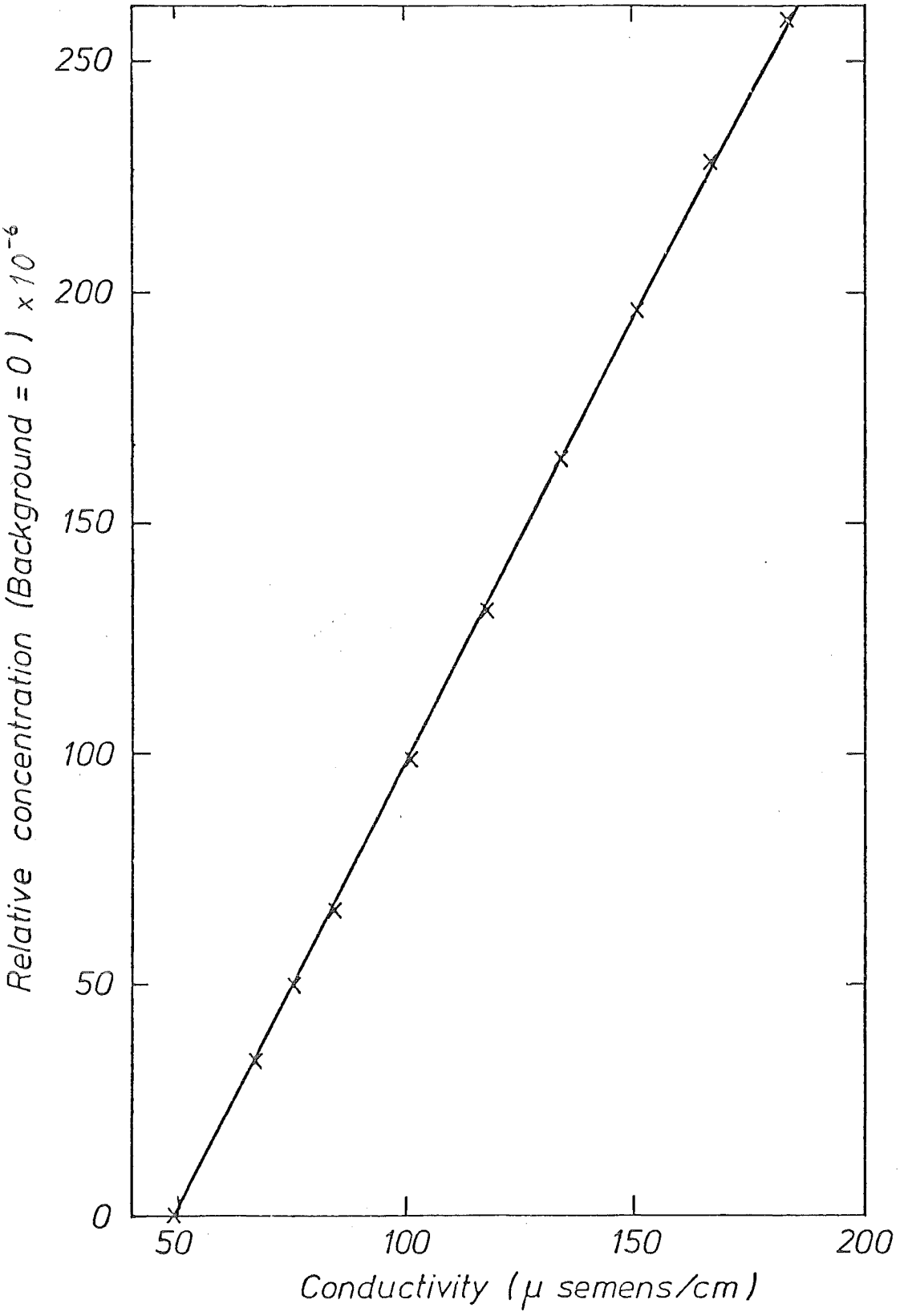

Figure 7.4 : Calibration curve for the Triac CM 100 meter used to measure conductivity in field experiments.

about some mean value. As it is this mean value in which we are interested, a record of conductivity readings should be capable of furnishing this information. There are two basic methods of recording data to obtain the mean conductivity; a complete time history of conductivity at each point (by chart recorder information or rapid discrete sampling) or a continuous sampling device resulting in a time averaged sample and thus a mean conductivity for the sampling period. The second method was chosen for the field work because it required less instrumentation and less time to complete an entire set of measurements. The length of time available for each experiment was limited by the amount of tracer available and the flow rate of the tracer. Time averaged samples were obtained using 5 litre plastic bottles with 35 mm neck, held in the flow at the desired point. This gave a continuous sample over approximately 30 seconds. Conductivities were measured in each bottle as soon as the sample had been taken to ensure that there were no possible temperature effects. The water temperature, background conductivity and fully mixed conductivity were also monitored throughout the experiment.

Single channel, Triac CM 100, salinity meters were used to measure field conductivities. These meters were extremely portable and were not susceptible to electronic drift as are many conductivity meters. Only one meter was used for sample conductivity measurements, while a second meter was used to monitor background and mixed conductivities.

7.4.3 Calibration

Figure 7.4 shows the relative conductivity (set to zero for background concentration) versus measured conductivity. As this plots as a linear curve (as expected) then it is appropriate to assume a linear relationship between measured conductivity and actual concentrations of salt. Probe calibration was achieved by background and equilibrium conductivity measurements, and with the knowledge of linearity between conductivity and concentration, non-dimensional concentrations were able to be calculated directly from these measurements. If there were any fluctuations in temperature readings, adjustments were made prior to calculating non-dimensional concentrations. This method of reducing data to non-dimensional concentrations is identical to that used in the laboratory experiments.

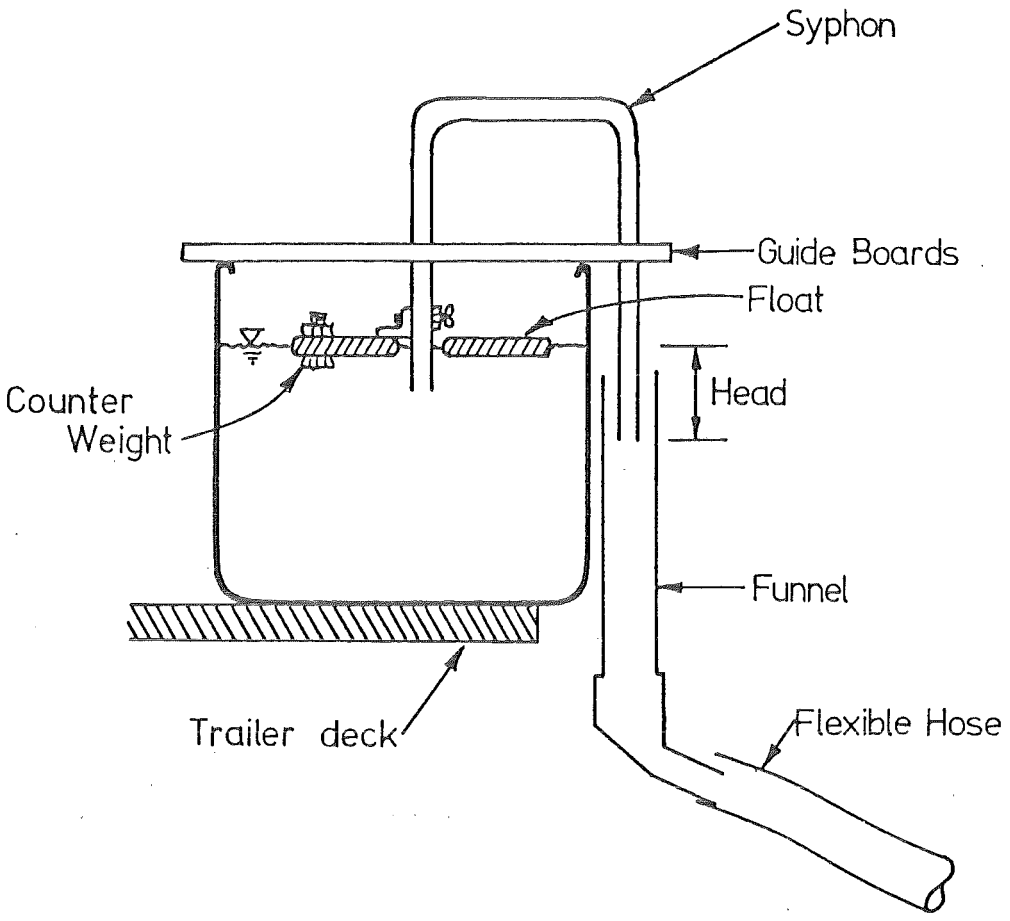

Figure 7.5 : Floating syphon device used to deliver tracer to the injection pipe (at the end of the flexible hose).

7.5 Tracer

A common salt (NaCl) solution was used as an electrolytic tracer. This was made up prior to each experiment, using water from the test reach, to a strength of approximately 11% by weight. As was the case in the laboratory experiments, the amount of tracer being released into the channel was small enough to neglect density effects.

7.6 Tracer Injection

It was desirable to inject tracer continuously into the channel over a period of about 45 minutes, in sufficient quantities to obtain approximately double the background conductivity in the fully mixed region. This involved large amounts of tracer for each experiment, the amount required depending on the channel discharge. For flows up to 1 cumec a 450 litre tank was sufficient although for some experiments a 900 ℓ tank was used to give longer run times. Tracer was delivered to the injection pipe using a floating syphon (figure 7.5). The tracer discharge was controlled by setting the head of solution over the syphon. This was usually set and tested prior to the field work on the basis of the expected flow.

For all field experiments tracer was injected into channels on the surface at either the side, quarter-or mid-point of the channel. This was achieved with a flexible hose from the injection funnel leading to a series of solid PVC connections which delivered the tracer into the channel in the flow direction (plate 7.3). The PVC pipework was supported by a dexion frame spanning the channel. This injection method simulated an ideal point release of pollutant at any transverse location on the surface of the water channel.

7.7 Typical Experimental Procedure

Field experiments were performed in two stages, the initial stage involved setting out equipment and selecting and marking sampling points. The second stage was the actual performance of an experiment or series of experiments. Due to the remoteness of some test reach locations, these experiments were set up on the day prior to actual experimental work. Sections were measured from the injection point at multiples of the channel width and at each section markers were placed at various points across the channel to indicate sampling positions. The injection framework and supply tank were located ready for use.

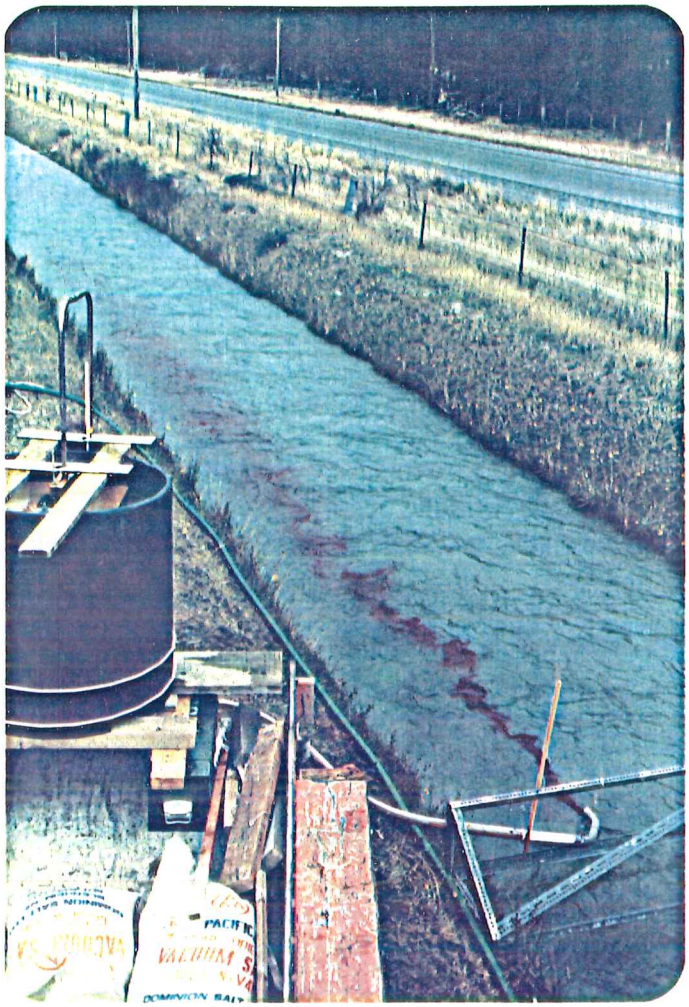

Plate 7.3 : Tracer injection equipment and dye test in the irrigation canal.

Prior to each experiment, while the salt solution was prepared, stream gauging was performed and sampling patterns determined from dye released at the injection point (see plate 7.3).

Tracer flow was then established in the syphon (recirculating tracer via buckets) and tracer discharge was gauged with a measuring cylinder and stop watch. Measurements were repeated until consistent readings were obtained. Tracer was released directly into the channel at the constant flow rate (this could be checked from background and fully mixed conductivities). Sampling was started, soon after tracer injection began, at the top section moving downstream from the release point. The initial time lapse between beginning tracer injection and sampling was minimized by sampling nearest the source first. Although sampling disturbs the flow downstream from the sampling section, there was sufficient time between sampling at sections to allow for flow and tracer distributions to stabilise. Samples were collected at each measurement point at a sampling section simultaneously and conductivities were measured immediately. Because of temperature sensitivity it was undesirable to sample any faster than conductivities could be recorded.

Once the entire test reach had been sampled, there was generally sufficient time remaining to check readings and if necessary repeat any sections. In cases where sections were re-sampled it was found that variations were within 6% and apparent discrepancies were in fact a correct record of the entire pollutant cloud persistantly swinging across the channel, (see following chapters).

When sampling had been completed the channel gauging was repeated. Dilution measurements were also performed with the tracer to cover the range of measured conductivities and produce a calibration curve. Details of the dilution procedure are outlined in Johnstone (1980).

BLANK PAGE IN ORIGINAL - PART OF PAGINATION

CHAPTER VIII

AN APPROXIMATE MODEL FOR THREE-DIMENSIONAL DISPERSION AND A COMPARISON WITH FIELD MEASUREMENTS

8.1 Introduction

In most natural waterways the channel width is far greater than the depth. In this situation a pollutant introduced as a point source will become well mixed over the depth of the channel before it is transversely well mixed. This chapter investigates the performance of the two-dimensional model applied to wide channels with a point source.

8.2 The Three-Dimensional Diffusion Problem

While a pollutant released at a point will certainly behave in a three-dimensional fashion near the source, the downstream behaviour will depend on the channel geometry. In a deep channel dispersion may continue three-dimensionally until complete mixing is achieved. On the other hand, in a shallow, wide channel the pollutant will become well mixed vertically long before complete mixing is achieved. For instance, if the channel width is equal to 15 channel depths the vertical mixing length is less than $\frac{1}{110}$ of the transverse mixing length (Rutherford 1981). Thus, in most natural channels the pollutant will become vertically well mixed in a fraction of the total mixing length (the mixing length is the distance required to reach some percentage of the final mixed concentration. In the example given the mixing length was taken as the distance at which the concentration anywhere in the section is within 5% of the final mixed concentration). Under such circumstances, the three-dimensional problem will reduce to a two-dimensional transverse mixing problem. The approximation made in using a two-dimensional scheme is that the point source is behaving as a vertical line source. The larger the ratio of width/depth becomes, the better the approximation. For the two reaches investigated in this Chapter the width to depth ratios were 12:1 and 30:1. Both of these cases are considered in section 9.7, where the three-dimensional model developed in Chapter 9 is used to predict the degree of vertical mixing at the first sampling station.

BLANK PAGE IN ORIGINAL - PART OF PAGINATION

The velocity and diffusivity profiles used in the two-dimensional transverse scheme will depend on the shape of the channel. For both profiles vertically averaged values must be used since the whole problem is being treated as vertically averaged. The form of these profiles is discussed in the following section.

8.3 Velocity and Diffusivity Profiles

The velocity field in a natural channel will vary in all three co-ordinate directions (vertically, transversely and longitudinally). However, if the dispersion is to be predicted with a two-dimensional transverse model, the velocity must be constant in all but the transverse direction. Therefore, a reach and depth averaged velocity profile is produced from velocity measurements taken in the experimental channels. A uniform velocity field is also available in the model. In many wide channels a uniform velocity distribution will be a good approximation to the actual mean transverse velocity distribution. This will depend on the cross-sectional shape of the channel since velocity variations across the channel are largely due to changes in depth (a function of the basic channel geometry). In a wide channel the banks will have a limited effect on the velocity distribution.

Many studies have been performed to determine transverse dispersion parameters, particularly the width-averaged transverse dispersion coefficient, D_z. As D_z is dependant on secondary currents as well as turbulent diffusion, it will vary from reach to reach in concert with the channel geometry. Although there is no theoretical basis for the local variation in the transverse dispersion coefficient some suggested distributions have been proposed.

If diffusivities are considered to be isotropic then Elder (1959) showed that the local transverse turbulent diffusivity is proportional to the product of the local water depth and the longitudinal velocity. Subsequent investigators have found, for a large number of experiments, the mean transverse diffusivity is (Fischer et al 1979),

$$\varepsilon_z \simeq 0.15\ \bar{y}_n\ u_* \qquad (8.1)$$

A model was suggested by Smith (1981) which combines both the above pieces of information to produce,

$$\varepsilon_z = 0.15\ y_n(z)\ u_*(z) \qquad (8.2)$$

BLANK PAGE IN ORIGINAL - PART OF PAGINATION

where $y_n(z)$ is the depth at z. Smith assumed that there is a constant ratio γ such that, $u_*(z) = \gamma u(z)$, to completely define equation 8.2. If an average depth profile is known for a reach then equation 8.2 can be used to estimate the average local diffusivity.

Again, a uniform diffusivity is also available in the model. In a wide channel with a uniform section this may be as good an approximation as any.

One of the main difficulties in defining a transverse diffusivity coefficient in any natural river is the occurrence of occasional unexplained transverse migrations of pollutant on a scale larger than the depth. Until the mechanisms causing transverse turbulence are fully understood approximations for transverse dispersion coefficients must be made. This study is limited to making comparisons between approximations and comparisons with field measurements.

8.4 Model Equations

The general convective-diffusive equation defined in chapter 2 for three dimensions is,

$$\frac{\partial c}{\partial t} + u \frac{\partial c}{\partial x} = \frac{\partial}{\partial x}\left(\varepsilon_x \frac{\partial c}{\partial x}\right) + \frac{\partial}{\partial y}\left(\varepsilon_y \frac{\partial c}{\partial y}\right) + \frac{\partial}{\partial z}\left(\varepsilon_z \frac{\partial c}{\partial z}\right) \qquad (8.3)$$

In the two-dimensional model developed in Chapters 3 and 4 the z-direction term is omitted and non-dimensional variables are defined in terms of the channel depth, y_n. For transverse dispersion, the equation is written in terms of the transverse and longitudinal terms only, resulting in the steady equation,

$$u \frac{\partial c}{\partial x} = \frac{\partial}{\partial x}\left(\varepsilon_x \frac{\partial c}{\partial x}\right) + \frac{\partial}{\partial z}\left(\varepsilon_z \frac{\partial c}{\partial z}\right) \qquad (8.4)$$

Non-dimensional variables are defined by the channel width,

$$\xi = \frac{x}{z_n}, \quad \zeta = \frac{z}{z_n}, \quad \chi(\zeta) = \frac{u}{\bar{u}} \qquad (8.5)$$

The longitudinal diffusivity remains unchanged and a transverse diffusivity is introduced,

$$\varepsilon_x = D_y \psi(\eta, \zeta), \quad \varepsilon_z = D_z \phi(\zeta) \qquad (8.6)$$

where D_y and D_z are constants determined from the average dispersion

BLANK PAGE IN ORIGINAL - PART OF PAGINATION

coefficients. The function $\psi(\eta, \zeta)$ is the complete vertical (and longitudinal) diffusivity function. In the model this function is replaced by a vertically averaged function to give $\varepsilon_x = D_y \psi(\zeta)$.

Thus equation 8.4 becomes

$$\frac{z_n}{y_n} \frac{8}{f} \chi \frac{\partial c}{\partial \xi} = \psi \frac{\partial^2 c}{\partial \xi^2} + \frac{D_z}{D_y} \frac{\partial}{\partial \zeta} \left(\phi \frac{\partial c}{\partial \zeta} \right) \tag{8.7}$$

where $\frac{8}{f} = \left[\frac{\bar{u}}{u*}\right]^2$. This equation is of an identical form to the equation developed in chapter 3, with η replaced by ζ.

The boundary conditions remain the same. There is no flow of tracer through the channel boundaries,

$$\phi(\zeta) \frac{\partial c}{\partial \zeta} = 0 \text{ for } \zeta = 0, 1 \tag{8.8}$$

Dead zones are neglected for this application of the model since it was demonstrated in chapter 4 that they produce no significant difference in model solutions. For wide channels, any dead zones at the channel sides may occupy a significant percentage of the flow width. These regions may be very slow to respond to changes in main flow concentrations but in the steady state situation it is assumed that such backwaters are also in an equilibrium state. When estimating the channel width the average waters edge should be used, with large backwaters and side channels being ignored.

Since there is no change in the form of any of the two-dimensional dispersion model equations for transverse dispersion, the same approach is used to obtain moments and ultimately produce concentration profiles. A complete discussion of the techniques used for solving equation 8.7 is given in chapter 3. Briefly, this involves the definition of the deficit concentration $\left(c_{d*} = \frac{c}{c_e} - 1\right)$ to ensure that moments of concentration are finite. Aris moment transforms are then applied to equation 8.7 to reduce the equation to a one-dimensional diffusion equation. This equation is then solved, using numerical integration, for all moments required and these moments are used to generate concentration profiles. The computer program used to produce this solution is identical to that described in chapter 4, with appropriate adjustments made for the constants in equation 8.7. This program is included in Appendix D.

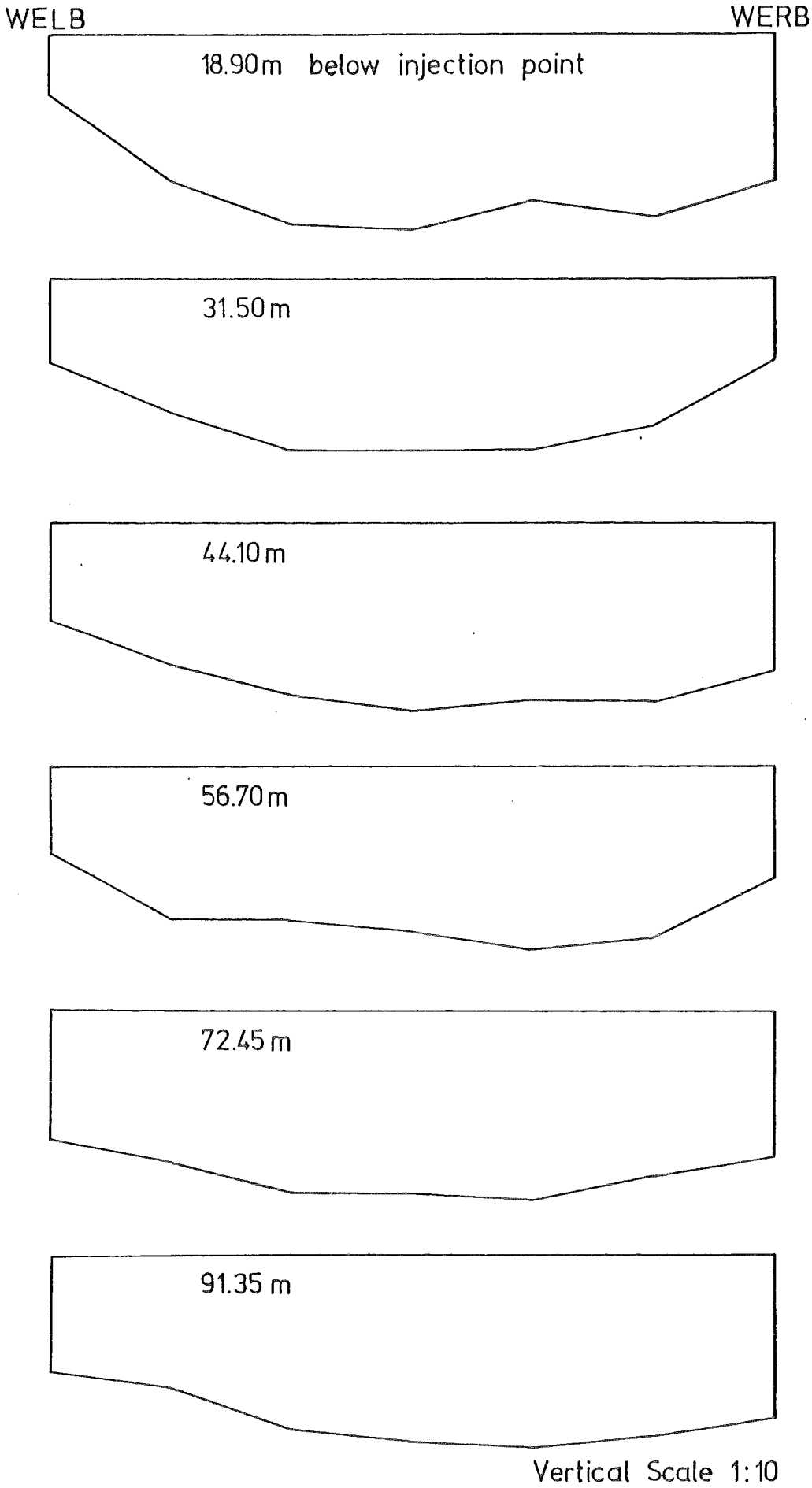

Figure 8.1 : Channel cross-sections at each sampling point in the irrigation canal.

WELB - Waters edge left bank, WERB - Waters edge right bank.

8.5 A Note on the Output of the Computer Program

As the same program is used for the transverse model as outlined in chapter 4, all output routines described in section 4.2.4 are available. The most information about the concentration distribution is portrayed in a contour diagram. Consequently, these plots were obtained from the computer solution for each experiment performed in the field. The measurements from the field experiments were plotted on the contour diagrams giving a comparison with expected concentrations. The measured points are also plotted as transverse profiles at each section. A routine was included in the program to produce similar predicted transverse concentration profiles. However, these theoretical profiles are not very meaningful, due to the inability of the program to fit the correct profile near the source. If a better fitting procedure was available, such plots would be useful to portray the transverse concentration distribution at a particular distance downstream from the source. It appears that the contour plots of concentration smooth any anomalies in the fitted profiles and therefore give a better overall picture of the dispersion.

8.6 Presentation of Field Experimental Results and Comparisons with Theoretical Predictions

Of the field experiments performed, only those in the first test reach (the irrigation race) and the "smoothed" second reach were directly comparable with the present computer model. In these two cases the channel shape appeared relatively constant over the reach considered. Thus, longitudinally constant flow conditions (which are required by the computer model) could be expected. In the remaining field experiments (described in Appendix C) natural and man-made obstructions in the channel preclude the approximation of longitudinally constant velocity and diffusivity profiles. In such cases an estimate of the additional mixing generated by individual obstructions would be necessary. Suitable adjustments would also be required to predict reach-averaged velocity profiles. Limited results may then be available using the model developed, however this investigation is beyond the scope of this study.

8.6.1 The Irrigation Canal

Channel cross-sections at each of the sampling points in the irrigation race illustrate the rectangular nature of the test reach (see figure 8.1). The average channel width is 3.22 m and the average depth

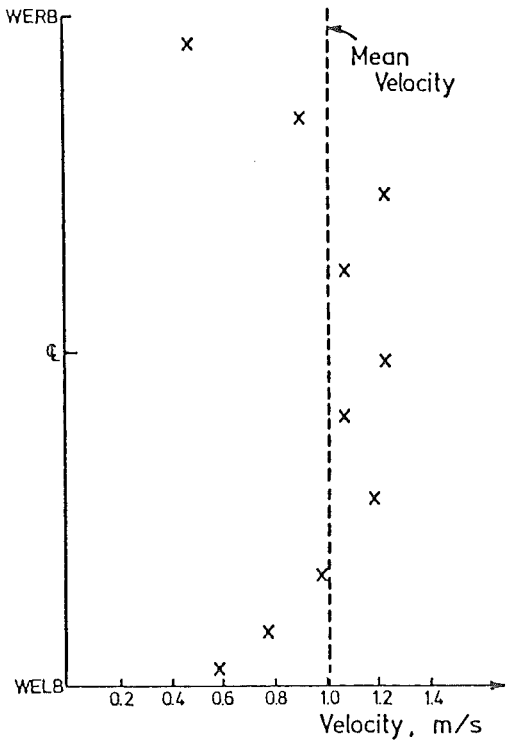

Figure 8.2 : Plot of mean vertical velocity versus transverse location in the irrigation canal.

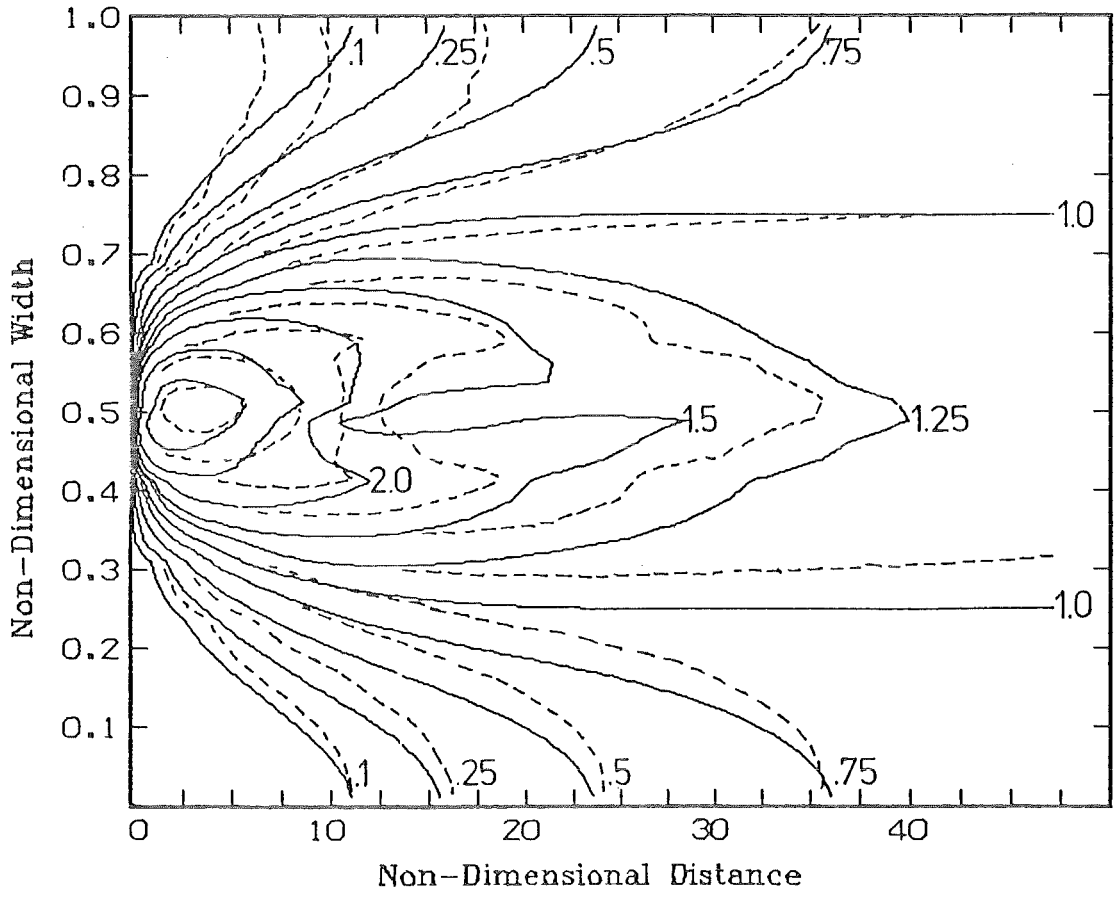

Figure 8.3 : Uniform Velocity With Source At 0.50 (f=.005)

----- Concentration distribution using the measured velocity.

——— Concentration distribution using a uniform velocity in the irrigation canal.

263 mm. As cross-sections appear to be nearly constant along the channel, the assumption of longitudinal uniformity should be good. Furthermore, a uniform velocity profile is most likely to be a close representation of the actual (transverse) velocity profile. A plot of mean velocities from vertical sections, shown in figure 8.2, is compared with the mean velocity for the entire section. Both of these velocity distributions were used in the computer model with a uniform diffusivity distribution. Contour plots for each velocity distribution were compared at each source location used in the field experiments. Figure 8.3 shows both cases for the source at the centre of the channel. The solid lines represent the constant velocity concentration contours and the dashed lines correspond to concentration contours obtained using the measured velocity profile. Closer agreement between such plots is obtained for the remaining source locations.

If a measured velocity profile is to be used to predict concentrations, then a large number of profiles at various points along the reach will be required to define a reach averaged profile. The resulting profile is likely to be some smoothed form of the measured points in figure 8.2, and it is likely to be closer to the uniform velocity. Therefore the uniform velocity distribution will be a good approximation for this channel.

Section 8.3 discussed the models for the local transverse diffusivity. In the irrigation channel there is little variation in depth across the channel (figure 8.1) and therefore diffusivity models based on the flow depth will have little advantage over a constant diffusivity. Accordingly, a constant diffusivity distribution was used for the irrigation channel ($D_z = 0.15\ u_* y_n$, since this flow is close to a laboratory type flow with no meandering).

Figures 8.4 - 8.6 illustrate results obtained for the three release points investigated in the first reach. Overall agreement between the measured concentrations and the predicted plot of concentration contours is reasonable. It is apparent that the main cause of the discrepancies observed in the contour plots is the tendency of the plume to be swept across the channel as it travels downstream. This can be seen clearly in figure 8.6a where the distributions at 44.10 m and 91.35 m (non-dimensional distances $\xi = 13.70$ and $\xi = 28.37$) have moved towards the right bank. With the release point in the centre of the channel the peak

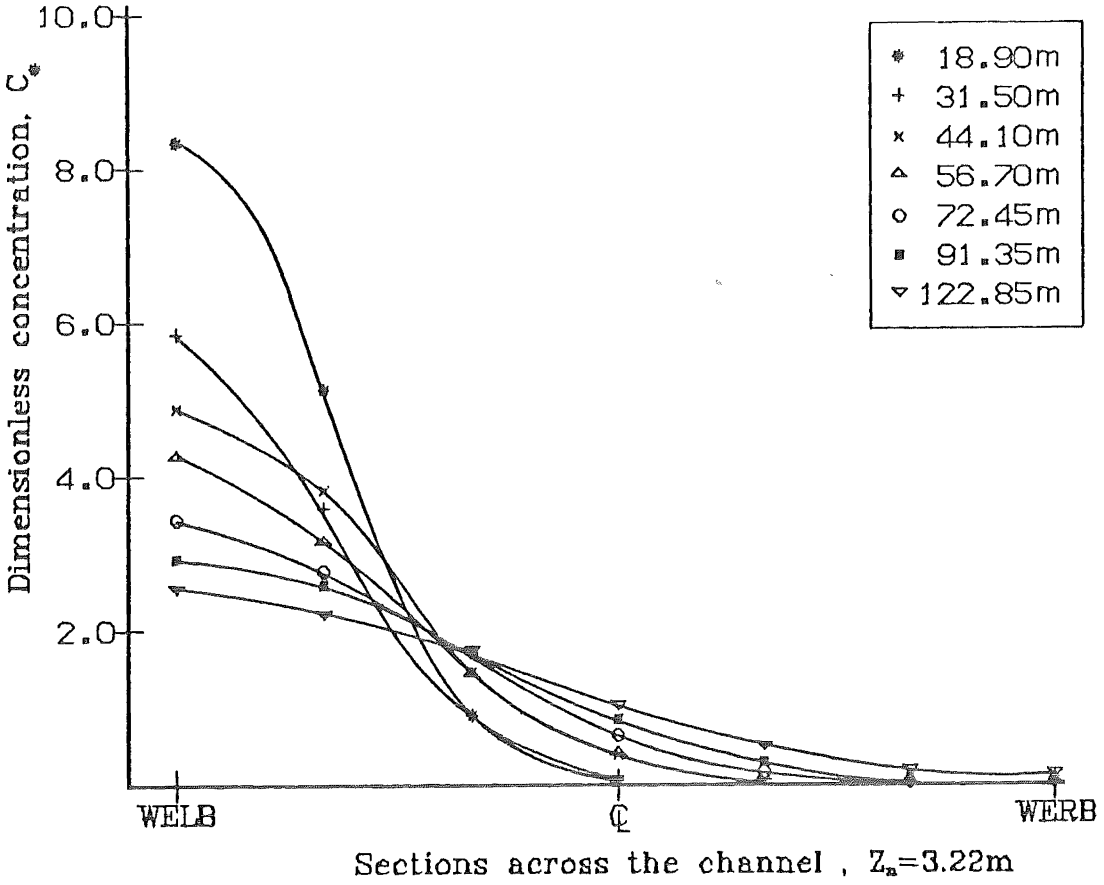

Figure 8.4a: Source at left bank, Run 1, 11/3/82

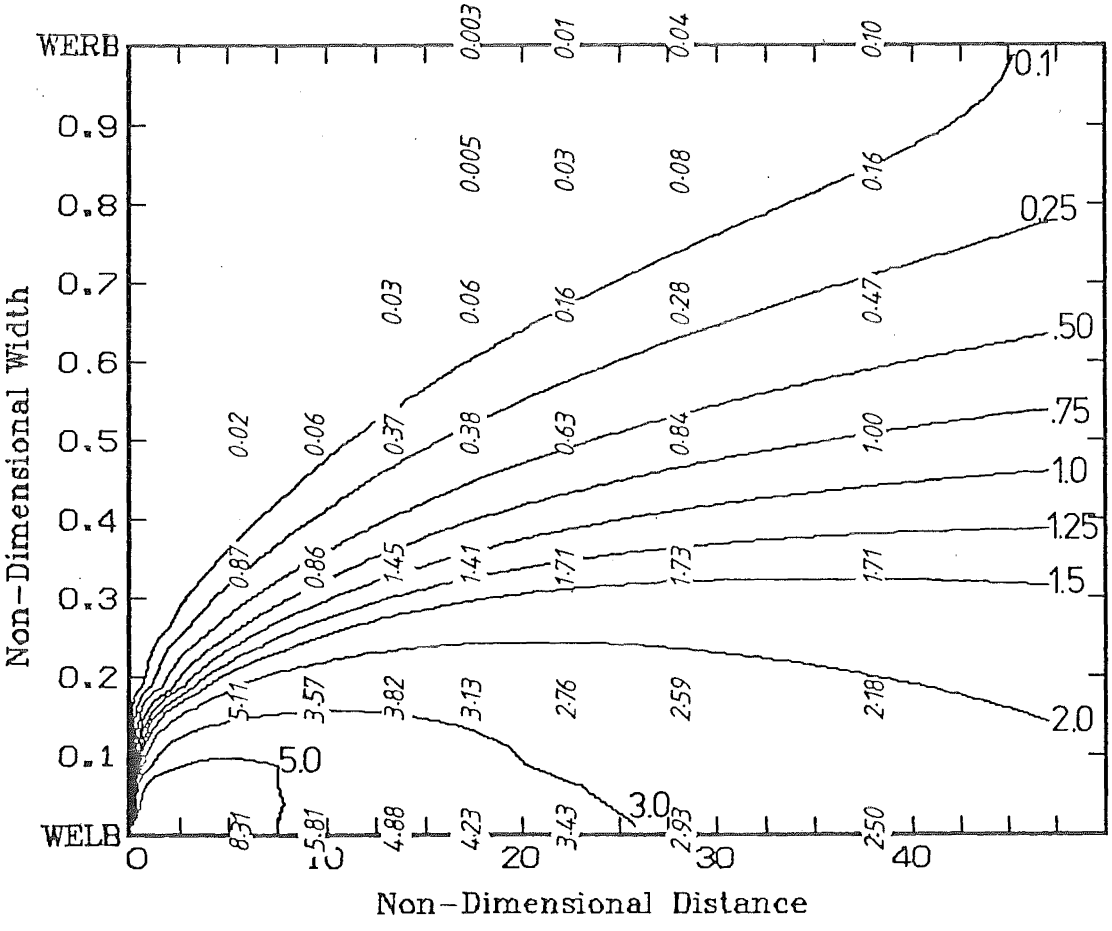

Figure 8.4b: Uniform Velocity With Source At 0.0 (f=.005)

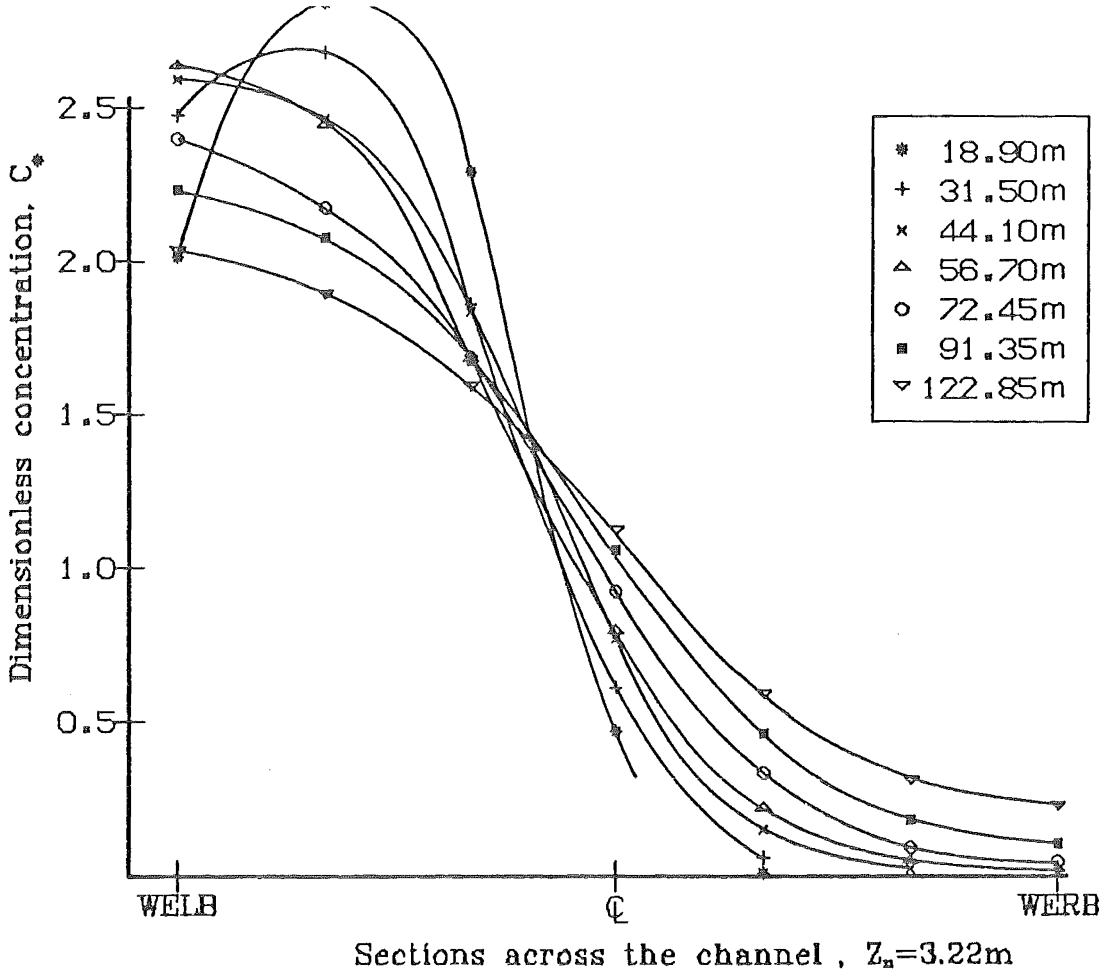

Figure 8.5a: Source at 1/4-point, Run 2, 11/3/82

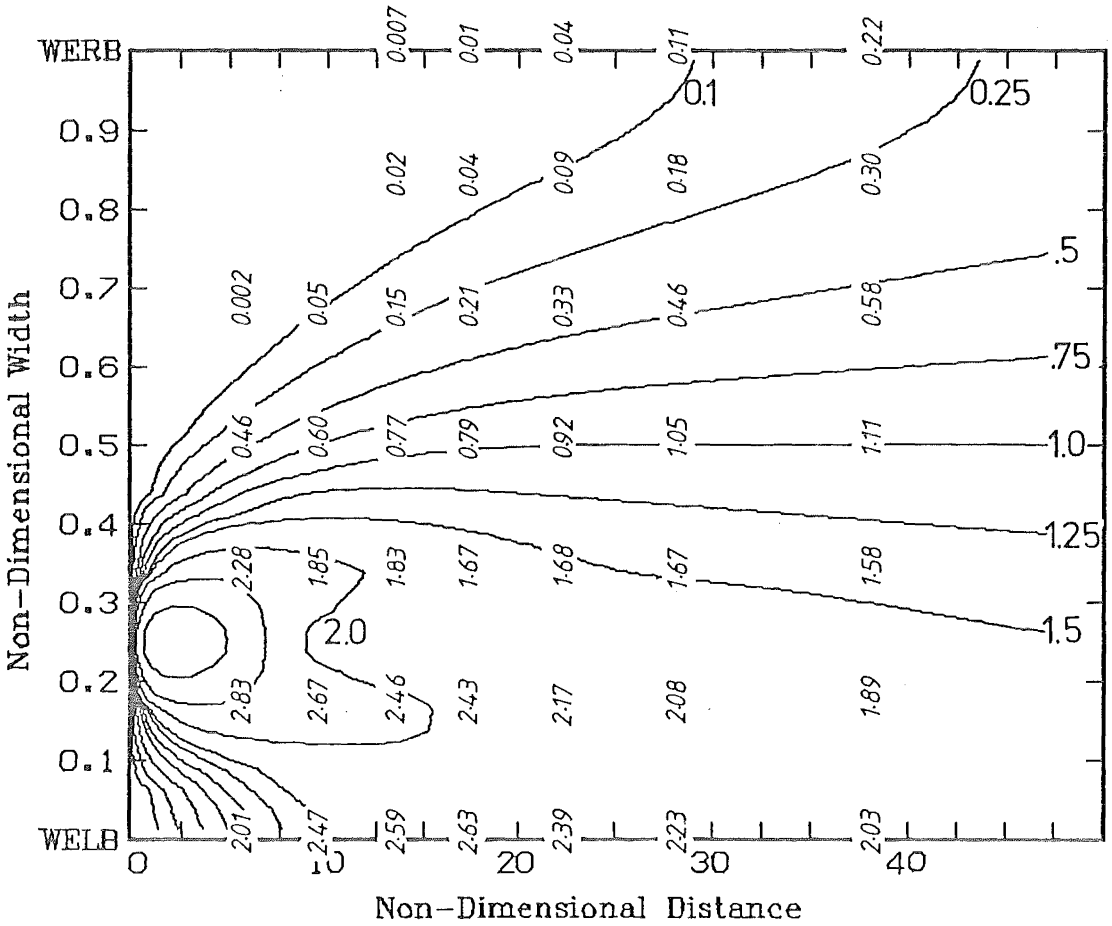

Figure 8.5b: Uniform Velocity With Source At 0.25 (f=.005)

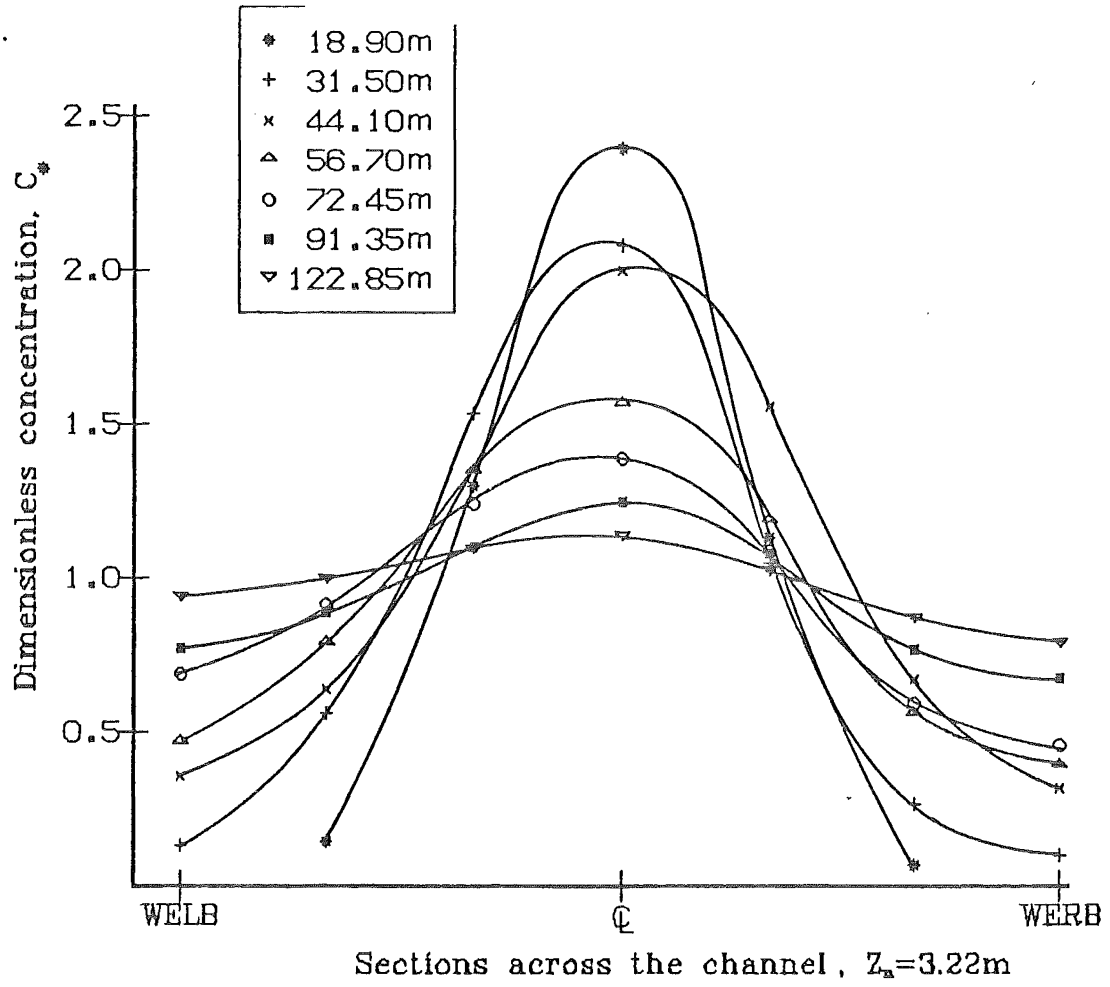

Figure 8.6a: Source at mid-point, Run 3, 11/3/82

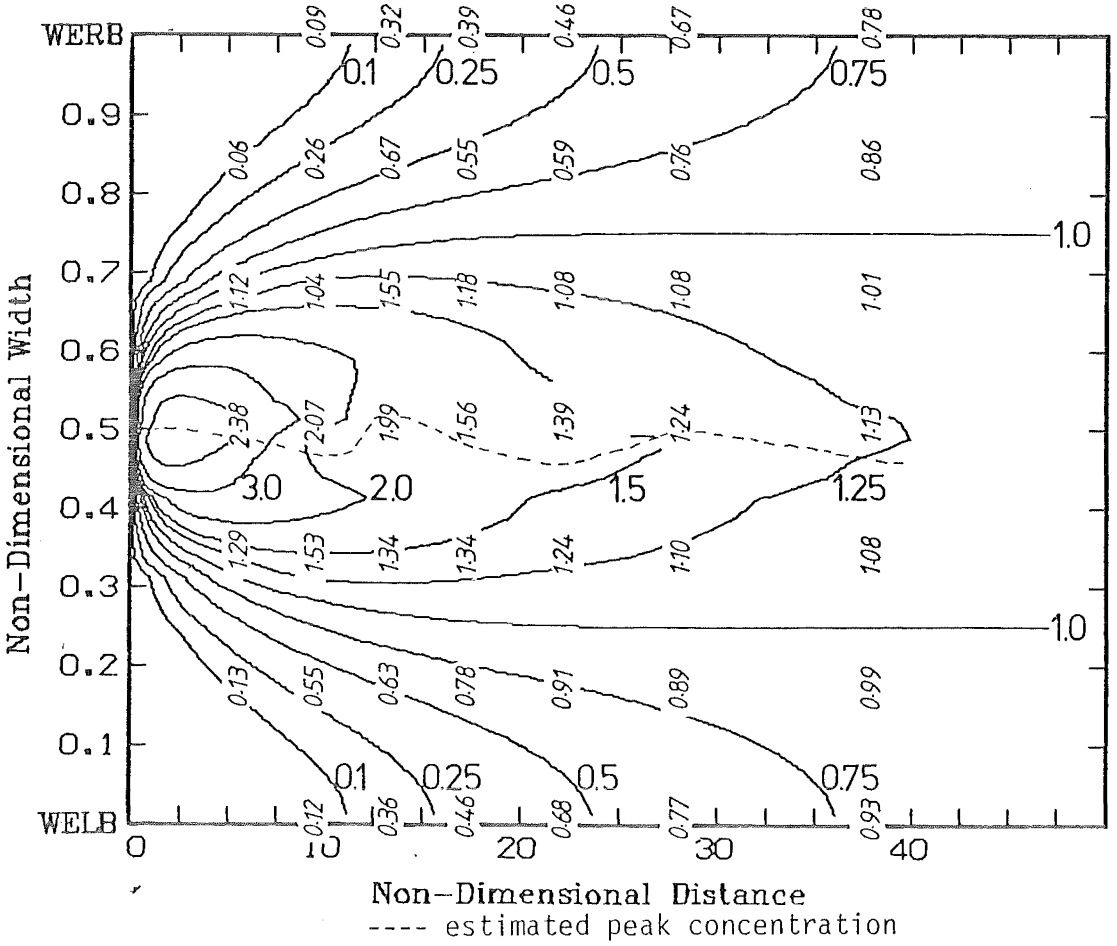

Figure 8.6b: Uniform Velocity With Source At 0.50 (f=.005)

concentration is expected to occur at the centre-line all along the reach. Using the field measurements the location of the peak concentration was estimated at each section. This is plotted on figure 8.6b as a dashed line, and clearly shows the way in which the plume is moving across the channel from section to section. On the whole, the pollutant appears to spend more time on the left hand side of the centreline. This is also reflected in the higher concentrations observed along the left bank and the better mixing that is achieved at this bank.

For the two other release points in the irrigation canal it is not possible to plot the plume movement. At most sections in these experiments the peak concentration occurs at the channel bank. Nevertheless, a visual inspection of diagrams 8.4a and 8.5a shows some of the profiles are slightly displaced from the positions in which they would be expected to appear. For instance, the second section (31.50 m, ξ = 9.78) in diagram 8.4a appears to have moved towards the left hand bank.

Although transverse convection was encountered in each of the experiments in the irrigation canal no account for this is possible in the model. The inclusion of this in the model would require the transverse convective term, $w \frac{\partial c}{\partial z}$, to be included in the original diffusion equation. Even if this term was introduced, the definition of the transverse velocity component, w, over the entire reach would be extremely difficult. Any allowance for transverse convection must therefore be made with the transverse diffusivity coefficient. Accordingly, it is expected that the model developed in this study will not give accurate predictions for any individual section in a natural channel. However, figures 8.4b, 8.5b and 8.6b indicate that if mean channel conditions are available overall dispersion predictions are still possible.

8.6.2 The Craigieburn River

Although this test reach had been "smoothed" (large rocks removed and large depressions filled) channel sections were not regular along the reach (see figure 8.7). The average channel width is 4.04 m and the average depth 131 mm. Approximations of uniformity in the channel are not likely to be as good as they were in the more regular irrigation channel. Although the model allows no longitudinal variation in velocity or diffusivity profiles, transverse profiles which are representative of distributions over the whole of the reach may be used. In the case of the velocity distribution, sufficient profiles must be available to confidently

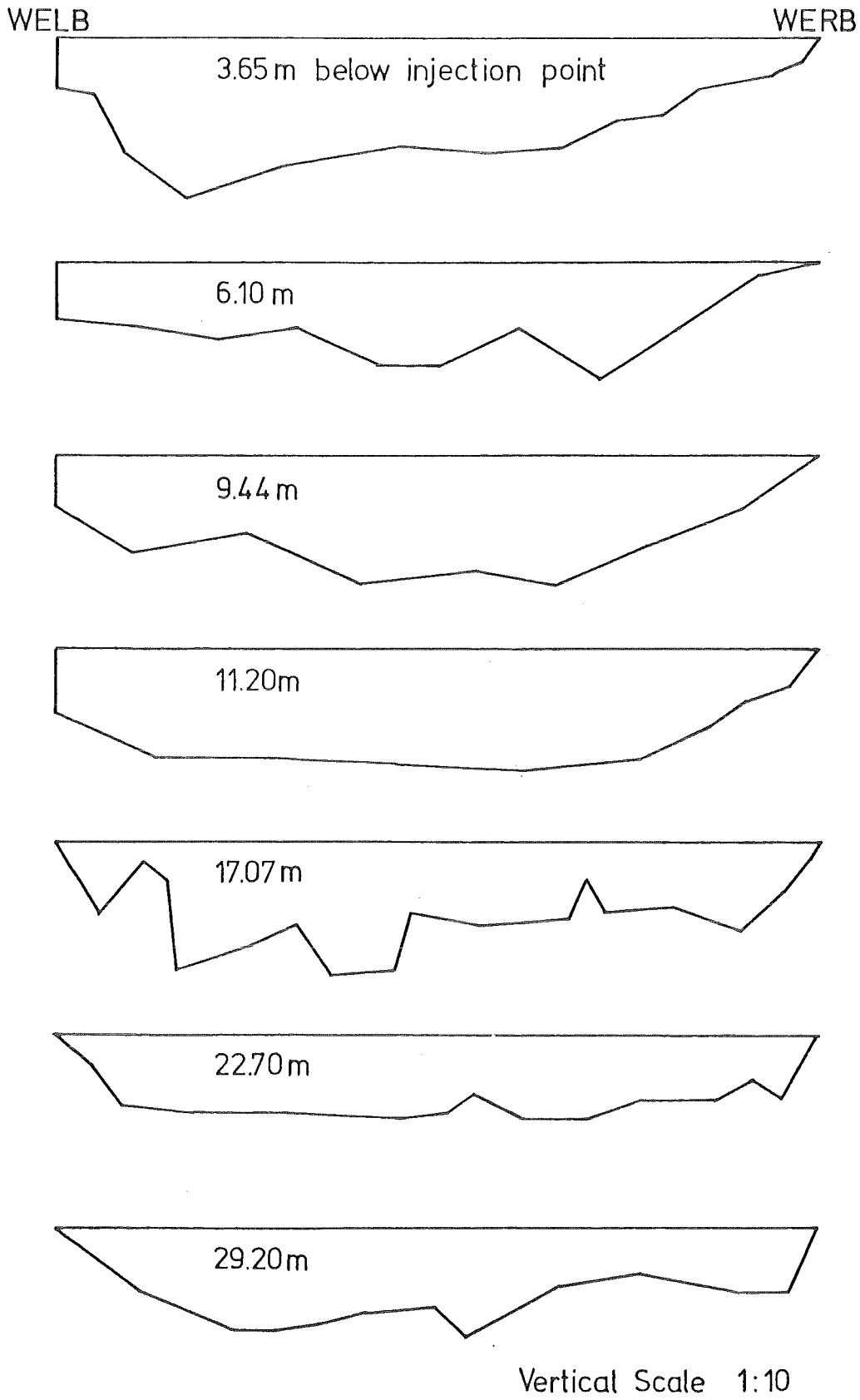

Figure 8.7 : Channel cross-sections at each sampling point in the Craigieburn River.

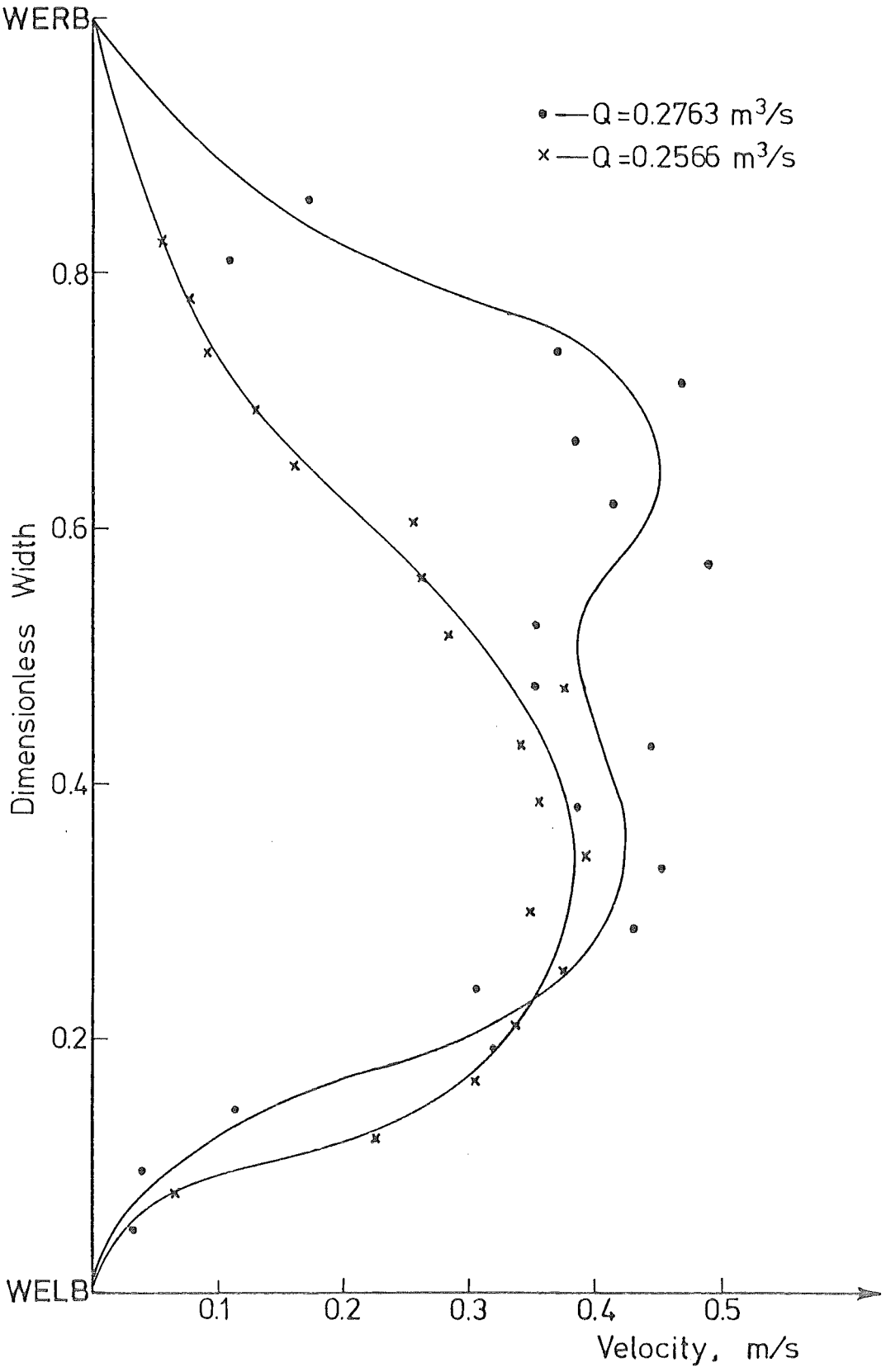

Figure 8.8 : Measured velocity profiles in the "smoothed" Craigieburn River test reach.

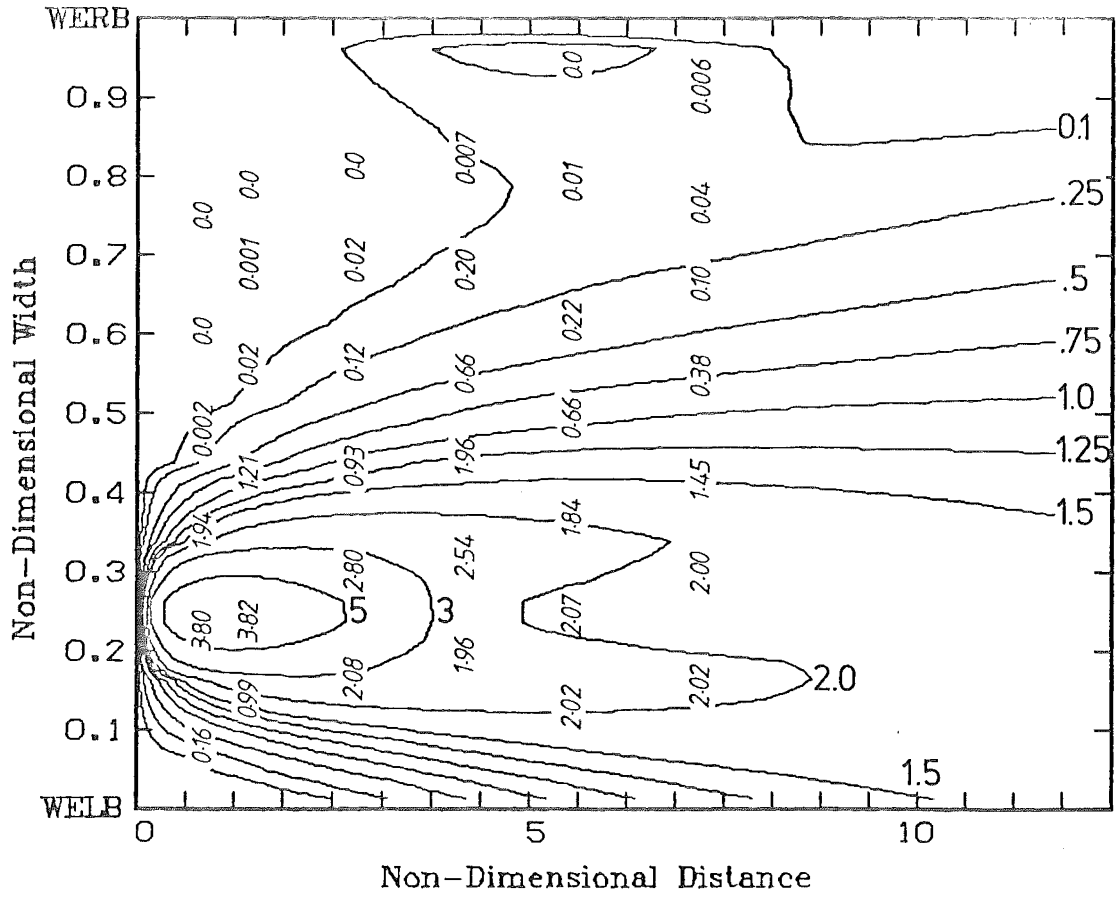

Plot for estimated local transverse diffusivity.

Figure 8.9 : Uniform Velocity With Source At 0.25 (f=.0115)

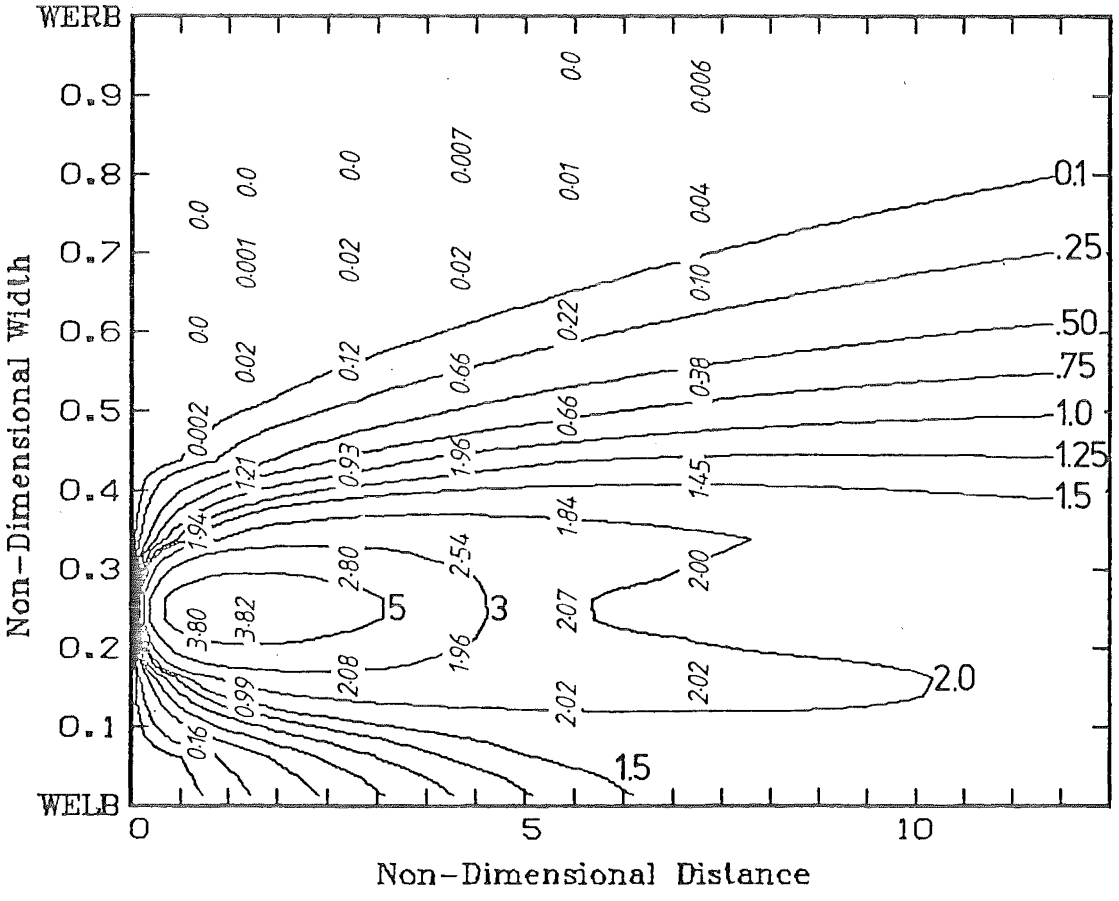

Plot for constant transverse diffusivity.

Figure 8.10: Uniform Velocity With Source At 0.25 (f=.0115)

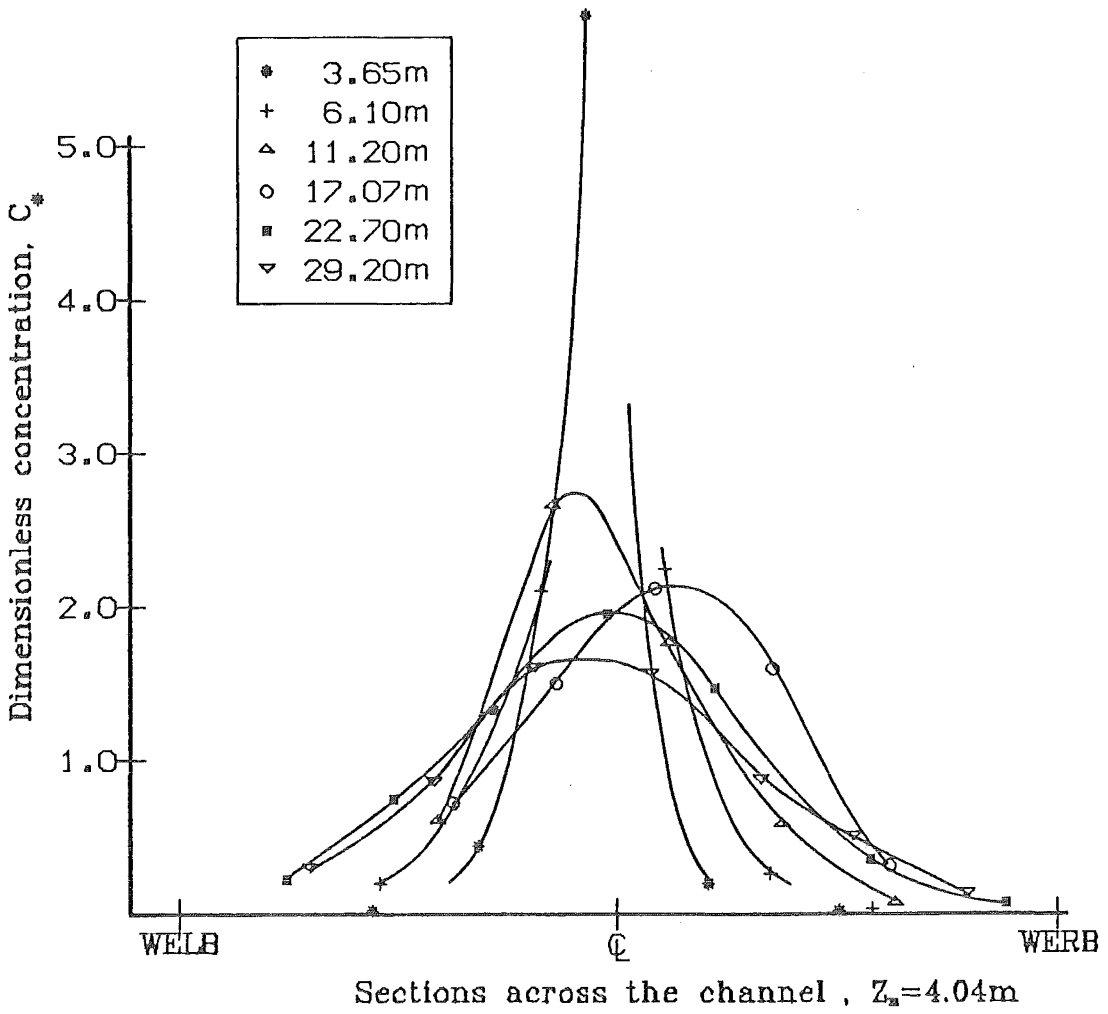

Figure 8.11a Source at mid-point, Run 1, 29/7/82

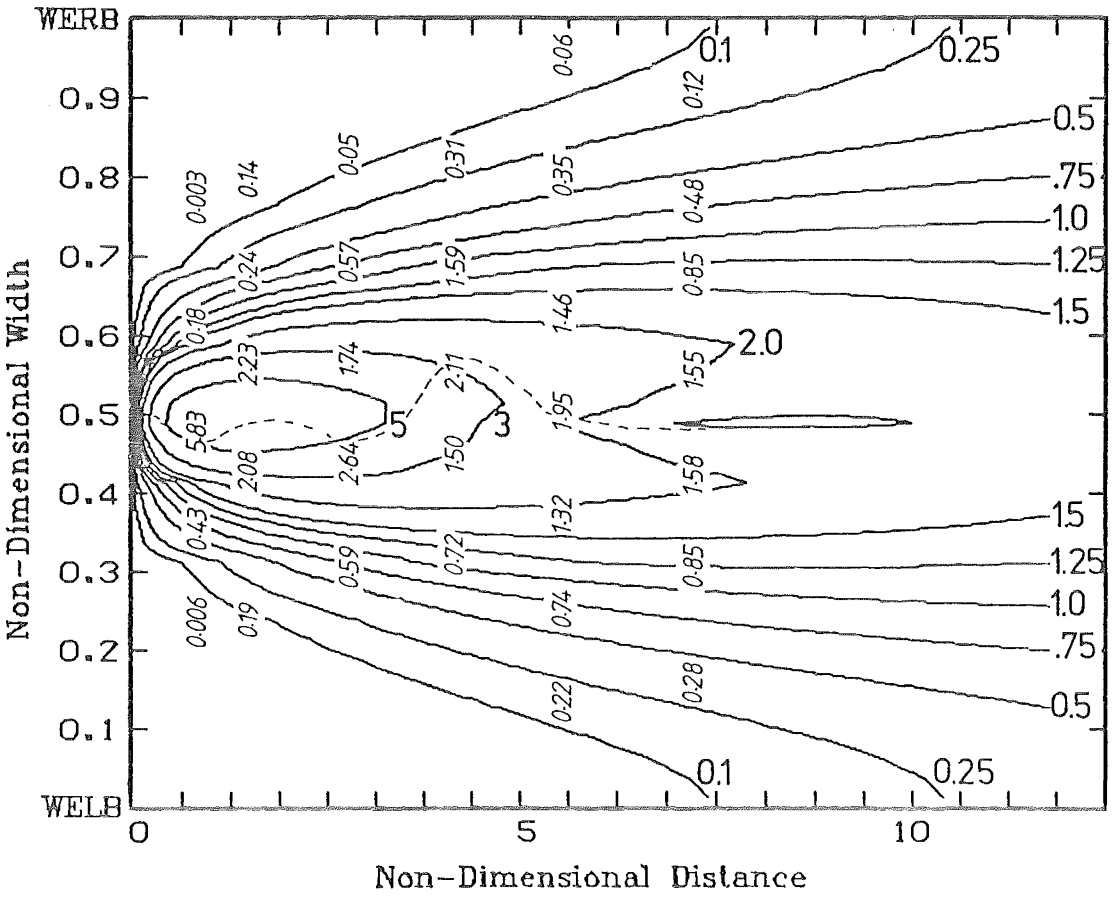

Figure 8.11b Uniform Velocity With Source At 0.50 (f=.0115)

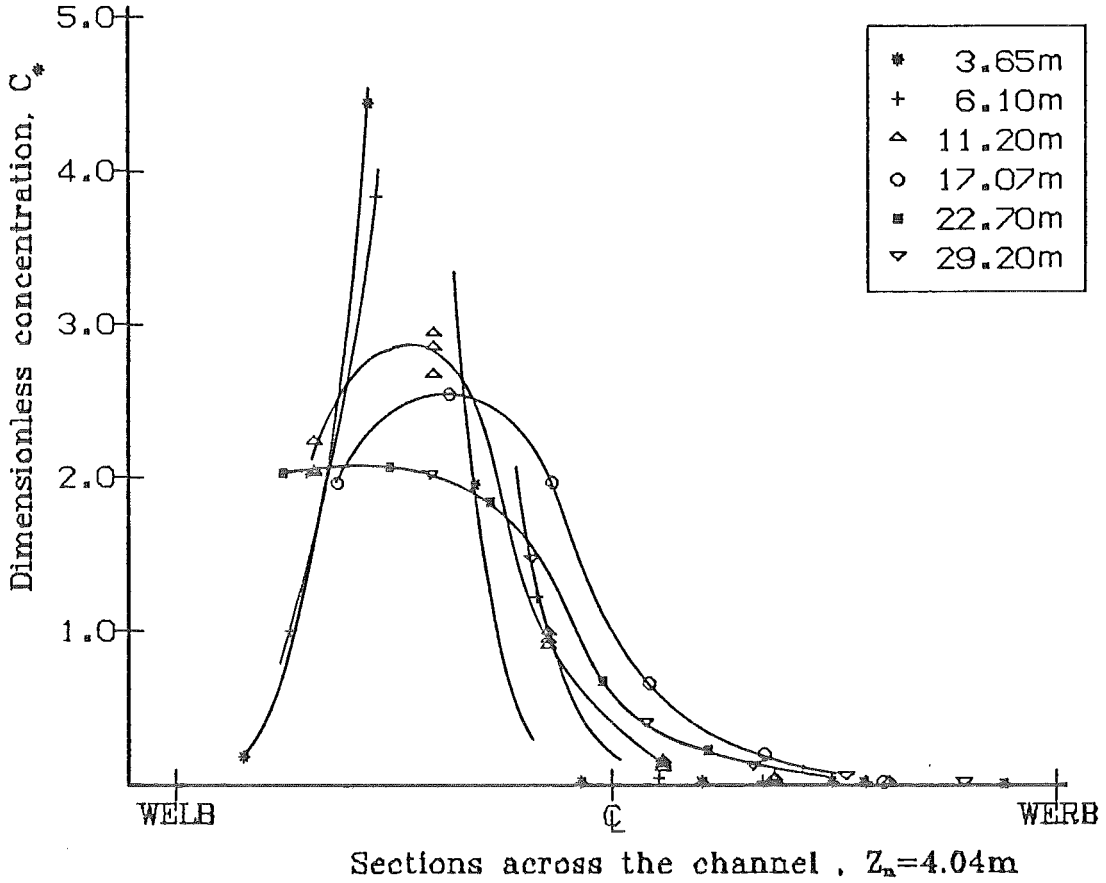

Figure 8.12a Source at 1/4-point, Run 3, 29/7/82

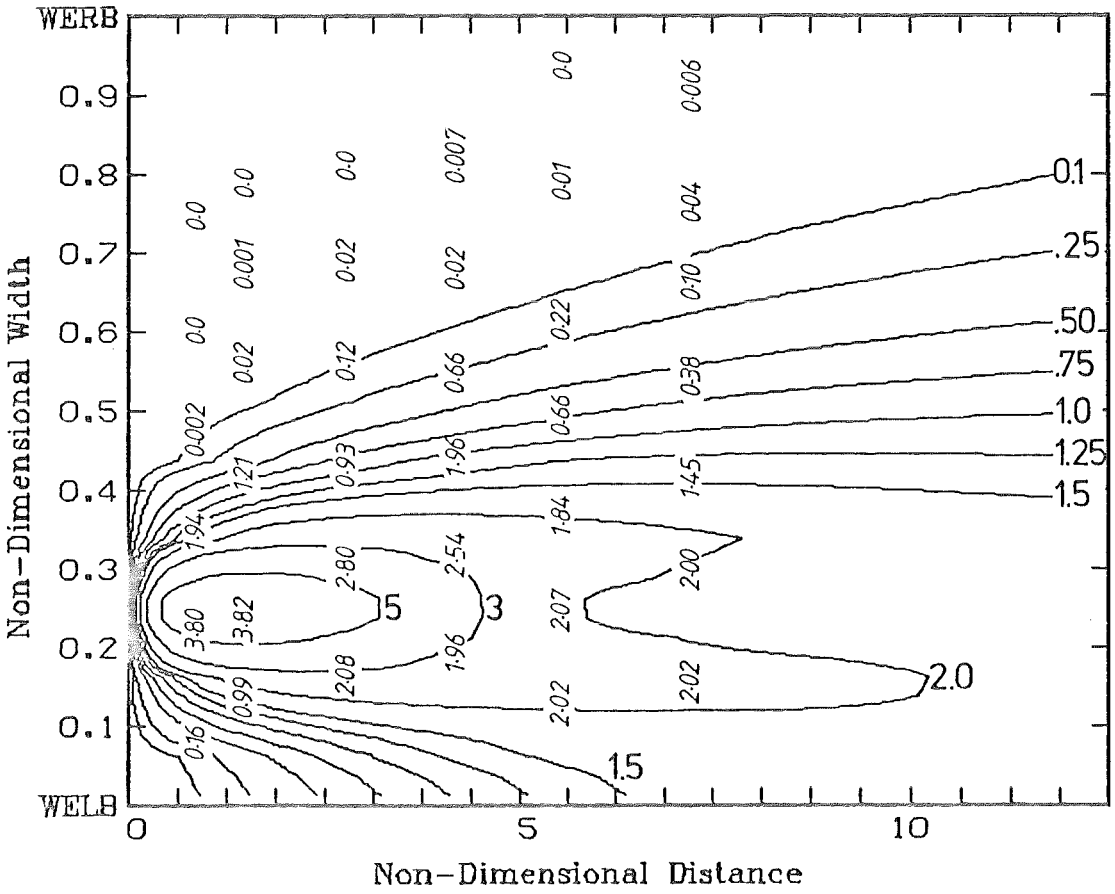

Figure 8.12b Uniform Velocity With Source At 0.25 (f=.0115)

predict a mean velocity profile at each section. Similarly, sufficient section mean profiles must be available to produce a reach averaged profile. Two typical measured velocity profiles for the smoothed channel are plotted in figure 8.8 (for slightly different discharges). Clearly, it is not possible to fit to these distributions a single profile to represent the velocity field at this section unless a large number of profiles are available. The limited manpower and time available for field work precluded such extensive velocity measurements. If one of the measured profiles shown in figure 8.8 is used in the computer model, numerical instabilities prevent a meaningful solution. It appears that such velocity distributions are not smooth enough to effect a computer solution. Hence for this initial study of the "smoothed" Craigieburn river reach a uniform velocity is used to obtain computer predictions.

While it is difficult to obtain a reach averaged velocity profile, an average section shape is more plausible. If such a mean section profile is available then an estimate of local diffusivity may be found via equation 8.2, $\varepsilon_z = 0.15\, y_\eta(\zeta)\, u_*(\zeta)$. An average bed profile was calculated from the sections shown in figure 8.4. The model was then used to compare the variable diffusivity solution with that obtained for a uniform diffusivity. This comparison is shown in figures 8.9 and 8.10. Although there is a marked difference in the predicted concentration contours neither appears to give significantly better agreement with the measured points. One section may be predicted better by the local diffusivity solution while the next section may favour the uniform diffusivity solution. Overall, a slight improvement is attained when the uniform diffusivity is used. This indicates the difficulty of trying to simplify turbulent dispersion in a real channel to produce a model.

In plots 8.11b and 8.12b, uniform velocity and diffusivity distributions are used to predict concentration distributions. Again the transverse convection of the plume is a significant factor influencing the measured concentrations. The estimated location of the measured peak concentration is plotted as a dashed line on figure 8.11b. In this rougher channel, larger transverse plume movements than those in the irrigation channel are observed. This is emphasised by the dishevelled appearance of figures 8.11a and 8.12a. Overall predictions shown in plots 8.11b and 8.12b are still reasonable considering the limited data available to calculate average channel conditions.

BLANK PAGE IN ORIGINAL - PART OF PAGINATION

8.7 Conclusions

The plots presented in this chapter indicate that overall dispersion predictions may be made with the computer model, providing reach-averaged flow properties are available. However, the inadequacy of the model to cope with varying velocities and channel shapes along the reach is also apparent. Since the solution technique involves length averaged properties it is not possible to improve on local predictions in this study.

BLANK PAGE IN ORIGINAL - PART OF PAGINATION

CHAPTER IX

THE EXTENSION OF THE MODEL TO THREE DIMENSIONS

9.1 Introduction

Results in the preceding chapter demonstrated the ability of the two-dimensional model to approximate a three-dimensional problem. In that application the two-dimensional approach will be good so long as vertical mixing is completed over a small fraction of the total mixing length. Thus the model will be suitable in most natural channels, which by nature are wide ($z_n >> y_n$). In situations where the near field is important (close to the release point) it will be necessary to choose a three-dimensional model. This will be the case when the so called near field is physically quite a large region, for example in atmospheric applications or in deep channels. In this chapter the general dispersion equation 2.8 is developed to produce moments of concentration along a streamline at any location in the channel cross-section. The employment of the three-dimensional model is limited by the fitting of concentration profiles to the computed moments of concentration. Although an accurate fit is still possible for the far field, it is the near field which is significant for three-dimensional problems.

9.2 The Three-Dimensional Model

The flow section for this model is idealised by a rectangular grid of variable dimensions. A rectangular section was chosen for simplicity but there is no reason why this could not be developed further to model any flow section desired. As in the previous chapter, dead zones are neglected.

The minimum dimensions of the grid used will depend on the number of points required for a reasonable representation of the vertical and horizontal velocity profiles. Sufficient points will also be needed to produce desired output plots. The maximum number of elements allowable is dependent on available computer space, and for this study up to 8190 elements could be used.

There is no flux of pollutant through the flow boundaries and the movement of pollutant within the flow region will be governed by the

BLANK PAGE IN ORIGINAL - PART OF PAGINATION

exchange of dispersant between adjacent elements. Diffusivities are defined at element interfaces and an average velocity assigned to each element.

9.3 Model Equations

9.3.1 Three-Dimensional Diffusion Equation

The general convective-diffusive equation in three-dimensions for turbulent open channel flow presented in chapter 2 is,

$$\frac{\partial c}{\partial t} + u \frac{\partial c}{\partial x} = \frac{\partial}{\partial x}\left(\varepsilon_x \frac{\partial c}{\partial x}\right) + \frac{\partial}{\partial y}\left(\varepsilon_y \frac{\partial c}{\partial y}\right) + \frac{\partial}{\partial z}\left(\varepsilon_z \frac{\partial c}{\partial z}\right) \qquad (9.1)$$

For the steady release case, $\frac{\partial c}{\partial t} = 0$ and longitudinal concentration gradients will be small so the longitudinal (x) turbulent diffusion term is neglected. The local eddy diffusivities are defined as,

$$\varepsilon_y = D_y \psi(y, z)$$

and

$$\varepsilon_z = D_z \phi(y, z) \qquad (9.2)$$

where D_y and D_z are constants and $\psi(y, z)$ and $\phi(y, z)$ are functions describing respectively the vertical and transverse eddy diffusivity distributions.

Equation 9.1 then becomes

$$u(y, z) \frac{\partial c}{\partial x} = D_y\left(\frac{\partial}{\partial y} \psi(y, z) \frac{\partial c}{\partial y}\right) + D_z\left(\frac{\partial}{\partial z} \phi(y, z) \frac{\partial c}{\partial z}\right) \qquad (9.3)$$

The equations describing the boundary conditions, zero flux of mass across any of the flow boundary, are

$$\psi(y, z) \frac{\partial c}{\partial y} = 0, \; y = 0, \; y_n$$

and

$$\phi(y, z) \frac{\partial c}{\partial z} = 0, \; z = 0, \; z_n \qquad (9.4)$$

Upstream and downstream boundary conditions are identical to those for the two-dimensional model; at $x = 0$, $c = 0$ everywhere except at the source position and at $x = \infty$, $c = c_e$, the equilibrium concentration. The solution developed below requires the source to occupy at least one complete element. The source strength will therefore depend on the number of elements containing the source and the total number of elements.

BLANK PAGE IN ORIGINAL - PART OF PAGINATION

9.3.2 Definition of Dimensionless Variables

Since the dominant length scale in the three-dimensional situation is the flow width, the average flow width, z_n replaces the average flow depth, y_n used to non-dimensionalise the two-dimensional parameters. The mean flow width will also be more consistent in proportion to its magnitude and easier to identify than the mean depth. The dimensionless parameters are

$$\xi = \frac{x}{z_n},\ \zeta = \frac{z}{z_n},\ \eta = \frac{y}{z_n}$$
$$\tau = \frac{\bar{u}t}{z_n},\ \chi(\eta, \zeta) = \frac{u}{\bar{u}} \tag{9.5}$$

Substituting these into the diffusion equation 9.3 gives,

$$\frac{z_n}{y_n}\frac{8}{f}\chi(\eta, \zeta)\frac{\partial c}{\partial \xi} = \frac{\partial}{\partial \eta}\psi(\eta, \zeta)\frac{\partial c}{\partial \eta} + \frac{D_z}{D_y}\frac{\partial}{\partial \zeta}\phi(\eta, \zeta)\frac{\partial c}{\partial \zeta} \tag{9.6}$$

where $D_y = \frac{u_*^2 y_n}{\bar{u}}$ and $D_z = \frac{u_*^2 z_n}{\bar{u}}$.

The boundary condition becomes,

$$\psi(\eta, \zeta)\frac{\partial c}{\partial \eta} = 0,\ \eta = 0, 1$$
$$\phi(\eta, \zeta)\frac{\partial c}{\partial \zeta} = 0,\ \zeta = 0, 1 \tag{9.7}$$

9.3.3 The Aris Moment Transforms

As the application of Aris moment transforms reduced the two-dimensional problem to a one-dimensional problem, the three-dimensional problem may be reduced to two-dimensions. Again transforms are expressed as integrals of the moment of concentration along any horizontal flow element in the ξ-direction,

$$c_p(\eta, \zeta) = c_p = \int_0^\infty c\ \xi^p\ d\xi \tag{9.8}$$

The deficit concentration is used once more to ensure moments obtained will be finite,

$$c_{d*} = c_* - 1 \tag{9.9}$$

resulting in, from equation 9.6,

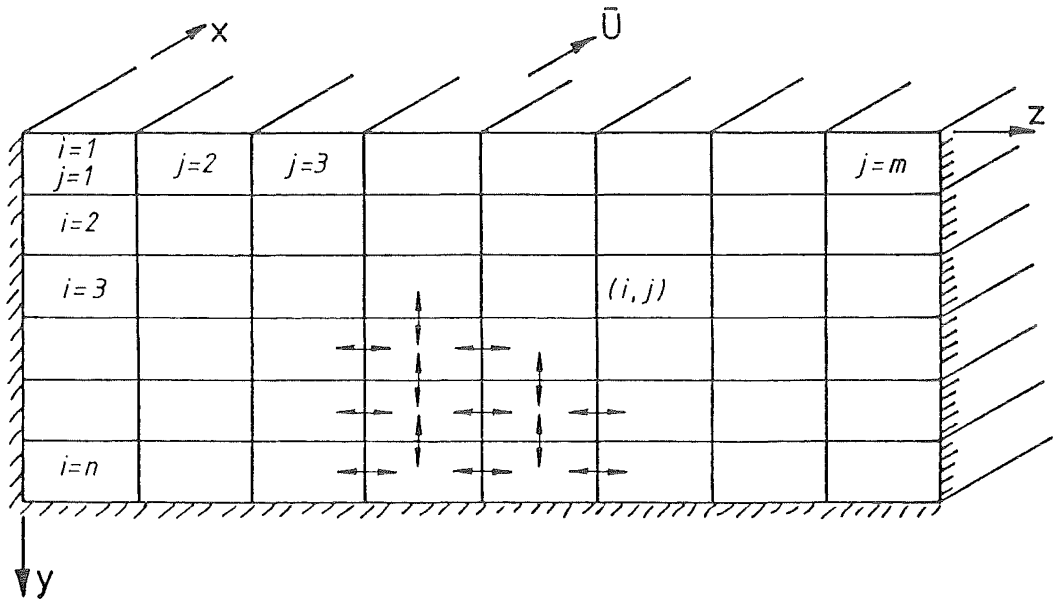

Figure 9.1 : Idealised flow section for the three-dimensional model.

$$\frac{z_n}{y_n}\frac{8}{f}\chi(\eta,\zeta)\frac{\partial c_{d*}}{\partial \xi} = \frac{\partial}{\partial \eta}\psi(\eta,\zeta)\frac{\partial c_{d*}}{\partial \eta} + \frac{D_z}{D_y}\frac{\partial}{\partial \zeta}\phi(\eta,\zeta)\frac{\partial c_{d*}}{\partial \zeta} \qquad (9.10)$$

If equation 9.10 is multiplied by ξ^p and integrated as per equation 9.8, then moment equations are obtained. The basic form of the equations is unchanged from the two-dimensional equations which are derived in Appendix A. The resulting moment equations are, for p = 0,

$$-\frac{8}{f}\frac{z_n}{y_n}\chi(\eta,\zeta)\,c_{d*}\Big|_{\xi=0} = \frac{\partial}{\partial \eta}\psi(\eta,\zeta)\frac{\partial c_{d0}}{\partial \eta} + \frac{D_z}{D_y}\frac{\partial}{\partial \zeta}\phi(\eta,\zeta)\frac{\partial c_{d0}}{\partial \zeta}$$

for p = 1,

$$-\frac{8}{f}\frac{z_n}{y_n}\chi(\eta,\zeta)\,c_{d0} = \frac{\partial}{\partial \eta}\psi(\eta,\zeta)\frac{\partial c_{d1}}{\partial \eta} + \frac{D_z}{D_y}\frac{\partial}{\partial \zeta}\phi(\eta,\zeta)\frac{\partial c_{d1}}{\partial \zeta} \qquad (9.11)$$

and for $p \geq 2$,

$$-p\frac{8}{f}\frac{z_n}{y_n}\chi(\eta,\zeta)\,c_{d(p-1)} = \frac{\partial}{\partial \eta}\psi(\eta,\zeta)\frac{\partial c_{dp}}{\partial \eta} + \frac{D_z}{D_y}\frac{\partial}{\partial \zeta}\phi(\eta,\zeta)\frac{\partial c_{dp}}{\partial \zeta}$$

The solution of equations 9.11 will provide c_{dp}, for p = 0, 1...

9.4 The Numerical Scheme

Previously, in the equations generated for the moments, the unknown c_{dp} appeared only once in each equation with all other terms being known. This enabled a solution by numerical integration, a technique which was found to be very stable and accurate. However, it can be seen in equation 9.11 that c_{dp} occurs twice in each equation. Of the methods available for the solution of equation 9.11 a finite difference technique was chosen. This formulation of the problem is well-known and appears sufficiently accurate for this application.

The idealised rectangular flow section is divided into elements as shown in figure 9.1. If elements are labelled in terms of i and j then each of the terms in equation 9.11 can be written in a difference form, such as,

$$\frac{\partial}{\partial \eta}\psi(\eta,\zeta)\frac{\partial c_{dp}}{\partial \eta} = \left[\frac{\psi_{i+\frac{1}{2},\,j}}{\Delta\eta^2}\left(c_{dp(i+1,\,j)} - c_{dp(i,\,j)}\right) - \frac{\psi_{i+\frac{1}{2},\,j}}{\Delta\eta^2}\left(c_{dp(i,\,j)} - c_{dp(i-1,\,j)}\right)\right] \qquad (9.12)$$

where $c_{dp(i,j)}$ is the pth moment in element (i, j) and $\psi_{i+\frac{1}{2},\,j}$ is the

BLANK PAGE IN ORIGINAL - PART OF PAGINATION

diffusivity at the interface of elements (i, j) and (i + 1, j). A similar equation may be written for the transverse term.

The numerical scheme developed to solve equation 9.11 for c_{dp} in each element may be split into two stages. The first section of the program calculates diffusivities at the interfaces surrounding each element, the velocity in each element and the boundary conditions, if any, to be imposed on each element. If an element is on the boundary then a phantom element is introduced across the appropriate interface and this element is given the same identification as the adjacent flow element. For instance, in equation 9.12, if i = n then $c_{dp(i+1,\ j)}$ is a phantom element which is actually identical to $c_{dp(i,\ j)}$ and consequently the term

$$\frac{\psi_{i+\frac{1}{2},\ j}}{\Delta\eta^2}\left(c_{dp(i+1,\ j)} - c_{dp(i,\ j)}\right)$$

is zero, satisfying the boundary condition. The above information is then used to generate a matrix of coefficients for c_{dp} in equation 9.11 (this is a constant matrix for all moments).

The second stage is a loop which is executed for each of the moments required. Inside this loop the left hand side of equation 9.11 is calculated and stored in an array. The solution for c_{dp} may now be obtained using matrix solving techniques since equation 9.11 can be written as,

$$Ax = b \qquad (9.13)$$

where A is the coefficient matrix, x is $c_{dp(i,\ j)}$ and b is the array corresponding to the left hand side of equation 9.11. A library package of subroutines for real sparse matrices is used to solve for the coefficients, c_{dp}, The routine uses a variant of Gaussian elimination, with a pivotal strategy designed to compromise between maintaining sparsity and controlling loss of accuracy through round-off. After the coefficient matrix has been operated on, the decomposed form is retained and may be used for all moments (i.e. the matrix is decomposed once only).

9.5 Flow Data Input

9.5.1 Velocity Distribution

As with the two-dimensional program the model should be able to calculate solutions for any particular velocity distribution. This was

Source Location	Moment	3-D Computer Solution	2-D Computer Solution	Percentage Difference
0.2	c_{d0}	25.9564143	25.9567566	0.00132
	c_{d1}	490.648528	490.630328	0.00371
	c_{d2}	16940.6519	16939.5971	0.00623
0.5	c_{d0}	-7.34358416	-7.34324344	0.00464
	c_{d1}	-40.2522946	-40.2466676	0.01398
	c_{d2}	-486.701983	-486.598274	0.02131
0.8	c_{d0}	-25.2150107	-25.2146720	0.00134
	c_{d1}	-477.593318	-477.575312	0.00377
	c_{d2}	-16942.0149	-16940.9827	0.00609

Table 9.1 : A comparison of moments obtained from the three-dimensional program (using 200 vertical elements with a horizontal line source) and the two-dimensional program, at $\eta = 0.0125$, in a uniform velocity field.

achieved by including in the computer program (see Appendix E) a subroutine containing possible velocity distributions. These velocity distributions were two-dimensional only, and were used to evaluate the model.

In the general situation vertical and transverse velocity profiles are required to describe a typical three-dimensional flow. In this case two possible methods may be used to input this data. If the distribution is able to be described mathematically then a velocity function ($\chi(\eta, \zeta)$) may be included in the velocity subroutine. However, often for a three-dimensional flow field the velocity is only described by a series of point measurements at various cross-sections. Enough measurements should be made along the reach to confidently predict an average velocity distribution for the entire reach under study. From the representative velocity distribution average element velocities can be calculated and input into the computer model as a matrix.

9.5.2 Diffusivity Distribution

Diffusivities may be input in a similar manner to velocity distributions. However, for the examples given later in this chapter a uniform diffusivity was used. While it is recognised that there is some cross-sectional variation in diffusivity, this is not fully understood at this stage. Of the limited work performed to examine the transverse variation of diffusivity the most promising study is that by Lau and Krishnappen (1981). They found that the best agreement was obtained with measured data if the model for local diffusivity was a function of the local velocity and depth, and the averaged transverse diffusivity was variable along the reach. Any such diffusivity profile may be included in the model by modifying one or two lines in the diffusivity subroutine.

9.6 Program Evaluation

The accuracy of the solution technique was judged in the same manner as the two-dimensional solution (Section 4.3.1). Moments computed using the three-dimensional model for a uniform velocity, two-dimensional (horizontal line source) problem, are compared with moments obtained using the two-dimensional model. Moments from the two-dimensional model were shown to be sufficiently accurate in section 4.3.1. Table 9.1 shows the comparison near the channel bed (η = 0.0125) for three source locations. As the source extends the entire width of the channel the number of horizontal elements used in the three-dimensional solution is not relevant.

Source Location	Moment	3-D Computer Solution	2-D Computer Solution	Percentage Difference
0.2	c_{d0}	38.4043856	38.4730140	0.1784
	c_{d1}	553.028389	553.333862	0.0552
	c_{d2}	16688.3404	16696.4644	0.0487
0.5	c_{d0}	-0.114592167	-.066790997	41.7142
	c_{d1}	95.2295961	95.9682595	0.7697
	c_{d2}	3812.84870	3835.24190	0.5839
0.8	c_{d0}	-21.9720331	-21.9461705	0.1178
	c_{d1}	-369.351787	-368.849025	0.1363
	c_{d2}	-11757.3083	-11740.7472	0.1411

Table 9.2 : A comparison of moments obtained from the three-dimensional program (using 200 vertical elements with a horizontal line source) and the two-dimensional program, at $\eta = 0.0125$, in a logarithmic velocity field.

The errors shown in table 9.1 are approximately one order of magnitude larger than those between the two-dimensional solution and analytical moments shown in table 4.1. However, errors are expected to be larger for the finite difference scheme than those arising from the numerical integration scheme used in the two-dimensional model. The moments are certainly accurate enough to be used for estimating concentration profiles.

An identical evaluation is presented in table 9.2 for a non-uniform (logarithmic) velocity distribution. Very large errors are noted when the source is at the centre of the channel, however the absolute errors for this source position are of the same order as for other source locations (the large percentage errors correspond to smaller moments). The main cause of the overall increase in the percentage errors is the representation of the logarithmic velocity profile in the model. For the uniform velocity, where the velocity is equal to the mean velocity everywhere, it is straightforward to apply the correct velocity to each flow element. However, if a logarithmic velocity profile is to be used in the model, the average velocity in each flow element must be used. Consequently, the larger the number of flow elements used, the better the representation of the velocity distribution, and the better the agreement with the correct moments. The limiting factor is the number of elements which the computer is able to handle in the three-dimensional model.

9.7 A Justification of the Applicability of the Two-Dimensional Model to the Field Experiments

In the previous chapter, the two-dimensional model developed earlier was used to predict the dispersion pattern for a continuous point source in a natural channel. Although the dispersion will initially be three-dimensional it was expected that the length required for complete vertical mixing would be much less than that for complete section mixing. On this basis it was assumed that vertical averages could be used at all sections along the reach. It is now possible to examine this assumption with the complete three-dimensional model presented in this chapter.

For both of the test reaches discussed in Chapter 8 the three-dimensional program was applied to obtain a concentration distribution at the first and last measurement section. As a first approximation to the velocity field, the same vertical logarithmic velocity distribution was taken at all points across the section. Secondary currents (across the

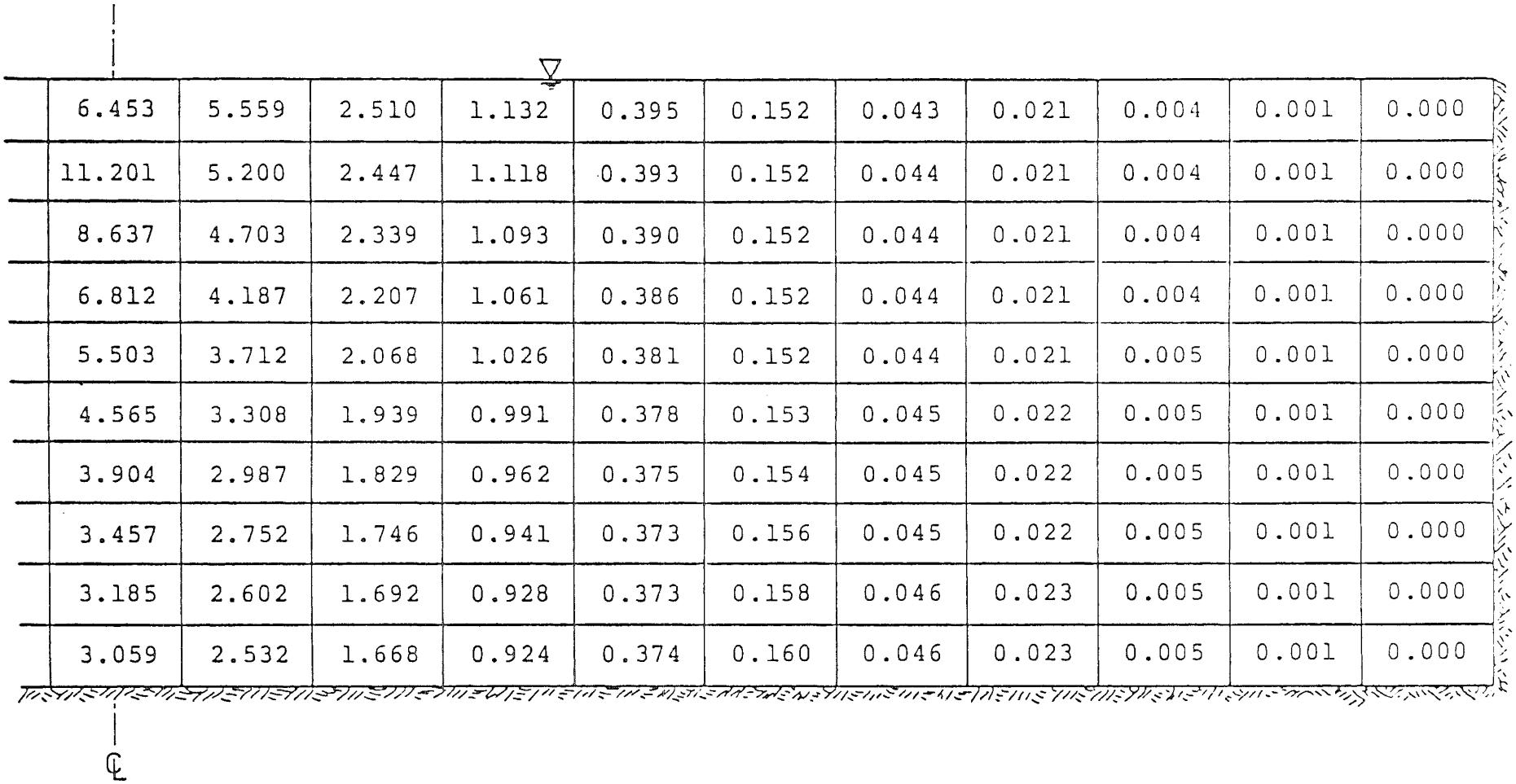

6.453	5.559	2.510	1.132	0.395	0.152	0.043	0.021	0.004	0.001	0.000
11.201	5.200	2.447	1.118	0.393	0.152	0.044	0.021	0.004	0.001	0.000
8.637	4.703	2.339	1.093	0.390	0.152	0.044	0.021	0.004	0.001	0.000
6.812	4.187	2.207	1.061	0.386	0.152	0.044	0.021	0.004	0.001	0.000
5.503	3.712	2.068	1.026	0.381	0.152	0.044	0.021	0.005	0.001	0.000
4.565	3.308	1.939	0.991	0.378	0.153	0.045	0.022	0.005	0.001	0.000
3.904	2.987	1.829	0.962	0.375	0.154	0.045	0.022	0.005	0.001	0.000
3.457	2.752	1.746	0.941	0.373	0.156	0.045	0.022	0.005	0.001	0.000
3.185	2.602	1.692	0.928	0.373	0.158	0.046	0.023	0.005	0.001	0.000
3.059	2.532	1.668	0.924	0.374	0.160	0.046	0.023	0.005	0.001	0.000

Figure 9.2 : Predicted concentrations at the first sampling section (x = 18.90 m, ξ = 5.97) in the irrigation canal.

channel) were ignored, as were any variations in channel geometry across and along the channel.

Figure 9.2 shows the predicted pollutant distribution (in non-dimensional form) for the first sampling section (x = 18.90 m, ξ = 5.87) in the irrigation canal (see plates 7.1 and 7.3). This channel had an average width of 3.22 m and an average depth of 263 mm $\left(\frac{z_n}{y_n} = 12.2\right)$. The plot of concentrations in figure 9.2 is for a source at the mid-point of the channel, on the water surface and is therefore symmetric about the centreline. Although there are some spurious concentrations (due to the fitting procedure), particularly near to the source, the overall distribution is easily perceivable. Clearly, there is still a significant vertical concentration gradient at the centre of the channel. If samples were collected at the mid-depth of the channel (as they were in both field tests) it would be expected that the vertical average concentration would be obtained. Towards the side of the channel the vertical mixing is complete and samples could be collected anywhere over the depth. For a release point away from the centreline of the channel there will be a similar distance either side of the source (depending on the proximity of the banks) where vertical concentration gradients exist.

At the final sampling section (x = 122.85 m, ξ = 38.14) in the irrigation canal (see figure 9.3) mixing is complete in all vertical sections except that containing the source. In most of the other sections there is a slight concentration gradient but it is opposite to any expected gradients (positive away from the source). This arises partly from the fitting procedure used to obtain the concentration distribution (near the source) and partly from numerical errors. In the vertical section containing the source problems arise from the assumption that the source initally occupies an entire flow element. If the source could be reduced to a point source it is expected that vertical mixing would also be complete over this section.

Figures 9.4 and 9.5 are the comparative diagrams for the Craigieburn River, the second field test reach, which had an average width of 4.04 m and an average depth of 131 mm. This channel is much wider than the irrigation canal, the average width to depth ratio is 30.8, as compared to 12.2 for the irrigation canal. Consequently the vertical mixing is achieved in a smaller number of channel widths. Even at x = 3.65 m (ξ = 0.90), the first sampling section shown in figure 9.3, all points

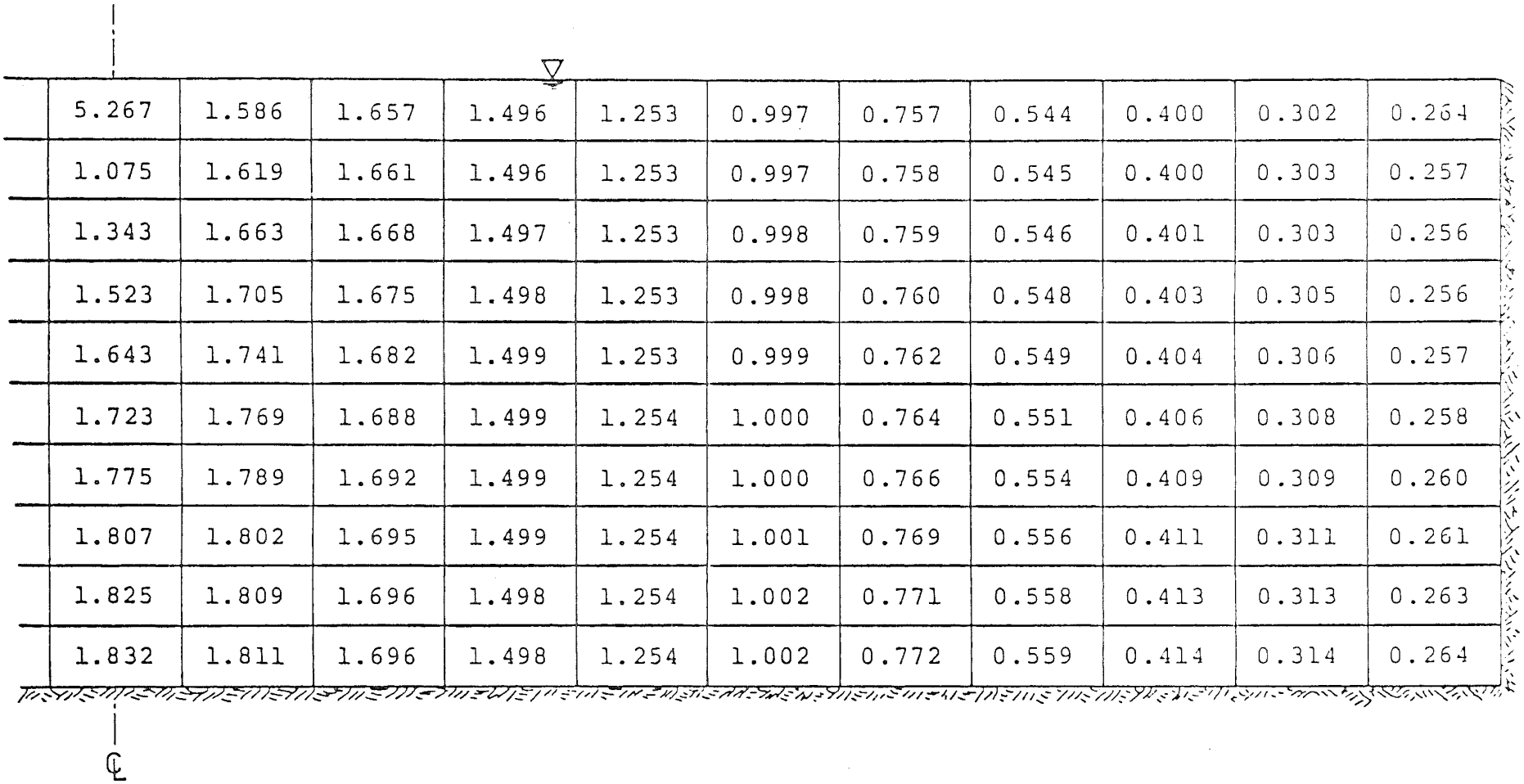

5.267	1.586	1.657	1.496	1.253	0.997	0.757	0.544	0.400	0.302	0.264
1.075	1.619	1.661	1.496	1.253	0.997	0.758	0.545	0.400	0.303	0.257
1.343	1.663	1.668	1.497	1.253	0.998	0.759	0.546	0.401	0.303	0.256
1.523	1.705	1.675	1.498	1.253	0.998	0.760	0.548	0.403	0.305	0.256
1.643	1.741	1.682	1.499	1.253	0.999	0.762	0.549	0.404	0.306	0.257
1.723	1.769	1.688	1.499	1.254	1.000	0.764	0.551	0.406	0.308	0.258
1.775	1.789	1.692	1.499	1.254	1.000	0.766	0.554	0.409	0.309	0.260
1.807	1.802	1.695	1.499	1.254	1.001	0.769	0.556	0.411	0.311	0.261
1.825	1.809	1.696	1.498	1.254	1.002	0.771	0.558	0.413	0.313	0.263
1.832	1.811	1.696	1.498	1.254	1.002	0.772	0.559	0.414	0.314	0.264

Figure 9.3 : Predicted concentrations at the final sampling section (x = 122.85 m, ξ = 38.14) in the irrigation canal.

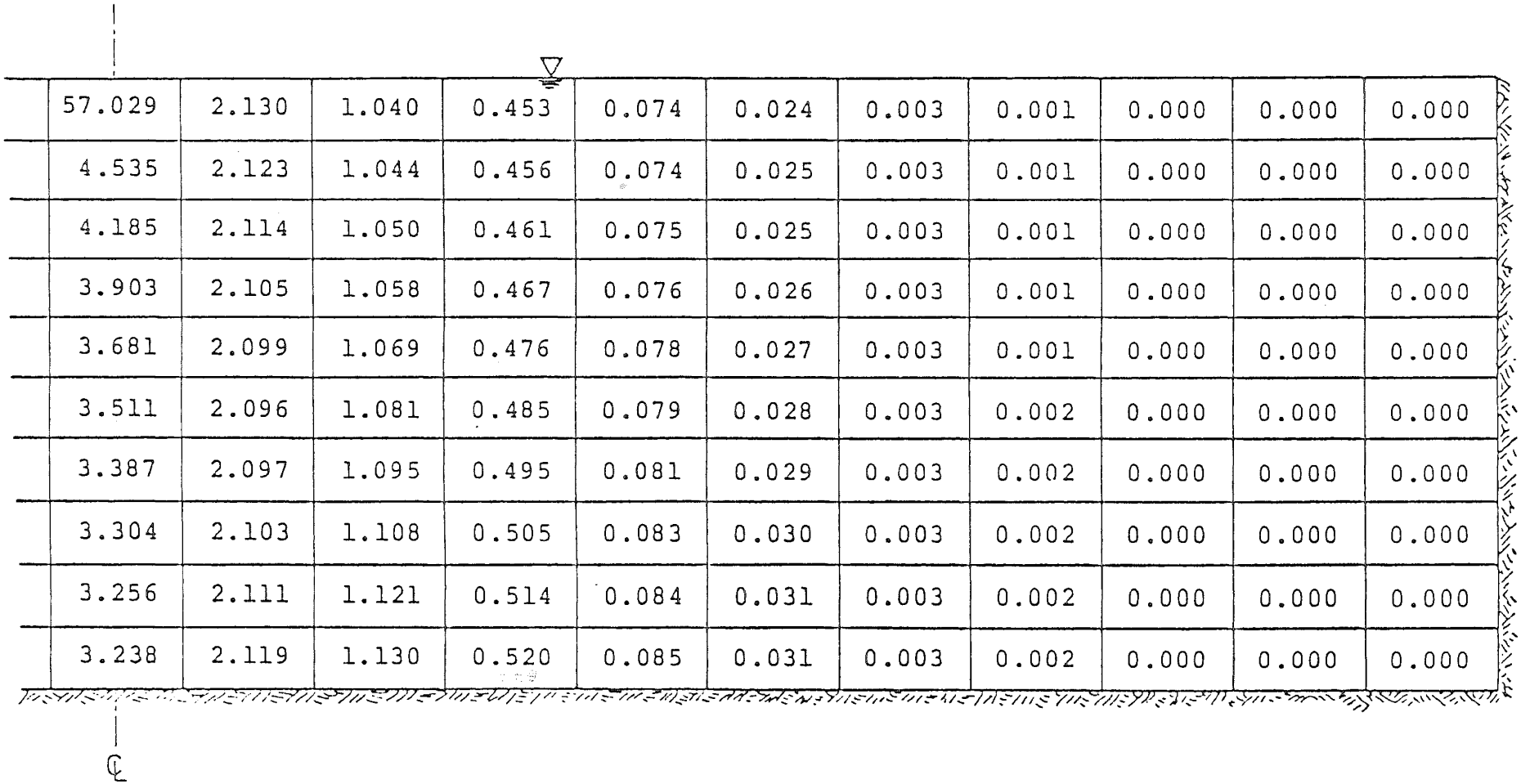

57.029	2.130	1.040	0.453	0.074	0.024	0.003	0.001	0.000	0.000	0.000
4.535	2.123	1.044	0.456	0.074	0.025	0.003	0.001	0.000	0.000	0.000
4.185	2.114	1.050	0.461	0.075	0.025	0.003	0.001	0.000	0.000	0.000
3.903	2.105	1.058	0.467	0.076	0.026	0.003	0.001	0.000	0.000	0.000
3.681	2.099	1.069	0.476	0.078	0.027	0.003	0.001	0.000	0.000	0.000
3.511	2.096	1.081	0.485	0.079	0.028	0.003	0.002	0.000	0.000	0.000
3.387	2.097	1.095	0.495	0.081	0.029	0.003	0.002	0.000	0.000	0.000
3.304	2.103	1.108	0.505	0.083	0.030	0.003	0.002	0.000	0.000	0.000
3.256	2.111	1.121	0.514	0.084	0.031	0.003	0.002	0.000	0.000	0.000
3.238	2.119	1.130	0.520	0.085	0.031	0.003	0.002	0.000	0.000	0.000

Figure 9.4 : Predicted concentrations of the first sampling section (x = 3.65 m, ξ = 0.90) in the Craigieburn River.

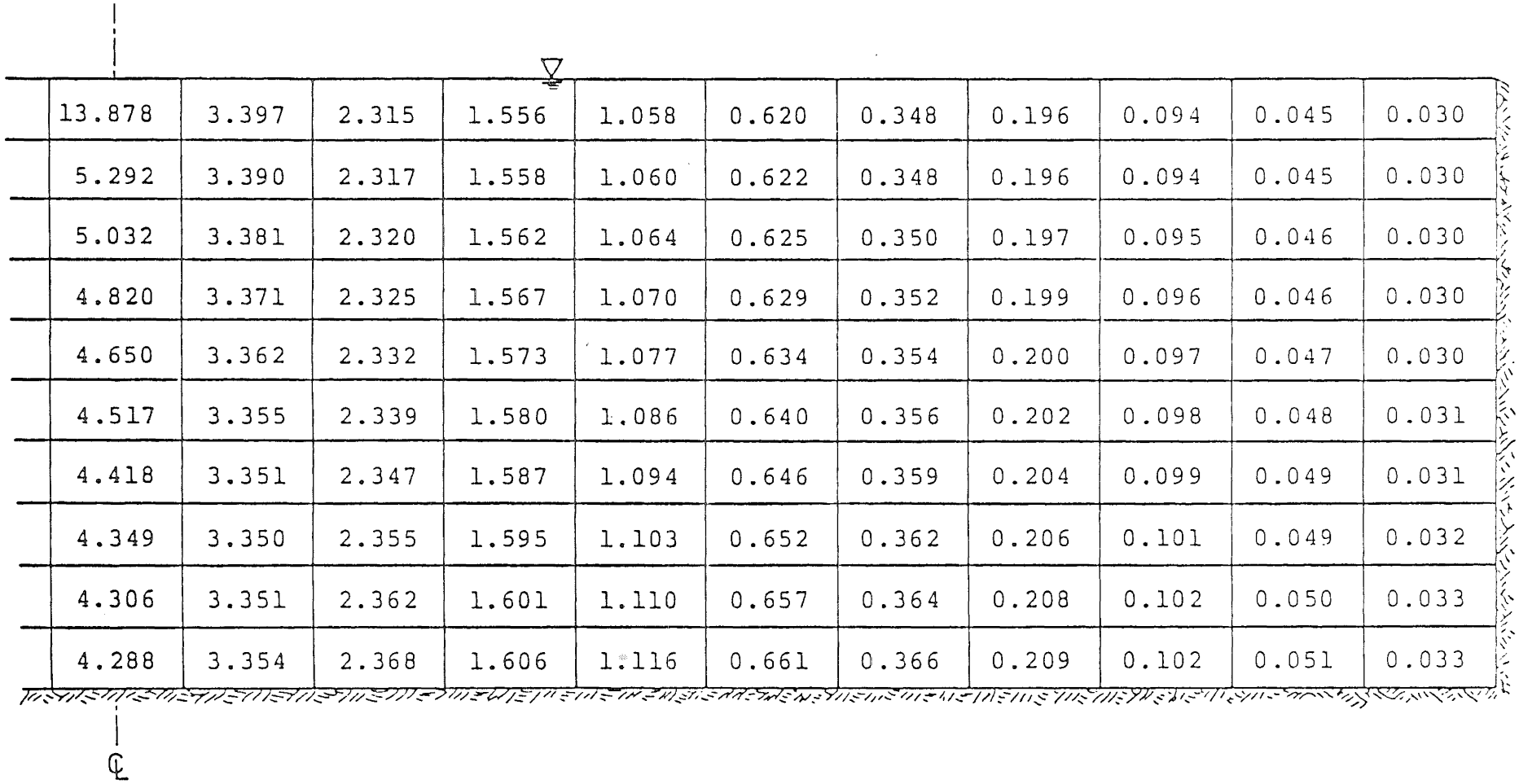

13.878	3.397	2.315	1.556	1.058	0.620	0.348	0.196	0.094	0.045	0.030
5.292	3.390	2.317	1.558	1.060	0.622	0.348	0.196	0.094	0.045	0.030
5.032	3.381	2.320	1.562	1.064	0.625	0.350	0.197	0.095	0.046	0.030
4.820	3.371	2.325	1.567	1.070	0.629	0.352	0.199	0.096	0.046	0.030
4.650	3.362	2.332	1.573	1.077	0.634	0.354	0.200	0.097	0.047	0.030
4.517	3.355	2.339	1.580	1.086	0.640	0.356	0.202	0.098	0.048	0.031
4.418	3.351	2.347	1.587	1.094	0.646	0.359	0.204	0.099	0.049	0.031
4.349	3.350	2.355	1.595	1.103	0.652	0.362	0.206	0.101	0.049	0.032
4.306	3.351	2.362	1.601	1.110	0.657	0.364	0.208	0.102	0.050	0.033
4.288	3.354	2.368	1.606	1.116	0.661	0.366	0.209	0.102	0.051	0.033

Figure 9.5 : Predicted concentrations at the final sampling section (x = 29.20 m, ξ = 7.24) in the Craigieburn River.

but the vertical section containing the source, may be considered to be vertically well mixed. Again the fitting and numerical accuracy accounts for most of the variation in each vertical section. It can be concluded that for this reach the samples may be collected at any depth in the flow to obtain a vertically averaged concentration.

In conclusion, the approximation of applying the two-dimensional model to a point release is well justified if the river channel is wide. Of the two reaches investigated, the Craigieburn River certainly falls into this category but a little caution must be exercised in applying the two-dimensional model to the irrigation channel. While it is possible to predict the distance from the source at which vertical mixing is complete it is not possible to incorporate the effect of the initial three-dimensional mixing region in the two-dimensional model. Considering the agreement between predicted concentrations and measured concentrations in the irrigation canal (section 8.6.1) it is possible that this initial three-dimensional effect is offset by the secondary current and local flow properties. In both channels an accurate forecast of the dispersion pattern is limited by the flow properties available and the fitting techniques used in the model to obtain a concentration profile from the concentration moments.

BLANK PAGE IN ORIGINAL - PART OF PAGINATION

CHAPTER X

SUMMARY, CONCLUSIONS AND RECOMMENDATIONS FOR FUTURE RESEARCH

10.1 Summary

A model has been developed to solve the complete dispersion equation for a conservative non-buoyant pollutant released continuously into an open channel. The model was verified by a set of laboratory experiments. The verified model was then used to examine the assumptions that previous investigators have made to obtain a concentration distribution for a continuous release of pollutant.

The technique was also applied to a natural channel and compared with data collected from field experiments.

10.2 Evaluation of Assumptions Made by Previous Investigators

This study has enabled comparisons to be made between the assumptions that were previously necessary to obtain a solution to the dispersion equation and conditions expected in laboratory situations. The conclusions which can be drawn from this comparison are:

(1) As previously assumed the effect of the longitudinal diffusion on the concentration distribution is negligible.

(2) The use of uniform flow conditions in the model produces conservative predictions of pollutant concentrations. The more realistic logarithmic velocity distribution resulted in approximately a 25% reduction in the mixing length.

The trapping mechanism that has been recognised by other investigators (Valentine 1978) as an important aspect for longitudinal dispersion was found to be of little consequence for a continuous release of contaminant. For any given channel the most significant channel boundary parameter is the friction factor. This may be determined from the flow conditions existing in the channel, independently of the nature of the channel roughness. That is to say, an identical friction factor may be obtained for a uniformly rough granular bed material as for a smoother material with trapping pockets of intervals along the bed. It was demonstrated in Chapter 4 that in both of these cases the concentration

BLANK PAGE IN ORIGINAL - PART OF PAGINATION

distribution downstream for a continuous source would be the same.

10.3 The Application of the Model to Laboratory and Field Experiments

Prior to applying the model to natural channels, a laboratory verification was carried out. It was shown in Chapter 6 that the model may be used to predict the concentration field provided an accurate description of the velocity distribution is available.

In Chapter 8 the two-dimensional model was applied to two field experimental situations. In each case it was found that reasonable predictions of the overall dispersion pattern were possible. Again the success of the model for such estimates is dependent on the availability of average channel conditions. In a typical natural channel, conditions along a reach will usually vary, requiring a large amount of data to obtain reach averaged channel properties (i.e. velocity profile, depth profile etc). Since the model uses the reach averaged conditions, local variations down the channel are not able to be predicted. However, the model may be extended following the method used by Yotsukura and Sayre (1976) to account for channel curvature and a meandering thalweg. This technique results in a smoothing of the flow conditions along the reach.

The applicability of the two-dimensional model, for three-dimensional experiments performed in an irrigation canal and in the Craigieburn River, was confirmed in Chapter 9. Although the three-dimensional model is not complete (in the sense that the fitting technique is not perfect), it was sufficient to estimate vertical mixing along a reach. In both test reaches vertical mixing was expected long before complete cross-sectional mixing. For the wider test reach (the Craigieburn River, $\frac{z_n}{y_n} = 30.8$) vertically uniform concentrations were predicted by the three-dimensional model for all sampling locations (beginning at $\xi = 0.90$, $x = 3.65$ m). As most natural streams are wide ($y_n << z_n$), the two-dimensional model applied to the transverse mixing problem will give accurate dispersion patterns, providing the channel flow properties are sufficiently defined.

10.4 Recommendations for Future Research

Future work should be directed at five major topics:

(1) The only limitation of the model developed in this study is its ability to correctly describe the concentration field in certain

BLANK PAGE IN ORIGINAL - PART OF PAGINATION

(1) Cont. extreme conditions, such as, close to the source where concentration gradients are large. Since it has been shown that the moments of concentration obtained in the first stage of the solution procedure are exact (within numerical accuracy), it is the fitting of concentration profiles to these moments which requires more attention. This is essentially a near-field problem, as the far field concentrations may be determined exactly from high order moments. In many cases including engineering applications, the model presented here is adequate for the concentration predictions required. However, a computer model capable of describing the complete concentration field would be very useful for situations where the near field is important, for instance in atmospheric pollution problems.

(2) If the model developed here is to be used in field situations, reliable and consistent methods of evaluating the average channel conditions are necessary. For a continuous pollutant release, the length of channel over which average conditions are required may be relatively short (of the order of hundreds of metres). Then the accurate identification of a typical section and typical flow parameters is not unreasonable. It will depend on the reach considered and the nature of the problem considered, whether or not a single section portrays enough information about the whole reach. If not, the modifications discussed in (4) below may be necessary.

(3) This model has only been applied to rectangular cross-sections, as an exact representation for the laboratory experiments and an approximate representation of the channel in the field experiments. Subsequent work should include the extension of the model to regular non-rectangular cross-sections in the laboratory (for instance trapezoidal or triangular).

(4) Most natural rivers have an inherent meandering thalweg, which is often imposed on a meandering bed. It has been demonstrated by many investigators (Fischer et al, 1979) that bends enhance the mixing across the channel. It was also shown (Yotsukura and Sayre, 1976) that the correct choice of co-ordinate system and dimensionless variables will enable most of the longitudinal irregularities of a meandering channel to be removed. Suitable modifications to the computer model would allow the techniques of Yotsukura and Sayre to be used to adapt the model for meandering channels.

BLANK PAGE IN ORIGINAL - PART OF PAGINATION

(5) In addition to mixing generated by bends, there are many other conditions in natural channels which may increase or decrease the mixing rate. Real streams have sandbars, side channels, pools, riffles, piers, changes in channel shape and other obstructions, all of which will be particular to the channel under consideration. The combination and interaction of these effects can further complicate the dispersion process. An investigation of each mechanism mentioned above will enable a composite estimate of the dispersive pattern for any natural channel.

Each of the above areas for study will enhance the understanding of mixing in natural channels. Ultimately, the knowledge of some simple channel properties (width, depth, sinuosity, flow rate, etc) should allow reasonable predictions of dispersion from a continuous source. It is not until all the problems raised in this section are answered that satisfactory predictions may be made in natural channels.

BLANK PAGE IN ORIGINAL - PART OF PAGINATION

REFERENCES

ABRAMOWITZ, M., and STEGUN, I.A., *Handbook of Mathematical Functions*, Dover Publications, Inc., New York, N.Y., 1964, pp. 1046.

ANTONIA, R.A. and WOOD, D.H., "Calculation of a Turbulent Boundary Layer Downstream of a Small Step Change in Surface Roughness," *Aeronautical Quarterly*, Aug., 1975, pp. 202-210.

ARIS, R., "On the Dispersion of a Solute in a Fluid Flowing Through a Tube," *Proceedings of the Royal Society of London*, Vol. 235A, 1956, pp. 67-77.

AYTEKIN, A. and BERGER, F.P., "Turbulent Flow in Rectangular Ducts With Low Aspect Ratios Having One Rough Wall," *Nuclear Energy*, Vol. 18, No. 1, Feb., 1979, pp. 53-63.

BATCHELOR, G.K., and TOWNSEND, A.A., "Turbulent Diffusion," *Surveys in Mechanics*, Batchelor, G.K., and Davies, R.M., ed., Cambridge University Press, Cambridge, England, 1956, pp. 352-399.

CARSLAW, H.S., and JAEGER, J.C., *Conduction of Heat in Solids*, 2nd ed., Oxford University Press, London, 1959, pp. 510.

CHATWIN, P.C., "On the Interpretation of Some Longitudinal Dispersion Experiments," *Journal of Fluid Mechanics*, Vol. 48, part 4, 1971, pp. 689-702.

DAGAN, G., "Dispersivity Tensor for Turbulent Uniform Channel Flow," *Journal of the Hydraulics Division*, ASCE, Vol. 95, No. HY5, Sept., 1969, pp. 1699-1712.

ELDER, J.W., "The Dispersion of Marked Fluid in Turbulent Shear Flow," *Journal of Fluid Mechanics*, Vol. 5, part 4, 1959, pp. 544-560.

FICK, A., "On Liquid Diffusion," *Philosophical Magazine*, Series 4, Vol. 4, No. 10, 1855, pp. 30-39.

FISCHER, H.B., "The Effect of Bends on Dispersion in Streams," *Water Resources Research*, Vol. 5, No. 2, April, 1969, pp. 496-596.

BLANK PAGE IN ORIGINAL - PART OF PAGINATION

FISCHER, H.B., discussion of "Dispersivity Tensor for Turbulent Uniform Channel Flow," by G. Dagan, *Journal of the Hydraulics Division,* ASCE, Vol. 96, No. HY4, April, 1970, pp. 1096-1100.

FISCHER, H.B., "Longitudinal Dispersion and Turbulent Mixing in Open-Channel Flow," *Annual Review of Fluid Mechanics,* Vol. 5, 1973, pp. 59-77.

FISCHER, H.B., LIST, E.J., KOH, R.C.Y., IMBERGER, J., and BROOKS, N.H., *Mixing in Inland and Coastal Waters,* 1st ed., Academic Press, Inc., New York, N.Y., 1979.

FOURIER, J.B.J., *Theorie Analytique de la Chaleur,* Didot, Paris, 1822.

GLOVER, J.R., "Multiple-Channel Conductometer For Measuring Salinity Concentrations in Laboratory Flows," *IIHR Report No. 128,* Iowa Institute of Hydraulic Research, The University of Iowa, Iowa, Nov., 1970, pp. 17.

HARDEN, T.O., and SHEN, H.T., "Numerical Simulation of Mixing in Natural Rivers," *Journal of the Hydraulics Division,* ASCE, Vol. 105, No. HY4, Proc. Paper 14501, April, 1979, pp. 393-408.

HENDERSON, F.M., *Open Channel Flow,* 1st ed., Macmillan Publishing Co., Inc., New York, N.Y., 1966.

JOBSON, H.E., and SAYRE, W.W., "Predicting Concentration Profiles in Open Channels," *Journal of the Hydraulics Division,* ASCE, Vol. 96, No. HY10, Oct., 1970, pp. 1983-1996.

JOHNSTONE, D.E., "A Procedure for Constant-Rate Injection Salt Dilution Gauging," *Report No. WS 396,* Ministry of Works and Development, Christchurch, New Zealand, Feb., 1981, pp. 35.

LAU, Y.LAM, and KRISHNAPPEN, B.G., "Transverse Dispersion in Rectangular Channels," *Journal of the Hydraulics Division,* ASCE, Vol. 103, No. HY10, Proc. Paper 13294, Oct., 1977, pp. 1173-1189.

LAU, Y.LAM, and KRISHNAPPEN, B.G., "Modelling Transverse Mixing in Natural Streams," *Journal of Hydraulics Division,* ASCE, Vol. 107, No. HY2, Proc. Paper 16048, Feb., 1981, pp. 209-226.

BLANK PAGE IN ORIGINAL - PART OF PAGINATION

OKOYE, J.K., "Characteristics of Transverse Mixing in Open Channel Flows," *Report No. KH-R-23,* W. M. Keck Laboratory of Hydraulics and Water Resources, California Institute of Technology, Pasadena, Calif., Nov., 1970, pp. 269.

PEACEMAN, D.W., and RACHFORD, H.H., Jr., "The Numerical Solution of Parabolic and Elliptic Differential Equations," *Journal on Applied Mathematics,* Society for Industrial and Applied Mathematics, Vol. 3, No. 2., Mar., 1955, pp. 28-41.

RASTOGI, A.K., and RODI, W., "Predictions of Heat and Mass Transfer in Open Channels," *Journal of the Hydraulics Division,* ASCE, Vol. 104, No. HY3, March, 1978, pp. 397-420.

ROHSENOW, W.M., and CHOI, H.Y., *Heat, Mass and Momentum Transfer,* Prentice-Hall, Englewood Cliffs, N.J., 1961, pp. 529.

RUTHERFORD, J.C., "Handbook on Mixing in Rivers," *Water and Soil Miscellaneous Publication No. 26,* Water and Soil Division of the Ministry of Works and Development, Wellington, New Zealand, 1981, pp. 60.

SAYRE, W.W., "Dispersion of Mass in Open-Channel Flow," *Hydraulics Papers,* No. 3, Colorado State University, Fort Collins, Colo., Feb., 1968, pp. 73.

SAYRE, W.W., "Natural Mixing Processes in Rivers," *Environmental Impact on Rivers,* H.W. Shen, ed., Hsieh Wen Shen, Fort Collins, Col., 1973, Chap. 6.

SMITH, R., "The Importance of Discharge Sitting Upon Contaminant Dispersion in Narrow Rivers and Estuaries," *Journal of Fluid Mechanics,* Vol. 108, 1981, pp. 43-53.

STONE, H.L. and BRIAN, P.L.T., "Numerical Solution of Convective Transport Problems," *Journal of the American Institute of Chemical Engineers,* Vol. 9, No. 5, 1963, pp. 681-688.

TAYLOR, G.I., "Diffusion By Continuous Movements," *Proceedings of the London Mathematical Society,* Series 2, Vol. 20, 1921, pp. 196-212.

TAYLOR, G.I., "Dispersion of Soluble Matter in Solvent Flowing Slowly Through a Tube," *Proceedings of the Royal Society London,* A, Vol. 219, 1953, pp. 186-203.

BLANK PAGE IN ORIGINAL - PART OF PAGINATION

TAYLOR, G.I., "The Dispersion of Matter in Turbulent Flow Through a Pipe," *Proceedings of the Royal Society London,* A, Vol. 223, 1954, pp. 446-468.

VALENTINE, E.M., "The Effect of Channel Boundary Roughness on Longitudinal Dispersion," thesis presented to the University of Canterbury, at Christchurch, New Zealand, in 1978, in partial fulfilment of the requirements for the degree of Doctor of Philosophy.

WOLMAN, M.G., "A Method of Sampling Coarse River-Bed Material," *Transactions,* American Geophysical Union, Vol. 35, No. 6, Dec., 1954, pp. 951-956.

YOTSUKURA, N., and FIERING, M.B., "Numerical Solution to a Dispersion Equation," *Journal of the Hydraulics Division,* ASCE, Vol. 90, No. HY5, pp. 83-104.

YOTSUKURA, N. and SAYRE, W.W., "Transverse Mixing in Natural Channels," *Water Resources Research,* Vol. 12, No. 4, Aug., 1976, pp. 695-704.

APPENDIX A

THE APPLICATION OF ARIS MOMENT TRANSFORMS TO THE DISPERSION EQUATION

To obtain equation 3.33 to 3.35 viz,

$$\frac{\partial}{\partial\eta}\left(\psi(\eta)\ \frac{\partial c_{d0}}{\partial\eta}\right) = -\mu\chi(\eta)\ c_{d*}\Big|_{\xi=0} + \psi(\eta)\ \frac{\partial c_{d*}}{\partial\xi}\Big|_{\xi=0}$$

$$\frac{\partial}{\partial\eta}\left(\psi(\eta)\ \frac{\partial c_{d1}}{\partial\eta}\right) = -\mu\chi(\eta)\ c_{d1} - \psi(\eta)\ c_{d*}\Big|_{\xi=0} \qquad (A.1)$$

and $$\frac{\partial}{\partial\eta}\left(\psi(\eta)\ \frac{\partial c_{dp}}{\partial\eta}\right) = -\mu\chi(\eta)p\ c_{dp-1} - \psi(\eta)\ p(p-1)\ c_{dp-2}$$

the steady state form of equation 3.30,

$$\mu\chi(\eta)\ \frac{\partial c_{d*}}{\partial\xi} = \psi(\eta)\ \frac{\partial^2 c_{d*}}{\partial\eta^2} + \frac{\partial}{\partial\eta}\psi(\eta)\ \frac{\partial c_{d*}}{\partial\eta} \qquad (A.2)$$

is multiplied by ξ^p and integrated from 0 to ∞. Thus

$$\int_0^\infty \mu\chi(\eta)\ \frac{\partial c_{d*}}{\partial\xi}\ \xi^p\ d\xi = \int_0^\infty \psi(\eta)\ \frac{\partial^2 c_{d*}}{\partial\xi^2}\ \xi^p\ d\xi + \int_0^\infty \frac{\partial}{\partial\eta}\psi(\eta)\ \frac{\partial c_{d*}}{\partial\eta}\ \xi^p\ d\xi \qquad (A.3)$$

(1) (2) (3)

Considering each term separately;

Term 1 If $p = 0$ then this term reduces to $\mu\chi(\eta)\int_0^\infty \frac{\partial c_{d*}}{\partial\xi}\,d\xi$. For $p > 0$ integration by parts gives

$$\int_0^\infty \mu\chi(\eta)\ \frac{\partial c_{d*}}{\partial\xi}\ \xi^p\ d\xi = \mu\chi(\eta)\left[c_{d*}\ \xi^p\Big|_{\xi=0}^{\xi=\infty} - \int_0^\infty c_{d*}\ p\ \xi^{p-1}\ d\xi\right]$$

$$= \mu\chi(\eta)\ [-p\ c_{dp-1}] \qquad (A.4)$$

Thus for $p = 0$, term 1 $= -\mu\chi(\eta)\ c_{d*}\Big|_{\xi=0}$

$p \geq 1$, term 1 $= -\mu\chi(\eta)p\ c_{dp-1}$

Term 2 If $p = 0$, this term reduces to $\int_0^\infty \psi(\eta)\ \frac{\partial^2 c_{d*}}{\partial\xi^2}\,d\xi$, then,

$$\text{term 2} = \psi(\eta)\ \frac{\partial c_{d*}}{\partial\xi}\Big|_{\xi=0}^{\xi=\infty}$$

For $p > 0$ integration by parts yields

$$\int_0^\infty \psi(\eta) \frac{\partial^2 c_{d*}}{\partial \xi^2} \xi^p \, d\xi = \psi(\eta) \left[\frac{\partial c_{d*}}{\partial \xi} \xi^p \Big|_{\xi=0}^{\xi=\infty} - \int_0^\infty \frac{\partial c_{d*}}{\partial \xi} p \, \xi^{p-1} \, d\xi \right] \qquad (A.5)$$

Then for $p = 1$, term 2 $= -\psi(\eta) \int_0^\infty \frac{\partial c_{d*}}{\partial \xi} d\xi$

$$= -\psi(\eta) \, c_{d*} \Big|_{\xi=0}^{\xi=\infty}$$

For $p > 1$, term 2 $= -\psi(\eta) \int_0^\infty \frac{\partial c_{d*}}{\partial \xi} p \, \xi^{p-1} \, d\xi$

$$= -\psi(\eta) \, p \left[c_{d*} \, \xi^{p-1} \Big|_{\xi=0}^{\xi=\infty} - \int_0^\infty c_{d*}(p-1) \, \xi^{p-2} \, d\xi \right]$$

$$= \psi(\eta) \, p(p-1) \, c_{dp-2}$$

Thus,
for $p = 0$, term 2 $= -\psi(\eta) \left. \frac{\partial c_{d*}}{\partial \xi} \right|_{\xi=0}$

for $p = 1$, term 2 $= \psi(\eta) \, c_{d*} \Big|_{\xi=0}$

and for $p > 1$, term 2 $= \psi(\eta) \, p(p-1) \, c_{dp-2}$

Term 3 $$\int_0^\infty \frac{\partial}{\partial \eta} \psi(\eta) \frac{\partial c_{d*}}{\partial \eta} \xi^p \, d\xi = \frac{\partial}{\partial \eta} \psi(\eta) \frac{\partial}{\partial \eta} \int_0^\infty c_{d*} \, \xi^p \, d\xi$$

$$= \frac{\partial}{\partial \eta} \psi(\eta) \frac{\partial c_{dp}}{\partial \eta} \qquad (A.6)$$

Clearly there will be three separate equations for $p = 0$, $p = 1$ and $p \geq 2$ and these are equations A.1.

This method may be extended to the three-dimensional dispersion equation by the inclusion of the term

$$\frac{\partial}{\partial \zeta} \phi(\zeta) \frac{\partial c_{d*}}{\partial \zeta}$$

to produce a further term similar to term (3),

$$\frac{\partial}{\partial \zeta} \phi(\zeta) \frac{\partial c_{dp}}{\partial \zeta}.$$

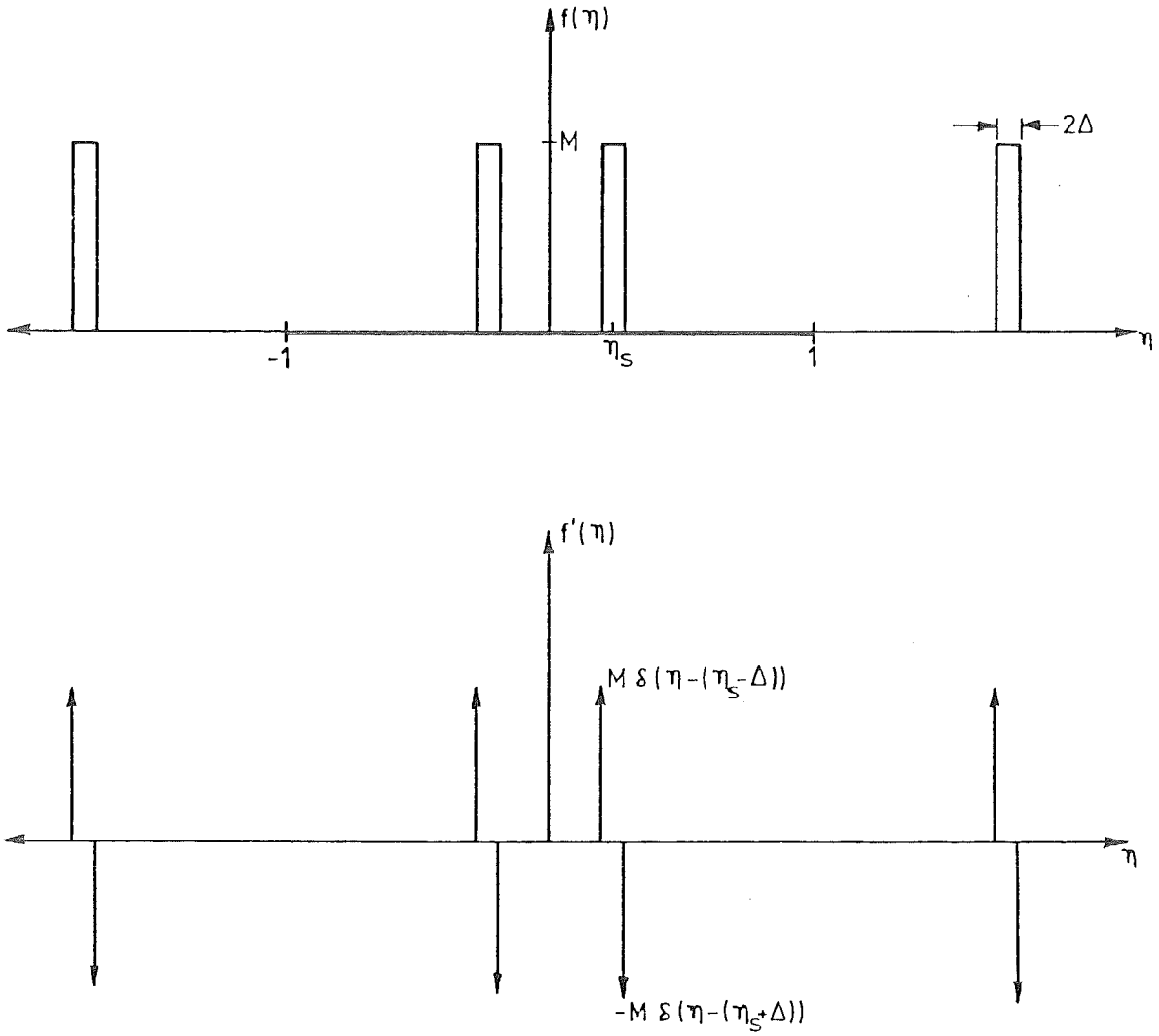

Figure B.1 : Source function and derivative of source function (at $\xi = 0$).

APPENDIX B

SOME ANALYTICAL SOLUTIONS FOR THE DISPERSION EQUATION

This Appendix contains the analytic solutions used to check the numerical solution obtained using the Aris moment transforms. A complete analytic solution is available for the uniform flow/uniform diffusivity case as outlined in Section 3.6.1. The scheme described in Chapter 4 was also checked with moments obtained analytically using a power velocity and uniform diffusivity distribution.

B.1 Uniform Conditions Solution

The basic diffusion equation 3.13,

$$\frac{8}{f}\frac{\partial c}{\partial \tau} + \frac{8}{f}\chi(\eta)\frac{\partial c}{\partial \xi} = \psi(\eta)\frac{\partial^2 c}{\partial \xi^2} + \frac{\partial}{\partial \eta}\psi(\eta)\frac{\partial c}{\partial \eta} \qquad (B.1)$$

is reduced to a simpler form by assuming $\chi(\eta) = 1$, $\psi(\eta)$ = constant and that the longitudinal concentration gradient is negligible, (note, we are interested in the steady state case only), such that:

$$\mu\frac{\partial c}{\partial \xi} = \alpha\frac{\partial^2 c}{\partial \eta^2} \qquad (B.2)$$

α is the value of constant $\psi(\eta)$ such that the average value of diffusivity over the depth is $D = \frac{\kappa}{6} y_n u_*$ (Fischer 1973), and $\mu = \frac{8}{f}$.

Then $\alpha = \frac{\sqrt{\mu}\kappa}{6}$ and the equation becomes

$$\beta\frac{\partial c}{\partial \xi} = \frac{\partial^2 c}{\partial \eta^2} \qquad (B.3)$$

where $\beta = \frac{6\sqrt{\mu}}{\kappa}$ (equation 3.18).

The boundary conditions will be

$$\left.\frac{\partial c}{\partial \eta}\right|_{\xi=0} = 0 \text{ for } \eta = 0,\ \eta = 1 \qquad (B.4)$$

and the source conditions as shown in figure B.1 are,

$$c\big|_{\xi=0} = f(\eta), \qquad (B,5)$$

with $f(\eta)$ the fourier series for the source, of the form

$$f(\eta) = a_0 + \sum_{n=1}^{\infty} (a_n \cos(nw_0\eta) + b_n \sin(nw_0\eta)) \qquad (B.6)$$

Since $f(\eta)$ is an even function, the sin term vanishes and $f'(\eta)$ is

$$f'(\eta) = \sum_{n=1}^{\infty} c_n \sin(nw_0\eta) \qquad (B.7)$$

Now $c_n = -nw_0 a_n$ and if T is the period of $f(\eta)$, then $w_0 = \frac{2\pi}{T} = \frac{2\pi}{2 \times 1} = \pi$. Then by applying a fourier inversion c_n can be solved for,

$$\begin{aligned} c_n &= \frac{4}{T} \int_0^{T/2} f'(\eta) \sin(nw_0\eta)\, d\eta \\ &= 2 \int_0^{1} [M\delta(\eta - (\eta_s - \Delta)) - M\delta(\eta - (\eta_s + \Delta))] \sin(n\pi\eta)\, d\eta \qquad (B.8) \\ &= -4M[\sin(n\pi\Delta) \cos(n\pi\eta_s)] \end{aligned}$$

Thus, $a_n = \frac{-c_n}{nw_0}$ and $a_0 = \frac{1}{T} \int_{-1}^{1} f(\eta)\, d\eta = \frac{1}{2}\, 2M.2\Delta = 2\Delta M$ so the complete fourier series for the source is

$$f(\eta) = 2\Delta M + \frac{4M}{\pi} \sum_{n=1}^{\infty} \frac{\sin(n\pi\Delta) \cos(n\pi\eta_s)}{n} \cos(n\pi\eta) \qquad (B.9)$$

A general solution to equation B.3 is obtained by separating the variables and since the ξ-dependency is an exponential (which disappears at $\xi = 0$) then

$$c(\xi, \eta) = a_0 + \sum_{m=1}^{\infty} a_m e^{-\frac{1}{\beta}(m\pi)^2 \xi} \cos(m\pi\eta) \qquad (B.10)$$

which reduces to $f(\eta)$ for $\xi = 0$, hence

$$c(\xi, \eta) = 2\Delta M + \frac{4M}{\pi} \sum_{n=1}^{\infty} \frac{\sin(n\pi\Delta) \cos(n\pi\eta_s)}{n} \cos(n\pi\eta)\, e^{-\frac{1}{\beta}(n\pi)^2 \xi} \qquad (B.11)$$

This solution may be reduced to $c_*(\xi, \eta)$ by dividing through by the equilibrium concentration, $c_e = 2\Delta M$, or to $c^p_{d*}(\eta)$ by applying the transformation,

$$c^{p}_{d*}(\eta) = \int_{0}^{\infty} \frac{[c(\xi, \eta) - 2\Delta M]}{2\Delta M} \xi^{p} \, d\xi \qquad (B.12)$$

It is also noted that the decay of the exponential function which in the numerical solution is α_n, is simply

$$\alpha_n = \frac{(n\pi)^2}{\beta} \qquad (B.13)$$

and clearly this will vary as n^2. An estimate for this coefficient in non-uniform flow conditions is described in section B.4.

If the effect of the longitudinal term is to be included (with a uniform velocity/diffusivity) then an analytical solution may still be obtained for moments using the same approach as is used in the numerical solution. The development of the relevant equations is described in section 3.7.1, and outlined in Appendix A. The equations for c_{dp}, the moments of the deficit concentration distribution, are (eqns. 3.33 - 3.35)

$$\text{for } p = 0, \; \frac{\partial}{\partial \eta}\left[\psi(\eta) \frac{\partial c_{d0}}{\partial \eta}\right] = -\mu\chi(\eta) \, c_{d*}\Big|_{\xi=0} + \psi(\eta) \frac{\partial c_{d*}}{\partial \xi}\Big|_{\xi=0}$$

$$p = 1, \; \frac{\partial}{\partial \eta}\left[\psi(\eta) \frac{\partial c_{d1}}{\partial \eta}\right] = -\mu\chi(\eta) \, c_{d0} - \psi(\eta) \, c_{d*}\Big|_{\xi=0} \qquad (B.14)$$

$$p \geq 2, \; \frac{\partial}{\partial \eta}\left[\psi(\eta) \frac{\partial c_{dp}}{\partial \eta}\right] = -\mu\chi(\eta) \, p \, c_{d(p-1)} - \psi(\eta) \, p(p-1) \, c_{d(p-2)}$$

As each of these equations will involve a different routine for the right hand side of the equation it is necessary to analytically solve for the first three moments.

The flux of moment, Q_p, is defined as $Q_p(\eta) = \psi(\eta) \frac{\partial c_{dp}}{\partial \eta}$ (equation 3.36), so for $p = 0$,

$$Q_0 = \int_{0}^{\eta} -\mu\chi(\eta) \, c_{d*}\Big|_{\xi=0} + \psi(\eta) \frac{\partial c_{d*}}{\partial \xi}\Big|_{\xi=0} \, d\eta \qquad (B.15)$$

However $\frac{\partial c_{d*}}{\partial \xi}\Big|_{\xi=0}$ is zero everywhere but at the source boundaries. If the source is shrunk to a point source then the effect of this term will become negligible. For uniform flow conditions the velocity and diffusivity distributions are defined by,

$$\chi(\eta) = 1, \quad \psi(\eta) = \frac{\sqrt{\mu\kappa}}{6} \tag{B.16}$$

Thus,
$$Q_0 = -\mu\left[-\eta + c_s\Big|_{\eta_{s\ell}}^{\eta_{su}} \{\eta - \eta_s\}\right] + K_Q \tag{B.17}$$

By definition of c_s, $c_s\Big|_{\eta_{s\ell}}^{\eta_{su}} = 1$ (for a point source c_s will become a delta function) and the curly brackets are defined such that

$$\begin{aligned} \{\eta - \eta_s\} &= 0, \quad \eta - \eta_s < 0 \\ \{\eta - \eta_s\} &= 1, \quad \eta - \eta_s \geqq 0 \end{aligned} \tag{B.18}$$

Now $Q_0 = \psi \frac{\partial c_{d0}}{\partial \eta}$, so $Q_0 = 0$ at $\eta = 0$ and $\eta = 1$, hence $K_Q = 0$, and

$$\begin{aligned} c_{d0} &= \frac{1}{\psi}\int_0^{\eta} -\mu[-\eta + \{\eta - \eta_s\}]\, d\eta \\ &= \frac{-6\sqrt{\mu}}{\kappa}\left[\frac{-\eta^2}{2} + (\eta - \eta_s)\{\eta - \eta_s\}\right] + K_0 \end{aligned} \tag{B.19}$$

The constant of integration K_0 is found from Q_1 by considering the boundary condition at $\eta = 1$ ($Q_1 = 0$ at $\eta = 1$)

$$\begin{aligned} Q_1 &= \int_0^{\eta} \left[-\mu\chi(\eta)\, c_{d0} - \psi(\eta)\, c_{d*}\Big|_{\xi=0}\right] d\eta \\ &= \frac{6\mu\sqrt{\mu}}{\kappa}\left(\frac{-\eta^3}{6} + \frac{(\eta - \eta_s)^2}{2}\{\eta - \eta_s\}\right) - \mu\eta K_0 + \frac{\sqrt{\mu\kappa}}{6}(\eta - \{\eta - \eta_s\}) \end{aligned} \tag{B.20}$$

With K_0 determined, Q_1 may be used to obtain c_{d1} etc.

$$\begin{aligned} c_{d1} &= \int_0^{\eta} \frac{Q_1}{\psi}\, d\eta + K_1 \\ &= \frac{6}{\sqrt{\mu\kappa}}\left[\frac{6\mu\sqrt{\mu}}{\kappa}\left(\frac{-\eta^4}{24} + \frac{(\eta - \eta_s)^3}{6}\{\eta - \eta_s\}\right) - \mu\frac{\eta^2}{2}K_0\right. \\ &\quad \left. + \frac{\sqrt{\mu\kappa}}{6}\left(\frac{\eta^2}{2} - (\eta - \eta_s)\{\eta - \eta_s\}\right)\right] + K_1 \end{aligned} \tag{B.21}$$

$$Q_2 = \int_0^{\eta} (-\mu 2c_{d1} - \psi(\eta) 2c_{d0})\, d\eta$$

$$= -\frac{12\sqrt{\mu}}{\kappa}\left[\frac{6\mu\sqrt{\mu}}{\kappa}\left(\frac{-\eta^5}{120} + \frac{(\eta - \eta_s)^4}{24}\{\eta - \eta_s\}\right) - \mu\frac{\eta^3}{6}K_0\right.$$

$$\left. + \frac{\sqrt{\mu\kappa}}{6}\left(\frac{\eta^3}{6} - \frac{(\eta - \eta_s)^2}{2}\{\eta - \eta_s\}\right)\right] - 2\mu\eta K_1 \qquad (B.22)$$

$$- 2\mu\left[\frac{\eta^3}{6} - \frac{(\eta - \eta_s)^2}{2}\{\eta - \eta_s\}\right] - \frac{2\sqrt{\mu\kappa}}{6}\eta K_0$$

$$c_{d2} = \int_0^{\eta} \frac{Q_2}{\psi}\, d\eta + K_2$$

$$= \frac{6}{\sqrt{\mu\kappa}}\left[\frac{-12\sqrt{\mu}}{\kappa}\left[\frac{6\mu\sqrt{\mu}}{\kappa}\left(\frac{-\eta^6}{720} + \frac{(\eta - \eta_s)^5}{120}\{\eta - \eta_s\}\right) - \mu\frac{\eta^4}{24}K_0\right.\right.$$

$$\left.\left. + \frac{\sqrt{\mu\kappa}}{6}\left(\frac{\eta^4}{24} - \frac{(\eta - \eta_s)^3}{6}\{\eta - \eta_s\}\right)\right] - \mu\eta^2 K_1\right. \qquad (B.23)$$

$$\left. - 2\mu\left[\frac{\eta^4}{24} - \frac{(\eta - \eta_s)^3}{6}\{\eta - \eta_s\}\right] - \frac{\sqrt{\mu\kappa}}{6}\eta^2 K_0\right] + K_2$$

$$Q_3 = \int_0^{\eta} (-\mu 3c_{d2} - \psi 6c_{d1})\, d\eta$$

$$= \frac{-18\sqrt{\mu}}{\kappa}\left[\frac{-12\sqrt{\mu}}{\kappa}\left[\frac{6\mu\sqrt{\mu}}{\kappa}\left(\frac{-\eta^7}{5040} + \frac{(\eta - \eta_s)^6}{720}\{\eta - \eta_s\}\right)\right.\right.$$

$$\left.\left. - \mu\frac{\eta^5}{120}K_0 + \frac{\sqrt{\mu\kappa}}{6}\left[\frac{\eta^5}{120} - \frac{(\eta - \eta_s)^4}{24}\{\eta - \eta_s\}\right]\right] - \mu\frac{\eta^3}{3}K_1\right.$$

$$\left. - 2\mu\left[\frac{\eta^5}{120} - \frac{(\eta - \eta_s)^4}{24}\{\eta - \eta_s\}\right] - \frac{\sqrt{\mu\kappa}}{18}\eta^3 K_0\right] - 3\mu\eta K_2 \qquad (B.24)$$

$$- \frac{36\mu\sqrt{\mu}}{\kappa}\left[\frac{-\eta^5}{120} + \frac{(\eta - \eta_s)^4}{24}\{\eta - \eta_s\}\right] - \mu\eta^3 K_0$$

$$+ \sqrt{\mu\kappa}\left(\frac{\eta^3}{6} - \frac{(\eta - \eta_s)^2}{2}\{\eta - \eta_s\}\right) + \sqrt{\mu\kappa}\,\eta K_1$$

Equations B.19, B.21 and B.23 completely describe the 1st, 2nd and 3rd moments for uniform flow conditions and constants of integration for each moment are determined by equations B.20, B.22 and B.24 respectively.

B.2 Moments Obtained for a Power Velocity and Uniform Diffusivity

An analytical solution may also be obtained for a power-law velocity (or a logarithmic velocity) with a uniform diffusivity. The method is identical to that used in the second solution for uniform flow conditions described in the preceeding section. Since the computer algorithm is unchanged from one velocity profile to another only the first two analytical moment solutions are given here. The agreement of the uniform solutions (analytical and computed) up to 3 moments and the agreement of the zeroeth moments for the power-law velocity - uniform diffusivity is sufficient to ensure higher moment compatibility for the power-law velocity. For the power-law velocity distribution and uniform diffusivity,

$$\begin{aligned} \chi(\eta) &= (1 + \alpha)\, \eta^{\alpha} \\ \psi(\eta) &= \frac{\sqrt{\mu\kappa}}{6} \end{aligned} \tag{B.25}$$

Then equation B.15 becomes,

$$\begin{aligned} Q_0 &= -\mu \int_0^{\eta} (1 + \alpha)\, \eta^{\alpha}\, c_{d*}\Big|_{\xi=0} d\eta + \text{constant } (K_Q) \\ &= -\mu[\eta^{(1+\alpha)}\, (-1) + \{\eta - \eta_s\}] + K_Q \end{aligned}$$

Since by definition of c_s, $\eta^{(1+\alpha)}\Big|_{\eta_{se}}^{\eta_{su}} c_s = 1$ and the curly brackets are defined by equation B.18.

As before, $Q_0 = \psi \frac{\partial c_{d0}}{\partial \eta}$ so $Q_0 = 0$ at $\eta = 0$, hence $K_Q = 0$

$$\begin{aligned} c_{d0} &= \int_0^{\eta} \mu \frac{6}{\sqrt{\mu\kappa}} [\eta^{(1+\alpha)} - \{\eta - \eta_s\}]\, d\eta + K_0 \\ &= \mu \frac{6}{\sqrt{\mu\kappa}} \left[\frac{\eta^{2+\alpha}}{(2+\alpha)} - (\eta - \eta_s)\, \{\eta - \eta_s\}\right] + K_0 \end{aligned} \tag{B.26}$$

To find K_0, the expression for Q_1 is used with the boundary condition that $Q_1 = 0$ at $\eta = 1$, thus

$$Q_1 = \int_0^{\eta} \left[-\mu\chi(\eta)\, c_{d0} - \psi(\eta)\, c_{d*}\Big|_{\xi=0}\right] d\eta$$

$$= -\mu(1+\alpha)\left[\frac{6\sqrt{\mu}}{\kappa}\left(\frac{\eta^{3+2\alpha}}{(2+\alpha)(3+2\alpha)} - \left[\frac{\eta^{2+\alpha}}{(2+\alpha)} - \frac{\eta^{1+\alpha}\eta_s}{(1+\alpha)} + \frac{\eta_s^{2+\alpha}}{(1+\alpha)(2+\alpha)}\right]\{\eta - \eta_s\}\right)\right.$$

$$\left. + \frac{\eta^{1+\alpha}}{1+\alpha} K_0\right] - \frac{\sqrt{\mu\kappa}}{6}\left(-\eta + \eta\Big|_{\eta_{s\ell}}^{\eta_{su}} c_s\{\eta - \eta_s\}\right) \qquad (B.28)$$

Using the value for K_0 from the above equation c_{d0} is completely defined and may be used to find the next moment, for p = 1,

$$c_{d1} = \int_0^{\eta} \frac{Q_1}{\psi}\, d\eta + K_1$$

$$= \frac{6}{\sqrt{\mu\kappa}}\left[-\mu(1+\alpha)\left[\frac{6\sqrt{\mu}}{\kappa}\left(\frac{\eta^{4+2\alpha}}{(2+\alpha)(3+2\alpha)(4+2\alpha)} - \left[\frac{\eta^{3+\alpha}}{(2+\alpha)(3+\alpha)} - \frac{\eta^{2+\alpha}\eta_s}{(1+\alpha)(2+\alpha)}\right.\right.\right.\right. \qquad (B.29)$$

$$\left.\left.\left. + \frac{\eta\eta_s^{2+\alpha}}{(1+\alpha)(2+\alpha)}\right]_{\eta_s}^{\eta}\{\eta - \eta_s\}\right) + \frac{\eta^{2+\alpha}}{(1+\alpha)(2+\alpha)} K_0\right]$$

$$\left.\left. - \frac{\sqrt{\mu\kappa}}{6}\left(-\frac{\eta^2}{2} + (\eta - \eta_s)\, c_s(\eta_{su} - \eta_{s\ell})\{\eta - \eta_s\}\right)\right] + K_1$$

Again to solve for K_1, the boundary condition on Q_2 is used,

$$Q_2 = \int_0^{\eta} \left[-\mu\chi(\eta) 2c_{d1} - \psi(\eta) 2c_{d0}\right] d\eta$$

$$= -\mu(1+\alpha)\, 2\left[\frac{6}{\sqrt{\mu\kappa}}\left[-\mu(1+\alpha)\left[\frac{6\sqrt{\mu}}{\kappa}\left(\frac{\eta^{5+3\alpha}}{(2+\alpha)(3+2\alpha)(4+2\alpha)(5+3\alpha)}\right.\right.\right.\right.$$

$$- \left[\frac{\eta^{4+2\alpha}}{(2+\alpha)(3+\alpha)(4+2\alpha)} - \frac{\eta^{3+2\alpha}\eta_s}{(1+\alpha)(2+\alpha)(3+2\alpha)} + \frac{\eta^{2+\alpha}\eta_s^{2+\alpha}}{(1+\alpha)(2+\alpha)(2+\alpha)}\right.$$

$$\left.\left. - \frac{\eta^{1+\alpha}\eta_s^{3+\alpha}}{(1+\alpha)(2+\alpha)(3+\alpha)}\right]_{\eta_s}^{\eta}\{\eta - \eta_s\}\right) + \frac{\eta^{3+2\alpha}}{(1+\alpha)(2+\alpha)(3+2\alpha)} K_0\Big]$$

$$\left.\left. - \frac{\sqrt{\mu\kappa}}{6}\left(\frac{-\eta^{3+\alpha}}{2(3+\alpha)} + \left(\frac{\eta^{2+\alpha}}{(2+\alpha)} - \frac{\eta^{1+\alpha}\eta_s}{(1+\alpha)} + \frac{\eta_s^{2+\alpha}}{(1+\alpha)(2+\alpha)}\right) c_s(\eta_{su} - \eta_{s\ell})\{\eta - \eta_s\}\right)\right]\right]$$

$$+ \frac{\eta^{1+\alpha}}{(1+\alpha)} K_1 \Bigg] - \frac{2\sqrt{\mu\kappa}}{6} \Bigg[-\frac{6\sqrt{\mu}}{\kappa} \Bigg(\frac{\eta^{3+2\alpha}}{(2+\alpha)(3+2\alpha)} \tag{B.30}$$

$$- \left(\frac{\eta^{2+\alpha}}{(2+\alpha)} - \frac{\eta^{1+\alpha}\eta_s}{(1+\alpha)} + \frac{\eta_s^{2+\alpha}}{(1+\alpha)(2+\alpha)} \right) \{\eta - \eta_s\} \Bigg) + \frac{\eta^{1+\alpha}}{(1+\alpha)} K_0 \Bigg]$$

When $\eta = 1$, $Q_2 = 0$ and the only unknown in equation B.30 is the constant of integration K_1. With K_1 determined Q_2 can be integrated to obtain c_{d2} and so on for higher moments.

B.3 Moments Obtained for a Logarithmic Velocity and Uniform Diffusivity

The procedure used to obtain these moments is identical to that of the previous section B.2. The velocity and diffusivity distributions are defined by,

$$\chi(\eta) = 1 + \frac{1}{\kappa\sqrt{\mu}} (\ln\eta + 1)$$
$$\psi(\eta) = \frac{\sqrt{\mu}\kappa}{6} \tag{B.31}$$

Substituting these into equation B.15 for Q_0 leads to,

$$Q_0 = -\mu \int_0^{\eta} \left(1 + \frac{1}{\kappa\sqrt{\mu}} (\ln\eta + 1)\right) c_{d*}\Big|_{\xi=0} d\eta$$
$$= \mu \left[\eta + \frac{1}{\kappa\sqrt{\mu}} (\eta\ln\eta) - \{\eta - \eta_s\} \right] \tag{B.32}$$

Thus,

$$c_{d0} = \int_0^{\eta} \frac{6}{\sqrt{\mu}\kappa} \left(\mu \left[\eta + \frac{1}{\kappa\sqrt{\mu}} \eta\ln\eta - \{\eta - \eta_s\}\right)\right) d\eta$$
$$= \frac{6}{\sqrt{\mu}\kappa} \left(\mu \left[\frac{\eta^2}{2} + \frac{1}{4\kappa\sqrt{\mu}} (2\eta^2\ln\eta - \eta^2) - (\eta - \eta_s)\{\eta - \eta_s\} \right] \right) + K_0 \tag{B.33}$$

$$Q_1 = \int_0^{\eta} \left[-\mu\chi(\eta) c_{d0} - \psi(\eta) c_{d*}\Big|_{\xi=0} \right] d\eta$$

$$= -\mu \Bigg[\left(1 + \frac{1}{\kappa\sqrt{\mu}}\right) \left[\frac{6}{\sqrt{\mu}\kappa} \left(\mu \left[\frac{\eta^3}{6} + \frac{1}{4\kappa\sqrt{\mu}} \left(2\frac{\eta^3}{3} \left(\ln\eta - \frac{1}{3} \right) - \frac{\eta^3}{3} \right) \right. \right. \right.$$

$$\left. \left. \left. - \frac{(\eta - \eta_s)^2}{2} \{\eta - \eta_s\} \right] \right) + K_0\eta \right]$$

$$+\frac{1}{\kappa\sqrt{\mu}}\left[\frac{6}{\sqrt{\mu}\kappa}\left(\mu\left[\frac{\eta^3}{6}\left(\ln\eta-\frac{1}{3}\right)\right.\right.\right. \tag{B.34}$$

$$+\frac{1}{4\kappa\sqrt{\mu}}\left(2\frac{\eta^3}{3}\left[(\ln\eta)^2-\frac{2}{3}\ln\eta+\frac{2}{9}\right]-\frac{\eta^3}{3}\left(\ln\eta-\frac{1}{3}\right)\right)-\left[\frac{\eta^2}{2}\left(\ln\eta-\frac{1}{2}\right)\right.$$

$$\left.\left.\left.-\eta_s\eta(\ln\eta-1)+\frac{\eta_s^2}{2}\left(\ln\eta_s-\frac{3}{2}\right)\right]\{\eta-\eta_s\}\right]\right)+K_0\eta(\ln\eta-1)\left.\right]\left.\right]$$

$$+\frac{\sqrt{\mu}\kappa}{6}\left(-\eta+c_s\,\eta\left|\begin{matrix}\eta_{su}\\ \eta_{s\ell}\end{matrix}\{\eta-\eta_s\}\right.\right)$$

As in section B.2 higher moments may be obtained by carrying out further integrations of equations 3.27 - 3.28. Since the procedure is identical to that for the power-law velocity, agreement of the zeroeth moment calculated analytically and that calculated using moment transforms is sufficient, provided that higher moments are in agreement in the power-law case.

B.4 Bessel's Function Solution

If the logarithmic velocity, parabolic diffusivity situation is truely representative of natural conditions, then it appears at present that the closest approach to natural conditions with an analytical solution is a power-law velocity, linear diffusivity case. If the velocity distribution is defined by

$$u(\eta) = (1+\alpha)\,\bar{u}\eta^{\alpha} \tag{B.35}$$

then the appropriate diffusivity field is,

$$\varepsilon(\eta) = \frac{u_*^2 y_n}{\alpha(1+\alpha)\,\bar{u}}\,\eta^{1-\alpha}\,(1-\eta) \tag{B.36}$$

To facilitate a solution it is assumed that $(1-\eta)$ is close to 1 (a good approximation near the bed) and then $\varepsilon(\eta)$ is a linear function of η,

$$\varepsilon(\eta) = \frac{u_*^2 y_n}{\alpha(1+\alpha)\,\bar{u}}\,\eta^{(1-\alpha)} \tag{B.37}$$

Again neglecting the effect of longitudinal concentration gradients, the steady state dispersion equation becomes,

$$u(\eta)\,\frac{\partial c_*}{\partial \xi} = \frac{\partial}{\partial \eta}\,\varepsilon(\eta)\,\frac{\partial c_*}{\partial \eta} \tag{B.38}$$

If a solution of the form $c_* = \phi_n(\xi)\psi_n(\eta)$ is assumed then

$$\frac{\phi_n'(\xi)}{\phi_n(\xi)} = \frac{1}{u(\eta)\psi_n(\eta)} \frac{\partial}{\partial \eta} \varepsilon(\eta) \frac{\partial \psi_n(\eta)}{\partial \eta} = -\lambda_n, \text{ say} \qquad (B.39)$$

where $\phi_n'(\xi) = \frac{d\phi_n(\xi)}{d\xi}$ and $\psi_n'(\eta) = \frac{d\psi_n(\eta)}{d\eta}$. Now the ξ-dependency of c_* will become $\phi_n = e^{-\lambda_n \xi}$ to satisfy the equation

$$\phi_n'(\xi) + \phi_n(\xi)\lambda_n = 0 \qquad (B.40)$$

and clearly the decay of exponential series is dependent on λ_n. To determine the value of λ_n, consider the second half of the function for c_*, that is

$$\frac{\partial}{\partial \eta} \varepsilon(\eta) \frac{\partial \psi_n(\eta)}{\partial \eta} + u(\eta)\psi_n(\eta)\lambda_n = 0 \qquad (B.41)$$

which becomes, on substitution of $u(\eta)$ and $\varepsilon(\eta)$,

$$\frac{\partial}{\partial \eta} \eta^{1-\alpha} \frac{\partial \psi_n(\eta)}{\partial \eta} + \lambda_n \alpha(1+\alpha)^2 \frac{\bar{u}^2}{\bar{u}_*^2} \eta^{\alpha}\psi_n(\eta) = 0 \qquad (B.42)$$

This is of identical form to equation 9.1.53 of Abramowitz and Stegun (1964) and has the solution,

$$\psi_n(\eta) = \eta^p J_\nu(\gamma_n \eta^q) \times \text{constant} \qquad (B.43)$$

where J_ν is a Bessel function of the first kind of order ν, and p, q, ν and γ are from the coefficients of B.42;

$$\begin{aligned} p &= \alpha/2 \\ q &= \tfrac{1}{2}+\alpha \\ \nu &= \frac{p}{q} = \frac{\alpha}{1+2\alpha} \\ \gamma_n^2 &= \frac{\lambda_n \alpha(1+\alpha)^2 \left[\frac{\bar{u}}{u_*}\right]^2}{(\tfrac{1}{2}+\alpha)^2} \end{aligned} \qquad (B.44)$$

To satisfy the boundary condition at $\eta = 1$,

$$\eta^{1-\alpha} \frac{\partial \psi_n(\eta)}{\partial \eta} = 0 \qquad (B.45)$$

then $$0 = \frac{\alpha}{2} J_\nu(\gamma_n) + \gamma_n(\tfrac{1}{2}+\alpha) J_\nu'(\gamma_n)$$

or $$0 = \nu J_\nu(\gamma_n) + \gamma_n J_\nu'(\gamma_n) \qquad (B.46)$$

So for ν small γ_n will tend to $j'_{\nu,n}$, the nth root of J_ν'. In this case, λ_n is described by

$$\lambda_n = \frac{(j'_{\nu,n})^2 \, u_*^2}{4\alpha(1-\nu)^2 \, \bar{u}^2} \tag{B.47}$$

A normalization procedure is then applied to $\psi_n(\eta)$, to solve for the constant in equation B.43, by setting $\frac{1}{\bar{u}} \int_0 u\psi_n^2 \, d\eta = 1$ to produce

$$\text{Constant} = \left(\frac{1+\alpha}{1+2\alpha}\right)^{\frac{1}{2}} J_\nu(\gamma_n) \tag{B.48}$$

Then combining boundary conditions on $\psi_n(\eta)$, that there is a source at $\eta = \eta_s$ and the constant, B.48, results in an expression for $\psi_n(\eta)$

$$\psi_n(\eta) = \frac{(\eta\eta_s)^{\frac{\alpha}{2}} J_\nu\left(j'_{n,\nu} \, \eta^{\alpha+\frac{1}{2}}\right) J_\nu\left(j'_{n,\nu} \, \eta_s^{\alpha+\frac{1}{2}}\right)}{(1-\nu)\left[1 - \frac{\nu^2}{(j'_{n,\nu})^2}\right] J_\nu(j'_{n,\nu})^2} \tag{B.49}$$

Since ν, α are assumed to be small then

$$c_*(\eta, \xi) \simeq 1 + \sum_{n=2}^{\infty} \exp\left(-j'^2_{n,0} \frac{u_*^2}{4\alpha \, \bar{u}^2} \xi\right) \frac{J_\theta\left(j'_{n,0} \, \eta^{\frac{1}{2}+\alpha}\right) J_0\left(j'_{n,0} \, \eta_s^{\frac{1}{2}+\alpha}\right)}{J_0(j'_{n,0})^2} \tag{B.50}$$

This result is discussed in Chapter 3.6.2.

APPENDIX C

DATA FROM FIELD EXPERIMENTS

In addition to the field experiments described in chapters 7 and 8, field tests were performed in the Craigieburn River in its natural form and in a modified form. These experiments were not included in the discussion in chapter 8 owing to the irregular nature of the reach and the inability of the present computer model to allow for such irregularities. The data presented in this chapter portrays some attempts to quantify the effects mentioned in chapter 10. That is, using sand-bags, polythene and considering the river in its natural state, some idea of the dispersive effects of particular features of the reach was obtained.

While the results presented in this appendix are limited and primarily for interest only, it is hoped that future studies will consider more carefully the dispersive characteristics of particular channel irregularities.

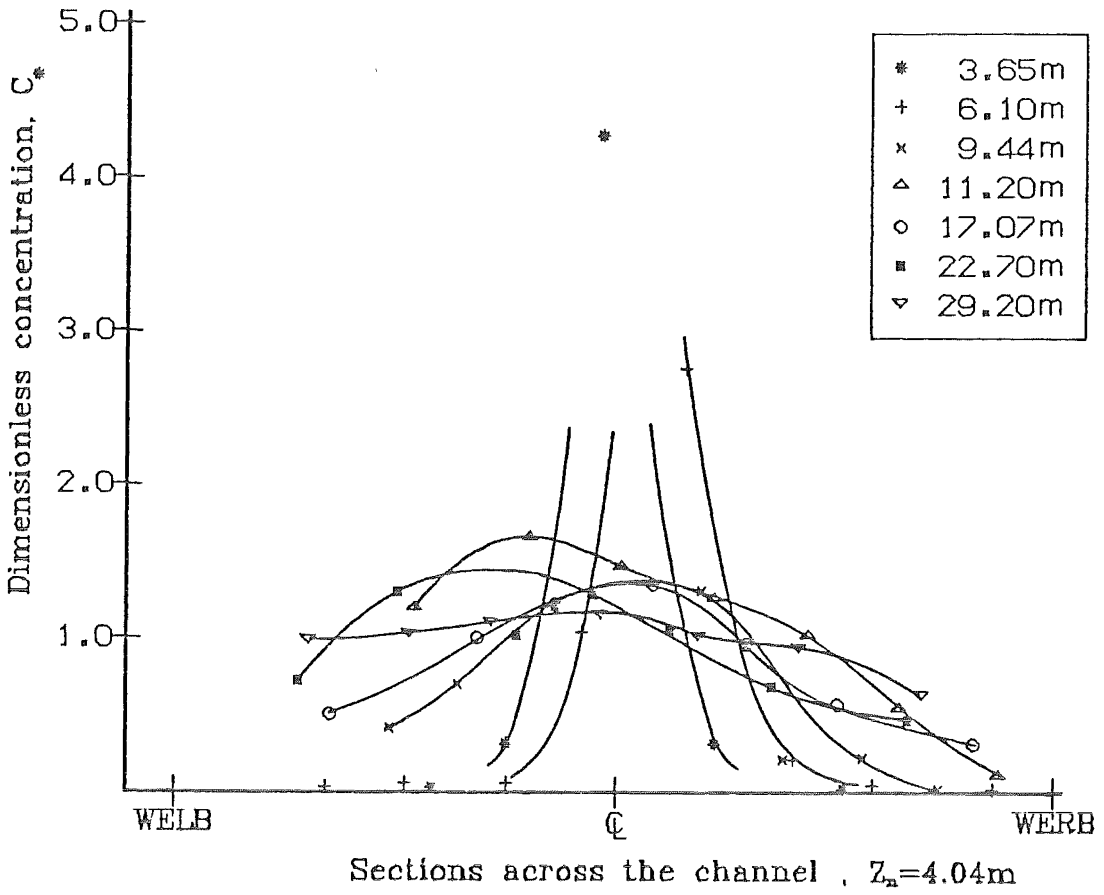

Figure C.1 : Source at mid-point, Run 1, 3/5/82

The first series of experiments (figures C.1 to C.3) in the Craigieburn River were performed with the reach in its unaltered state. This is illustrated in plate 7.2. In its natural form the Craigieburn River is typical of the many small mountainous streams in New Zealand, with numerous rocks generating local mixing and a pool/riffle type composition. The test reach shown in plate 7.2 is completely within a riffle region with pools at both ends. When figures C.1 and C.2 are compared with the corresponding figures for the "smoothed" reach (figures C.4 and C.6) it is clear that the irregularities in natural channels enhance the mixing. The final section in figure C.1 has concentrations varying from 0.61 to 1.14 compared with a range of 0.12 to 1.58 in the smoothed reach (figure C.4).

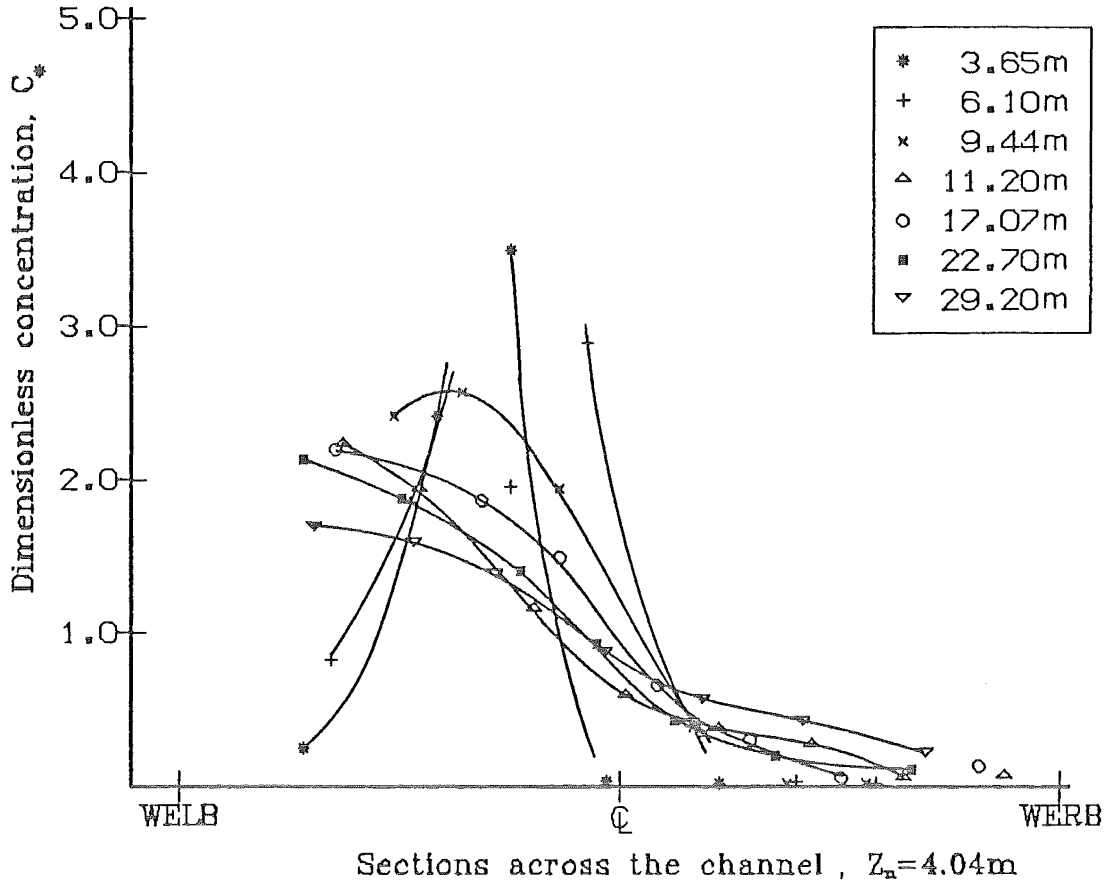

Figure C.2 : Source at 1/4-point, Run 2, 3/5/82

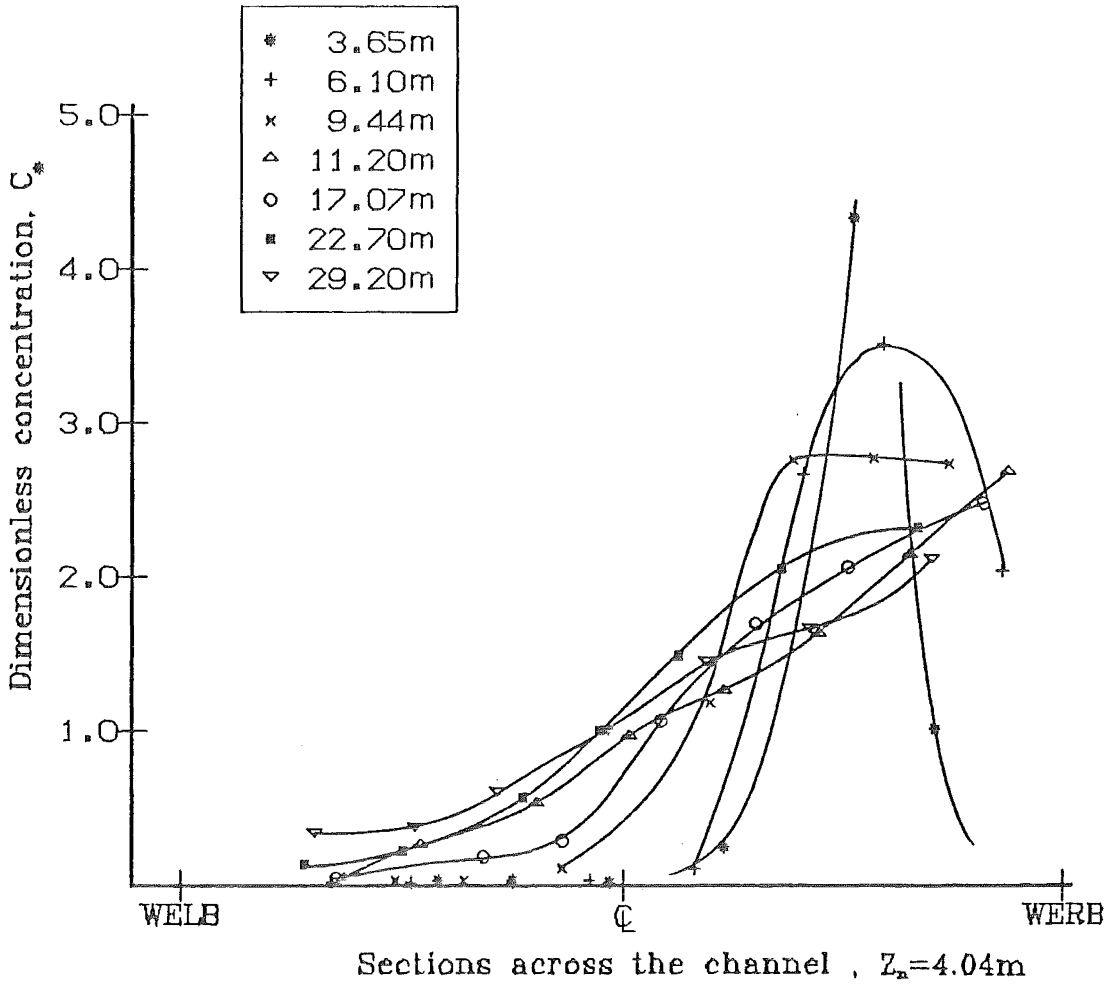

Figure C.3 : Source at 3/4-point, Run 3, 3/5/82

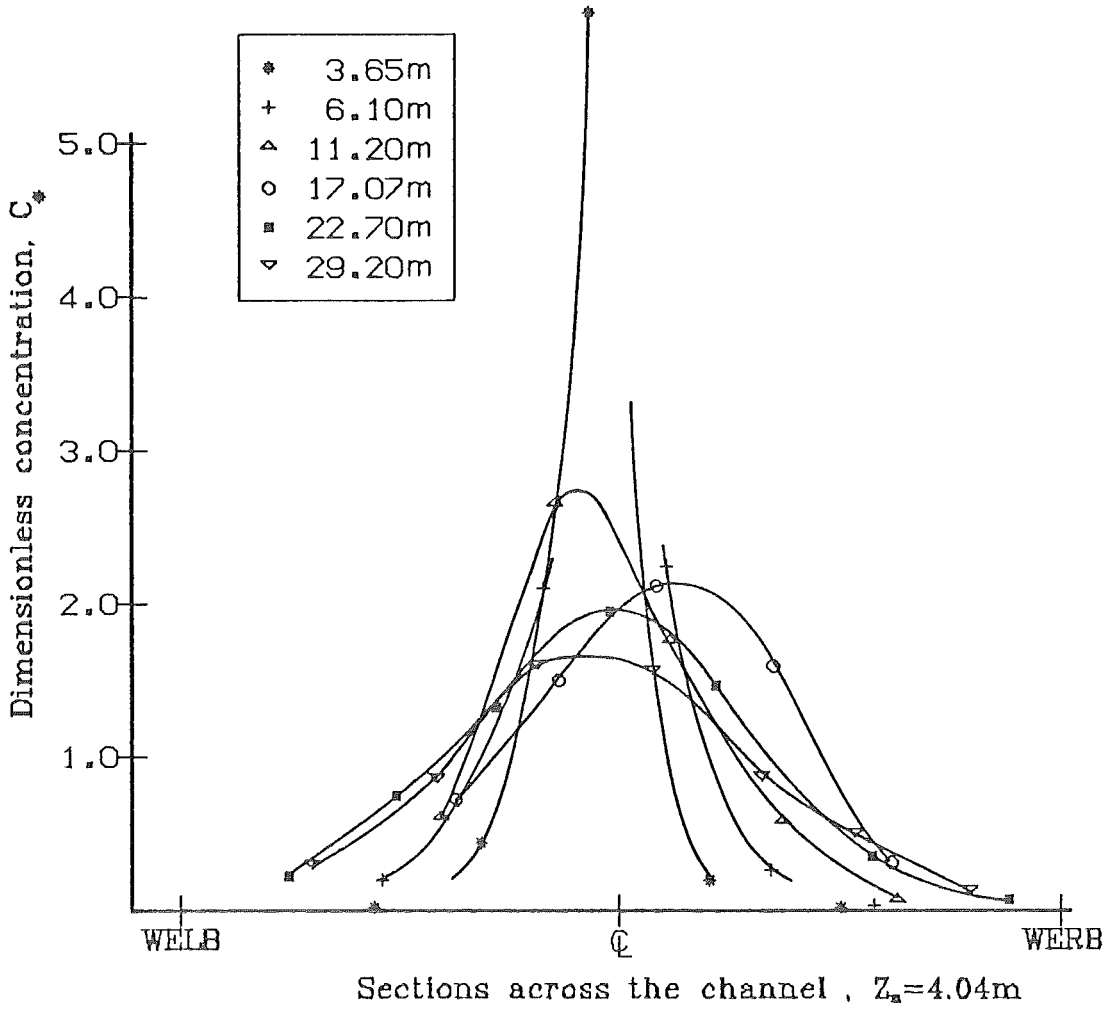

Figure C.4 : Source at mid-point, Run 1, 29/7/82

The following figures (C.4 - C.12) show dispersion patterns for the smoothed channel. In some cases obstructions were placed in the flow to simulate effects found in natural streams in a controlled manner.

Figures C.4 and C.6 were discussed in Chapter 8, where measured results were compared with predicted concentrations, for the smoothed channel.

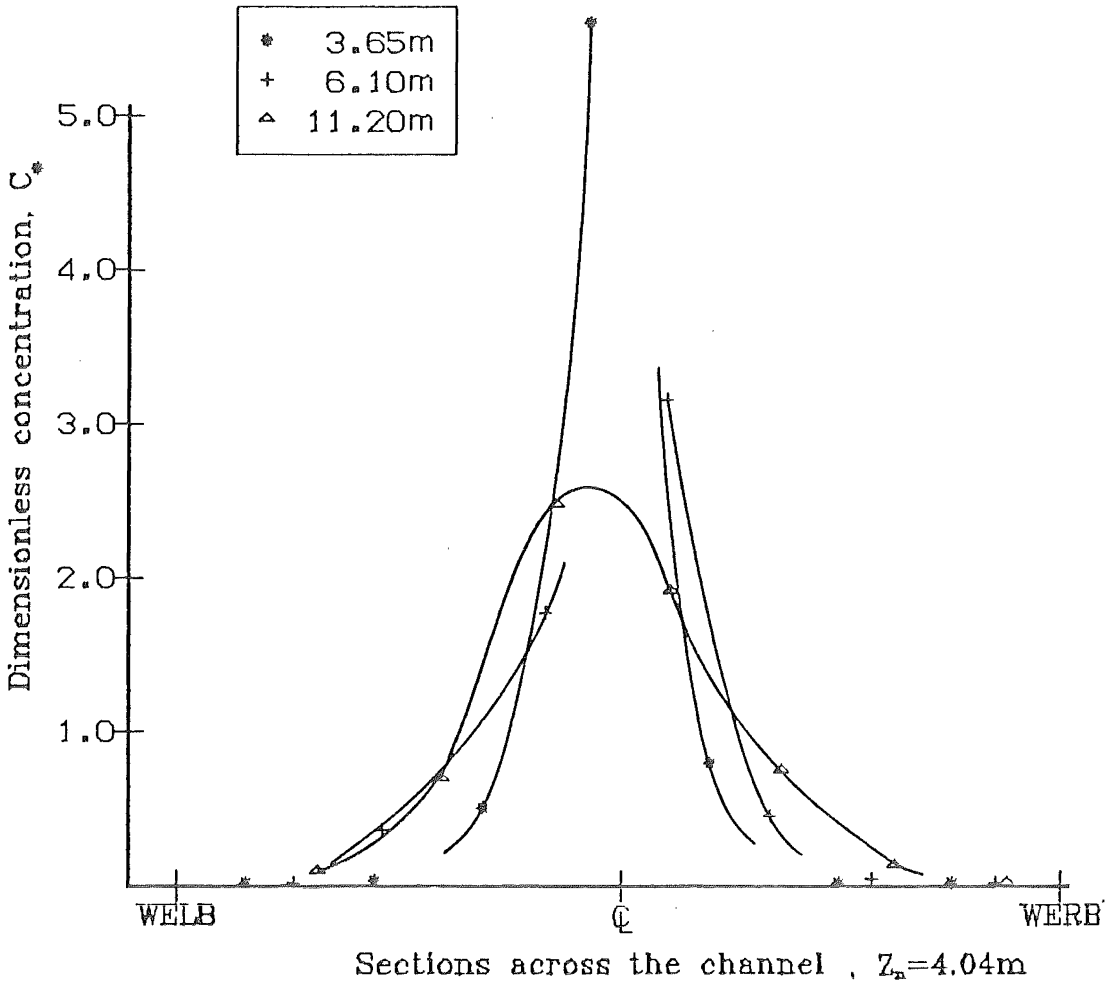

Figure C.5 : Source at mid-point, Run 2, 29/7/82

For this run three sand-bags were placed 1 m directly downstream from the point source to investigate the mixing generated by an obstruction in the flow. The corresponding run without any obstructions in the flow is shown in figure C.4. A slight improvement in the mixing is observed at 11.20 m from the source.

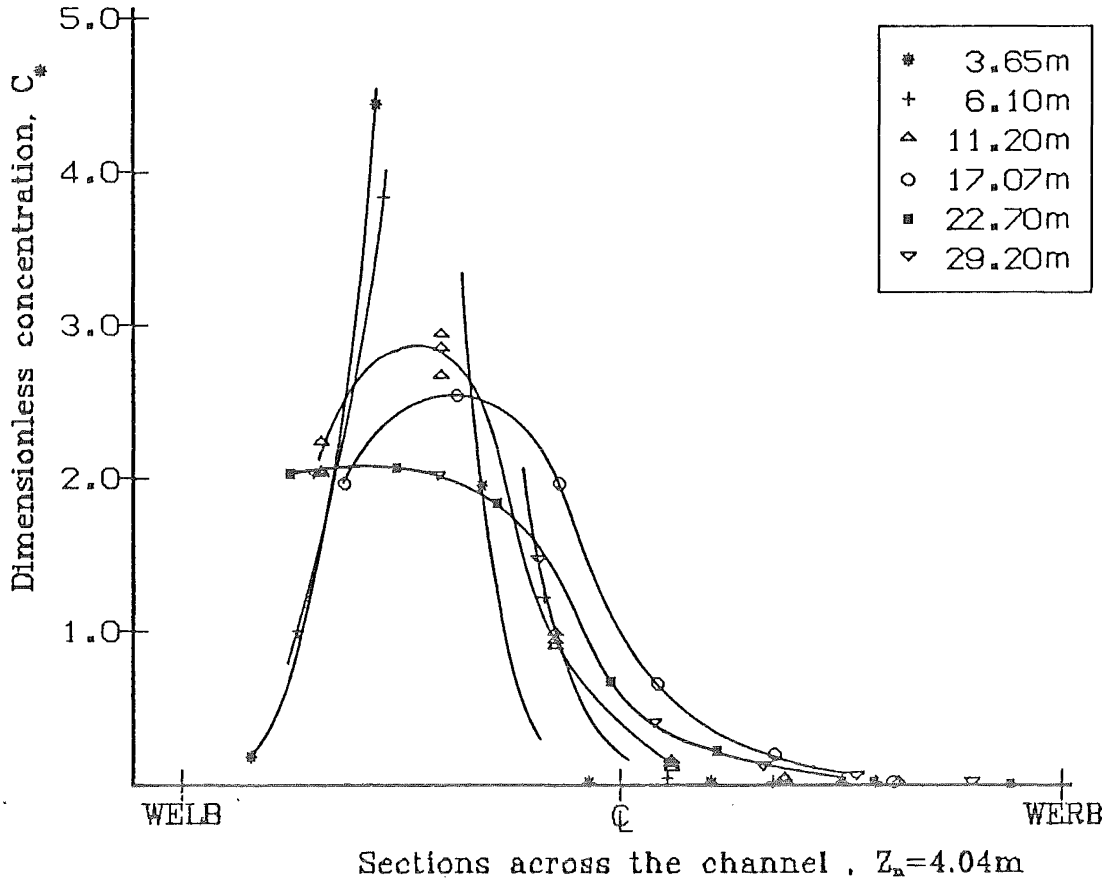

Figure C.6 : Source at 1/4-point, Run 3, 29/7/82

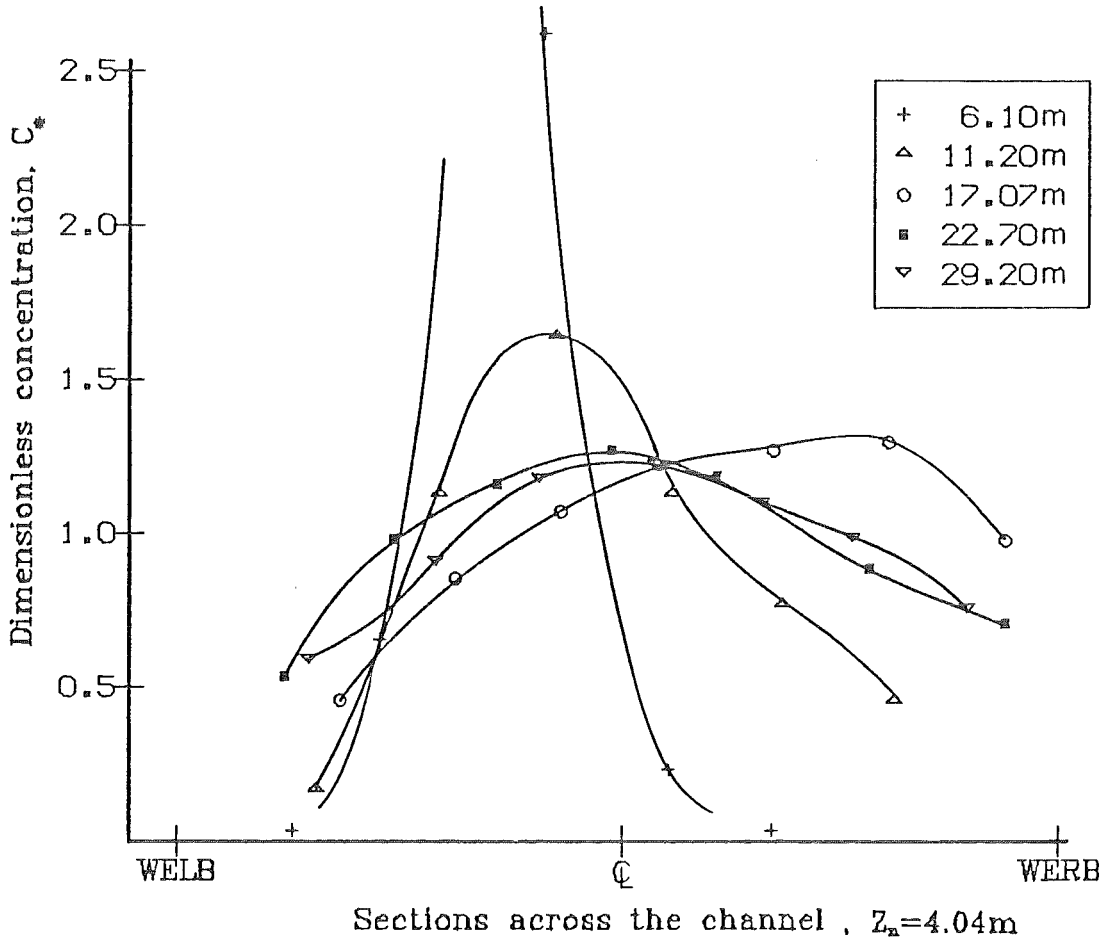

Figure C.7 : Source at mid-point, Run 4, 29/7/82

A significant improvement in mixing is attained when two groynes are included in the test reach. Groynes extending approximately two-thirds the width of the channel were placed at 7.0 m (on the right bank) and at 12.5 m (on the left bank) from the source. A comparison with figure C.1 (note scales are different) shows that a similar dispersion pattern to that observed in the natural channel is achieved when two groynes are placed in the smoothed channel.

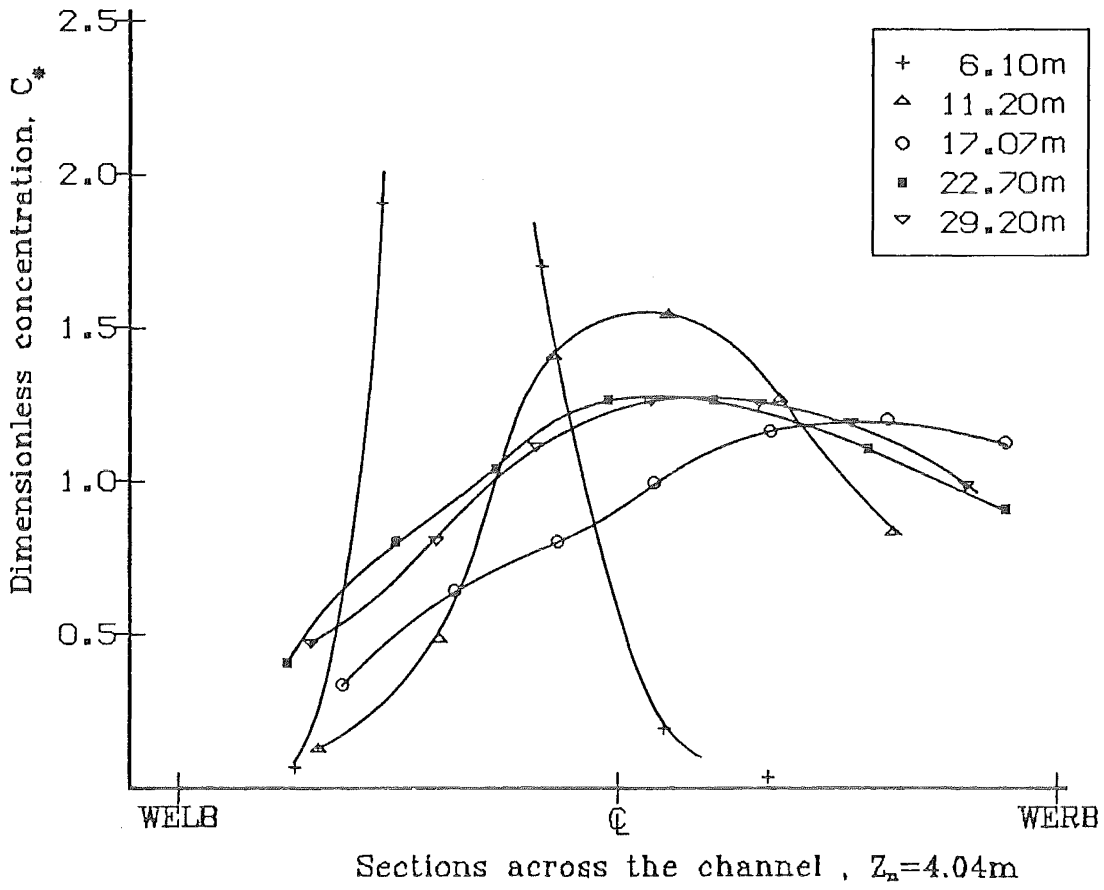

Figure C.8 : Source at mid-point, Run 1, 30/7/82

A further improvement in mixing was observed when the groynes were extended to cover three-quarters of the channel, as shown in figure C.8.

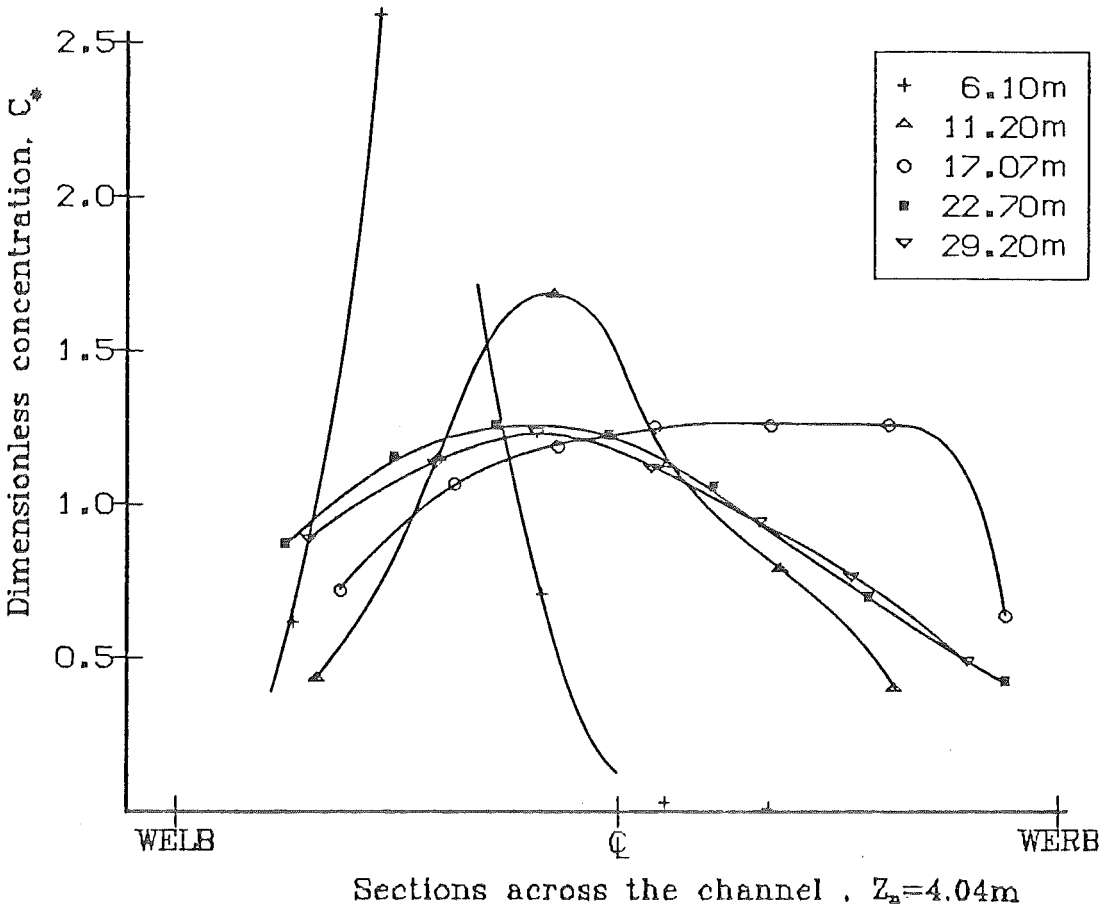

Figure C.9 : Source at 1/3-point, Run 2, 30/7/82

Identical groynes were used in this run as for the previous run, however the source was located at a third of the width from the left bank. A slight improvement is noted from the mid-point release shown in figure C.8.

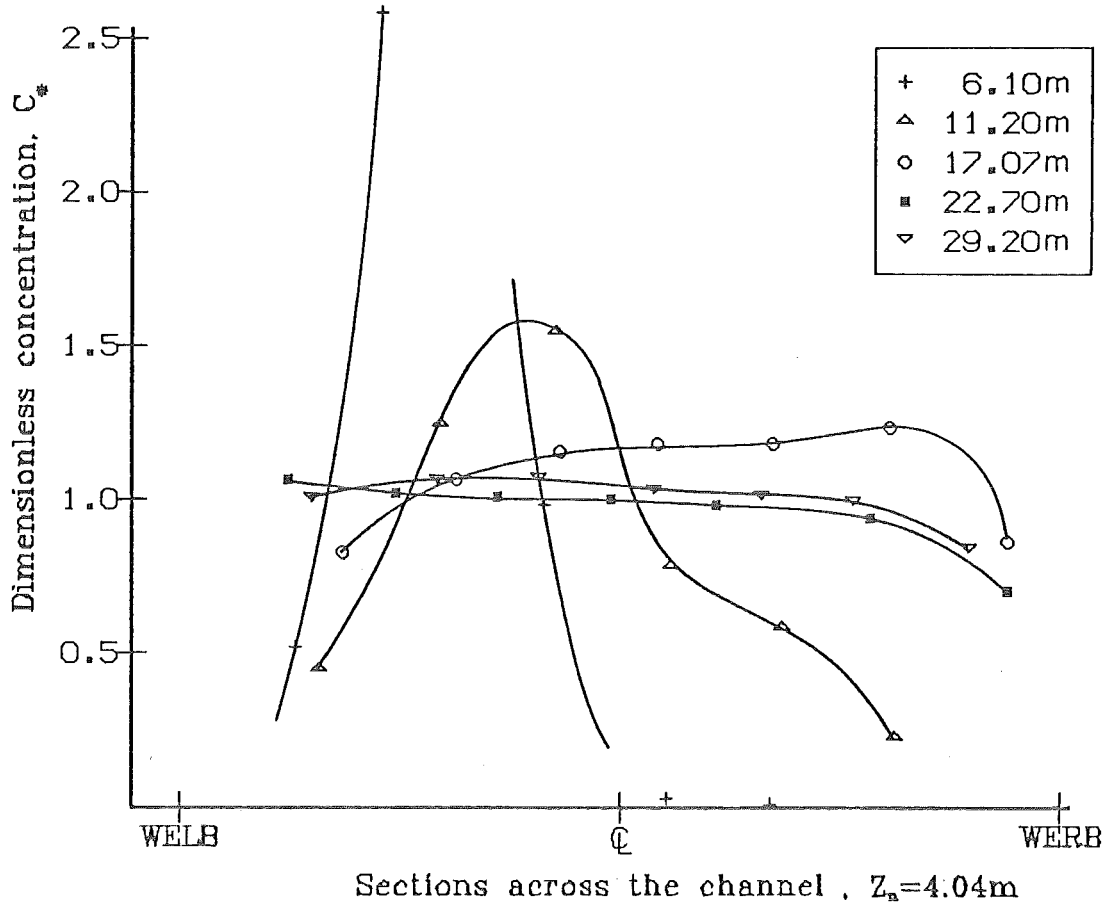

Figure C.10: Source at 1/3-point, Run 3, 30/7/82

A vast improvement in mixing is observed with a third groyne is introduced at 18.8 m from the injection point (on the right bank). This groyne extended over three-quarters of the channel and resulted in the depth below the first groyne increasing up to double the depth observed when only two groynes were present in the channel.

It is apparent from figures C.7 to C.10 that the contraction and expansion of the flow is a powerful mixing tool. A similar effect may be present in a meandering stream where the mainstream moves from one bank to the other.

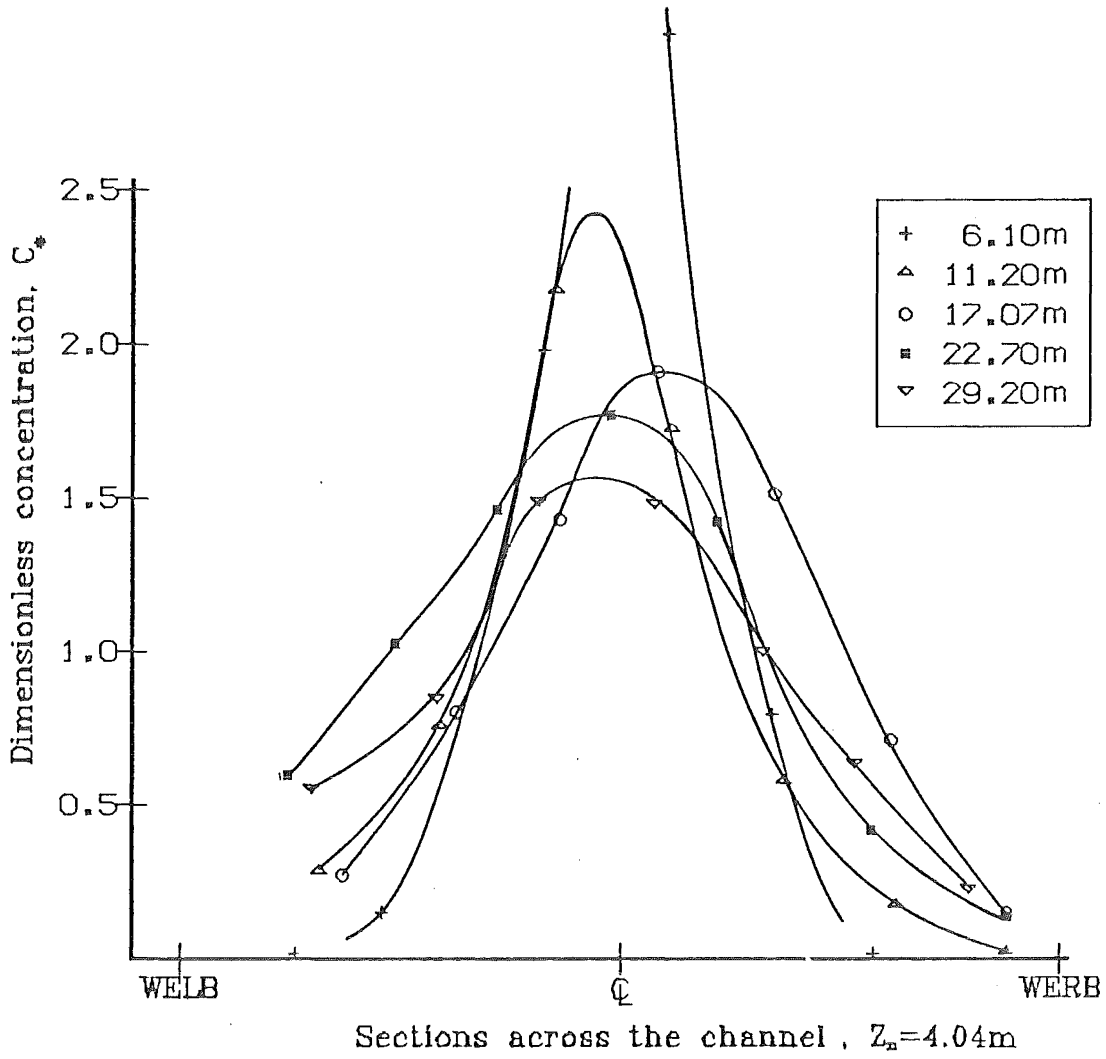

Figure C.11 : Source at mid-point, Run 4, 30/7/82

The final two runs involved grids of sand-bags placed along the reach. Figure C.11 shows some improvement in mixing (c.f. figure C.4) when a line of sand-bags is placed across the channel with two 750 mm gaps in the line, at the quarter-points. These sand-bags were placed just prior to the 3rd sampling section, at 9.0 m from the source.

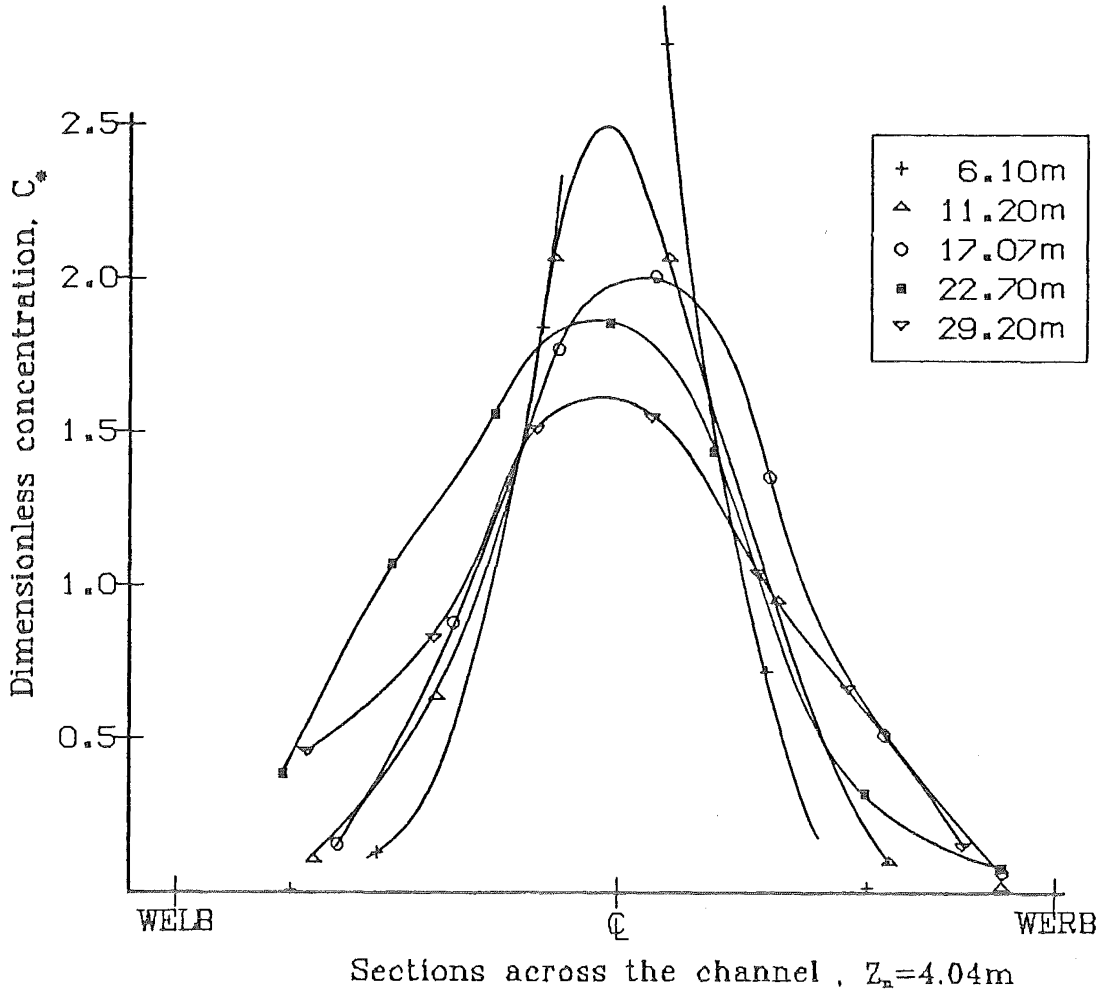

Figure C.12 :Source at mid-point, Run 5, 30/7/82

A similar dispersion pattern is observed for two grids of sand-bags (two or three rows of sand-bags at 1 m centres, 1 m apart). Grids were centred at 8.5 m (three rows) and at 18.0 m (two rows) from the source.

It is apparent from the experimental runs presented in this chapter, that the mixing generated by natural obstacles and meanders is significant in natural channels. Until more extensive experimental data is available, individual mixing effects of obstructions, meanders and so on must be neglected or crudely approximated.

APPENDIX D

TWO-DIMENSIONAL MODEL COMPUTER PROGRAM

Most of the parameters used in the computer model are described, along with general comments, at the beginning of the main program. Some selected parameters not described in the program are listed below;

DUMPM - set $\neq 0$ to output the matrix generated to solve for coefficients in the fitting procedure.

COEFF - set $\neq 0$ to output coefficients in $c = A_n e^{-\alpha_n x}$.

MOMUSE - set $\neq 0$ to output moments of deficit concentration.

NOM - (maximum -1) number of moments used to fit concentration profiles.

NOD - minimum number of derivatives used to fit concentration profiles.

SLE - set $\neq 0$ to make plot length = LPLO.

IX=IXX - longitudinal spacing of points plotted on contour plots (in $\frac{1}{100}$ths of an inch).

IY=IYY - vertical/transverse spacing of points (in $\frac{1}{100}$ths of an inch).

NCON - number of concentration contours on a contour plot.

ZCC - an array of NCON concentration contours.

```
C
C ***********************************************************************
C *                                                                     *
C *     STEADY STATE SOLUTION OF THE TWO-DIMENSIONAL DISPERSION         *
C *     -------------------------------------------------------         *
C *                                                                     *
C *               EQUATION FOR CONCENTRATION DEFICIT.                   *
C *               -----------------------------------                   *
C *                                                                     *
C ***********************************************************************
C
C*****INPUT REQUIRED********
C          GENERAL PARAMETERS:
C             KO - NUMBER OF MOMENTS CALCULATED
C             MU - DIMENSIONLESS AVERAGE VELOCITY (MU=8/f)
C             CE - EQUILIBRIUM CONCENTRATION
C             YS - THE LOCATION OF SOURCE ( DIMENSIONLESS: 0<YS<1 )
C             NDIM - NUMBER OF STEPS FOR NUMERICAL INTEGRATION (<2001)
C             AK - VON KARMAN'S CONSTANT
C             EPS - ERROR LIMIT FOR MATRIX SOLUTION (PIVOT CHECK)
C             S - A USER COMMENT CARD TO PRECEED OUTPUT
C
C
C    VELOCITY AND DIFFUSIVITY PROFILES ARE DEFINED AS FUNCTIONS OF Y,
C          WHERE Y IS DIMENSIONLESS DEPTH.
C
C             VELTYP = 0 , FOR UNIFORM VELOCITY
C                    = 1 , FOR PARABOLIC VELOCITY
C                    = 2 , FOR LOGARITHMIC VELOCITY
C                    = 3 , FOR POWER VELOCITY
C
C             ETYP   = 0 OR 1 , FOR UNIFORM DIFFUSIVITY
C                    = 2 , FOR PARABOLIC DIFFUSIVITY (FROM LOG. VEL.)
C                    = 3 , FOR PARABOLIC DIFFUSIVITY (FROM POWER VEL.)
C       THE PROGRAM IS DESIGNED TO PRODUCE ONE OF THREE TYPES OF PLOT
C       OF THE CONCENTRATION DISTRIBUTION WHICH IS GENERATED.
C       FOR ALL CASES THE USER MUST SPECIFY NL (OR NL2) , THE
C       NUMBER OF HIEGHTS AT WHICH CONCENTRATION PROFILES ARE
C       REQUIRED. THE TYPE OF PLOT IS SPECIFIED BY TYOP ;
C
C               TYOP = 0, CONC. PROFILE IS PLOTTED FOR EACH HEIGHT
C                    = 1-4, PRODUCES 3-D PLOTS OF VARIOUS DESCRIPTION
C                    = 5 , PRODUCES CONTOUR PLOTS OF CONCENTRATION
C
C       FOR TYOP=0 THE USER MUST INPUT THE NUMBER OF SUCH PLOTS
C       REQUIRED ( NL ) AND AN ARRAY YH OF NL HIEGHTS
C       FOR TYOP>0 THE USER MUST INPUT THE NUMBER OF HORIZONTAL
C       SECTIONS ( NL2 ) ALONG WITH THE HEIGHT OF THE FIRST SECTION
C       ( YIN ) AND THE SPACING OF SECTIONS ( YSP ).
C       THE SPACING OF LONGITUDINAL SECTIONS IS DETERMINED BY XSPACE
C       AND THE LENGTH OF PLOT BY LPLO
C
C    DEAD ZONE PARAMETERS:
C       FIVE PARAMETERS ARE REQUIRED TO DEFINE THE PROPERTIES
C       OF THE TRAPPING ELEMENT.
C               AREA - THE DEAD ZONE FRACTION OF THE BED
C               DZO - THE DEPTH OF THE DEAD ZONE
C               PTZ - THE FRACTION OF DEAD ZONE OCCUPIED BY EDDY
C               E - THE DEPTH INTO THE EDDY TO Y=0 (FRACTION OF PTZ)
C               INTR - IF INTR IS NOT EQUAL TO 0 THE SOURCE IS PLACED
C                      IN THE DEAD ZONE
C
C               THE VALUE FOR DZO IS A REAL MEASUREMENT WHICH IS
C               NON-DIMENSIONALISED BY THE MEAN FLOW DEPTH, YNN.
C
C
C    INITIALISE VARIABLES
C    --------------------
C
      INTEGER P
      REAL MU
      EXTERNAL Q
C
      COMMON/AL1/YS,CS,MU,P,SUM(2001,2),XSPACE,LE,YY(1001,50)
      COMMON/AL2/C(2001),DIM,AC(50),K7,AL,YH(50),JM,TYOP,NL
      COMMON/AL3/A(25,25),EPS
      COMMON/AL4/YNN,LEM(50),SER,SLE,LPLO
      COMMON/AL5/YSC,XINC,ZINC,PHI,THETA,XLTH,FR,CONTR,MSKN,IS,NCR
      COMMON/AL6/NCON,ZCC(100),IX,IY,IXX,IYY,LOGPL,NPLS,MX
      COMMON/AL7/VELTYP,SCTI(2001,2),H,AK,YST,ETYP,FLA,UJ(2001)
      COMMON /AL8/INTR,VPT(50),DIST(50),NPTS,DEPT(50)
      COMMON/AL9/PSIB(2001),U(2001),S1,UBAR
      COMMON/AL10/FL1,PSU(2001)
C
      DIMENSION Z(2001),CC(50,25),CM(50),LH(50),S(10)
     1,PL(2000),YD(1001,25),OL(2000)
C
      READ(5,180)S
      READ(5,/) EPS,MU,NL,AK
      READ(5,/)VELTYP,ETYP
      READ(5,/)AREA,DZO,YNN
      READ(5,/) PTZ,E,INTR
      READ(5,/)CE,YS,NDIM,KO
      READ(5,/)XSPACE,DUMPM,COEFF,MOMUSE,SER
      READ(5,/) (YH(I),I=1,NL)
      READ(5,/)TYOP
      READ(5,/)YSP,YIN,NL2
      READ(5,/)NOM,NOD
      READ(5,/)SLE,LPLO
      READ(5,/)YSC,XINC,ZINC,PHI,THETA,XLTH,FR,CONTR,MSKN,IS,NCR
      READ(5,/)IX,IY,IXX,IYY
      READ(5,/)NCON,(ZCC(I),I=1,NCON)
      READ(5,/)LOGPL,NPLS
      READ(5,/)NPTS,UBAR,(VPT(I),DIST(I),DEPT(I),I=1,NPTS)
```

```
      IF(TYOP.GE.1.)NL=NL2
C
      DATE=TIME(15)
      WT2=TIME(11)*2.4E-6
      WT1=AINT(WT2/3600.)*100
      WTT=(WT2-WT1*36.)/60.+WT1
      RM=CONCAT(RM,DATE,15,47,16)
      RD=CONCAT(RD,DATE,15,31,16)
      RY=CONCAT(RY,DATE,15,15,16)
      WRITE(6,505)RD,RM,RY,WTT
      WRITE(6,180)S
      WRITE(6,*) EPS,MU,NL,AK
      WRITE(6,*)VELTYP,ETYP
      WRITE(6,*)AREA,DZO,YNN
      WRITE(6,*)PTZ,E,INTR
      WRITE(6,*)CE,YS,NDIM,KO
      WRITE(6,)XSPACE,DUMPM,COEFF,MOMUSE,SER
      WRITE(6,*) (YH(I),I=1,NL)
      WRITE(6,*)TYOP
      WRITE(6,*)YSP,YIN,NL
      WRITE(6,)NOM,NOD
      WRITE(6,*)SLE,LPLO
      WRITE(6,)YSC,XINC,ZINC,PHI,THETA,XLTH,FR,CONTR,MSKN,IS,NCR
      WRITE(6,)IX,IY,IXX,IYY
      WRITE(6,)NCON,(ZCC(I),I=1,NCON)
      WRITE(6,*)LOGPL,NPLS,UBAR
C     WRITE(6,171)(VPT(I),DIST(I),DEPT(I),I=1,NPTS)
 171  FORMAT(5X,3(1X,F6.4,3X))
C
C*********ADJUST INPUT VARIABLES FOR DEAD ZONE EFFECTS
C         ------------------------------------------
C
      DIM=NDIM
      H=1.0/NDIM
      YNN=YNN+DZO*AREA
      DZO=DZO/YNN
      YST=AREA*DZO*E*PTZ
      YE=AREA*DZO*PTZ
      YS=YS-(1-YS)*YE/(1-YE)
      IF(YS.LT.0.)YS=4./DIM
      YL=YS-1E-5
      YU=YS+1E-5
      IF(INTR.NE.0)YS=4./DIM
      CS=MU/(UI(YS+1E-5)-UI(YS-1E-5))
      WRITE(6,) YST,YE,DZO,YS,YU,YL,CS
C
C    SET UP ARRAYS OF PROFILE HEIGHTS
C
      DO 31 I=1,NL
      IF(TYOP.GE.1.0)YH(I)=YIN+(I-1)*YSP
      IF(TYOP.LT.1.)YH(I)=(YH(I)/YNN)
      YH(I)=YH(I)-(1-YH(I))*YE/(1-YE)
      IF(YH(I).LT.0.)YH(I)=0.
 31   LH(I)=AINT(YH(I)*DIM)+1
      IF(SER.NE.0.)GO TO 68
C
C         CALCULATE ARRAY OF VELOCITIES AND DIFFUSIVITIES
C         THEN ENTER LOOP TO SOLVE FOR MOMENTS
C
      CALL VELDIF(NDIM)
      SUM1=-PSIA(1)+CS*(PSIA(YS+1E-5)-PSIA(YS-1E-5))
 15   CONTINUE
      J=P+1
C
C    NUMERICAL INTEGRATION TO SOLVE FOR C
C
      CALL QTFE(H,Q,C,NDIM)
C
C    ADJUST C TO FIT BOUNDARY CONDITION ( Q(1)=0 )
C
      CALL BOUND(NDIM,SCT2,SUM2,SUM1)
      ADD=(-SCT2-SUM1)/MU
        WRITE(6,*)ADD,SCT2,SUM1,S1
      DO 16 I=1,NDIM
 16   C(I)=C(I)+ADD
C
C    CALCULATE "SOURCE" TERM FOR NEXT CYCLE
C
      CALL QTFF(H,SUM,NDIM)
      SUM1=S1
      DO 18 I=1,NL
      CC(I,J)=C(LH(I))
C
 18   CONTINUE
      P=P+1
      IF(P.GT.KO)GO TO 20
      GO TO 15
 20   CONTINUE
 68   CONTINUE
      P=KO+1
C
C    FIT A CONCENTRATION PROFILE AT EACH HEIGHT
C    ------------------------------------------
C
      DO 8 JM=1,NL
      Y=YH(JM)
      IF(SER.NE.0.)GO TO 69
      CAX0=-CE
      IF(MOMUSE.NE.0) WRITE(6,51) Y
      DO 1 I=1,P
      II=I-1
      CM(I)=CC(JM,I)
 1    IF(MOMUSE.NE.0)WRITE(6,50) CM(I),II
      PI=3.1415926536
```

```
      AL=CM(P-1)*(P-1)/CM(P)
      AC(1)=AL**(P)*CM(P)/FACT(P-1)
   79 CONTINUE
      YK=ABS(Y-YS)
C
C     DETERMINE THE NUMBER OF MOMENT AND DERIVATIVE EQUATIONS
C       REQUIRED TO SOLVE AT A PARTICULAR HEIGHT IN THE FLOW
C       (THIS IS A FUNCTION OF THE DISTANCE FROM THE SOURCE AT X = 0 )
C
      IF(YK.GT..175)IF((YK-.25))71,72,72
      IF(YK.GT..075)GO TO 172
      NM=NOM+1
      ND=NOD
      GO TO 24
      GO TO 24
  172 NM=NOM
      ND=NOD
      GO TO 24
   71 NM=NOM
      ND=NOD+1
      GO TO 24
   72 IF((YK-.35).GT.0.0)IF((YK)-.4)73,74,74
      NM=NOM-1
      ND=NOD+2
      GO TO 24
   73 NM=NOM-1
      ND=NOD+3
      GO TO 24
   74 IF(YK.GT..5)IF(YK-.6)75,76,76
      NM=NOM-2
      ND=NOD+4
      GO TO 24
   75 NM=NOM-3
      ND=NOD+5
      GO TO 24
   76 IF(YK.GT..7)IF(YK-.8)77,78,78
      NM=NOM-5
      ND=NOD+6
      GO TO 24
   77 NM=NOM-5
      ND=NOD+7
      GO TO 24
   78 NM=NOM-5
      ND=NOD+8
   24 CONTINUE
      NM=AMAX0(3,NM)
      NOM1=NM+1
      NOM2=NOM1+1
      K6=ND+NOM1
      K7=K6+1
C
C     SET UP COEFFICIENT MATRIX FOR A(N), WHERE CD* = A(N) * EXP(...)
C
      A(1,K7)=-AC(1)+CAX0
      DO 3 II=1,NOM1
      DO 2 K=1,K7
      I=II
    2 A(II,K)=1.0/(ALPN(K))**(I-1)
    3 CONTINUE
      A(1,K7)=-AC(1)+CAX0
      DO 4 II=2,NOM1
      I=II
    4 A(II,K7)=CM(I-1)*(AL**(I-1))/FACT(I-2)-AC(1)
      NOM2=NOM1+1
      IF(ND.EQ.0)GO TO 22
      DO 23 K=NOM2,K6
      DO 21 I=1,K6
   21 A(K,I)=(ALPN(I))**(K-NOM1)
   23 A(K,K7)=-AC(1)
   22 CONTINUE
      IF(DUMPM.EQ.0.)GO TO 41
      DO 25 I=1,K7
   25 WRITE(6,/) (A(I,K),K=1,K7)
   41 CONTINUE
C
C     SOLVE COEFFICIENT MATRIX
C
      CALL MATSOL(K6,K7)
      DO 7 I=2,K7
    7 AC(I)=A((I-1),K7)
      IF(COEFF.EQ.0.)GO TO 42
      WRITE(6,53)K7,NM,ND
      I=1
      WRITE(6,52) I,AC(1)
      DO 6 I=1,K6
      II=I+1
    6 WRITE(6,52) II,AC(II)
   42 CONTINUE
      IF(COEFF.NE.0.) WRITE(6,54) AL
   69 CONTINUE
C
C       CALL PLOTTING ROUTINE REQUIRED
C
      IF(TYOP.GT.6.0.OR.TYOP.LT.0.)GO TO 8
      IF(TYOP.LT.1)CALL GRA(Y)
      IF(TYOP.GE.1..AND.SER.EQ.0.)CALL CONI(Y,PL)
      IF(TYOP.GE.1..AND.SER.NE.0.)CALL CON(Y,PL,OL)
    8 CONTINUE
      DO 45 I=1,NL
   45 LE=MAX0(LEM(I),LE)
      IF(SLE.NE.0.)LE=LPLO
      IF(TYOP.GE.1.AND.TYOP.LT.5.)CALL PLO(TYOP,YD)
      IF(TYOP.EQ.5)CALL FLATCO(YD)
  100 FORMAT(I5,E7.1,F6.2)
```

```
110 FORMAT(F4.2,2F5.3,I4,I2)
120 FORMAT(2F6.4)
160 FORMAT('1',10X,'SOLUTION FOR C',I1,' IS:'///10X,'  Y=    '
   1,10X,'C',I1/)
170 FORMAT('0',13X,F5.3,8X,E15.7)
180 FORMAT(1X,10(A6))
505 FORMAT(2X,C2,"/",C2,"/19",C2,5X,"TIME IS",F10.3,//)
 50 FORMAT(5X,E17.9,5X,'C',I2,5X,E17.9,5X,E17.9,5X,E17.9,5X,E17.9/)
 51 FORMAT(/10X,"VALUE OF ITH MOMENT USED FOR Y=",F5.3,//)
 52 FORMAT(10X,'A',I1,10X,E15.7,/)
 53 FORMAT(////10X,'PROGRAM HAS SOLVED FOR THE FIRST ',I1,
   1' COEFFICIENTS',//10X,'USING ',I1,' MOMENTS AND ',I1
   2,' DERIVATIVES',/)
 54 FORMAT(//10X,'ALPHA=',F12.10,///)
    STOP
    END
```

```
C
C     ..................................................................
C
C        FUNCTION ALPN
C        -------------
C
C          ROUTINE TO RETURN ALPN, WHERE ALPHA(N)=ALPHA(0)*ALPN
C
C     ..................................................................
C
      FUNCTION ALPN(I)
      COMMON/AL7/VELTYP,SCTI(2001,2),H,AK,YST,ETYP
      IF(VELTYP.NE.0)GO TO 1
    2 ALPN=(I+1)**2
      RETURN
    1 IF(I.GT.0)GO TO 3
      ALPN=1
      RETURN
    3 ALPN=0.614186979*(I+2)**2-0.853060009*(I+2)+0.248891628
      RETURN
      END
C
C     ..................................................................
C
C        FUNCTION FACT
C        -------------
C
C          ROUTINE TO CALCULATE FACTORIALS
C
C     ..................................................................
C
      FUNCTION FACT(I)
      F=1.0
      DO 1 J=1,I+1
      F=F*(J-1)
      IF(F.EQ.0.0) F=1.0
    1 CONTINUE
      FACT=F
      RETURN
      END
C
C     ..................................................................
C
C        SUBROUTINE MATSOL
C        -----------------
C
C     ..................................................................
C
      SUBROUTINE MATSOL(K5,K6)
      COMMON/AL3/A(25,25),EPS
      DO 90 K=1,K5
      KP1=K+1
```

```
C
      IF(ABS(A(K,K)).GE.EPS)GO TO 50
C
      WRITE(6,150)
  150 FORMAT(////10X,'PIVOT ELEMENT TOO SMALL.STOP')
      STOP
C
   50 DO 60 J=KP1,K6
   60 A(K,J)=A(K,J)/A(K,K)
      A(K,K)=1.0
C
      DO 90 I=1,K5
      IF(I.EQ.K.OR.A(I,K).EQ.0.) GO TO 90
      DO 80 J=KP1,K6
   80 A(I,J)=A(I,J)-A(I,K)*A(K,J)
      A(I,K)=0.0
   90 CONTINUE
      RETURN
      END
C
C     .....................................................................
C
C        SUBROUTINE CONI
C        ---------------
C
C
C          SUBROUTINE TO COMPUTE CONCENTRATION ALONG ONE STREAMLINE
C             USING COEFFICIENTS CALCULATED FROM MOMENTS
C
C     .....................................................................
C
      SUBROUTINE CONI(Y,PL)
      COMMON/AL1/YS,CS,MU,P,SUM(2001,2),XSPACE,LE,YY(1001,50)
      COMMON/AL2/C(2001),DIM,AC(50),K7,AL,YH(50),JM,TYOP,NL
      COMMON/AL4/YNN,LEM(50),SER
      COMMON/AL6/NCON,ZCC(100),IX,IY,IXX,IYY,LOGPL,NPLS,MX
      DIMENSION PL(2000)
      DO 2 M=1,1001
      PL(M)=-1.0
    2 YY(M,JM)=1.0
      X=XSPACE
      PL(1)=-1.0
      YY(1,JM)=0.0
      I=2
    4 IF(LOGPL.NE.0) X=-5.0
      DO 5 L=1,MX
    5 YY(L,JM)=0.0
   20 PL(I)=0.0
      AX=X
      IF(LOGPL.NE.0) AX=10**(X)
      DO 1 J=1,K7
    1 PL(I)=AC(J)*EXP(-AL*ALPN(J-1)*AX)+PL(I)
      YY(I,JM)=PL(I)+1.0
      LE=I
      LEM(JM)=I
      IF(ABS(PL(I)).LT.2E-02.AND.X.GT.85.)GO TO 3
      IF(ABS(PL(I)).LT.2E-02.AND.AX.GT.1E04)GO TO 3
      I=I+1
      X=X+XSPACE
      GO TO 20
    3 CONTINUE
      RETURN
      END
C
C     .....................................................................
C
C        SUBROUTINE CON
C        --------------
C
C
C          SUBROUTINE CALCULATING CONCENTRATIONS FOR THE SERIES SOLN.
C
C     .....................................................................
C
      SUBROUTINE CON(Y,PL,OL)
      COMMON/AL1/YS,CS,MU,P,SUM(2001,2),XSPACE,LE,YY(1001,50)
      COMMON/AL2/C(2001),DIM,AC(50),K7,AL,YH(50),JM,TYOP,NL
      COMMON/AL4/YNN,LEM(50),SER,SLE,LPLO
      COMMON/AL6/NCON,ZCC(100),IX,IY,IXX,IYY,LOGPL,NPLS
      COMMON/AL7/VELTYP,SCTI(2001,2),H,AK,YST,ETYP
      DIMENSION PL(2000),OL(2000)
      XDT=XSPACE*LPLO
      IF(SLE.EQ.0.)XDT=70.
      REAL MU
      BETA=6*SQRT(MU)/AK
      PI=3.14159265359
      DO 2 M=1,1001
    2 YY(M,JM)=1.0
      X=XSPACE
      YY(1,JM)=0.0
      I=2
    3 IF(LOGPL.NE.0) X=-5.0
      D=.00001
   20 SU=0.0
      AX=X
      IF(LOGPL.NE.0) AX=10**(X)
      DO 1 M=1,25
      SU=SU+SIN(M*PI*D)*COS(M*PI*(YS))*COS(M*PI*Y)/
     1M*EXP(-1.0/BETA*(M*PI)**2*AX)
    1 CONTINUE
      PL(I)=2*D*CS+4*CS/PI*SU-1.0
      YY(I,JM)=PL(I)+1.0
      OL(I)=X
      LE=I
      LEM(JM)=I
      IF(ABS(PL(I)).LT.2E-02.AND.AX.GT.1E04)RETURN
```

```
      IF(ABS(PL(I)).LT.2E-02.AND.X.GT.XDT)RETURN
      I=I+1
      X=X+XSPACE
      GO TO 20
      END
C
C     ..................................................................
C
C        FUNCTION UI(Y)
C        --------------
C
C     ..................................................................
C
      FUNCTION UI(Y)
      COMMON/AL1/YS,CS,MU,P
      COMMON/AL7/VELTYP,SCTI(2001,2),H,AK,YST,ETYP,FLA,UJ(2001)
      YW=Y
      NDIM=1/H+.1
      YW=(1-YW)*YST/(1+YST)+YW
      REAL MU
      IF(VELTYP.GT.0.)IF(VELTYP-2.)1,2,3
C
C         UNIFORM VELOCITY
C
      UI=MU*YW
      RETURN
C
C         PARABOLIC VELOCITY
C
    1 CONTINUE
      UI=MU*YW+SQRT(MU)/AK*(-YW**3+3*YW*YW-2*YW)
      RETURN
C
C         LOGARITHMIC VELOCITY
C
    2 CONTINUE
      IF(YW.GT.0.)  Z=MU*YW+SQRT(MU)/AK*(YW*ALOG(YW))
      UI=Z
      RETURN
C
C         POWER VELOCITY
C
  3   IF(VELTYP-4)4,4,6
   4    UI=MU*YW**(1.+1./7.)
        RETURN
   6    IF(FLA.NE.0)GO TO 7
        FLA=1
        US=0
        DO 10 I=1,NDIM
        YK=I*H-H/2.
        US=US+H*VELM(YK)
  10    UJ(I)=US
   7    CONTINUE
        UI=UJ(AINT(YW*NDIM+.6))
      RETURN
      END
C
C     ..................................................................
C
C        FUNCTION PSI(Y)
C        ---------------
C
C     ..................................................................
C
      FUNCTION PSI(Y)
      COMMON/AL7/VELTYP,SCTI(2001,2),H,AK,YST,ETYP
      COMMON/AL1/YS,CS,MU,P,SUM(2001,2),XSPACE,LE,YY(1001,50)
      COMMON /AL8/INTR,VPT(50),DIST(50),NPTS,DEPT(50)
      YW=Y
      YW=(1-YW)*YST/(1+YST)+YW
      REAL MU
      PI=3.14159265358979
      IF(ETYP-2.)1,2,3
C
C         UNIFORM DIFFUSIVITY
C
  1   PSI=SQRT(MU)*AK/6.
      RETURN
C
C         PARABOLIC DIFFUSIVITY  (FROM LOG VELOCITY)
C
   2  CONTINUE
      PSI=SQRT(MU)*AK*YW*(1-YW)
      IF(PSI.LT.H)PSI=H
      RETURN
  3   IF(VELTYP-4)4,5,6
C
C         PARABOLIC DIFFUSIVITY  (FROM POWER VELOCITY)
C
  4    PSI=AK*SQRT(MU)/6.*(2-1./7.)*(3.-1./7.)*YW**(1-1./7.)*(1-YW)
       RETURN
C
C         SINUSOIDAL DIFFUSIVITY
C
  5    PSI=SQRT(MU)*AK/12.*PI*SIN(PI*YW)
       RETURN
   6   PSI=.15*DEP(YW)*VELM(YW)/6.5*SQRT(MU)
       RETURN
      END
C
C     ..................................................................
C
C        FUNCTION PSIA(Y)
C        ----------------
```

```
C
C     ..................................................................
C
      FUNCTION PSIA(Y)
      COMMON/AL7/VELTYP,SCTI(2001,2),H,AK,YST,ETYP
      COMMON/AL1/YS,CS,MU,P,SUM(2001,2),XSPACE,LE,YY(1001,50)
      COMMON/AL10/FL1,PSU(2001)
      YW=Y
      NDIM=1/H+.1
      YW=(1-YW)*YST/(1+YST)+YW
      REAL MU
      PI=3.141592653589793
      IF(ETYP-2.)1,2,3
C
C          UNIFORM DIFFUSIVITY
C
    1 PSIA=YW*SQRT(MU)*AK/6.
      RETURN
C
C          PARABOLIC DIFFUSIVITY  (FROM LOG VELOCITY)
C
    2 CONTINUE
      PSIA=SQRT(MU)*AK/6.*(3*YW**2-2*YW**3-(3*YST**2-2*YST**3))
      RETURN
    3 IF(ETYP-4)4,5,6
C
C          PARABOLIC DIFFUSIVITY  (FROM POWER VELOCITY)
C
    4  PSIA=AK*SQRT(MU)/6.*((3.-1./7.)*YW**(2-1./7.)-YW**(3-1./7.)*
     - (2.-1./7.))
      RETURN
C
C          SINUSOIDAL DIFFUSIVITY
C
    5  PSIA=SQRT(MU)*AK/12.*(1-COS(PI*YW))
      RETURN
    6  CONTINUE
      IF(FL1.NE.0)GO TO 7
      FL1=1
      UP=0
      DO 10 I=1,NDIM
      YK=I*H-H/2.
      UP=UP+H*PSI(YK)
   10 PSU(I)=UP
    7 CONTINUE
      UI=PSU(AINT(YW*NDIM+.6))
      RETURN
      END
C
C     ..................................................................
C
C        FUNCTION Q(Y)
C        -------------
C
C     ..................................................................
C
      FUNCTION Q(Y)
      INTEGER P
      COMMON/AL1/YS,CS,MU,P,SUM(2001,2),XSPACE,LE
      COMMON/AL2/C(2001),DIM,AC(50),K7,AL,YH(50),JM,TYOP,NL
      COMMON/AL7/VELTYP,SCTI(2001,2),H,AK,YST
      COMMON/AL9/PSIB(2001),U(2001)
      YL=YS-1E-5
      YU=YS+1E-5
      N=AINT((Y+H/2.)*DIM)
      IF(P-1)7,8,9
C
C     P=0
C
    7 Q=UI(Y)
      RETURN
C
C     P=1
C
    8 CONTINUE
      IF(Y-YS)10,10,11
   10 IF(Y.NE.0.)GO TO 12
      Q=0.0
      RETURN
   12 CONTINUE
      Q=-SCTI(N,2)
      RETURN
   11 IF(Y-YS.GT.H)GO TO 14
   13 Q=PSIA(Y)-SCTI(N,2)-(CS)*(PSIA(Y)-PSIA(YS-1E-5))
      RETURN
   14 Q=PSIA(Y)-SCTI(N,2)-(CS)*(PSIA(YS+1E-5)-PSIA(YS-1E-5))
      RETURN
C
C     P>1
C
    9 CONTINUE
      IF(Y.NE.0)GO TO 17
      Q=0.
      RETURN
   17 Q=-P*(P-1)*SUM(N,1)-P*SCTI(N,2)
      RETURN
      END
C
C     ..................................................................
C
C        FUNCTION VELM(Y)
C        ----------------
C
C            THIS FUNCTION RETURNS LINEARLY INTERPOLATED VALUES
```

```
C            OF VELOCITY FROM A DISCRETE VELOCITY INPUT
C     ..................................................................
C
        FUNCTION VELM(Y)
        COMMON/AL1/YS,CS,MU,P
        COMMON /AL8/INTR,VPT(50),DIST(50),NPTS,DEPT(50)
        IF(Y.GE.1..OR.Y.LE.0.)RETURN
        DO 1 I=1,NPTS
    1   IF(Y.LE.DIST(I))GO TO 2
    2   VELM=VPT(I-1)+(VPT(I)-VPT(I-1))*(Y-DIST(I-1))/(DIST(I)
      - -DIST(I-1))
        VELM=VELM*MU
        RETURN
        END
C
C     ..................................................................
C
C        FUNCTION DEP(Y)
C        ---------------
C
C     ..................................................................
C
        FUNCTION DEP(Y)
        COMMON/AL1/YS,CS,MU,P
        COMMON /AL8/INTR,VPT(50),DIST(50),NPTS,DEPT(50)
        IF(Y.GE.1..OR.Y.LE.0.)GO TO 2
        DO 1 I=1,NPTS
    1   IF(Y.LE.DIST(I))GO TO 2
    2   CONTINUE
        DEP=DEPT(I-1)+(DEPT(I)-DEPT(I-1))*(Y-DIST(I-1))/
      -  (DIST(I)-DIST(I-1))
        RETURN
        END
C
C     ..................................................................
C
C        SUBROUTINE QTFE
C        ---------------
C
C     ..................................................................
C
        SUBROUTINE QTFE(H,Q,Z,NDIM)
        INTEGER P
        COMMON/AL1/YS,CS,MU,P,SUM(2001,2),XSPACE,LE,YY(1001,50)
        COMMON/AL9/PSIB(2001),U(2001),S1
C
C
        DIMENSION Z(2001)
C
        IF(NDIM-1)4,3,1
     1  HH=.5*H
        SUM2=HH/2.*Q(HH)/PSIB(1)
        Z(1)=SUM2
C       INTEGRATION LOOP
        S3=0
        DO 2 I=2,NDIM
        A=H*(I)-HH
        SUM2=SUM2+HH*(Q(A)/PSIB(I)+Q(A-H)/PSIB(I-1))
        IF(P.GT.0)GO TO 2
        IF(A.LT.YS)GO TO 2
        H1=AMIN1((A-YS),H)
        S3=S3-MU*H1/PSIB(I)
    2   Z(I)=SUM2+S3
    3   CONTINUE
    4   RETURN
        END
C
C     ..................................................................
C
C        SUBROUTINE BOUND
C        ----------------
C
C            THIS ROUTINE FINDS THE CONSTANT OF INTEGRATION
C            FOR THE CURRENT MOMENT BEING CALCULATED
C     ..................................................................
C
        SUBROUTINE BOUND(NDIM,SCT2,SUM2,SUM1)
        INTEGER P
        COMMON/AL1/YS,CS,MU,P
        COMMON/AL2/C(2001),DIM,AC(50),K7,AL,YH(50),JM,TYOP,NL
        COMMON/AL7/VELTYP,SCTI(2001,2),H,AK,YST,ETYP
        COMMON/AL9/PSIB(2001),U(2001)
          HH=0.5*H
          SCT2=0.5*C(1)/DIM*U(1)
          DO 2 I=1,NDIM-1
          A=I*H
    2     SCT2=SCT2+HH*(U(I)*C(I)+U(I+1)*C(I+1))
          SCT2=SCT2+HH*U(NDIM)*C(NDIM)
          RETURN
          END
C
C     ..................................................................
C
C        SUBROUTINE QTFF
C        ---------------
C
C     ..................................................................
C
        SUBROUTINE QTFF(H,SUM,NDIM)
        INTEGER P
        COMMON/AL1/YS,CS,MU,P
        COMMON/AL2/C(2001),DIM,AC(50),K7,AL,YH(50),JM,TYOP,NL
        COMMON/AL7/VELTYP,SCTI(2001,2)
        COMMON/AL9/PSIB(2001),U(2001),S1
```

```
C
C
      DIMENSION SUM(2001,2)
      DO 5 I=1,NDIM
      SCTI(I,1)=SCTI(I,2)
    5 SUM(I,1)=SUM(I,2)
C
      SUM(1,2)=H/2.*C(1)*PSIB(1)
      S1=SUM(1,2)
      SCTI(1,2)=H/2.*C(1)*U(1)
      IF(NDIM-1)4,3,1
    1 HH=.5*H
C     INTEGRATION LOOP
      DO 2 I=2,NDIM
      SUM(I,2)=SUM(I-1,2)+HH*(C(I)*PSIB(I)+C(I-1)*PSIB(I-1))
    2 SCTI(I,2)=SCTI(I-1,2)+HH*(C(I)*U(I)+C(I-1)*U(I-1))
      S1=(SUM(NDIM,2)+HH*C(NDIM)*PSIB(NDIM))*(P+1)
      RETURN
    3 SUM(NDIM,2)=SUM2
    4 RETURN
      END
C
C     ..................................................................
C
C        SUBROUTINE VELDIF
C        -----------------
C
C     ..................................................................
C
      SUBROUTINE VELDIF(NDIM)
      COMMON/AL1/YS,CS,MU,P
      COMMON/AL7/VELTYP,SCTI(2001,2),H,AK,YST,ETYP
      COMMON/AL9/PSIB(2001),U(2001),DU,UBAR
C
        REAL MU
        PI=3.14159265358979
        IF(ETYP-2)1,2,3
C
C          UNIFORM DIFFUSIVITY
C
    1   DO 11 I=1,NDIM
        Y1=(1-I*H)*YST/(1+YST)+I*H
        Y2=(1-(I-1)*H)*YST/(1+YST)+(I-1)*H
   11   PSIB(I)=SQRT(MU)*AK/6./H*(Y1-Y2)
        GO TO 20
C
C          PARABOLIC DIFFUSIVITY  (FROM LOG VELOCITY)
C
    2   DO 12 I=1,NDIM
        Y1=(1-I*H)*YST/(1+YST)+I*H
        Y2=(1-(I-1)*H)*YST/(1+YST)+(I-1)*H
   12   PSIB(I)=SQRT(MU)*AK/6./H*((3*(Y1)**2-2*(Y1)**3)-
     -  (3*(Y2)**2-2*(Y2)**3))
        GO TO 20
    3   CONTINUE
        IF(ETYP-4)4,5,6
C
C          PARABOLIC DIFFUSIVITY  (FROM POWER VELOCITY)
C
    4   CONTINUE
        A1=2.-1./7.
        A2=3.-1./7.
        DO 13 I=1,NDIM
        Y1=(1-I*H)*YST/(1+YST)+I*H
        Y2=(1-(I-1)*H)*YST/(1+YST)+(I-1)*H
   13   PSIB(I)=SQRT(MU)*AK/6./H*((A2*(Y1)**A1-A1*(Y1)**A2)-
     -  (A2*(Y2)**A1-A1*(Y2)**A2))
        GO TO 20
C
C          SINUSOIDAL DIFFUSIVITY
C
    5   DO 15 I=1,NDIM
        Y1=(1-I*H)*YST/(1+YST)+I*H
        Y2=(1-(I-1)*H)*YST/(1+YST)+(I-1)*H
   15   PSIB(I)=SQRT(MU)*AK/12./H*(COS(Y2*PI)-COS(Y1*PI))
        GO TO 20
    6   CONTINUE
        DO 16 I=1,NDIM
        Y1=I*H-H/2.
   16   PSIB(I)=PSI(Y1)
   20   CONTINUE
        IF(VELTYP.GT.0.)IF(VELTYP-2.)8,9,10
C
C          UNIFORM VELOCITY
C
        DO 21 I=1,NDIM
   21   U(I)=MU
        RETURN
C
C          PARABOLIC VELOCITY
C
    8   CONTINUE
        DO 22 I=1,NDIM
        Y1=(1-I*H)*YST/(1+YST)+I*H
        Y2=(1-(I-1)*H)*YST/(1+YST)+(I-1)*H
   22   U(I)=MU+SQRT(MU)/AK/H*((-(Y1**3)+3*Y1*Y1-2*Y1)-(-Y2**3+3*Y2**2
     -  -2*Y2))
        RETURN
C
C          LOGARITHMIC VELOCITY
C
    9   CONTINUE
        DO 23 I=1,NDIM
        Y1=(1-I*H)*YST/(1+YST)+I*H
```

```
      Y2=(1-(I-1)*H)*YST/(1+YST)+(I-1)*H
      IF(Y1.GT.H)Z=1+1/AK/H/SQRT(MU)*(Y1*ALOG(Y1)-Y2*ALOG(Y2))
      IF(Y1.LE.H)Z=1+1/AK/SQRT(MU)*(1+ALOG(H/2))
   23 U(I)=MU*Z
      RETURN
C
C       POWER VELOCITY
C
   10 IF(VELTYP-4)30,30,31
   30 CONTINUE
      DO 24 I=1,NDIM
      Y1=(1-I*H)*YST/(1+YST)+I*H
      Y2=(1-(I-1)*H)*YST/(1+YST)+(I-1)*H
   24 U(I)=MU/H*(Y1**(1+1./7.)-(Y2)**(1+1./7.))
      RETURN
   31 CONTINUE
      DO 32 I=1,NDIM
      Y1=I*H-H/2.
   32 U(I)=VELM(Y1)/UBAR
      RETURN
      END
C
C     ------------------------------------------------------------
C
C       SUBROUTINE PLO
C       --------------
C
C           TO USE THIS 3-D PLOTTIMG ROUTINE REFER TO
C           G.HARRINGTON OF NZAEI.
C     ------------------------------------------------------------
C
      SUBROUTINE PLO(NTY,YD)
      COMMON/AL1/YS,CS,MU,P,SUM(2001,2),XSPACE,LE,YY(1001,50)
      COMMON/AL2/C(2001),DIM,AC(50),K7,AL,YH(50),JM,TYOP,NL
      COMMON/AL5/YSC,XINC,ZINC,PHI,THETA,XLTH,FR,CONTR,MSKN,IS,NCR
      DIMENSION YD(LE,NL)
      DO 1 J=1,NL
      DO 1 I=1,LE
    1 YD(I,J)=YY(I,J)
      MC3D=NTY-1
      DIMENSION XINIT(2001),ZINIT(2001),MASK(7000)
      CALL AINIT(4500)
      CALL CNTR3D(YD,LE,NL,YSC,XINIT,XINC,ZINIT,ZINC,PHI,THETA,
     -XLTH,FR,MASK,CONTR,MC3D,MSKN,IS,NCR)
      CALL AEND
      RETURN
      END

C
C     ------------------------------------------------------------
C
C       SUBROUTINE GRA
C       --------------
C
C     ------------------------------------------------------------
C
      SUBROUTINE GRA(Y)
      COMMON/AL2/C(2001),DIM,AC(50),K7,AL,YH(50),JM,TYOP,NL
      COMMON/AL1/YS,CS,MU,P,SUM(2001,2),XSPACE,LE,YY(1001,50)
      COMMON/AL4/YN,LEM(50),SER,SLE,LPLO
      COMMON/STORE/MAXJA,NUMJA,JA(3,500)
      COMMON/AL6/NCON,ZCC(100),IX,IY,IXX,IYY,LOGPL,NPLS
      COMMON/AL7/VELTYP,SCTI(2001,2),H,AK
      COMMON/AL8/INTR
      DATA CHAR/'.'/
      IF(SLE.NE.0.)LE=LPLO
      IF(SER.NE.0.)GO TO 9
      CALL CONI(Y,PL)
      IF(SLE.NE.0.)LE=LPLO
      DO 13 I=1,LE
   13 PL(I)=PL(I)+1
    9 IF(SER.NE.0.)CALL CON(Y,QL,OL)
      IF(SLE.NE.0.)LE=LPLO
      LE4=LE/4
      H=XSPACE*LE
      N=(IFIX(H/10)+1)*2
      DIMENSION ZL(2),PL(2000),X(100),XY(100),QL(2000),OL(2000)
      IF(TYOP.EQ..5) GO TO 5
      REAL TMF(1)/'F5.1'/
      REAL T1(3)/'CONCENTRATION'/
      REAL MU
      REAL FIT(1)/'F4.1'/
      REAL FFT(1)/'F5.3'/
      REAL XT(1)/'F6.2'/
      REAL VT(1)/'F6.4'/
      REAL FMT(1)/'F4.2'/
      REAL T4(1)/3HY= /
      REAL R1(4)/19H UNIFORM VELOCITY  /
      REAL R2(4)/19HPARABOLIC VELOCITY /
      REAL R3(4)/20HLOGARITHMIC VELOCITY/
      REAL R9(4)/19H  POWER  VELOCITY  /
      REAL R4(3)/15HSOURCE          /
      REAL R7(3)/15H        HEIGHT /
      REAL R5(1)/2HF=/
      REAL R8(1)/4H,YN=/
      REAL T2(5)/26HNON-DIMENSIONAL DISTANCE  /
      REAL T3(6)/"PLEASE PUT .35MM PEN IN CALCOMP"/
      REAL R6(2)/12HIN DEAD ZONE/
      REAL FT(1)/'I2'/
      CALL AINIT(2000)
      CALL ASPEED(6)
      CALL AORIG(200,100)
      CALL ABOX(0,0,N,1,50,1,1)
      CALL ABOX(0,0,1,11,1,78,1)
```

```
      G=40.0/N*XSCALE
      ZL(2)=1.0
      ZL(1)=1.0
      IC=N*50
      NN=N/2
    5 CONTINUE
      YSP=0.2
      YO=-1.2
      DO 1 I=1,LE4
    1 IF(PL(I).GT.1.3.OR.QL(I).GT.1.3)GO TO 3
      GO TO 2
    3 YO=-1.25
      YSP=0.25
      DO 66 I=1,LE4
   66 IF(PL(I).GT.3.0.OR.QL(I).GT.3.0)GO TO 44
      GO TO 2
   44 YO=-1.5
      YSP=0.5
      DO 6 I=1,LE4
    6 IF(PL(I).GT.4.5.OR.QL(I).GT.4.5)GO TO 4
      GO TO 2
    4 YO=-3.0
      YSP=2.0
      GO TO 2
    2 YSC=YSP*10.0/7.8
      YO=0.0
      IF(TYOP.EQ.0.5)GO TO 7
      FU=8./MU
      CALL ASCALE(570,595,0,0,YN,0,1,2,2,XT,6)
      CALL ASCALE(370,595,0,0,FU,0,1,2,2,VT,6)
      CALL ALAB(330,595,R5,6,2,2)
      CALL ALAB(490,595,R8,6,2,2)
      IF(VELTYP.EQ.0.)CALL ALAB(330,665,R1,24,2,2)
      IF(VELTYP.EQ.1.)CALL ALAB(330,665,R2,24,2,2)
      IF(VELTYP.EQ.2.)CALL ALAB(330,665,R3,24,2,2)
      IF(VELTYP.EQ.3.)CALL ALAB(330,665,R9,24,2,2)
      CALL ALAB(330,630,R4,18,2,2)
      IF(INTR.NE.0)GO TO 20
      CALL ASCALE(650,630,0,0,YSP,0,1,2,2,FFT,5)
      CALL ALAB(330,630,R7,18,2,2)
      GO TO 24
   20 CONTINUE
      CALL ALAB(470,630,R6,12,2,2)
   24 CONTINUE
      CALL ASCA(-85,-35,100,0,0,10,NN,2,2)
      CALL ALAB(-105,170,T1,18,2,4)
      CALL ALAB(250,-80,T2,30,2,2)
      CALL ALINEX(0,IC,ZL,2,YO,YSC)
      CALL ALAB(465,700,T4,6,2,2)
      IX=XSPACE*10.+.1
      IF(SER.EQ.0.)CALL ALINEX(1,IX,PL,LE,YO,YSC)
      IF(YSP.LT.1.5) CALL ASCALE(-85,-10,0,78,0.0,YSP,11,2,2,FMT,4)
      IF(YSP.GE.1.5) CALL ASCALE(-85,-10,0,78,0.0,YSP,11,2,2,FIT,4)
      IF(SER.NE.0.) CALL ALINEX(1,IX,QL,LE,YO,YSC)
      CALL ASCALE(500,700,0,0,Y,0,1,2,2,FFT,5)
      CALL AEND
      DO 21 I=1,LE
   21 PL(I)=0.0
      RETURN
    7 CONTINUE
      WRITE(7,10)
      DO 8 I=1,LE
      B=I
      XP=B/(N*25.)*9999.
      YP=(YY(I,JM)-(YO+1.))/(12*YSP)*9999
      IA=I/2.
      IB=IA*2
    8 IF(I.NE.IB) WRITE(7,12)XP,YP
      WRITE(7,11)
   10 FORMAT(" PLTL")
   11 FORMAT(" PLTT")
   12 FORMAT(1X,F5.0,1X,F5.0)
      END
C
C     ------------------------------------------------------------
C
C        SUBROUTINE FLATCO
C        -----------------
C
C     ------------------------------------------------------------
C
      SUBROUTINE FLATCO(YD)
      COMMON/AL1/YSP,CS,MU,P,SUM(2001,2),XSPACE,LE,YY(1001,50)
      COMMON/AL2/C(2001),DIM,AC(50),K7,AL,YH(50),JM,TYOP,NL
      COMMON/STORE/MAXJA,NUMJA,JA(3,500)
      COMMON/AL4/YNN,LEM(50),SER,SLE,LPLO
      COMMON/AL6/NCON,ZCC(100),IX,IY,IXX,IYY,LOGPL,NPLS
      COMMON/AL8/INTR
      REAL MU
      REAL FFT(1)/'F5.3'/
      REAL VT(1)/'F6.4'/
      COMMON/AL7/VELTYP,SCTI(2001,2),H,AK
      REAL FMT(1)/'F4.2'/
      REAL R1(4)/19HUNIFORM VELOCITY   /
      REAL R2(4)/19HPARABOLIC VELOCITY /
      REAL R3(4)/20HLOGARITHMIC VELOCITY/
      REAL R9(4)/19H  POWER  VELOCITY  /
      REAL R4(3)/15HSOURCE          /
      REAL R7(3)/15H        HEIGHT /
      REAL R5(1)/2HF=/
      REAL R6(2)/12HIN DEAD ZONE/
      REAL S1(3)/15HSERIES SOLUTION/
      REAL FT(1)/'I2'/
      REAL T1(5)/26HNON-DIMENSIONAL DEPTH     /
```

```
      REAL T2(5)/26HNON-DIMENSIONAL DISTANCE  /
      REAL T3(6)/"PLEASE PUT .35MM PEN IN CALCOMP"/
      DIMENSION YD(LE,NL)
      INTEGER MC(60)/60*10000/
      F=8./MU
      DO 1 J=1,NL
      DO 1 I=1,LE
    1 YD(I,J)=YY(I,J)
      MAXJA=500
      NUMJA=0
      CALL AINIT(2000)
      NX=LE*IX
      IF(LOGPL.NE.0) GO TO 3
      NY=NL*IY/10.
      CALL ASPEED(6)
      NYOR=IY/2.
      CALL AORIG(200,200)
      CALL ASCALE(750,340,0,0,F,0,1,2,2,VT,6)
      CALL ALAB(710,340,R5,6,2,2)
      CALL ABOX(0,0,20,10,50,NY,2)
      IF(SER.NE.0.)GO TO 5
      IF(VELTYP.EQ.0.)CALL ALAB(590,410,R1,24,2,2)
      IF(VELTYP.EQ.1.)CALL ALAB(590,410,R2,24,2,2)
      IF(VELTYP.EQ.2.)CALL ALAB(590,410,R3,24,2,2)
      IF(VELTYP.EQ.3.)CALL ALAB(590,410,R9,24,2,2)
    5 CONTINUE
      IF(SER.NE.0.)CALL ALAB(590,410,S1,18,2,2)
      CALL ALAB(570,375,R4,18,2,2)
      IF(INTR.NE.0)GO TO 2
      CALL ASCALE(890,375,0,0,YSP,0,1,2,2,FFT,5)
      CALL ALAB(570,375,R7,18,2,2)
      GO TO 4
    2 CONTINUE
      CALL ALAB(710,375,R6,12,2,2)
    4 CONTINUE
      CALL ASCALE(-85,-10,0,NY,0.0,0.1,11,2,2,FMT,4)
      IX=XSPACE*10.+.2
      IXX=IX
      WRITE(6,*/)LE,NL,IX,IY,IXX,IYY,NYOR,NCON
      CALL CONTR(YD,LE,NL,IX,IY,ZCC,MC,IXX,IYY,0,NYOR,NCON)
      CALL SPLOTM
      CALL ASCA(-85,-35,100,0,0,10,10,2,2)
      CALL ALAB(-105,170,T1,30,2,4)
      CALL ALAB(250,-80,T2,30,2,2)
      CALL AEND
      RETURN
    3 CONTINUE
      CALL AORIG(100,100)
      NY=NL*IY/10.
      IX=NPLS*XSPACE
      IXX=IX
      CALL ABOX(0,0,8,10,NPLS,NY,2)
      CALL ASCALE(-55,-5,0,NY,0.0,0.1,11,1,2,FMT,4)
      NYOR=IY/2.
      CALL CONTR(YD,LE,NL,IX,IY,ZCC,MC,IXX,IYY,0,NYOR,NCON)
      CALL ASCA(-85,-40,NPLS,0,10,0,9,2,2)
      CALL ASCA(-25,-20,NPLS,0,-5,1,9,1,2)
      CALL SPLOTM
      CALL AEND
      RETURN
      END
```

APPENDIX E

THREE-DIMENSIONAL MODEL COMPUTER PROGRAM

Additional parameters required for this program that are not used in the two-dimensional program are:

YYNO, ZZNO - number of elements in the vertical and horizontal directions, respectively.

YDEPTH, ZDEPTH - relative channel dimensions (consistent units).

ZS - horizontal source location.

UBAR - mean velocity, required if actual velocities are used as input.

ISP, INY - output parameters describing the spacing between output concentrations (ISP) and the number of concentrations required (INY).

NSEC, XSEC - number of transverse contour plots (NSEC) and longitudinal location of each plot (XSEC).

```
C
C ********************************************************************
C *                                                                  *
C *     STEADY STATE SOLUTION OF THE THREE-DIMENSIONAL DISPERSION    *
C *     ---------------------------------------------------------    *
C *                                                                  *
C *               EQUATION FOR CONCENTRATION DEFICIT.                *
C *               -----------------------------------                *
C *                                                                  *
C ********************************************************************
C
C
C*****INPUT REQUIRED********
C
C          GENERAL PARAMETERS:
C             NM - NUMBER OF MOMENTS CALCULATED
C             MU - DIMENSIONLESS AVERAGE VELOCITY (MU=8/f)
C             YS,ZS - THE LOCATION OF SOURCE ( DIMENSIONLESS: 0<YS<1
C                                                             0<ZS<1 )
C             AK - VON KARMAN'S CONSTANT
C             EPPSS - ERROR LIMIT FOR MATRIX SOLUTION (PIVOT CHECK)
C             S - A USER COMMENT CARD TO PRECEED OUTPUT
C
C
C    VELOCITY AND DIFFUSIVITY PROFILES ARE DEFINED AS FUNCTIONS OF Y,
C             WHERE Y IS DIMENSIONLESS DEPTH.
C
C             VELTYP = 1 , FOR UNIFORM VELOCITY
C                    = 2 , FOR LOGARITHMIC VELOCITY
C                    = 3 , FOR POWER VELOCITY
C
C             ETYP   = 0 OR 1 , FOR UNIFORM DIFFUSIVITY
C                    = 2 , FOR PARABOLIC DIFFUSIVITY (FROM LOG. VEL.)
C                    = 3 , FOR PARABOLIC DIFFUSIVITY (FROM POWER VEL.)
C
C       THE PROGRAM IS DESIGNED TO PRODUCE ONE OF TWO TYPES OF PLOT
C       OF THE CONCENTRATION DISTRIBUTION WHICH IS GENERATED.
C       FOR ALL CASES THE USER MUST SPECIFY NL (OR NL2) , THE
C       NUMBER OF HIEGHTS AT WHICH CONCENTRATION PROFILES ARE
C       REQUIRED. THE TYPE OF PLOT IS SPECIFIED BY NTYOP ;
C
C              NTYOP = 1, PRODUCES LONGITUDINAL CONTOUR PLOTS OF
C                         CONCENTRATION (VERTICAL OR HORIZONTAL)
C                    = 2 , PRODUCES CROSS-SECTIONAL CONTOUR PLOTS OF
C                          CONCENTRATION
C
C
C
C
C    INITIALISE VARIABLES
C    --------------------
C
      DIMENSION NODE(3000,4),P(3000,2),Q(3000,2),FC(3000),S(12)
      DIMENSION LY(100),PL(100),XSEC(20),YD(501,100),PG(20)
      DIMENSION AB(8000),W(8000),X(8000),IW(8000,8),ICN(8000),IRN(8000)
     - ,IKE(8000,5),IDISP(10)
      LOGICAL LBLOCK,GROW,ABORT(4)
      COMMON /C1/AMI,ZS,DELY,DELZ,SK,NC,YN,YYNO,ZZNO
      COMMON /C2/UBAR,ZN,YDEPTH,ZDEPTH,VYTYP,VZTYP,EYTYP,EZTYP
      COMMON/C3/YH(3000),ZH(3000),BIN(3000),CM(3000)
      COMMON/C4/CD(3000,21)
      COMMON/AL1/YS,MU,XSPACE,LE,LE1,YY(501,100)
      COMMON/AL2/AC(0:15),K7,AL,JM,NTYOP,NL
      COMMON/AL3/A(25,25)
      COMMON/AL4/LEM(50),SER,X0,SLE,LPLO
      COMMON/AL5/YSC,XINC,ZINC,PHI,THETA,XLTH,FR,CONTR,MSKN,IS,NCR
      COMMON/AL6/NCON,ZCC(100),IX,IY,IXX,IYY,LOGPL,NPLS
      COMMON/AL7/VELTYP,SCTI(2220,2),H,AK,YST,ETYP
      COMMON/AL8/YU1,YL1,INTR
C
C    INPUT DATA
C
      REAL MU
      READ(4,180)S
      READ(4,/)YYNO,ZZNO,NM
      READ(4,/)YDEPTH,ZDEPTH,EPPSS
      READ(4,/)YS,ZS
      READ(4,/)UBAR,MU,AK
      READ(4,/)VYTYP,VZTYP,EYTYP,EZTYP
      READ(4,/)ISP,INY,NL2
      READ(4,/)LZ,LPLO,NEW
      READ(4,/)NTYOP
      READ(4,/)NCON,(ZCC(I),I=1,NCON)
      READ(4,/)NSEC,(XSEC(I),I=1,NSEC)
C
      DATE=TIME(15)
      WT2=TIME(11)*2.4E-6
      WT1=AINT(WT2/3600.)*100
      WTT=(WT2-WT1*36.)/60.+WT1
      RM=CONCAT(RM,DATE,15,47,16)
      RD=CONCAT(RD,DATE,15,31,16)
      RY=CONCAT(RY,DATE,15,15,16)
      WRITE(6,505)RD,RM,RY,WTT
      WRITE(6,180)S
      WRITE(6,*/)YYNO,ZZNO,NM
      WRITE(6,*/)YDEPTH,ZDEPTH,EPPSS
      WRITE(6,*/)YS,ZS
      WRITE(6,*/)UBAR,MU,AK
      WRITE(6,*/)VYTYP,VZTYP,EYTYP,EZTYP
      WRITE(6,*//)ISP,INY,NL2
      WRITE(6,*/)LZ,LPLO,NEW
      WRITE(6,*/)NTYOP
      WRITE(6,*/)NCON,(ZCC(I),I=1,NCON)
      WRITE(6,*/)NSEC,(XSEC(I),I=1,NSEC)
```

```
C
C     SET CONSTANTS
C
        YN=YDEPTH/ZDEPTH
        YS=YS*YN
        DELZ=1./FLOAT(ZZNO)
        DELY=1./FLOAT(YYNO)*YN
        DYZ=(DELY/DELZ)**2
        LICN=8000
        LIRN=8000
        ZN=1.0
        MTYPE=1
        LBLOCK=.TRUE.
        GROW=.TRUE.
        ABORT(1)=.TRUE.
        ABORT(2)=.TRUE.
        ABORT(4)=.TRUE.
        ABORT(3)=.FALSE.
        M=YYNO
        N=ZZNO
        MN=YYNO*ZZNO
        NC=1
C
C     SET UP GRID OF ELEMENTS FOR SOLUTION
C
        DO 4 I=1,YYNO
         DO 5 J=1,ZZNO
         K=N*(I-1)
         Y=FLOAT(I-1)*DELY+DELY/2.
         Z=FLOAT(J-1)*DELZ+DELZ/2.
         YH(NC)=Y
         ZH(NC)=Z
         NODE(NC,1)=K-N+J
         NODE(NC,2)=K+J+1
         NODE(NC,3)=K+N+J
         NODE(NC,4)=K+J-1
         P(NC,1)=EY(Y-DELY/2.,Z)
         Q(NC,1)=0.15*SQRT(MU)*EZ(Y,Z+DELZ/2.)*DYZ
         P(NC,2)=EY(Y+DELY/2.,Z)
         Q(NC,2)=0.15*SQRT(MU)*EZ(Y,Z-DELZ/2.)*DYZ
    5    NC=NC+1
    4   CONTINUE
         DO 6 I=1,ZZNO
         NODE(I,1)=NODE(I,1)+ZZNO
    6    NODE((YYNO-1)*ZZNO+I,3)=NODE((YYNO-1)*ZZNO+I,3)-ZZNO
         DO 7 I=1,YYNO
         NODE((I-1)*ZZNO+1,4)=NODE((I-1)*ZZNO+1,4)+1
         NODE(I*N,2)=NODE(I*N,2)-1
    7    CONTINUE
         SK=0.0
C
C     CALCULATE SOURCE PROPERTIES
C
         DO 11 J=1,MN
         YL=YH(J)-DELY/2.
         YU=YH(J)+DELY/2.
         ZL=ZH(J)-DELZ/2.
         ZU=ZH(J)+DELZ/2.
         Z=ZH(J)
         Y=YH(J)
         IF(YS.GE.YL.AND.YS.LT.YU.AND.ZS.GE.ZL.AND.ZS.LT.ZU)SK=SK+1.*
     -   VYZ(Y,Z)
   11    CONTINUE
        AMI=FLOAT(MN)/SK
        J=0
        SUM1=0
        DO 195 I=1,MN
  195   SUM1=SUM1+EY(YH(I),ZH(I))*CDI1(YH(I),ZH(I))/MN
C
C     CALCULATE COEFFICIENT MATRIX A FOR Ax=b
C
        NZ=MN*(MN-5)+2*(ZZNO+YYNO)
        NONZ=(MN*MN)-NZ
        LP=1
        L=0
        LL=0
        DO 250 I=1,YYNO
        DO 250 M=1,ZZNO
        IF(I.EQ.IFIX(YYNO).AND.M.EQ.IFIX(ZZNO))NONZ=LP-1
        LL=LL+1
        FL=0.
        L=L+1
        IF(NODE(L,3).NE.MN)GO TO 249
        GO TO 151
  249   IF(NODE(L,3).EQ.L)GO TO 261
        AB(LP)=P(L,2)
        ICN(LP)=NODE(L,3)
        IRN(LP)=LL
        LP=LP+1
  151   AB(LP)=-P(L,2)
        FL=1
        LPT=LP
        ICN(LP)=L
        IRN(LP)=LL
        LP=LP+1
  261   IF(NODE(L,1).NE.MN)GO TO 251
        GO TO 152
   251  IF(NODE(L,1).EQ.L)GO TO 262
        AB(LP)=P(L,1)
        ICN(LP)=NODE(L,1)
        IRN(LP)=LL
        LP=LP+1
  152   IF(FL.NE.0)GO TO 240
        AB(LP)=-P(L,1)
```

```
      FL=1
      LPT=LP
      ICN(LP)=L
      IRN(LP)=LL
      LP=LP+1
      GO TO 262
  240 AB(LPT)=AB(LPT)-P(L,1)
  262 CONTINUE
      IF(NODE(L,2).NE.MN)GO TO 252
      GO TO 153
  252 IF(NODE(L,2).EQ.L)GO TO 263
      AB(LP)=Q(L,1)
      ICN(LP)=NODE(L,2)
      IRN(LP)=LL
      LP=LP+1
  153 IF(FL.NE.0)GO TO 241
      FL=1.
      LPT=LP
      AB(LP)=-Q(L,1)
      ICN(LP)=L
      IRN(LP)=LL
      LP=LP+1
      GO TO 263
  241 AB(LPT)=AB(LPT)-Q(L,1)
  263 IF(NODE(L,4).NE.MN)GO TO 253
      GO TO 154
  253 IF(NODE(L,4).EQ.L)GO TO 250
      AB(LP)=Q(L,2)
      ICN(LP)=NODE(L,4)
      IRN(LP)=LL
      LP=LP+1
  154 IF(FL.NE.0)GO TO 243
      FL=1.
      LPT=LP
      AB(LP)=-Q(L,2)
      ICN(LP)=L
      IRN(LP)=LL
      LP=LP+1
      GO TO 250
  243 AB(LPT)=AB(LPT)-Q(L,2)
  250 CONTINUE
      U=1.0
      JN=MN-1
C
C    LOOP TO SOLVE FOR MOMENTS x,IN Ax=b
C
   89 CONTINUE
      J=J+1
       DO 178 L1=1,MN
       NC=L1
       Y=YH(L1)
       Z=ZH(L1)
      IF(J.EQ.1)FC(L1)=-MU/YN*VYZ(Y,Z)*CDI1(Y,Z)*DELY**2
      IF(J.EQ.2)FC(L1)=-(EY(Y,Z)*CDI1(Y,Z)+MU/YN*VYZ(Y,Z)*CD(L1,J-1))
     1 *DELY**2
      IF(J.GT.2)FC(L1)=-(EY(Y,Z)*(J-2)*(J-1)*CD(L1,J-2)+(J-1)*MU/YN*
     1 VYZ(Y,Z)*CD(L1,J-1))*DELY**2
  178 CONTINUE
      IF(J.GT.1)GO TO 93
      CALL F01BRF(JN,NONZ,AB,LICN,IRN,LIRN,ICN,U,IKE,IW,W,LBLOCK,
     -            GROW,ABORT,IDISP,IFLAG)
   93 CALL F04AXF(JN,AB,LICN,ICN,IKE,FC,W,MTYPE,IDISP,RESID)
      DO 192 I=1,MN
  192 CD(I,J)=FC(I)
      CALL BOUND(SUM1,MN,J)
      ADD=(SUM1+SUM2)/MU/YN
C     WRITE(6,*//)ADD,SUM1,SUM2
      SUM2=0.
      DO 193 I=1,MN
      CD(I,J)=FC(I)-ADD
  193 SUM2=EY(YH(I),ZH(I))*CD(I,J)*DELZ*DELY+SUM2
   94 CONTINUE
      IF(J.LT.NM)GO TO 89
      PP=J
      MKL=4
C     WRITE(6,120)(I,I=1,6)
      DO 95 I=1,NL2
      KY=INY+(I-1)*ISP
C     WRITE(6,121)YH(KY),(CD(KY,J),J=1,MKL)
      AL=CD(KY,PP-1)*(PP-1)/CD(KY,PP)
      AC1=AL**(PP)*CD(KY,PP)/FACT(PP-1)
      XM=-ALOG(0.05/ABS(AC1))/AL
       Y=YH(KY)
       Z=ZH(KY)
C     WRITE(6,*//)Y,Z,AL,AC1,XM
   95 CONTINUE
C      STOP
      NOM=3
      NOD=0
      PP=NM
      NK=NL2*ISP
      DO 8 JM=INY,NK,ISP
      Y=YH(JM)
      Z=ZH(JM)
      CAX0=CDI1(Y,Z)
      YSO=YS
      ZSO=ZS
      DO 1 I=1,PP
      II=I-1
      CM(I)=CD(JM,I)
    1 IF(MOMUSE.NE.0)WRITE(6,50) CM(I),II
      PI=3.1415926536
      AL=CM(PP-1)*(PP-1)/CM(PP)
      AC(1)=AL**(PP)*CM(PP)/FACT(PP-1)
```

```
      YK=SQRT((Y-YSO)**2+(Z-ZSO)**2)
      IF(YK.GT..175)IF((YK-.25))71,72,72
      NM=NOM
      ND=NOD
      GO TO 24
   71 NM=NOM
      ND=NOD+1
      GO TO 24
   72 IF((YK-.35).GT.0.0)IF((YK)-.4)73,74,74
      NM=NOM-1
      ND=NOD+2
      GO TO 24
   73 NM=NOM-1
      ND=NOD+3
      GO TO 24
   74 IF(YK.GT..5)IF(YK-.6)75,76,76
      NM=NOM-2
      ND=NOD+4
      GO TO 24
   75 NM=NOM-3
      ND=NOD+5
      GO TO 24
   76 IF(YK.GT..7)IF(YK-.8)77,78,78
      NM=NOM-5
      ND=NOD+6
      GO TO 24
   77 NM=NOM-5
      ND=NOD+7
      GO TO 24
   78 NM=NOM-5
      ND=NOD+8
   24 CONTINUE
      NM=AMAX0(2,NM)
      NOM1=NM+1
      NOM2=NOM1+1
      K6=ND+NOM1
      K7=K6+1
      A(1,K7)=-AC(1)
      DO 83 II=1,NOM1
      DO 82 K=1,K7
      I=II
      IF(II.GT.2)I=II+(II-2)*MT
   82  A(II,K)=1.0/((K+1)**2)**(I-1)
   83  CONTINUE
      A(1,K7)=CAX0-AC(1)
      DO 84 II=2,NOM1
      I=II+(II-2)*MT
   84  A(II,K7)=CM(I-1)*(AL**(I-1))/FACT(I-2)-AC(1)
      NOM2=NOM1+1
      IF(ND.EQ.0)GO TO 22
      DO 23 K=NOM2,K6
      DO 26 I=1,K6
   26 A(K,I)=((I+1)**2)**(K-NOM1)
   23 A(K,K7)=-AC(1)
   22 CONTINUE
   41 CONTINUE
      CALL MATSOL(K6,K7)
      DO 87 I=2,K7
   87  AC(I)=A((I-1),K7)
      AC(0)=AL
       IF(NTYOP.EQ.4.AND.FL3.EQ.0)WRITE(6,124)(XSEC(I),I=1,NSEC)
       FL3=1
       IF(NTYOP.NE.4)GO TO 79
       DO 122 I1=1,NSEC
       XD=XSEC(I1)
       PG(I1)=1.0
       DO 122 I2=1,K7
  122  PG(I1)=PG(I1)+AC(I2)*EXP(-AL*I2**2*XD)
       WRITE(6,123)Y,Z,(PG(I),I=1,NSEC)
   79  CONTINUE
C  8  WRITE(8)AC
    8 CONTINUE
      STOP
   47  CONTINUE
      GO TO (111,112,113)NTYOP
       Z=ZH(LZ)
       IC1=1
       NL=YYNO
      DO 101 I=1,YYNO
  101 LY(I)=LZ+(I-1)*ZZNO
       DO 102 I=1,NL
       READ(8=LY(I))(AC(J),J=0,NM)
       REWIND 8
       Y=YH(LY(I))
       K7=NM
       JM=I
       CALL CONI(Y)
  102  CONTINUE
      LE=LPLO
      LE1=LE/XSPACE
       IX=123
       IXX=123
      CALL FLATCO(YD)
      GO TO 113
  111 NL=ZZNO
      K7=NM
      Y=YH((LZ-1)*ZZNO+1)
      DO 104 I=1,ZZNO
  104 LY(I)=(LZ-1)*ZZNO+I
      DO 105 I=1,ZZNO
      READ(8=LY(I))(AC(J),J=0,NM)
      REWIND 8
      Z=ZH(LY(I))
      JM=I
```

```
      CALL CONI(Y)
  105 CONTINUE
      LE=LPLO
      LE1=LE/XSPACE
      CALL FLATCO(YD)
      GO TO 113
  112 CONTINUE
      LE1=ZZNO
      NL=YYNO
      DO 107 I=1,NSEC
      XD=XSEC(I)
      DO 109 J=1,YYNO
      DO 110 J3=1,ZZNO
      READ(8)(AC(J1),J1=0,NM)
      PP=0.0
      DO 108 J2=1,NM
  108 PP=AC(J2)*EXP(-AC(0)*J2**2*XD)+PP
  110 YY(J3,J)=PP+1.0
  109 CONTINUE
      CALL PLOSEC(YD)
  107 CONTINUE
  113 CONTINUE
    3 FORMAT(4I4)
    2 FORMAT(4F10.5)
   50 FORMAT(10X,E15.7,10X,'C',I2,/)
  505 FORMAT(2X,C2,"/",C2,"/19",C2,5X,"TIME IS",F10.3,//)
   51 FORMAT(/10X,"VALUE OF ITH MOMENT USED FOR Y=",F5.3,
     1'    Z=',F5.3,//)
   52 FORMAT(10X,'A',I1,10X,E15.7,/)
   53 FORMAT(////10X,'PROGRAM HAS SOLVED FOR THE FIRST ',I1,
     1' COEFFICIENTS',//10X,'USING ',I1,' MOMENTS AND ',I1
     2,' DERIVATIVES',/)
   54 FORMAT(//10X,'ALPHA=',F12.10,///)
  120 FORMAT(14X,'C',7(I2,14X,'C'))
  121 FORMAT(/1X,F6.4,7E17.9,/)
  123  FORMAT(1X,2HY=,F5.3,2HZ=,F5.3,14(1X,F7.4))
  124  FORMAT(13X,2HX=,14(3X,F5.1))
  180 FORMAT(1X,12(A6))
      IF(TYOP.EQ.5)CALL FLATCO(YD)
      STOP
      END
C
C     ..................................................................
C
C        FUNCTION FACT
C        -------------
C
C     ..................................................................
C
      FUNCTION FACT(I)
      F=1.0
      DO 1 J=1,I+1
      F=F*(J-1)
      IF(F.EQ.0.0) F=1.0
    1 CONTINUE
      FACT=F
      RETURN
      END
C
C     ..................................................................
C
C        FUNCTION CDI1
C        -------------
C
C              FUNCTION TO CALCULATE SOURCE EFFECT IN EACH ELEMENT
C
C     ..................................................................
C
      FUNCTION CDI1(Y,Z)
      COMMON /C1/AMI,ZS,DELY,DELZ,SK,NC,YN,YYNO,ZZNO
      COMMON/AL1/YS,MU,XSPACE,LE,LE1,YY(501,100)
      CDI1=-1.0
      YU=Y+DELY/2.
      YL=Y-DELY/2.
      ZL=Z-DELZ/2.
      ZU=Z+DELZ/2.
      IF(YS.GE.YL.AND.YS.LT.YU.AND.ZS.GE.ZL.AND.ZS.LT.ZU)
    1 CDI1=AMI-1.0
      RETURN
      END
C
C     ..................................................................
C
C        FUNCTION VYZ
C        ------------
```

```
C
C               FUNCTION TO CALCULATE VELOCITY IN AN ELEMENT
C
C     ..................................................................
C
      FUNCTION VYZ(Y,Z)
      COMMON /C1/AMI,ZS,DELY,DELZ,SK,NC,YN,YYNO,ZZNO
        COMMON /C2/UBAR,ZN,YDEP,ZDEP,VTY,VTZ,ETY,ETZ
        COMMON/AL1/YS,MU,XSPACE,LE,LE1,YY(501,100)
        COMMON/AL7/VELTYP,SCTI(2220,2),H,AK,YST,ETYP
        IF(VTY-2)1,2,3
    1   VYZ=1.0
        RETURN
  2     H=DELY
        Y1=Y+.5*H
        Y2=Y-0.5*H
C       WRITE(7,*/)VYZ,Y,H,Y1,Y2,AK,SQRT(MU)
        IF(Y2.GE.H)V=1+1/AK/H/SQRT(MU)*(Y1*ALOG(Y1)-Y2*ALOG(Y2))
        IF(Y2.LT.H)V=1+1/AK/SQRT(MU)*(1+ALOG(H/2))
         VYZ=V
C   2   VYZ=1+(1+ALOG(Y))/AK/SQRT(MU)
C       WRITE(7,*/)VYZ,Y,H,Y1,AK,SQRT(MU)
        RETURN
    3   VYZ=Y**(1./7.)
C       WRITE(7,*/)VYZ,Y,AK,SQRT(MU)
        RETURN
        VYZ=1.0+1./0.42/SQRT(MU)*(1+ALOG(Y))
        RETURN
        Y=AMAX1(Y,0.0001)
        Z=AMAX1(Z,0.0001)
        UB=UBAR*1000.
        ZD=(ZN/2.-ABS(ZN/2.-Z))/ZN*2.
        YD=Y/YN
        VMEAN=1.165*UB+0.165*UB*ALOG(ZD)
        B=175.362+48.3456*ALOG(ZD)
        VYZ=(VMEAN+B+B*ALOG(YD))
        VYZ=AMAX1(Y,Z,VYZ)/1000.
        RETURN
        END
C
C     ..................................................................
C
C        FUNCTION EY
C        -----------
C
C              VERTICAL DIFFUSIVITY FUNCTION
C
C     ..................................................................
C
      FUNCTION EY(Y,Z)
       COMMON/AL1/YS,MU,XSPACE,LE,LE1,YY(501,100)
       COMMON/AL7/VELTYP,SCTI(2220,2),H,AK,YST,ETYP
        EY=SQRT(MU)*AK/6.
        RETURN
        END
C
C     ..................................................................
C
C        FUNCTION EZ
C        -----------
C
C              HORIZONTAL DIFFUSIVITY FUNCTION
C
C     ..................................................................
C
      FUNCTION EZ(Y,Z)
       COMMON/AL1/YS,MU,XSPACE,LE,LE1,YY(501,100)
       COMMON/AL7/VELTYP,SCTI(2220,2),H,AK,YST,ETYP
        EZ=1.0
        RETURN
        END
C
C     ..................................................................
C
C        SUBROUTINE MATSOL
C        -----------------
C
C     ..................................................................
C
      SUBROUTINE MATSOL(K5,K6)
      COMMON/AL3/A(25,25)
      DO 90 K=1,K5
      KP1=K+1
C
      IF(ABS(A(K,K)).GE.EPS)GO TO 50
C
      WRITE(6,150)
  150 FORMAT(////10X,'PIVOT ELEMENT TOO SMALL.STOP')
      STOP
C
   50 DO 60 J=KP1,K6
   60 A(K,J)=A(K,J)/A(K,K)
      A(K,K)=1.0
C
      DO 90 I=1,K5
      IF(I.EQ.K.OR.A(I,K).EQ.0.) GO TO 90
      DO 80 J=KP1,K6
   80 A(I,J)=A(I,J)-A(I,K)*A(K,J)
      A(I,K)=0.0
   90 CONTINUE
      RETURN
      END
C
C     ..................................................................
```

```
C
C       SUBROUTINE FLATCO
C       -----------------
C
C     ..................................................................
C
      SUBROUTINE FLATCO(YD)
      COMMON /C1/AMI,ZS,DELY,DELZ,SK,NC,YN,YYNO,ZZNO
      COMMON/AL1/A1,A2,MU,XSPACE,LE,LE1,YY(501,100)
      COMMON/AL2/AC(0:15),K7,AL,JM,NTYOP,NL
      COMMON/STORE/MAXJA,NUMJA,JA(3,3000)
      COMMON/AL6/NCON,ZCC(100),IX,IY,IXX,IYY,LOGPL,NPLS
      COMMON/AL8/YS,INTR
      REAL MU
      REAL FFT(1)/'F5.3'/
      REAL VT(1)/'F6.2'/
      COMMON/AL7/VELTYP,SCTI(2220,2),H,AK
      REAL FMT(1)/'F4.2'/
      REAL R1(4)/19H UNIFORM VELOCITY  /
      REAL R2(4)/19HPARABOLIC VELOCITY /
      REAL R3(4)/20HLOGARITHMIC VELOCITY/
      REAL R4(3)/15HSOURCE         /
      REAL R7(3)/15H              TO/
      REAL R5(1)/4H$R$=/
      REAL R6(2)/12HIN DEAD ZONE/
      REAL FT(1)/'I2'/
      REAL T1(5)/26HNON-DIMENSIONAL DEPTH     /
      REAL T3(5)/26HNON-DIMENSIONAL WIDTH     /
      REAL T2(5)/26HNON-DIMENSIONAL DISTANCE  /
      DIMENSION YD(LE1,NL)
      INTEGER MC(60)/60*10000/
      DO 1 J=1,NL
      DO 1 I=1,LE1
    1 YD(I,J)=YY(I,J)
      MAXJA=3000
      NUMJA=0
      CALL AINIT(2000)
      NX=LE/XSPACE
      IY=800./NL
      CALL ASPEED(6)
      NYOR=IY/2.
      CALL AORIG(200,200)
      CALL ASCALE(750,340,0,0,MU,0,1,2,2,VT,6)
      CALL ALAB(710,340,R5,6,2,2)
      CALL ABOX(0,0,20,10,50,80,2)
      IF(VELTYP.EQ.0.)CALL ALAB(590,410,R1,24,2,2)
      IF(VELTYP.EQ.1.)CALL ALAB(590,410,R2,24,2,2)
      IF(VELTYP.EQ.2.)CALL ALAB(590,410,R3,24,2,2)
      CALL ALAB(570,375,R4,18,2,2)
      IF(INTR.NE.0)GO TO 2
      CALL ASCALE(710,375,0,0,YL,0,1,2,2,FFT,5)
      CALL ASCALE(890,375,0,0,YU,0,1,2,2,FFT,5)
      CALL ALAB(570,375,R7,18,2,2)
      GO TO 3
    2 CONTINUE
      CALL ALAB(710,375,R6,12,2,2)
    3 CONTINUE
      YIN=.1
      IF(NTYOP.EQ.0)YIN=YN/10.
      CALL ASCALE(-85,-10,0,80,0.0,YIN,11,2,2,FMT,4)
      IX=XSPACE*10.+.2
      IXX=IX
      IYY=IY
      WRITE(6,*/)LE,NL,IX,IY,IXX,IYY,NYOR,NCON
      CALL CONTR(YD,LE1,NL,IX,IY,ZCC,MC,IXX,IYY,0,NYOR,NCON)
      CALL SPLOTM
      CALL ASCA(-85,-35,100,0,0,10,10,2,2)
      IF(NTYOP.EQ.0)CALL ALAB(-105,170,T1,30,2,4)
      IF(NTYOP.EQ.1)CALL ALAB(-105,170,T3,30,2,4)
      CALL ALAB(250,-80,T2,30,2,2)
      CALL AEND
      RETURN
      RETURN
      END
C
C     ..................................................................
C
C        SUBROUTINE PLOSEC
C        -----------------
C
C     ..................................................................
C
      SUBROUTINE PLOSEC(YD)
      COMMON /C1/AMI,ZS,DELY,DELZ,SK,NC,YN,YYNO,ZZNO
      COMMON/AL1/YS,MU,XSPACE,LE,LE1,YY(501,100)
      COMMON/AL2/AC(0:15),K7,AL,JM,NTYOP,NL
      COMMON/AL6/NCON,ZCC(100),IX,IY,IXX,IYY,LOGPL,NPLS
      REAL T1(5)/26HNON-DIMENSIONAL DEPTH     /
      REAL T3(5)/26HNON-DIMENSIONAL WIDTH     /
      REAL FFT(1)/'F4.2'/
      REAL FMT(1)/'F3.1'/
      DIMENSION YD(LE1,NL)
      INTEGER MC(60)/60*10000/
      DO 1 J=1,NL
      DO 1 I=1,LE1
    1 YD(I,J)=YY(I,J)
      WRITE(6,*/)YD
      IZ=1200./ZZNO
      IZZ=IZ
      IY=800./YYNO
      IYY=IY
      NYOR=IY/2.
      NZOR=IZ/2.
      YIN=YN/10.
```

```
      CALL AINIT(2000)
      CALL AORIG(200,200)
      CALL ABOX(0,0,20,10,60,80,2)
      CALL ASCALE(-85,-10,0,80,0.0,YIN,11,2,2,FFT,4)
      CALL ASCALE(93,-30,120,0,0.1,0.1,10,2,2,FMT,3)
      CALL CONTR(YD,ZZNO,YYNO,IZ,IY,ZCC,MC,IZZ,IYY,NZOR,NYOR,NCON)
      CALL SPLOTM
      CALL ALAB(-105,170,T1,30,2,4)
      CALL ALAB(250,-80,T3,30,2,2)
      CALL AEND
      RETURN
      END
C
CCCCCC.....................................................................
C
C        SUBROUTINE CONI
C        ---------------
C
CCCCCC.....................................................................
C
      SUBROUTINE CONI(Y)
      COMMON/AL1/YS,MU,XSPACE,LE,LE1,YY(501,100)
      COMMON/AL2/AC(0:15),K7,AL,JM,NTYOP,NL
      COMMON/AL4/LEM(50),SER,X0
      COMMON/AL6/NCON,ZCC(100),IX,IY,IXX,IYY,LOGPL,NPLS
      DO 2 M=1,501
    2 YY(M,JM)=1.0
      XSPACE=0.5
      X=0.0
      WRITE(6,*/)AC
      I=1
   20  PL=0.0
      AX=X
      DO 1 J=1,K7
    1 PL=AC(J)*EXP(-AC(0)*J**2*AX)+PL
      YY(I,JM)=PL+1.0
      IF(ABS(PL).LT.2E-02.AND.X.GT.85.)GO TO 3
      IF(ABS(PL).LT.2E-02.AND.AX.GT.1E04)GO TO 3
      I=I+1
      X=X+XSPACE
      GO TO 20
    3 CONTINUE
      RETURN
      END
C
CCCCCC.....................................................................
C
C        SUBROUTINE BOUND
C        ----------------
C
CCCCCC.....................................................................
C
      SUBROUTINE BOUND(SUM1,MN,J)
      COMMON/C3/YH(3000),ZH(3000),BIN(3000),CM(3000)
      COMMON/C4/CD(3000,21)
      COMMON/AL1/YS,MU
      COMMON/C1/AMI,ZS,DELY,DELZ,SK,NC,YN,YYNO,ZZNO
      ZY=1./(YYNO*ZZNO)
      SUM1=0.
      DO 1 I=1,MN
    1 SUM1=MU*YN*VYZ(YH(I),ZH(I))*CD(I,J)*ZY+SUM1
      RETURN
      END
```